Cíntia Catarina Sousa Carreira

Mestre em Biotecnologia

Insights into the structure and reactivity of the catalytic site of nitrous oxide reductase

Dissertação para obtenção do Grau de Doutor em Bioquímica – Especialidade em Bioquímica Física

Orientador: Doutora Isabel Maria Andrade Martins Galhardas de Moura, Professora Catedrática Aposentada da Faculdade de Ciências e Tecnologia da Universidade Nova de Lisboa

Co-orientador: Doutora Sofia Rocha Pauleta, Investigadora Principal da Faculdade de Ciências e Tecnologia da Universidade Nova de Lisboa

Co-orientador: Doutor Oliver Einsle, Professor da Universidade de Freiburg, Alemanha

Júri:

Presidente: Prof. Doutor Manuel Luís de Magalhães Nunes da Ponte
Arguentes: Prof. Doutor José João Galhardas de Moura
Prof. Doutor Simone Dell'Acqua
Vogais: Prof. Doutora Margarida Maria Portela Correia dos Santos Romão
Prof. Doutora Maria Alice Santos Pereira
Prof. Doutora Isabel Maria Andrade Martins Galhardas de Moura

FACULDADE DE CIÊNCIAS E TECNOLOGIA
UNIVERSIDADE NOVA DE LISBOA

Outubro 2017

Cíntia Catarina Sousa Carreira

Mestre em Biotecnologia

Insights into the structure and reactivity of the catalytic site of nitrous oxide reductase

Dissertação para obtenção do Grau de Doutor em Bioquímica – Especialidade em Bioquímica Física

Orientador: Doutora Isabel Maria Andrade Martins Galhardas de Moura, Professora Catedrática Aposentada da Faculdade de Ciências e Tecnologia da Universidade Nova de Lisboa

Co-orientador: Doutora Sofia Rocha Pauleta, Investigadora Principal da Faculdade de Ciências e Tecnologia da Universidade Nova de Lisboa

Co-orientador: Doutor Oliver Einsle, Professor da Universidade de Freiburg, Alemanha

Júri:

Presidente: Prof. Doutor Manuel Luís de Magalhães Nunes da Ponte
Arguentes: Prof. Doutor José João Galhardas de Moura
Prof. Doutor Simone Dell'Acqua
Vogais: Prof. Doutora Margarida Maria Portela Correia dos Santos Romão
Prof. Doutora Maria Alice Santos Pereira
Prof. Doutora Isabel Maria Andrade Martins Galhardas de Moura

Outubro 2017

Insights into the structure and reactivity of the catalytic site of nitrous oxide reductase

Outubro 2017

Acknowledgments

O meu percurso científico iniciou-se neste laboratório e tornou-se mais fácil com a presença de muitas pessoas que me apoiaram em vários momentos e que contribuíram para o meu desenvolvimento como pessoa e como investigadora. Estas pessoas não ficarão esquecidas, e a todas o meu sincero obrigada!

Em primeiro lugar, agradeço à Professora Isabel Moura, pela orientação do trabalho e discussões científicas e por me ter apoiado e motivado desde a licenciatura.

Quero fazer um agradecimento especial à Doutora Sofia Pauleta por me ter orientado, por todos os conhecimentos que me transmitiu e oportunidades que me concedeu. Estas são poucas palavras para descrever todo o apoio, disponibilidade e incentivo que sempre me deu e por isso estou-lhe grata.

Ao Professor Oliver Einsle, agradeço ter aceite ser co-orientador desta tese e por me receber sempre bem no seu laboratório.

Agradeço ao Professor José Moura a possibilidade de poder trabalhar no seu laboratório e pelo seu entusiasmo pela ciência e cultura, sempre contagiante.

À Professora Margarida Romão agradeço por me ter recebido no seu laboratório e por todo o conhecimento científico que me transmitiu, bem como a sua disponibilidade para discutir o trabalho.

Aos autores e co-autores dos trabalhos publicados e em fase de escrita, agradeço o seu contributo, nomeadamente ao Professor Edward Solomon, Esther Johnson, Simone Dell'Acqua, Olga Mestre e Rute Nunes.

Quero também agradecer à Anja Wüst por todo o apoio na execução e desenvolvimento do trabalho no laboratório do Professor Oliver Einsle.

Aos colegas de laboratório que estão e que por ali foram passando, obrigada pela preciosa ajuda, amizade, boa disposição e bom ambiente que me proporcionaram durante estes anos. O vosso apoio e motivação foram essenciais para concluir esta etapa. Não posso ainda deixar de mencionar algumas pessoas que me marcaram neste percurso:

À Susana, à Olga e ao Rui que me apoiaram e proporcionaram imensos risos, obrigada por todos esses momentos! À Luísa e à Célia agradeço por sempre se mostrarem disponíveis para me ajudar e aconselhar.

Rute, aprender e trabalhar contigo foi muito gratificante, mas mais que isso é reconfortante a amizade que permanece. Obrigada por tudo!

À Cláudia agradeço a amizade, discussões científicas e partilha de conhecimento e por toda a calma que sempre me tenta transmitir. Muito tenho a agradecer-te por todo o apoio que me deste. Foi muito bom partilhar este percurso contigo!

Aos amigos mais próximos e família agradeço por me incentivarem e se mostrarem sempre positivos, em especial durante a escrita da dissertação.
Deixo um especial agradecimento à Ana Maria por toda a amizade e paciência, sobretudo nestes últimos meses.

Aos meus pais e à minha irmã agradeço todo o carinho e apoio incondicional que me deram. Obrigada por tudo o que fizeram por mim, pelas oportunidades que me proporcionaram e por acreditarem sempre em mim!

Finalmente, agradeço à Fundação para a Ciência e Tecnologia pelo apoio financeiro através da bolsa de doutoramento atribuída (SFRH/BD/87898/2012).

Abstract

Substantial part of the emissions of nitrous oxide (N_2O), a powerful greenhouse gas, to the atmosphere comes from the incomplete denitrification in bacteria. N_2O can only be detoxified by nitrous oxide reductase (N_2OR), which catalyzes the last step of this pathway. This enzyme contains two distinct centers per monomer: CuA, the electron transfer center and "CuZ", a tetranuclear copper-sulfide center, which can exists in two forms CuZ(4Cu2S) and CuZ*(4Cu1S).

Most of the studies on the denitrification pathway have used soil denitrifying bacteria as models, while marine bacteria are understudied. This thesis presents an analysis of denitrification pathway of *Marinobacter hydrocarbonoclasticus* a marine bacterium capable of respiring nitrate under oxygen-limiting conditions. Here, the effect of pH (6.5, 7.5 and 8.5) on the denitrification pathway of this organism, as well as on the N_2OR isolated from each of those growths, was investigated. These enzymes were characterized through biochemical, spectroscopic and structural studies.

The expression profile of genes encoding the enzymes and accessory proteins involved in denitrification was analyzed, together with quantification of the by-products, nitrate and nitrite. These results showed lower levels of *nirS* expression at pH 6.5, which correlates with the accumulation of nitrite detected. In parallel, whole-cells reduction rates of NO and N_2O demonstrated that denitrification is impaired at more acidic conditions, as the whole-cells are not able to reduce external N_2O when grown at pH 6.5.

The N_2OR isolated from each growth exhibits differences at the "CuZ center". At acidic growth conditions, N_2OR has "CuZ center" mainly as CuZ*(4Cu1S), whereas when isolated from growths at 7.5 and 8.5, it is mainly as CuZ(4Cu2S). This was supported by spectroscopic data, sulfide quantification, and inspection of "CuZ center" X-ray structure, demonstrating the presence of an additional sulfur atom in the CuZ(4Cu2S) form. The effect of exogenous ligands on both forms of the "CuZ center" was re-visited and clarified.

Direct electrochemistry of N_2OR is reported for the first time, with the two signals observed, assigned to CuA and CuZ(4Cu2S) centers, with reduction potentials being in line with the ones determined by potentiometry (272 ± 10 mV and 65 ± 10 mV *vs* SHE at pH 7.6, respectively). This form of N_2OR has lower specific activity (0.004 ± 0.001 U/mg) in the presence of physiological electron donor, cytochrome c_{552}, compared to a N_2OR with CuZ*(4Cu1S) (1.25 ± 0.07 U/mg).

Fully reduced CuZ*(4Cu1S) is catalytically competent and in the presence of a stoichiometric amount of N_2O originates CuZ^o intermediate. CuZ^o species can be reduced through intramolecular electron transference (IET) from CuA center, in a reaction 10^4 faster than IET in the CuZ*(4Cu1S). In the absence of substrate or electrons a novel "CuZ center" intermediate species is formed with a maximum absorption band at 617 nm, and having a [$1Cu^{2+}$-$3Cu^{1+}$] oxidation state. These studies shed new lights on the catalytic cycle, which was reassessed and discussed here.

Keywords: *Marinobacter hydrocarbonoclasticus*, denitrification, nitrous oxide reductase, "CuZ center", catalytic cycle, CuZ^o species.

Resumo

Uma parte substancial das emissões de óxido nitroso (N_2O), um potente gás causador de efeito de estufa advém da incompleta desnitrificação em bactérias. O N_2O só pode ser biologicamente reduzido por acção da reductase do óxido nitroso (N_2OR), que cataliza a última etapa desta via. Esta enzima contém dois centros distintos por monómero: CuA, o centro de transferência de electrões e o "CuZ", um centro tetranuclear de cobre-enxofre, que pode existir em duas formas CuZ(4Cu2S) e CuZ*(4Cu1S).

Na maioria dos estudos existentes referentes à via da desnitrificação, foram utilizadas bactérias desnitrificantes do solo como modelos, enquanto em bactérias marinhas esta via foi parcamente estudada. Nesta tese é apresentada uma análise da via da desnitrificação de *Marinobacter hydrocarbonoclasticus*, uma bactéria marinha capaz de respirar nitrato em condições limitantes de oxigénio. Aqui, o efeito do pH (6.5, 7.5 e 8.5) na via da desnitrificação deste organismo, assim como na enzima isolada a partir de cada um desses crescimentos, foi investigado. Estas enzimas foram caracterizadas por estudos bioquímicos, espectroscópicos e estruturais.

O perfil de expressão dos genes que codificam para as enzimas e proteínas auxiliares envolvidas na desnitrificação foi analisada, em conjunto com a quantificação dos seus subprodutos, nitrato e nitrito. Estes resultados mostraram baixos níveis de expressão de *nirS* a pH 6.5, que está correlacionado com a acumulação de nitrito detectada. Em paralelo, a taxa de redução de NO e N_2O pelas células-inteiras demonstrou que a desnitrificação é comprometida em condições mais acídicas, uma vez que quando crescidas a pH 6.5 as células não são capazes de reduzir o N_2O externo.

O "centro CuZ" da N_2OR isolada de cada crescimento é diferente. Em condições de crescimento acídicas, a N_2OR tem o "centro CuZ" maioritariamente como CuZ*(4Cu1S), enquanto quando isolada a partir de crescimentos a pH 7.5 e 8.5, está maioritariamente como CuZ(4Cu2S). Estes resultados foram sustentados por dados espectroscópicos, quantificações de sulfureto e inspecção do "centro CuZ" por estrutura de raios-X, demonstrando a presença de um átomo de enxofre adicional na forma CuZ(4Cu2S). O efeito de ligandos exógenos a ambas as formas do "centro CuZ" foi revisitado e clarificado.

A electroquímica da N_2OR é reportada pela primeira vez, com os dois sinais observados, atribuídos aos centros CuA e CuZ(4Cu2S), com potenciais de redução em linha com os determinados por potenciometria (272 ± 10 mV e 65 ± 10 mV *vs* SHE a pH 7.6, respectivamente). Esta forma da N_2OR tem baixa actividade específica (0.004 ± 0.001 U/mg) na presença do dador de electrões fisiológico, citocromo c_{552}, em comparação à N_2OR com CuZ*(4Cu1S) (1.25 ± 0.07 U/mg).

A forma do CuZ*(4Cu1S) totalmente reduzida é cataliticamente competente e na presença de uma quantidade estequiométrica de N_2O origina o intermediário CuZ^o. A espécie CuZ^o pode ser reduzida por transferência de electrões intramolecular prevenientes do centro CuA, reduzido por ascorbato de sódio, numa reacção 10^4 vezes mais rápida que a transferência de electrões

intramolecular no CuZ*(4Cu1S). Na ausência de substrato ou electrões uma nova espécie intermediária do "centro CuZ" é formada com uma banda de absorção máxima a 617 nm, no estado redox [$1Cu^{2+}$-$3Cu^{1+}$].

Estes estudos elucidam o ciclo catalítico, que foi discutido e reavaliado.

Palavras-chave: *Marinobacter hydrocarbonoclasticus*, desnitrificação, reductase do óxido nitroso, "centro CuZ", ciclo catalítico, espécie CuZº

Table of contents

Figure Index

Table Index

Scheme Index

List of abbreviations and symbols

μ	specific growth rate
a.a.	amino acids
Abs	absorbance
Anammox	anaerobic ammonium oxidation
ASW	artificial seawater
ATCC	American type cell culture
BSA	bovine serum albumin
BV	benzyl viologen
CAPS	3-(cyclohexylamino)-1-propanesulfonic acid
C*c*O	cytochrome *c* oxidase
cd_1NiR	cytochrome cd_1 nitrite reductase
cDNA	complementary desoxyribonucleic acid
CHAPS	3-[(3-cholamidopropyl)dimethylammonio]-1-propanesulfonate
CHES	2-(cyclohexylamino)ethanesulfonic acid
CNTs	carbon nanotubes
CT	charge transfer
CV	cyclic voltammetry
Cyt	cytochrome
DAD	2,3,5,6-tetramethyl-1,4-benzenediamine
DEAE FF	sepharose CL 6B-2-(diethylamino)ethyl ether fast flow
DFT	density functional theory
DNA	desoxyribonucleic acid
DNase	desoxiribonuclease
DNR	dissimilatory nitrate respiration regulator
DNRA	dissimilatory nitrate reduction to ammonium
DP	differential pulse
DSC	differential scanning calorimetry
DT	sodium dithionite
DTT	DL-dithiothreitol
E°	standard reduction potential
EGTA	ethylene glycol-bis(2-aminoethylether)-N,N,N′,N′-tetraacetic acid
E_{lp}	reduction potential at low pH (fully protonated)
$E_{m,x}$	reduction potential at pH x
E°’	standard formal potential

E_{pa}	anodic peak potential
E_{pc}	cathodic peak potential
EPR	electron paramagnetic resonance
ET	electron transfer
EXAFS	extended X-ray absorption fine structure
ε	extinction coefficient
F_0	observed structure factor
F_c	calculated structure factor
FNR	fumarate-nitrate reduction regulator
GC	glassy carbon
HEPES	2-[4-(2-hydroxyethyl)piperazin-1-yl]ethanesulfonic acid
HH cyt *c*	horse heart cytochrome c
I	current
i_{cat}	catalytic current
ICP	inductive coupled plasma emission
IEF	isoelectric focusing
IET	intramolecular electron transfer
IHF	integration host factor
I_{pa}	anodic peak current
I_{pc}	cathodic peak current
IPG	imobiline dry strip
IT	inter-valence transition
MCD	magnetic circular dichroism
MES	2-(N-Morpholino)ethanesulfonic acid
MS	mass spectrometry
MV	methyl viologen
MWCNTS	multi-walled carbon nanotubes
N_2OR	nitrous oxide reductase
NaR	nitrate reductase
ND	not determined
NDH	NADH dehydrogenase
NiR	nitrite reductase
Nn	not named
NOR	nitric oxide reductase
Ø	diameter
OD	optical density

ox	oxidized
PAGE	polyacrylamide gel electrophoresis
Paz	pseudoazurin
PDB	protein data bank
PGE	pyrolytic graphite electrode
pI	isoelectric point
PWM	position weight matrix
Q	charge
qPCR	quantitative real time - polymerase chain reaction
r.m.s.	root mean square
red	reduced
Ref	reference
RNA	ribonucleic acid
rRNA	ribosomal ribonucleic acid
RT	room temperature
SDH	succinate dehydrogenase
SDS	sodium dodecyl sulfate
SHE	standard hydrogen electrode
TAPS	N-[Tris(hydroxymethyl)methyl]-3-aminopropanesulfonic acid
TCA	trichloroacetic acid
T_m	melting temperature
Tris	tris(hydroxymethyl)aminomethane
UV	ultra-violet
v	scan rate
vs	versus
$\Delta Ep,_{1/2}$	half-height peak
ΔH_{cal}	calorimetric enthalpy
ΔH_{vH}	van't Hoff enthalpy

Microorganisms

A. cycloclastes	*Achromobacter cycloclastes*
A. xylosoxidans	*Alcaligenes xylosoxidans*
B. japonicum	*Bradyrhizobium japonicum*
E. coli	*Escherichia coli*
M. hydrocarbonoclasticus	*Marinobacter hydrocarbonoclasticus*
P. aeruginosa	*Pseudomonas aeruginosa*

P. denitrificans	*Paracoccus denitrificans*
P. pantotrophus	*Paracoccus pantotrophus*
P. putida	*Pseudomonas putida*
P. stutzeri	*Pseudomonas stutzeri*
R. capsulatus	*Rhodobacter capsulatus*
R. eutropha	*Ralstonia eutropha*
R. sphaeroides	*Rhodobacter sphaeroides*
S. denitrificans	*Shewanella denitrificans*
S. meliloti	*Sinorhizobium meliloti*
T. thermophiles	*Thermus thermophiles*
W. succinogenes	*Wolinella succinogenes*

Chapter 1

Introduction

This Chapter was partially published in:

Carreira, C.; Pauleta, S. R.; Moura, I., The catalytic cycle of Nitrous Oxide Reductase – The enzyme that catalyses the last step of denitrification. *J. Inorg. Biochem.* **2017 –** *Accepted*. Doi: 10.1016/j.jinorgbio.2017.09.007

1 Introduction

1.1 Overview of the biogeochemical nitrogen cycle

Nitrogen is essential to all organisms as a component of numerous biomolecules, such as nucleic acids, amino acids, proteins and many additional cofactors [1]. Despite being the most frequent element in atmosphere (~ 78 %), as dinitrogen (N_2), its bioavailability is limited since N_2 is a stable and inert molecule containing a triple bond that requires a catalyst to overcome its large activation energy barrier [2, 3]. In fact, the N-containing compounds can be interconverted by enzymes and nitrogen can exist in nature in different oxidation states, ranging from + 5 to - 3. These reactions are mostly mediated by prokaryotes in six biological processes that constitute the biogeochemical N-cycle (Figure 1.1): nitrogen fixation, nitrification, denitrification, assimilatory nitrate reduction to ammonium (also known as assimilatory ammonification), dissimilatory nitrate reduction to ammonium (DNRA) and anaerobic ammonium oxidation (Anammox).

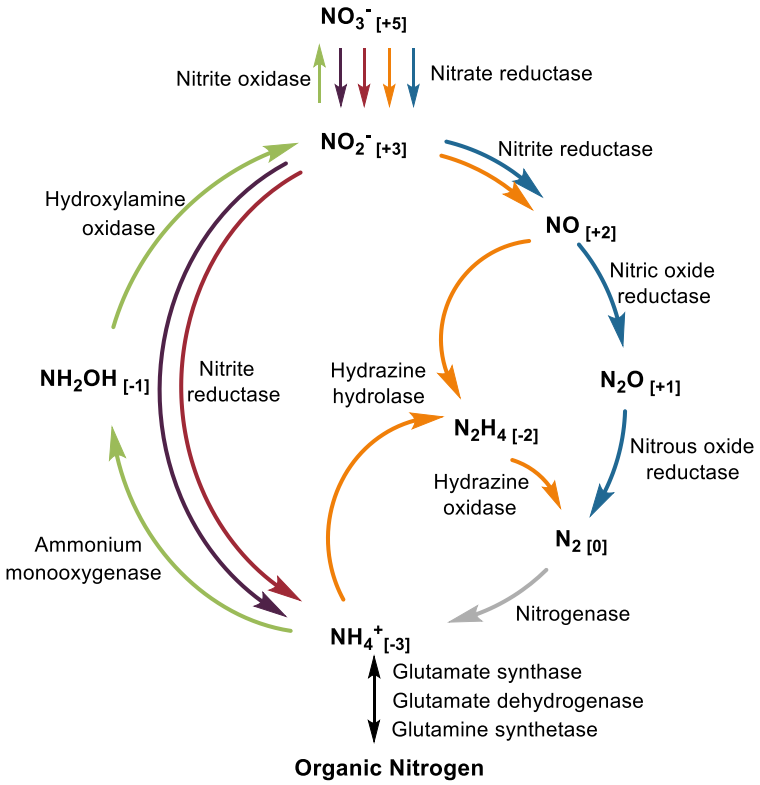

Figure 1.1 - The biogeochemical nitrogen cycle. Each pathway is identified in a different color by arrows as follow: denitrification (blue), nitrogen fixation (grey), nitrification (green), assimilatory (violet) and dissimilatory (red) nitrate reduction to ammonium and anaerobic ammonium oxidation (orange). The black arrow represents the incorporation of ammonium into organic N-compounds. The enzymes involved in each step of the cycle are identified. The oxidation state of nitrogen atoms is indicated in brackets.

The biological nitrogen fixation into ammonium is an anaerobic process catalyzed by nitrogenase, carried out by free-living or symbiotic bacteria and archaea [3, 4] (Figure 1.1-grey arrow). Though, most organisms cannot fixate N_2, the nitrogen element is incorporated into biomolecules through

ammonium or indirectly through assimilatory ammonification, which occurs in prokaryotes and also in plants [5]. While ammonium can be incorporated into glutamine or glutamate, which are used as N-donors for the synthesis of other amino acids and heterocyclic N-compounds [4-6], the assimilatory ammonification involves nitrate reduction via nitrite to ammonium in two consecutive reactions, catalyzed by assimilatory nitrate reductase and siroheme-dependent nitrite reductase, respectively, which accepts electrons from NAD(P)H [7, 8] (Figure 1.1- violet arrows).

On the other hand, ammonium can be oxidized into nitrate by autotrophic and heterotrophic microorganisms in an aerobic biological process called nitrification [5, 9] (Figure 1.1- green arrows). In this pathway, the ammonium is first oxidized to hydroxylamine, in a reaction catalyzed by ammonium monooxygenase, and then oxidized *via* nitrite to nitrate, in a two reactions process involving the enzymes hydroxylamine oxidase and nitrite oxidase, respectively. Both nitrite and nitrate generated can be reduced through two biological processes that are energy conserving, denitrification or DNRA, that occur in oxygen depleted environments or under low oxygen tensions. In the denitrification pathway, nitrate is reduced to dinitrogen in a four sequential enzymatic step process (Figure 1.1- blue arrows) (Section 1.2), while in the DNRA pathway the nitrite is directly reduced to ammonium in a reaction catalyzed by a multi-*c*-type heme containing nitrite reductase, that accepts electrons from the quinone pool [10] (Figure 1.1- red arrows).

The pathway most recently considered as part of the N-cycle is called Anammox, whereas several microorganisms, known as planctomycetes, have the ability to oxidize ammonium coupled with nitrite reduction to generate nitrogen [11, 12] (Figure 1.1- orange arrows). In this reaction ammonium is oxidized by nitric oxide (NO) to hydrazine, in a reaction catalyzed by hydrazine hydrolase, which is subsequently oxidized to dinitrogen through hydrazine oxidase [13].

Over the last century, an unbalance of N-cycle has been detected by the increasing emissions of its by-products to the atmosphere, particularly nitric oxide and nitrous oxide (N_2O), whose emissions cause severe environmental impacts.

Anthropogenic emissions of nitrous oxide to the atmosphere are one of the main environmental concerns of the 21st century [14, 15]. Direct emissions from the soils and human activities, such as burning of biomass, human sewage, wastewater treatment and fossil fuel combustion and industrial processes have been contributing to this increase [3, 16].

N_2O is a potent greenhouse gas that has a global warming impact 300-fold higher than CO_2 and a long half-life in atmosphere, estimated to be 120 years [14, 17]. Its removal from the stratosphere occurs through photodissociation, generating nitrogen oxides (NOx) compounds capable of reacting with ozone, causing its depletion [14, 15]. The exponential increase of N_2O in the atmosphere and its implication on the climate change (together with CO_2 and CH_4) have led to the development of potential strategies to mitigate emissions, especially those produced by prokaryotes in soils, thereby stabilizing the N_2O concentration in the atmosphere [3, 17-19]. As a matter of fact, about 60 % of N_2O emissions arise from soils through the nitrification and denitrification processes, partially

due to the increasing use of fertilizers, while its biological reduction is performed by nitrous oxide reductase (N_2OR), the last enzyme of the denitrification pathway [3, 14, 20] (Figure 1.1). This pathway is stimulated under abundant nitrogen input and oxygen limiting tensions [21].

1.2 Denitrification pathway

When complete, the bacterial denitrification is a four enzymatic step pathway consisting on the dissimilatory reduction of inorganic nitrate via nitrite to nitric oxide and nitrous oxide gases and then to the stable dinitrogen gas [21]. Each reaction is catalyzed by a different metalloenzyme, nitrate reductase (NaR), nitrite reductase (NiR), nitric oxide reductase (NOR) and N_2OR, respectively (Figure 1.2, Table 1.1). In fact, for each reaction more than one type of metalloenzyme can co-exist in a microorganism, as suggested by the genome analysis of some microorganisms [22], or as the case of *Paracoccus pantotrophus* in which both periplasmic and respiratory nitrate reductases were proved to co-exist [23]. The denitrification enzymes, containing molybdenum, heme and non-heme iron or copper in their active site, are involved in a conservative energy process with reduction of metabolites linked with the generation of a proton electrochemical gradient across the inner membrane, coupled with ATP synthesis [18, 21].

Table 1.1 - Metalloenzymes involved in the denitrification pathway and the genes encoding for its catalytic subunits [24].

Reaction	Enzyme	Genes	Ref.
$NO_3^- + 2e^- + 2H^+ \rightarrow NO_2^- + H_2O$	Respiratory nitrate reductase (NaR)	*narG*	25
	Periplasmic nitrate reductase (NaP)	*napA*	26
$NO_2^- + e^- + 2H^+ \rightarrow NO + H_2O$	Nitrite reductase cytochrome cd_1 (cd_1NiR)	*nirS*	27
	Copper nitrite reductase (CuNiR)	*nirK*	28
	Three domain T1Cu_CuNiR [a]	*Cu_nirK*	29
	Three domain cyt*c*_CuNiR [b]	*Cyt_nirK*	30
$2NO + 2e^- + 2H^+ \rightarrow N_2O + H_2O$	Cytochrome *c* nitric oxide reductase (*c*-NOR)	*c-norB*	31
	Quinol nitric oxide reductase (*q*-NOR)	*q-norB* [c]	32, 33
	CuA nitric oxide reductase (Cu_ANOR)	*N.n.*	34
$N_2O + 2e^- + 2H^+ \rightarrow N_2 + H_2O$	Nitrous oxide reductase (N_2OR)	*nosZ*	35
	Cytochrome *c* nitrous oxide reductase (*c*N_2OR) – atypical N_2OR	*cnosZ*	36

Notes: [a] This is a hexameric nitrite reductase isolated from *Hyphomicrobium denitrificans* that contains an additional N-terminal cupredoxin domain. [b] The gene coding for this enzyme has been identified at the genome level and it is proposed to present an additional C-terminal class I *c*-type cytochrome domain. [c] Also known as *norZ*. N.n. -Not named.

Nitrate reduction is catalyzed by molybdenum-dependent enzymes, respiratory nitrate reductase (NaR), which is a membrane-bound complex composed by three subunits NarG, NarH and NarI, or periplasmic nitrate reductase (NaP). Typical *narGHJI* operon encodes NaR proteins, being NarJ required for the assembly of molybdenum and iron-sulfur cofactors into NarGH, located in the cytoplasm, but anchored to NarI, and also for NarI insertion into the inner membrane [37, 38] (Figure

1.2). Moreover, NarGHI is a heterotrimeric enzyme containing 8 redox centers that accept electrons from menaquinol or ubiquinol (a reaction coupled with proton translocation to the periplasm) via the 2 *b*-type hemes of NarI subunit. An electron transfer relay from NarI hemes cofactors to the active site of NarG subunit is made through five iron-sulfur centers, involving [3Fe-4S] and 3 [4Fe-4S] centers of NarH and the [4Fe-4S] center of NarG. Then, the electrons are transferred to the molybdopterin-guanine-dinucleotide active site, where nitrate reduction occurs [37, 39].

In turn, *nap* operons show higher variability between them, but usually comprise the *napEDABC* genes, with *napA* encoding the catalytic subunit containing a molybdopterin active site and an iron-sulfur center [40]. NaP enzymes have been isolated as monomeric or as heterodimeric enzymes [40, 41]. In the heterodimeric NaP enzymes, the electron transfer to the NapA is through a second subunit, NapB, containing a [4Fe-4S] center [37].

The periplasmic respiratory nitrite reductase have been isolated with two distinct metals in its active site, with copper centers identified in CuNiR and heme cofactors are characteristic of cd_1NiR [42]. Both types of NiR are located in the periplasm and contain a redox electron transfer center, that are able to accept electrons from small electron shuttle proteins, and a catalytic center [42]. CuNiR is a homotrimeric enzyme containing a Type 1 Cu center in each monomer, as the electron transfer center, and a Type 2 Cu center located at the monomers interface, which is the catalytic center [29]. CuNiR is encoded by *nirK* and does not require obligatory ancillary genes, although in some organisms it is proceed by *nirV* [43], that may have a role in copper insertion. Recently, two new classes of CuNiR, containing a third domain, emerged: T1Cu_CuNiR and cyt*c*_CuNiR. The T1Cu_CuNiR comprises an additional N-terminal domain with Type 1 Cu center, which was first observed in the structure of CuNiR isolated from *Hyphomicrobium denitrificans* [29]. The three domain cyt*c*_CuNiR was first isolated from *Ralstonia Pickettii*, in which was identified two copper centers (a Type 1 and a Type 2 Cu center) and also an attached *c*-type heme domain at the C-terminal [44].

cd_1NiR, encoded by *nirS* gene, is a homodimeric enzyme comprising one *c*-type and one d_1-type hemes, the electron transfer and the catalytic centers, respectively [42, 45] (Figure 1.2). cd_1NiR operon is quite different from CuNiR, as *nirFDLGHJE* genes are required for the biosynthesis and insertion of d_1-type heme of cd_1NiR [46].

Three types of heterodimer membrane-bound NOR were identified, *c*-NOR, *q*-NOR and Cu_ANOR, being distinguished by their architecture and electron donor, in which *c*-type cytochrome, quinone pool and membrane-bound *c*-type cytochrome are the respective donors [47]. The *c*-NOR, encoded by the *norCBQD* operon, has two subunits, one anchored to the membrane, NorC, and another embedded in the inner membrane, NorB. Electrons from small electron carriers are transferred to the *c*-type heme and then transferred via the low–spin *b*-type heme to the binuclear catalytic center, containing another *b*-type heme and a non-heme iron [48] (Figure 1.2). On the other hand, *q*-NOR, encoded by *q-norB* gene, is a single subunit containing two *b*-type hemes and a non-heme iron,

similar to the NorB subunit found in *c*-NOR, but with an extended N-terminal domain possibly involved in quinol oxidation [33]. The Cu_ANOR contains, beside the centers typically found in the others NORs, a binuclear CuA center. This type of NOR, isolated from *Bacillus azotoformans*, previously reported to be qCu_A-NOR [49], was recently shown to lack menaquinol activity, being in fact able to accept electrons from the endogenous cytochrome c_{551} through its CuA center [34, 50].

The enzyme N_2OR catalyzes the last step of denitrification pathway and so far, two types were isolated, N_2OR and *c*N_2OR, which contains an additional *c*-type heme domain. N_2OR is a multicopper enzyme containing two copper centers: CuA center and "CuZ center". This protein is the major subject of this thesis and the known N_2OR properties will be discuss in the next Sections.

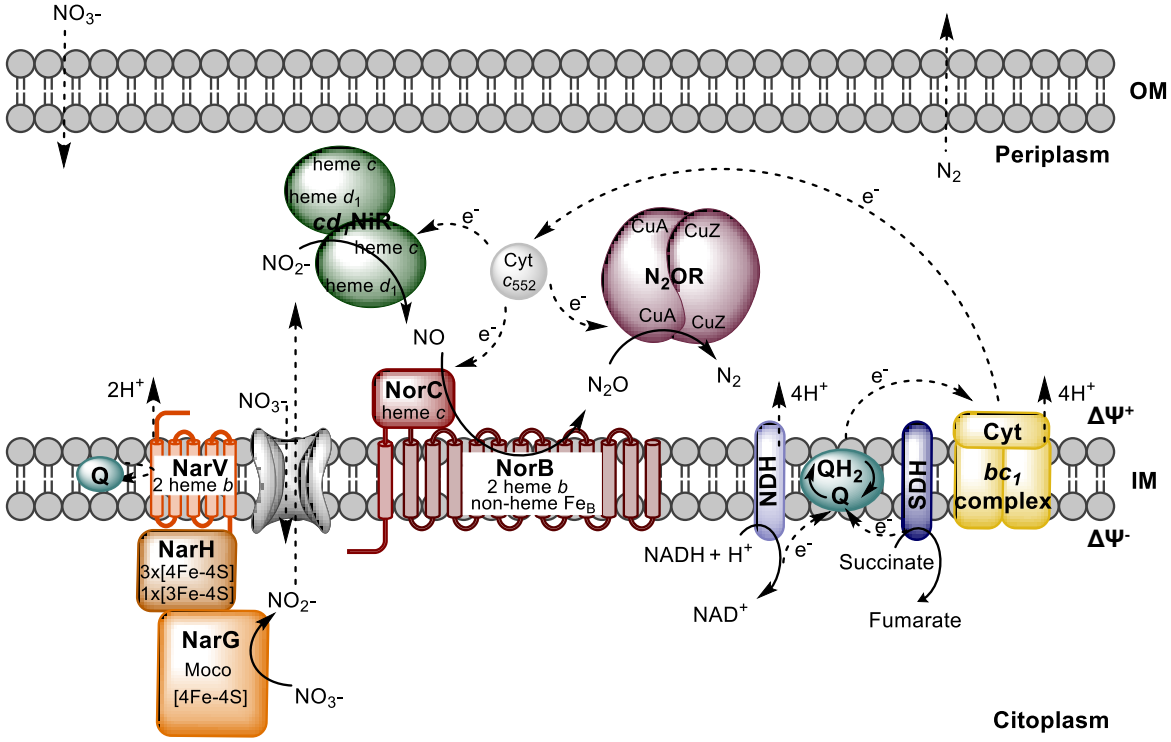

Figure 1.2 - Schematic representation of denitrification enzymes in *Marinobacter hydrocarbonoclasticus*. The membrane-bound nitrate reductase (NarGHI) and nitric oxide reductase (NorBC), as well as the periplasmic cytochrome cd_1 nitrite reductase (cd_1NiR) and the nitrous oxide reductase (N_2OR) are shown. The reactions trigger a proton gradient across the membrane, creating a positive potential outside of the inner membrane. The electrons for each reaction come from the quinone pool, which are replenished with inorganic electron donors or organic carbon. NDH and SDH are the NADH dehydrogenase and succinate dehydrogenase, respectively. Cyt is the abbreviation used for cytochrome and Moco for the molybdenum cofactor. IM and OM are the inner and outer membranes, respectively. Nitrate and nitrite type of transportation across the membrane is envisaged to be performed through NarK homologues.

Although the denitrification pathway has been identified in bacteria and most of the studies were performed in Gram-negative denitrifiers isolated from soils, there are evidences that some fungi [51, 52] and archaea may also denitrify, though not completely [20]. The denitrification by these organisms will be worth to investigate, as well as denitrification by bacteria from other niches as aquatic

systems. Part of this thesis focuses on the denitrification pathway of *M. hydrocarbonoclasticus*, a marine bacteria, used here as a denitrifying model organism of aquatic systems (Figure 1.2).

M. hydrocarbonoclasticus 617, formerly classified as *Pseudomonas nautica* 617 [53, 54], is a Gram-negative bacteria of *γ*-subdivision, isolated from the Mediterranean seawater [55]. This moderately halophilic bacterium requires sodium to grow, uses a wide range of carbon sources and is not only able to respire oxygen, but also nitrate, citrate, succinate or acetate, under microaerobic or anaerobic conditions from pH 6 to 9.5.

A schematic representation of the enzymes, as well as the physiological electron donors involved in the denitrification pathway of this species is presented in Figure 1.2. In this microorganism, the nitrate reduction occurs in the cytoplasm by NaR, being the nitrite directed to the periplasm possibly through NarK homologue transporters. Catalysis of nitrite to nitric oxide, followed by nitrous oxide and then by dinitrogen is ensured in this organism by cd_1NiR, *c*-NOR and N_2OR, respectively, which receive electrons from cytochrome c_{552} to perform the catalysis.

1.2.1 Regulation of denitrification pathway

The incomplete denitrification or the slower rate of denitrification, has been observed in some denitrifiers that lack the *nos* genes involved in the biosynthesis of N_2OR, or encode an inactive form of N_2OR, and in the presence of nitrate or nitrite release N_2O to the atmosphere. Indeed, being N_2OR a copper-dependent enzyme, a significant accumulation of N_2O gas is observed when the copper availability is limited [56, 57], and also under certain environmental conditions as low pH [58, 59].

This incomplete denitrification pathway is still used for energy conservation, as N_2O has not been shown to cause inhibition of any of the enzymes of this pathway and is not involved in its regulation, contrary to nitric oxide, a potent cytotoxic and major regulatory molecule of this pathway, as will be described [47, 60, 61]. Besides NO, other molecules are listed as signal regulators of denitrification, such as oxygen, nitrate, nitrite and cell redox changes [47, 60]. The current knowledge on the regulation of denitrification is based on model organisms which can be found on soils, such as *Pseudomonas stutzeri*, *Pseudomonas aeruginosa* and *Paracoccus denitrificans* but the regulation of this pathway in other microorganisms as *Bradyrhizobium japonicum* associated to plants, have also been extensively explored and thus an overview of these mechanisms will be discussed below (Figure 1.3) (reviewed in [47, 60, 62]).

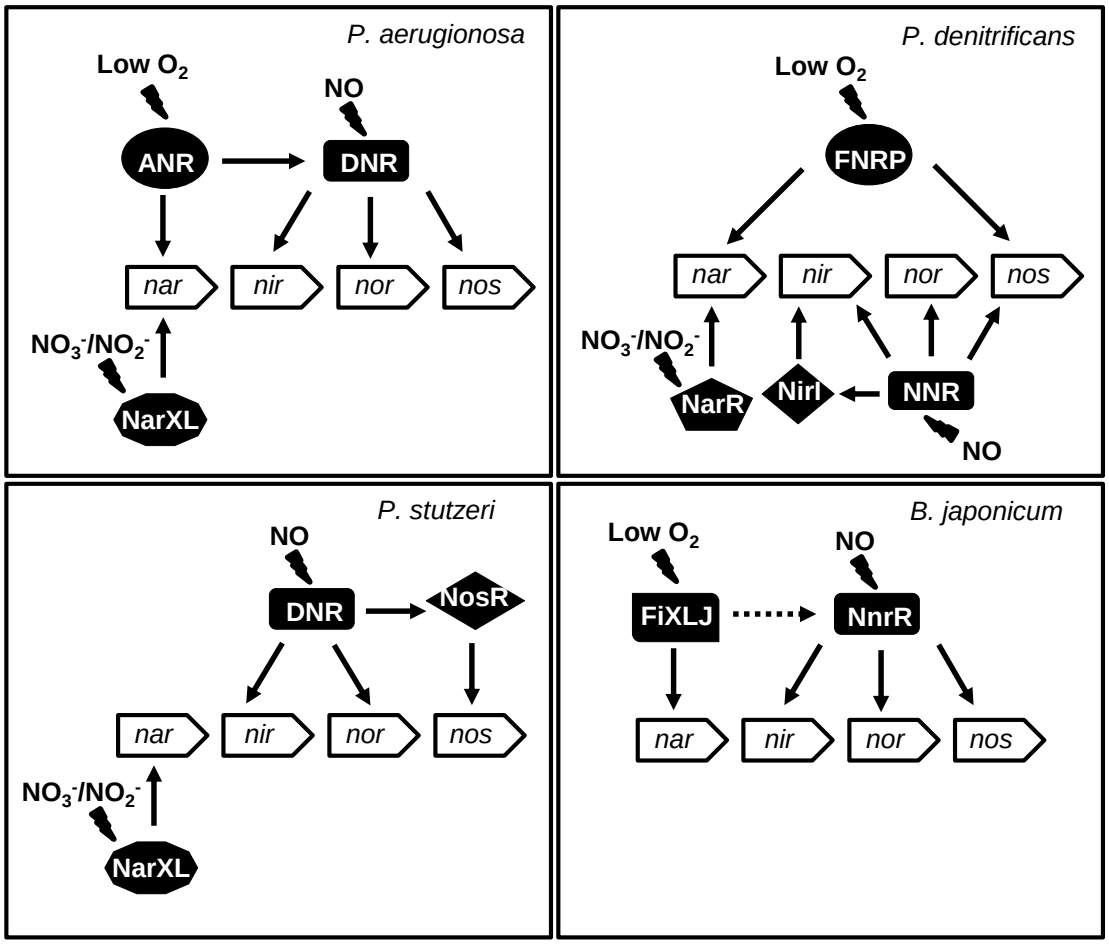

Figure 1.3 - Gene regulation of the denitrification pathway in response to nitrate/nitrite, low O_2 and nitric oxide. The regulatory network is based on the current knowledge of regulation of denitrification from *P. aeruginosa*, *P. denitrificans*, *P. stutzeri* and *B. japonicum*. Positive regulation is indicated by solid arrows and indirect regulation is indicated by dashed arrows. Adapted from [47].

Under oxygen-limiting conditions, many bacteria have the ability to switch respiration and use another available electron acceptor. In many of these organisms the switching to anaerobic metabolism is under the control of fumarate-nitrate reduction regulator (FNR), a protein containing an iron-sulfur oxygen sensitive cluster, which is the signal sensing domain, an RNA polymerase contact site, an α-helical domain postulated to be involved in dimerization and a DNA binding domain that recognizes $TTGATN_4ATCAA$ motifs (called FNR binding box) [63, 64]. In its activate form, FNR (or its orthologous, ANR in *P. aeruginosa* or FnrP in *P. denitrificans*), is a dimeric protein containing a $[4Fe\text{-}4S]^{2+}$ cluster per protomer able to recognize the specific DNA regions, of the FNR-regulated promoters. FNR becomes inactivate by oxygen exposure in which the $[4Fe\text{-}4S]^{2+}$ cluster is rapidly and reversibly converted *via* $[3Fe\text{-}4S]^{1+}$ to $[2Fe\text{-}2S]^{2+}$, leading to dissociation of the dimer into monomeric units [65, 66]. Prolonged exposure to oxygen lead to the inactive apo-FNR form that can be reactivated by incorporation of $[4Fe\text{-}4S]^{2+}$ cluster under proper oxygen conditions [65, 66]. Furthermore, FNR also responds to NO, as it exposure up to a certain NO

threshold leads to the nitrosylation of [4Fe-4S] cluster and consequently down-regulation of genes whose promoters are under the activation of FNR [67, 68].

In others microorganisms, as *B. japonicum* and *Sinorhizobium meliloti*, a different type of oxygen sensor, named FixL, is involved in the regulation of denitrification (Figure 1.3). FixL is a sensor kinase containing three domains, an ATPase, a kinase and a PAS domain, being PAS the oxygen sensing domain through a heme bound group [62]. In response to anoxic conditions FixL phosphorylates FixJ, which is able to activate FixK protein that in turn, activates the denitrification genes and other genes involved in the response to low O_2 [47, 62]. Therefore, under low oxygen tensions, FNR or FixLJ proteins can activate the expression of *nar* and *nap* operons.

Besides the low oxygen tension required for *nar* cluster expression, these genes in some organisms are induced by nitrate or nitrite, through the regulatory systems NarXL or NarR. The two component systems NarXL (or their orthologous NarQP) have been identified in γ- and β-proteobacteria, as activators of the *nar* and *nap* operons [69, 70]. NarX is a histidine sensor kinase that in contact with nitrate or nitrite phosphorylates NarL, which in turn activates the *nar* transcription by recognition of a motif in its promoter. NarR, a FNR/CRP family member identified in α-proteobacteria, controls the expression of NaR and the nitrate transport system (NarK) in the case of *P. pantotrophus*, however its mechanism of action is still speculative [71, 72].

Several transcriptional regulators respond to NO, such as nitrite and nitric oxide reductase regulator (NnrR or NNR), dissimilatory nitrate respiration regulator (DNR), NorR and NsrR. NNR and DNR are also CRP/FNR family members but lack the N-terminal cysteines required for [4Fe-4S] center formation and therefore a different sensing mechanism has been evidenced [73-75]. Indeed, these are heme-dependent proteins that in response to NO are postulated to trigger a response through the heme, activating the transcription of *nir* and *nor* operons, although the mechanism is still not completely clear [73-75].

NorR also responds to NO, being first evidenced in *Rasltonia eutropha* as capable of activating the *norB* gene through a σ factor dependent *norAB* promotor [76]. On the other hand, NsrR is a repressive regulator of the *nir* and *nor* operons that is inactivated in the presence of NO [47, 77].

The multidomain proteins NirI (under the control of NNR in *P. denitrificans*) and NosR, both containing a flavin domain and motifs for the binding of two [4Fe-4S] centers, are also regulators of the denitrification, since they are required for the transcription of *nirS* and *nosZ* genes, respectively [78, 79]. However, the signal that triggers its response is unknown.

The genes of denitrification are also under the control of redox sensors that respond to the alteration of the redox state of the cell [60, 62], however the mechanisms involved are still poorly understood and will not be discuss in here.

1.3 Biogenesis of nitrous oxide reductase

1.3.1 The *nos* operon

N_2OR is encoded by *nosZ*, that is usually included in the *nos* gene cluster, that comprises several other genes encoding proteins required for expression and maturation of N_2OR, and are also proposed to sustain a catalytic competent state of N_2OR *in vivo* [79-82]. These genes, highly conserved in the majority of the denitrifying bacteria, are arranged usually as *nosRZDFYL* in three transcriptional units, as the case of *P. stutzeri*, *P. denitrificans* and *S. meliloti* [80, 83, 84] or as a single transcriptional unit, as proposed to be the case in *P. aeruginosa* [61].

In some proteobacteria, the cluster *nosRZDFYL* can be preceded or followed by *nosX* gene, although the mechanisms involved in the cluster regulation are complex and variable between species (Figure 1.4) [20, 21, 47, 60].

In *P. denitrificans*, a paralogue gene of *nosX* termed *nirX*, was identified in a distinct gene cluster and mutational studies of those genes showed that *nosZ* transcription is unaffected in a double *nosXnirX* mutant, however only this double mutant is defective in N_2O reduction [81, 85], as NosX is essential for the flavin cofactor assembly in NosR, which in turn is necessary for an active N_2OR [82, 86].

This *nos* cluster organization is typical in bacteria that expresses a Z-type N_2OR (now called clade I N_2OR) that was first isolated from *Alcaligenes faecalis* in 1972 [87]. However, the requirement of copper in the N_2O respiration was only identified 8 years later, in *A. faecalis* cultures [88]. Since then, clade I N_2OR has been isolated and characterized from different α-, β- and γ-proteobacteria as periplasmic proteins (Figure 1.4) [89-97].

The ε-proteobacteria *Wolinella succinogenes* was reported to express an "atypical" N_2OR (classified now as a clade II N_2OR), containing an additional *c*-type heme domain at the C-terminal that has been proposed to function as an electron donor [36, 98]. The primary sequences of clade II N_2ORs share low identity (< 50 %) with those of clade I N_2ORs [99, 100].

Although, to date there has not been any report of the isolation of a N_2OR from Gram-positive bacteria, this enzyme is likely to be membrane-associated (in accordance with the bioinformatics analysis of its primary sequence) [22], being its atypical *nos* gene cluster commonly arranged as *nosCZ*-ORF-*nosDYF*-ORF (Figure 1.4) [22, 60, 101]. In fact, clade II *nos* clusters consistently exhibit a gene upstream *nosZ*, which encodes a transmembrane protein, and are frequently associated with *c*- and *b*-type cytochromes, as well as iron-sulfur proteins [100]. The different cluster arrangement, as well as the lacking of *nosR* and *nosX* genes in clade II [100], reported as essential to maintain the activity of clade I N_2ORs [79, 81, 85], pin pointed to the hypothesis of an alternative electron transfer route *via* menaquinol in these enzymes [36]. Most of the current knowledge on the clade II N_2OR is based on genome analysis and therefore this overview will focus mainly on clade I N_2ORs, which is also the main subject of this thesis.

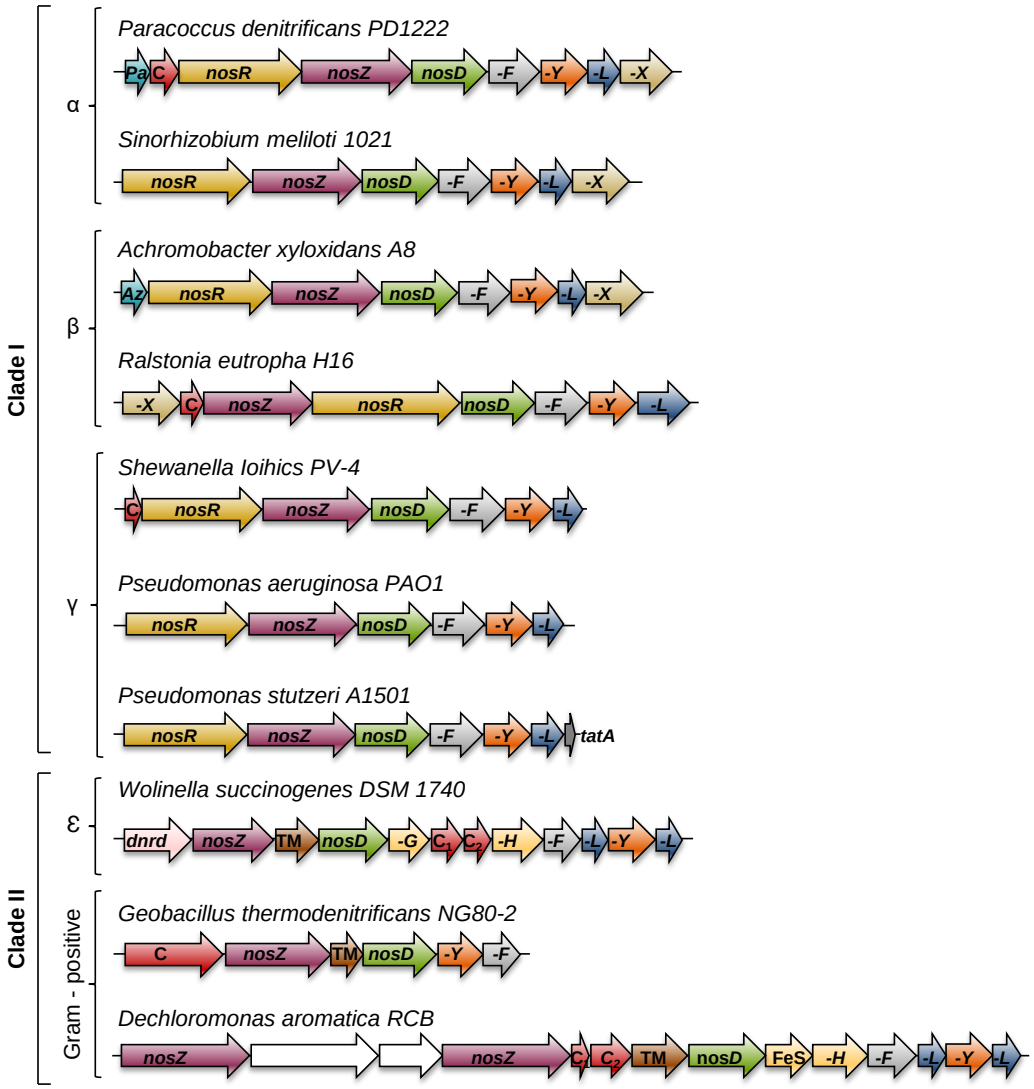

Figure 1.4 - Organization of *nos* gene clusters of selected genomes of Gram-negative (*α*-,*β*-,*γ*- and *ε*-subdivision) and Gram-positive bacteria representing the two clades. *PA* – gene encoding a pseudoazurin, *Az* - gene encoding an azurin, TM - transmembrane protein, C - protein containing either a *c*-type heme motif (CXXCH) or a CXXC motif, FeS-protein contain a Fe-S motif, *dnr* - dissimilative nitrate respiration regulator, *tat* - twin-arginine translocation. Undesignated genes are represented in white.

1.3.2 Protein export and maturation

Bacterial Tat (Twin arginine translocation) and Sec (the general Secretion) systems are responsible for exporting Nos proteins to the membrane or to the periplasm. NosR, NosD, and NosL are probably translocated by the Sec system, as they contain a signal peptide for this system [20, 79, 80]. In contrast, both, NosX and NosZ have a N-terminal signal peptide with a consensus motif, containing two consecutive arginine residues -(S/T)RRxFLK-, that is recognized by the Tat machinery, which comprises the proteins TatA, TatB, TatC and TatE, being TatA and TatE homologous proteins [102, 103]. In fact, the Zumft group reported that in the *P. stutzeri tatC* mutant, N_2OR is unable to be exported to the periplasm leading to the isolation of an apo-form of the enzyme [104]. Unlike most metal-sulfur proteins, whose centers are assembled in the cytoplasm prior to export, N_2OR is

exported to the periplasm as a folded apo-protein, where the assembly process of CuA and "CuZ" centers, takes place [80, 102]. Clade I NosZ proteins are exported by the TAT machinery, while clade II are exported by the Sec system, as a sec-signal peptide is often found in their primary sequence [60, 100]. Another difference between the two clades lies on the "CuZ center" binding motifs, as DXHHXH, EPHD motifs are conserved in clade I, but in clade II only DXHH, EPH motifs are conserved [60, 100] (Figure 1.5).

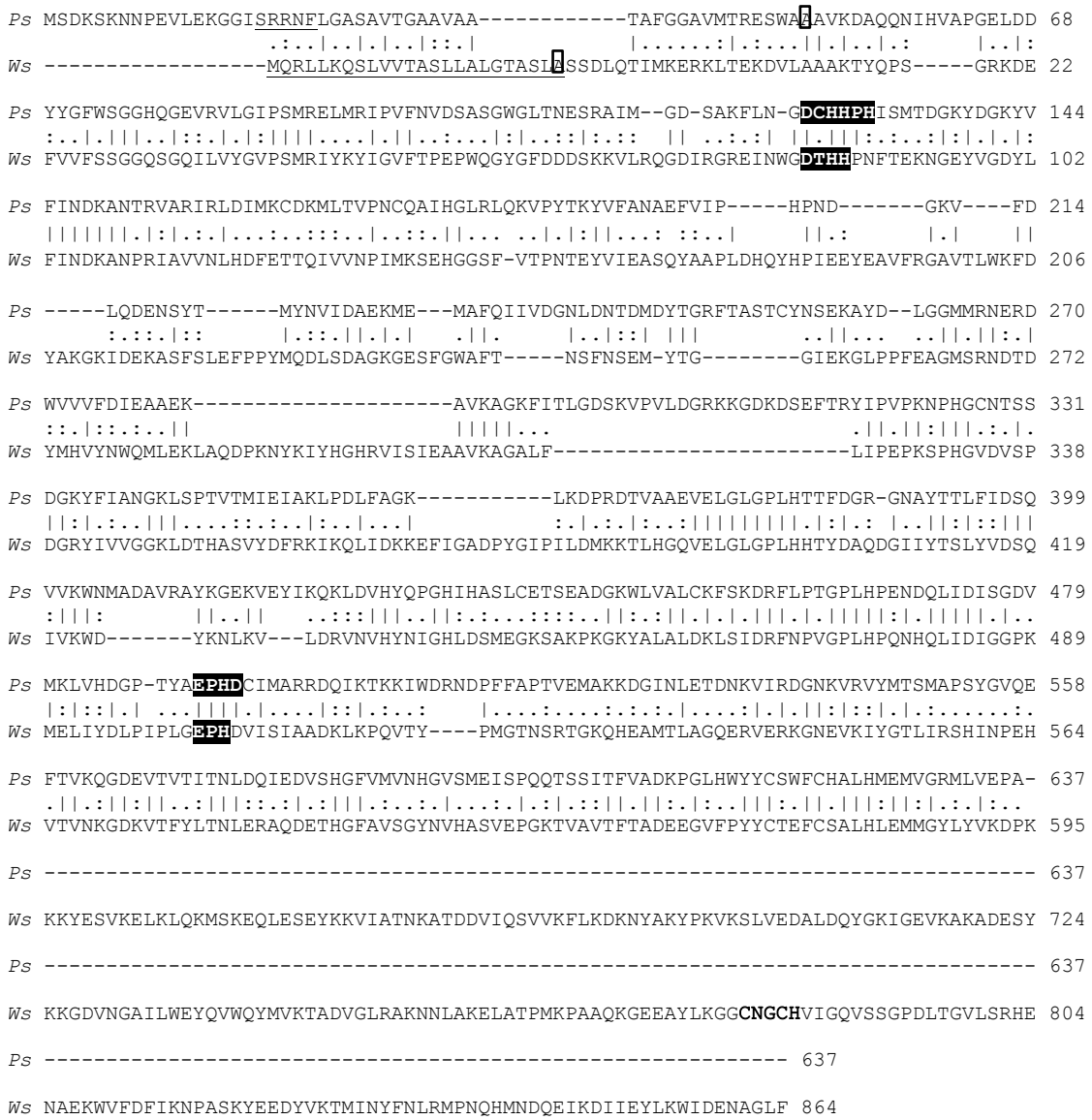

Figure 1.5 - Comparison of primary sequence alignment of N_2ORs from clade I and clade II. Clade I N_2OR is from γ-proteobacteria *Pseudomonas stutzeri* A1501 (*Ps*) and clade II N_2OR is from ε-proteobacteria *Wolinella succinogenes* (*Ws*). TAT- and Sec-motifs are underlined and the start of mature protein is identified with a square. Clade I and clade II CuZ binding motifs are highlighted on black filled rectangles. The *c*-type heme binding motif is highlighted in bold. Vertical lines, colons or stops below the sequence indicate matches, high conservation or conservation of the residues, respectively.

The uptake of copper into the periplasm is not well known, but most probably occurs through porins like NosA in *P. stutzeri*, or copper chelators [105] (Figure 1.6). Evidences of post-translational assembly of CuA center in folded N_2OR also arise from the metallation of a common center in cytochrome *c* oxidase (C*c*O), probably using a similar mechanism, whereas chaperone COX 17 directly transfers copper to the Sco1, that can binds Cu^{1+} through two cysteine (-CXXXCP- motif) and one histidine conserved residues, and is implicated in the copper insertion in C*c*O [106-108]. Homologous of Sco1 are usually present in bacteria harbouring the *nosZ* gene, as the cases of ScoP protein from *P. stutzeri* or the *senC2* in *P. denitrificans*, and thus this protein is a possible candidate for CuA insertion into N_2OR, but also proven nonessential for the CuZ assembly [82]. Furthermore, Cu assembly is most likely also related to NosL, a 20 kDa periplasmic lipoprotein anchored to the outer membrane that is capable of binding Cu^{1+} and has been postulated to have a role as metallochaperone for the Cu incorporation into N_2OR [109, 110]. Although *nosL* is conserved in the majority of clade I and clade II *nos* cluster (Figure 1.4), it is unnecessary for the biogenesis of a functional N_2OR [82]. Therefore, the existence of other mechanism independent of NosL and ScoP cannot be ruled out. In addition, a periplasmic CuA chaperone, PCu_AC, which contains a binding motif ($H(M)X_{10}MX_{21}HXM$) for Cu^{1+} insertion, was recently pointed out to be essential for the insertion and maintenance of the copper centers in *P. denitrificans* N_2OR [111].

An N_2OR containing only the CuA center was isolated from heterologous expression of *nosRZ* genes, evidencing that contrary to "CuZ center", CuA insertion is not dependent of the *nosDFY* coexpression [82]. In fact, previous studies reported that mutants of *nosDFY* genes from *P. stutzeri* express a N_2OR lacking "CuZ center", which is a Cu-S center and therefore the NosDFY has been postulated to have a role in the S supply [112] (Figure 1.6). NosD, NosF and NosY form a putative ABC-type transporter, being NosD a 45 kDa periplasmic protein member of the carbohydrates-binding proteins and sugar hydrolase family, NosF is a cytoplasmic 34 kDa protein structurally similar to an ATPase of the ABC transporters shown to have ATPase activity and NosY is a 26 kDa 5-spanning membrane protein with a putative export role [20, 83, 112].

Another highly conserved gene in the *nos* operon is NosR, an iron-sulfur transmembrane flavoprotein of 78 kDa, with a flavin cofactor covalently bound to the periplasmic domain, while the cytoplasmic domain carries motifs for the binding of two [4Fe-4S] centers [79, 113]. This protein has been shown to be essential for the *nosZ* transcription in *P. stutzeri*, though the mechanism is not explained [113]. Moreover, deletion of NosR domains and/or conserved motifs showed to affect the capacity of the whole-cells to reduce N_2O despite the complete assembly of the N_2OR centers, indicating that NosR does not affect the copper assembly process of the N_2OR but is crucial for its *in vivo* activity [79].

Furthermore, the recently characterized ApbE (NosX ortholog) from *P. stutzeri*, a 37 kDa protein containing a flavin adenine dinucleotide (FAD) cofactor, has been postulated to be involved in the flavinylation of the flavin mononucleotide (FMN) binding domain of NosR (Figure 1.6) [86].

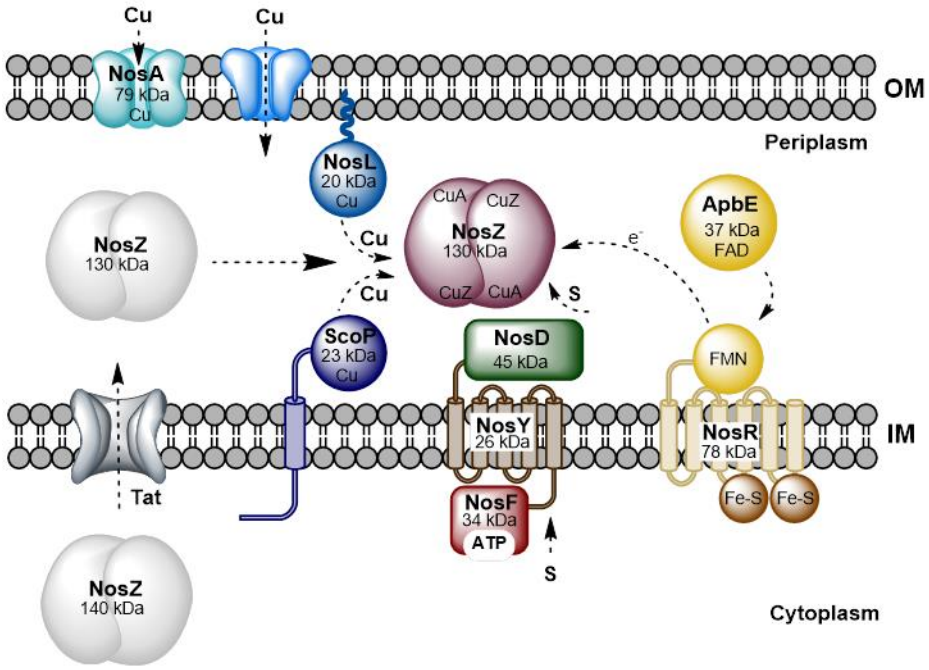

Figure 1.6 - Model of N_2OR biogenesis in *P. stutzeri*. Apo-NosZ as a dimer is exported to the periplasm by Tat translocon. The copper may enter to the periplasm by a transporter not encoded by the *nos* operon and also possibly through NosA. ScoP and NosL are putatively involved in the copper assembly. Sulfur is putatively provided by NosDFY. NosX is involved in the biosynthesis of NosR flavin center. NosR is essential to N_2OR activity and may provide electrons. Each protein is labeled with its name, molecular mass and cluster. IM and OM are the inner and outer membranes respectively. Adapted from [20].

1.4 Nitrous oxide reductase

Although the reaction of N_2O reduction is highly exergonic ($N_2O + 2e^- + 2H^+ \rightarrow N_2 + H_2O$; $\Delta G°' = -339.5$ kJ mol^{-1}) [20, 24], a catalyst is required to overcome the activation barrier of + 250 kJ mol^{-1} (in the gas phase) [114]. N_2OR is capable of reducing nitrous oxide to dinitrogen and water in a two-electron two-proton process, completing the denitrification process [20].

N_2OR is a stable homodimer with a molecular weight of 120 to 160 kDa [21], containing ~ 6 copper atoms per monomer arranged in two distinct copper centers, a binuclear CuA center, responsible for electron transfer and a sulfide-bridged tetranuclear copper center, termed "CuZ center", where the catalysis occurs (Figure 1.7).

CuA center has the ability to accept electrons from small electron shuttle proteins, usually small soluble *c*-type cytochromes or cupredoxins [21]. In fact, whole-cells and *in vitro* studies have been performed to identify the probable physiological electron donors of N_2OR in several microorganisms. Studies performed with whole-cells of *Rhodobacter capsulatus*, *Rhodobacter sphaeroides* and *P. denitrificans* indicated an oxidation of a cytochrome in the N_2O reduction [115, 116]. Moreover, the whole-cells of *R. capsulatus* in which a gene encoding cytochrome c_2 was deleted, were not able to reduce N_2O [117]. These results point out for the role of a *c*-type cytochrome as the physiological electron donor of N_2ORs from *P. denitrificans*, *R. capsulatus* and

R. sphaeroides [94, 115, 117]. In the case of *P. pantotrophus* N_2OR, the enzyme is able to receive electrons from pseudoazurin from the same organism [94, 118], while mammalian cytochrome *c* can donate electrons to *P. pantotrophus*, *Achromobacter cycloclastes* and *W. succinogenes* N_2ORs, as a non-physiological electron donor protein [119-121]. On the other hand, *in vitro* studies indicate that cytochrome c_{552} is the strongest candidate to be the physiological electron donor of *M. hydrocarbonoclasticus* N_2OR, which was also highlighted in molecular docking studies [122], while in the case of *A. cycloclastes*, pseudoazurin was assigned as the probable physiological donor [123, 124]. Although these proteins can donate electrons to N_2OR *in vitro*, being suggested as the probable physiological relevant electron donors, their role *in vivo* has not yet been demonstrated and the possibility of others proteins with the same role cannot be excluded.

The residues involved in the metal coordination of both copper centers are strictly conserved among N_2ORs [24]. In CuA center, the copper atoms are μ_2-bridged by two cysteine residues and also linked to two histidines, a methionine and a tryptophan residue, with each copper atoms adopting a distorted tetrahedral geometry [125] (Figure 1.8). "CuZ center" is a tetranuclear copper center with a central sulfide coordinating the four copper atoms, each of which is coordinated by the side chain of two histidine ligands, with the exception of Cu_{IV}, that is only coordinated by one [125, 126] (Figure 1.9).

CuA center is bound to the C-terminal domain, which is arranged in an antiparallel β-sandwich fold, feature common to Type 1 copper proteins [127], while "CuZ center" is located at the N-terminal domain, which has a seven-bladed β-propeller fold [125] (Figure 1.7). In the dimer, these two centers are oriented in a head-to-tail configuration: in the same monomer CuA and "CuZ" centers are separated by 40 Å, a long distance for efficient electron transfer, though CuA and "CuZ" centers from different monomers are only 10 Å apart, which confers a functional character to the dimer (Figure 1.7) [128]. The function of the calcium ions present in the X-ray structure of all N_2ORs was recently elucidated through the studies on the apo-N_2OR structure from *Shewanella denitrificans*. These studies revealed that calcium ions are not required for dimer formation, as calcium binding occurred after the complete assembly of the centers [129]. Thus, calcium binding seems to have an essential role in the stabilization of the enzyme structure, since in its absence the domains of the protein stand apart [129].

Since early years, various forms of N_2OR have been isolated and named according to the color of their solution as pink, purple or blue [130]. In-depth investigations over the years determined that those forms of the enzyme had different redox, spectroscopic and structural properties, due to the oxidation state of CuA center but mainly due to differences in the "CuZ center".

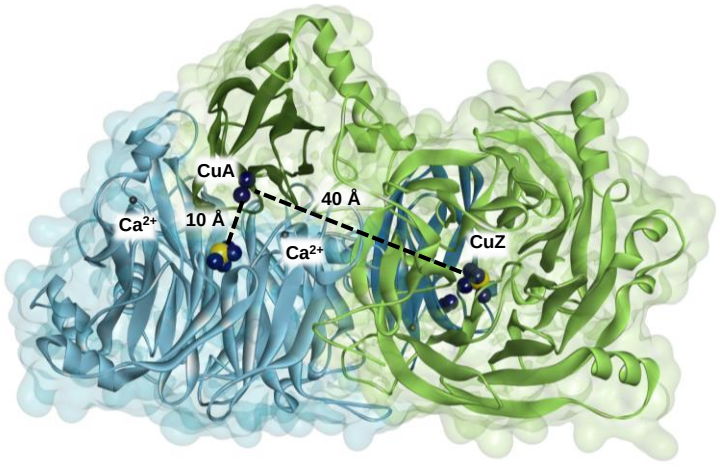

Figure 1.7 - Structure of *M. hydrocarbonoclasticus* N_2OR. The surface is colored according to the subunit. One monomer is represented in blue and the other in green, with the C-terminal dark colored and the N-terminal light colored. The copper atoms are represented as dark blue spheres and the sulfur atoms are represented as yellow spheres. The calcium ions in the dimer are evidenced as grey small spheres, being the two Ca^{2+} of the monomer labeled. The distance between CuA center and "CuZ centers" is represented. Figure was prepared with DS visualizer 4.5 using PDB ID: 1QNI.

Distinct forms of the "CuZ center" have been attributed to differences in growth conditions and purification strategies [90, 130-133]. Currently, it is generally accepted that N_2OR can be isolated with "CuZ center" in two forms, named herein as CuZ(4Cu2S) and CuZ*(4Cu1S). Indeed, the enzyme can be isolated mainly with CuZ(4Cu2S), in the oxidized or reduced state or mainly with CuZ*(4Cu1S) (in only one oxidation state, the resting state), and with CuA center in either the oxidized or reduced state. However, in a purified sample of N_2OR there is always a mixture of both "CuZ center" species, ranging so far from 5 % to 90 % of the CuZ(4Cu2S) form [133]. Thus, it has been a challenge to distinguish the spectroscopic features and kinetic parameters of the two forms of the "CuZ center".

1.5 Properties of copper centers in nitrous oxide reductase

1.5.1 CuA center - The electron entry point

CuA center of N_2OR is similar to the one identified in cytochrome *c* oxidase (C*c*O). The existence of copper in C*c*O is known since 1930s, however the properties of the enzyme were not in line with any of the existing classifications for copper containing proteins (Type 1, Type 2 and Type 3) [134]. The nature of CuA center in C*c*O was understood decades later, with significant contributions from Beinert, Greenwood and their colleagues, in recognizing the presence of two copper atoms with distinct spectral features from the other known coppers centers, using electron paramagnetic resonance (EPR) [134, 135] and magnetic circular dichroism (MCD) spectroscopies [136, 137].

The evidence of the presence of a similar CuA center in N_2OR was initially pointed out by Kroneck and his colleagues, who used multifrequency EPR spectroscopy to reveal the properties of N_2OR

metal centers [138-141]. A direct copper-copper interaction was identified, with similar features to the CuA center of C*c*O, demonstrating that this center is a mixed-valence metal site [$1Cu^{1.5+}$-$1Cu^{1.5+}$] [138-140].

The electronic properties of CuA center in N_2OR were since then extensively studied and are now well known.

The visible spectrum of the oxidized CuA center, in the [$1Cu^{1.5+}$-$1Cu^{1.5+}$] oxidation state, exhibits absorption bands at 480 ($\varepsilon \approx 4000\ M^{-1}\ cm^{-1}$), 540 ($\varepsilon \approx 4000\ M^{-1}\ cm^{-1}$) and 800 nm ($\varepsilon \approx 3000\ M^{-1}\ cm^{-1}$), while in the reduced state it becomes spectroscopically silent, due to the d^{10} electronic configuration of the copper atoms (Table 1.2) [142]. The intense absorption bands at 480 and 540 nm are associated to a S(cys)→Cu charge transfer (CT) in agreement with the strongest Cu-S(cys) stretching modes observed by resonance Raman, upon excitation at 488 nm, 259 and 347 cm^{-1} that are ^{34}S and ^{65}Cu isotope sensitive. The 259 cm^{-1} stretching mode observed has been assigned to a Cu-N(His) vibration [143-145]. The transition at 800 nm is assigned to a mix valence Ψ→Ψ* CT detected in absorption and MCD spectra and also supported by resonance Raman spectroscopy through an additional enhanced vibration (Cu_2S_2 "accordion" bending mode) at ~130 cm^{-1} [142, 144, 146].

The X-band EPR spectrum of CuA center in N_2OR is characterized by an axial signal, with $g_{\|}$ = 2.18 and $g_{\perp}$ = 2.03 and a 7-line hyperfine pattern in the $g_{\|}$ region, showing intensity ratios of 1:2:3:4:3:2:1, with a $A_{\|}$= 3.83 mT (Table 1.2) [90, 138]. The hyperfine splitting is due to the mix valence state (S = 1/2), in which an unpaired electron is delocalized over the two copper atoms (I_{cu} = 3/2) [90, 138, 140]. Nevertheless, the 7-line pattern is not always well resolved since, for the enzyme with "CuZ center" mainly as CuZ*(4Cu1S), an overlap of signals in this region from CuZ*(4Cu1S) was detected [20, 147] (see below).

Redox titrations followed by EPR or visible spectroscopy have been used to determine the reduction potential of CuA center and a value of + 260 mV *vs* SHE (standard hydrogen electrode), at pH 7.5, was estimated for this center in *P. stutzeri* N_2OR [90], in accordance with the reduction potential determined for CuA center in the enzymes isolated from *P. pantotrophus* [131] and *M. hydrocarbonoclasticus* [91, 148].

Table 1.2 - Summary of CuA center spectroscopic properties.

Oxidation State	Visible Absorption[a]	Resonance Raman Spectroscopy	Spin State	EPR	Ref.
$[1Cu^{1.5+}:1Cu^{1.5+}]$	480 nm ($\approx 4000\ M^{-1}cm^{-1}$) 540 nm ($\approx 4000\ M^{-1}cm^{-1}$) 800 nm ($\approx 3000\ M^{-1}cm^{-1}$)	Stretching modes: 259 and 347 cm^{-1} "Accordion" bending mode: 130 cm^{-1}	S = 1/2	$g_{\parallel}$=2.18, $g_{\perp}$=2.03 $A_{\parallel}$=3.83 mT	24, 133, 142, 144, 146
$[1Cu^{1+}:1Cu^{1+}]$	-	-	S = 0	silent	

[a]Molar extinction coefficients are given by concentration of N_2OR monomer.

Extended X-ray absorption fine structure (EXAFS) studies on N_2OR reinforced the existence of a direct metal-metal bond in the mixed valence CuA center with a distance of 2.43 Å and provided evidences of a Cu_2S_2 core with a 2.2 Å Cu-S interactions [149], which is in agreement with the EXAFS studies in C*c*O [150]. These data were confirmed some years later when the first X-ray structure of a N_2OR was solved at a 2.4 Å resolution, for the enzyme isolated from *M. hydrocarbonoclasticus*, confirming the coordination sphere of CuA center and showing identical Cu-Cu (2.47 Å) and Cu-S (2.26 Å - 2.31 Å) distances [125]. The two cysteine residues (C630 and C634) coordinate, through their S_γ atoms, both coppers atoms (CuA_1 and CuA_2), being CuA_1 also coordinate by $N_{\varepsilon 2}$ atoms of a histidine (H595) and a S_γ of a methionine (M641) and CuA_2 by $N_{\varepsilon 2}$ atom of a histidine (H638) and the carbonyl group of the tryptophan (W632) (numbering according to *P. denitrificans* primary sequence) (Figure 1.8A). CuA center is bound to the C-terminal cupredoxin folded domain in the loop region between β8 and β9 strands [125] of the β-barrel domain.

Besides the initial *M. hydrocarbonoclasticus* N_2OR structure, higher resolution structures of N_2ORs also purified in the presence of oxygen were solved for *P. denitrificans* (1.6 Å) [126] and *A. cycloclastes* (1.86 Å) [151]. More recently, a structure of N_2OR purified and crystallized under anoxic conditions was obtained for the enzyme isolated from *P. stutzeri* [152]. Interestingly, an alternative conformation of CuA center was reported for most of the monomers in the asymmetric unit of *P. stutzeri* N_2OR, in which the imidazole ring of H583 (equivalent to H595 in *P. denitrificans*) is rotated ~130°, no longer coordinating CuA_1 and forming two hydrogen bonds with two highly conserved residues, S550 and D576 (Figure 1.8B) [152, 153]. Also in the recently reported structure of the apo-form of *S. denitrificans* N_2OR [129], only this histidine was in the flipped conformation and hydrogen bonded to D576 (numbering as in *P. stutzeri* N_2OR primary sequence), though the causes and function of that different orientation are still poorly understood.

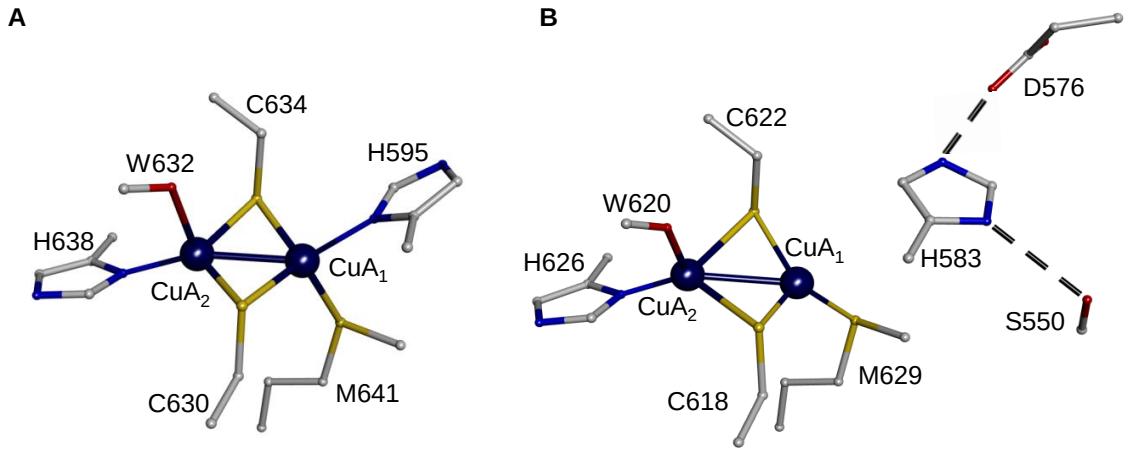

Figure 1.8 - Structures of CuA center of N_2OR. Representation of the CuA center of (A) *P. denitrificans* N_2OR and (B) *P. stutzeri* N_2OR. In Panel B, H583 does not coordinate CuA_1 atom. The copper atoms are represented as blue dark spheres and numbered 1-2. Figure was prepared with DS visualizer 4.5 using PDB ID: 1FWX (A) and 3SBP (B). The residues were numbered according to the primary sequence of N_2OR in each microorganism.

Furthermore, the conserved D576 residue has been proposed to be the entry point for the electrons donated from the small electron shuttle protein in *P. stutzeri* N_2OR, based on the docking studies between N_2ORs and its redox partners [154]. Indeed, these same studies applied to *M. hydrocarbonoclasticus* N_2OR, *P. denitrificans* N_2OR and *A. cycloclastes* N_2OR with the respective redox partners, also identified this conserved aspartate to be involved in the intermolecular electron transfer pathway [154].

Moreover, in the case of *P. stutzeri*, the mechanism involving the switching of H583 has been postulated to play a role in the intramolecular electron transfer from CuA center to the catalytic "CuZ center", as it is flipped away and non-coordinating CuA_1 in the absence of substrate but switches to its coordinating position in the presence of substrate [152], though the enzyme is in the fully oxidized form and no change in the oxidation state of the copper centers was reported upon data acquisition or substrate incubation.

1.5.2 "CuZ center" - The catalytic center

The existence of a catalytic center in N_2OR, assigned as "CuZ center", is long known [147, 155]. However, its spectroscopic and structural characteristics took years to discern and are still a matter of debate due to its unusual features and difficulties in obtaining an enzyme preparation with a single form of "CuZ center", either as CuZ(4Cu2S) or as CuZ*(4Cu1S).

In the early studies, as it was recurrent to obtain enzyme preparations with low copper content of ~8 Cu atoms per functional dimer (currently known to bind 12 Cu atoms [125]) was recurrent. Therefore, in combination with the available spectroscopic data, it was postulated the existence of a

second binuclear copper center coordinated by a thiolate group [90, 130, 147]. Although the S bridging character was detected [156], it could only be assigned to an inorganic sulfur, as there are only two conserved cysteine residues in the primary sequence of N_2ORs, which are located at the C-terminal domain and coordinate CuA center. The copper atoms of "CuZ center" were proposed to be coordinated by seven conserved histidine residues located at the N-terminal domain. The overall coordination was clarified when the three-dimensional structure of N_2OR was solved, in which a central inorganic sulfur atom was identified to be μ_4-bridging the copper atoms (here assigned as $Cu_{I\text{-}IV}$) arranged in a distorted tetrahedron [126, 151, 157].

However, the electron density coordinating the four copper atoms of "CuZ center" was fitted to an oxygen atom in the first reported N_2OR structure [125]. Although the oxygen was assigned as the central atom, early spectroscopic studies had suggested the presence of another copper-sulfide center, with different properties from CuA center [156].

At the same time as the release of the first X-ray structure of *M. hydrocarbonoclasticus* N_2OR, sulfide quantifications and analysis of resonance Raman spectra undoubtedly showed the presence of labile sulfide in the composition of "CuZ center" [143, 158]. Afterwards, new structural data and re-analysis of the first "CuZ center" electron density, together with sulfur quantifications in *M. hydrocarbonoclasticus* and in *P. denitrificans* N_2ORs showed that the magnitude of the electron density of the central atom corresponded to a sulfide instead of an oxygen atom [126].

Common to all structures, Cu-S_1 bonds have a similar length (~ 2.3 Å), while copper-copper distances are variable, with distances between Cu_I-Cu_{IV} and Cu_I-Cu_{III} being longer (ranging from 3.3 to 3.6 Å) than Cu_{II}-Cu_{IV} and Cu_{II}-Cu_{III} distances (ranging from 2.4 to 2.8 Å) [126, 151, 159].

As mentioned, different properties of the "CuZ center" have been observed mostly due to the mixture of "CuZ center" forms in each enzyme preparation, CuZ(4Cu2S) and CuZ*(4Cu1S). However, the understanding that the oxidation states of each of these "CuZ center" forms can be studied by selectively reducing the other "CuZ center" form and also CuA center (using reducing agents, such as sodium ascorbate, dithionite or reduced viologens), and that the amount of each form of the "CuZ center" in an enzyme preparation can be determined by EPR spin quantification, as led to unprecedented advances in the spectroscopic and structural characterization of "CuZ center" [91, 160].

1.5.2.1 Structural and spectroscopic features of CuZ*(4Cu1S)

A N_2OR sample with "CuZ center" mainly as CuZ*(4Cu1S) is usually obtained when its purification is performed from long term frozen crude extracts [125, 126, 151, 157], with either CuA center oxidized or reduced. Such an enzyme sample can also be isolated in the absence of oxygen from a *P. denitrificans* double mutant in *nirXnosX* [81, 85].

Up-to-date, N_2OR structures containing "CuZ center" mainly as CuZ*(4Cu1S) have been reported for the enzyme isolated from three microorganisms *M. hydrocarbonoclasticus*, *P. denitrificans* and *A. cycloclastes*, solved at 2.4, 1.6 and 1.9 Å resolution, respectively [125, 126, 151, 157].

The coordination sphere of the tetranuclear CuZ*(4Cu1S) in *P. denitrificans* consists of five histidine residues H337, H392, H443, H146 and H194, coordinating the copper atoms by $N_{\varepsilon 2}$ and the other two, H145 and H504, coordinating the copper atoms via $N_{\delta 1}$ (numbered according to *P. denitrificans* primary sequence) (Figure 1.9A) [125, 126]. These residues are located either in the blades (H145, H146, H194, H392 and H443) or on the top of the β-propeller domain (H270 and H495) [125, 126]. In those structures, a water-derived ligand had been identified in the edge of Cu_I-Cu_{IV}. Nevertheless, comparison between the three known structures of CuZ*(4Cu1S) highlights the difference that lies in the Cu_I-Cu_{IV} edge: an oxygen atom is bound to Cu_{IV}, assigned to a water molecule or a hydroxide, in the cases of *M. hydrocarbonoclasticus* and *P. denitrificans* N_2ORs, while two oxygen atoms bound to a different copper atom (Cu_I and Cu_{IV}) were modeled in the electron density in *A. cycloclastes* N_2OR [126, 151, 157].

Properties of resting CuZ*(4Cu1S) have been investigated in detail using different spectroscopies (Table 1.3) [91, 143, 161, 162]. The resting CuZ*(4Cu1S), in the [$1Cu^{2+}$-$3Cu^{1+}$] oxidation state, is characterized by a strong absorption band at 640 nm ($\varepsilon \approx 4000\ M^{-1}\ cm^{-1}$) (Table 1.3) and intense transitions in the visible region in both CD and MCD spectra, assigned to S→Cu CT, His→Cu CT, Cu→Cu inter-valence transition (IT) and also d→d transitions [91, 147, 158, 161, 162]. Additionally, the MCD spectra of the CuZ*(4Cu1S), acquired at variable temperature and field, were simulated for a $S_{Total} = 1/2$, indicating a paramagnetic behavior for the resting state [163]. The oxidation state of the resting CuZ*(4Cu1S) was determined by Cu K-edge X-ray absorption spectroscopy to be [$1Cu^{2+}$-$3Cu^{1+}$], attending to the possible oxidation states of the copper atoms for a $S_{Total} = 1/2$ [163].

The resonance Raman spectrum at pH ~7.3, excited at 624.4 nm (or 647 nm, which showed similar vibrational frequencies) presented three vibrational modes at 366, 386 and 415 cm^{-1}, being 366 and 415 cm^{-1} assigned to Cu-S stretching vibrations, and 386 cm^{-1} to μ_4S, as they exhibited ^{34}S shift [143, 162]. When the sample is enriched with $^{16}O/^{18}O$, no ^{18}O shifts were observed, upon excitation at 600 nm [161]. Moreover, at pH 10.5 a 9 cm^{-1} $^{16}O/^{18}O$ shift of the 415 cm^{-1} peak was detected, suggesting a Cu-O vibrational mode at high pH [161].

Selective reduction of CuA center with sodium ascorbate enabled the determination of the EPR features of the resting CuZ*(4Cu1S), in a sample with high content of this form. Q- and X-band EPR showed axial signals and hyperfine splitting in the $g_{\parallel}$ region, however the X-band hyperfine pattern was not very well resolved due to the broadening of the signals, which could be improved in the second derivative spectrum [163, 164]. Thus, accurate *g*-values, $g_{\parallel} = 2.16$ and $g_{\perp} = 2.04$, were determined based on the Q-band EPR spectra of *M. hydrocarbonoclasticus* N_2OR, which presented similar values to those previously reported for *P. pantotrophus* N_2OR (Table 1.3) [163, 165]. Two

hyperfine coupling constants were estimated ($A_{\parallel}$ = 6.1 mT and $A_{\parallel}$ = 2.4 mT) due to the unpaired spin density delocalized over two coppers in a ratio of ~5:2 [163].

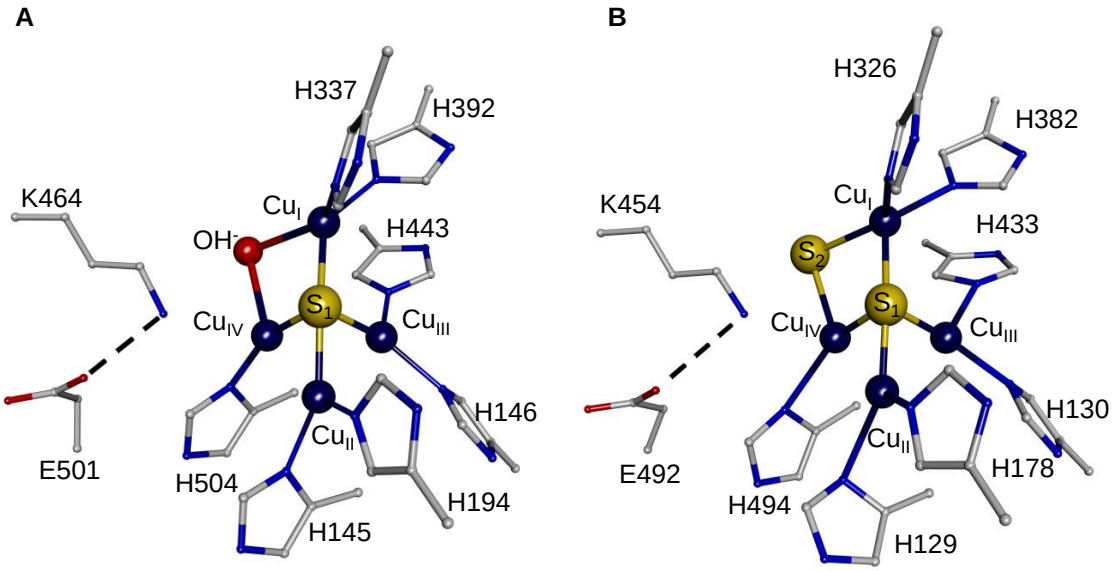

Figure 1.9 - Structures of the "CuZ center" of N_2OR. (A) Representation of the CuZ*(4Cu1S) from *P. denitrificans* N_2OR with the first and second coordination sphere residues. This form contains one sulfur atom named S_1 and one oxygen atom (from either a hydroxide or a water molecule) at the Cu_I-Cu_{IV} edge. (B) Representation of the "CuZ center" as CuZ(4Cu2S) from *P. stutzeri* N_2OR with first and second coordination sphere residues. This form contains two sulfur atoms named S_1 and S_2. The copper atoms are represented as dark blue spheres and numbered I-IV. The residues are numbered according to the primary sequence of each N_2OR. Figure was prepared with DS visualizer 4.5 using PDB ID: 1FWX (A) and 3SBP (B).

The crystallographic structure of *M. hydrocarbonoclasticus* N_2OR has been used in density functional theory (DFT) calculations to investigate the electronic configuration of the ground-state of CuZ*(4Cu1S) [163, 166]. Taking into account that the spin distribution is affected by the ligand in the Cu_I-Cu_{IV} edge, different models were considered. Initially a model with a water molecule in the Cu_I-Cu_{IV} edge was proposed, in which the spin density would be distributed over Cu_I and Cu_{II} atoms [163]. Other models, involving the following ligands, have been also analyzed: a H_2O bond to Cu_I, a OH^- in the Cu_I-Cu_{IV} edge, a OH^- in the Cu_I-Cu_{IV} edge bound to a lysine residue or a OH^- ligand H-bonding to a protonated lysine residue [161]. DFT calculations combined with spectroscopic studies, lead Solomon and collaborators to propose that a OH^- ligand occupies the Cu_I-Cu_{IV} edge, being closer to Cu_I (2.00 Å) than to Cu_{IV} (2.09 Å) [161]. This model at low pH also includes two residues nearby the Cu_{IV} atom, a protonated lysine and a glutamate residue, that establishes with each other a H-bond (K447 and E485 residues in the primary sequence of *M. hydrocarbonoclasticus* N_2OR), but not with the OH^- ligand at the Cu_I-Cu_{IV} edge (Figure 1.9A) [161, 167].

Thus, the edge of Cu_I-Cu_{IV} in CuZ*(4Cu1S) is proposed to be occupied by a hydroxide that is mainly bond to Cu_I, as the spin density resides mainly on this atom (26 %), with Cu_{IV} (13 %) also having a contribution [164]. At higher pH, no changes in the position of K447 was observed, with the

enhance vibration (shift of 9 cm^{-1}) observed in the resonance Raman spectra explained by a close proximity of the ligand to both Cu_I and Cu_{IV} atoms [167].

This form of the catalytic center is redox inert and can only be fully reduced to the [$4Cu^{1+}$] oxidation state after prolonged incubation (3 – 5 h) with a large excess of reduced viologens [122, 160, 168]. The reduction potential of the redox couple [$1Cu^{2+}$-$3Cu^{1+}$]/[$4Cu^{1+}$] has not yet been determined, since reducing the resting CuZ*(4Cu1S) in a potentiometric redox titration is very difficult [148].

1.5.2.2 Structural and spectroscopic features of CuZ(4Cu2S)

N_2OR can be isolated with "CuZ center" mainly as CuZ(4Cu2S), in an oxidized [$2Cu^{2+}$-$2Cu^{1+}$] or a reduced [$1Cu^{2+}$-$3Cu^{1+}$] state, and with CuA center either oxidized or reduced. This form of "CuZ center" can be easily reduced and oxidized and the reduction potential of the reversible redox couple [$2Cu^{2+}$-$2Cu^{1+}$]/[$1Cu^{2+}$-$3Cu^{1+}$] was estimated to be + 60 mV *vs* SHE at pH 7.5, in *P. pantotrophus* N_2OR [131].

The crystallographic structures of *P. stutzeri* N_2OR, isolated with "CuZ center" mainly as CuZ(4Cu2S), in the oxidized state, were solved at 1.7 and 2.1 Å resolution and reported for the first time in 2011 [152] (Figure 1.9B). The coordination is similar to that observed for CuZ*(4Cu1S), with the exception of the ligand at the Cu_I-Cu_{IV} edge modeled as a sulfur atom [152]. Typical metal-sulfur bonds were observed with Cu_I-S_2 and Cu_{IV}-S_2 being 2.5 Å and 2.3 Å, respectively [152]. Spectroscopically, the oxidized [$2Cu^{2+}$-$2Cu^{1+}$] state is characterized by a strong absorption band at 545 nm ($\varepsilon \approx 5000\ M^{-1}\ cm^{-1}$) and a shoulder at 635 nm [131, 156, 164] (Table 1.3), corresponding to five transitions at room temperature, assigned to S→Cu CT [164]. This CT character was addressed by resonance Raman spectroscopy upon excitation at 568 or 676 nm, whose profiles exhibited enhanced vibrational modes at 350 and 405 cm^{-1}, that are S isotope-sensitive. The resonance Raman profiles combined with DFT calculations associated the nature of the transitions to the presence of a sulfide (μ_2S^{2-}) edge ligand that has a $pK_a \leq 3$ [164]. Moreover, upon reduction of CuA center with sodium ascorbate, neither MCD or EPR spectra presented signals of the oxidized CuZ(4Cu2S) confirming the diamagnetic behavior (S = 0) of this oxidation state [131].

The [$1Cu^{2+}$-$3Cu^{1+}$] state is characterized by a strong absorption band in the visible spectrum at 670 nm ($\varepsilon \approx 3000\ M^{-1}\ cm^{-1}$) (Table 1.3) [131]. Different transitions were observed by simultaneous analyses of low temperature absorption and MCD spectra, which were assigned to S→Cu CT transitions, IT transitions and low d→d transitions [147, 161, 164].

Table 1.3 - Summary of "CuZ center" properties. The different oxidation states of the four copper atoms in "CuZ center" are presented for each of the "CuZ center" forms, together with their spectroscopic and kinetic properties.

Forms of "CuZ center"	**Oxidation State**	**Cu_I - Cu_{IV} Edge ligand**	**Spin State**	**Turnover Number**	**Visible Absorption[b]**	**EPR**	**Ref.**
Oxidized CuZ(4Cu2S)	$[2Cu^{2+}:2Cu^{1+}:2S]^{2+}$	bridging S^{2-}	S = 0	None	545 mn ($\approx 5000\ M^{-1}cm^{-1}$)	Silent	90, 131, 156, 164
Reduced CuZ(4Cu2S)	$[1Cu^{2+}:3Cu^{1+}:2S]^{1+}$	bridging SH^-	S = 1/2	0.6 h^{-1}	670 nm ($\approx 3000 - 4400\ M^{-1}cm^{-1}$)	$g_{\parallel}$=2.150, $g_{\perp}$=2.035 $A_{\parallel}$=5.6 mT[c]	89, 90, 96, 131, 132, 156, 160, 163, 164
Resting CuZ*(4Cu1S)	$[1Cu^{2+}:3Cu^{1+}:S:OH]^{2+}$	bridging OH^-	S = 1/2	None	640 nm ($\approx 4000\ M^{-1}cm^{-1}$)	$g_{\parallel}$=2.160, $g_{\perp}$=2.040 $A_{\parallel}$=6.1 mT $A_{\parallel}$=2.4 mT[d]	91, 131, 147, 156, 158, 163, 166
CuZ^{0} [a]	$[1Cu^{2+}:3Cu^{1+}:S:OH]^{2+}$	bridging OH^-	S = 1/2	> 200 s^{-1}	680 nm ($\approx 2000\ M^{-1}cm^{-1}$)	$g_{\parallel}$=2.177, $g_{\perp}$=2.05 $A_{\parallel}$=4.2 mT[e]	148, 167
Fully reduced CuZ*(4Cu1S)	$[4Cu^{1+}:S]^{2+}$	Empty/H_2O	S = 0	> 200 s^{-1}	No bands	Silent	90, 160, 161, 164, 168

Notes: [a]CuZ^0 is an intermediate of CuZ*(4Cu1S) catalytic cycle. [b]Molar extinction coefficient is given by concentration of N_2OR monomer. [c]Consider 3 identical hyperfine coupling constants. [d]With a 5/2 ratio. [e]Consider 2 identical hyperfine coupling constants.

Additionally, the resonance Raman spectrum, acquired by excitation at 676 or 697 nm, presented enhanced Cu-S stretching modes, particularly at 203, 378, 450 and 492 cm^{-1}, being the 378 cm^{-1} vibration assigned to the μ_4S, since is common to the CuZ*(4Cu1S) profile [164]. On the other hand, vibrations at 203 cm^{-1} were assigned to the Cu-S stretching modes of the edge sulfur ligand, while 450 and 492 cm^{-1} vibrations are D_2O-isotope sensitive and assigned as S-H bending modes, suggesting that this oxidation state has a thiolate (μ_2SH^-) edge ligand between Cu_I and Cu_{IV} [164] (Table 1.3). The resonance Raman profiles obtained at pH 7.8 and pH 10 showed unperturbed behavior of S-H bending modes, suggesting that the thiolate has a p$K_a \geq 11$ [164].

The reduced CuZ(4Cu2S), [$1Cu^{2+}$-$3Cu^{1+}$], is characterized by an X-band EPR axial spectrum due to the delocalized spin density ($S_{Total} = 1/2$) over the copper atoms d_{x2-y2} orbitals [164]. The simulation of the derivative spectrum estimated a $g_{\parallel} = 2.152$, a $g_{\perp} = 2.042$ and three identical hyperfine coupling constants of $A_{\parallel} = 5.6$ mT, were required to explain the five hyperfine lines observed in the EPR spectrum [164]. Moreover, the requirement of the three hyperfine coupling constants is attributed to the spin density being distributed over Cu_I (17 %), Cu_{II} (11 %) and Cu_{IV} (10 %), in a ratio 2:1:1, since these atoms are localized in the same plane as the sulfur ligands [164].

Besides the oxidation states described above, no other oxidation states have been reported for CuZ(4Cu2S). Indeed, even upon prolonged incubation with reduced viologens, the fully reduced [$4Cu^{1+}$] state cannot be attained by CuZ(4Cu2S) [160], which can be attributed to the presence of the sulfur atom in the Cu_I-Cu_{IV} edge.

1.6 Substrate binding site

The combined studies on the structural, kinetics and spectroscopic properties of N_2OR pin pointed the Cu_I-Cu_{IV} water-derived edge as the probable substrate binding site of CuZ*(4Cu1S) [122, 125, 162, 166]. The unveiling of crystallographic structures of N_2OR was one of the major findings for this assumption, showing that Cu_{IV} is coordinated by the side chain of only one histidine, while the other copper atoms are coordinated by two histidines, together with the ligand in the Cu_I-Cu_{IV} edge, regarded as a labile water-derived molecule that would be easily replaced by the substrate nitrous oxide [146, 157].

EPR studies on the resting CuZ*(4Cu1S) have identified a spin density delocalized over Cu_I and Cu_{IV} that favored the N_2O interaction, and supported this hypothesis [163]. Additionally, DFT calculations on "CuZ center" models performed by Solomon and collaborators, suggested a μ-1,3-N_2O coordination as the most favorable binding mode of N_2O at the Cu_I-Cu_{IV} edge, in the lowest energy configuration of CuZ*(4Cu1S) in the [$4Cu^{1+}$] oxidation state [168]. In this configuration the terminal N-atom of the N_2O molecule is coordinating the Cu_I and the O atom is bound to Cu_{IV}, forming a ~139° angle [146, 166-168] (Figure 1.10A).

Several synthetic model compounds of CuZ*(4Cu1S) have been developed, however only few evidenced features similar to those observed for this center on the enzyme [169, 170]. The first promising model compound shown to be capable of convert N_2O into N_2 was a mixed-valent tricopper cluster $[Cu_3S_2]^{2+}$ supported by amino ligands, reported by Bar-Nahum *et al* [171]. In fact, this compound was dissociated in two species, $[Cu_2S_2]^{1+}$ and $[Cu]^{1+}$, being $[Cu_2S_2]^{1+}$ species the most favorable for the N_2O bridging [171]. DFT calculations predicted a μ-1,1-bridging coordination mode through the oxygen atom [171], showing a different coordination from the μ-1,3-Cu_{IV}-ON_2-Cu_I proposed in N_2OR. More recently, a tetranuclear copper compound model synthesized with bis(diphenilphospinoamine), $[Cu_4(\mu_4\text{-}S)]$, has been shown to be a relevant functional model of CuZ*(4Cu1S) [170]. This compound contains all the coppers as Cu^{1+} and was able to bind analogous triatomic molecules, such as azide or nitrite, and also iodide, a proposed inhibitor of N_2OR [170]. Iodide can rapidly and strongly bind to this synthetic complex originating an unreactive species [170]. However, no reactivity of this compound with N_2O was reported so far.

The proposed N_2O coordination to the enzyme was strengthen by the X-ray structure of an inhibited form of *A. cycloclastes* N_2OR, solved at 1.7 Å resolution [151]. The exposure of N_2OR to the inhibitor iodide lead to the formation of a blue adduct characterized by a strong absorption band at 650 nm [151]. In the structure of the adducted-N_2OR, the iodide was modeled in the electron density maps between Cu_I and Cu_{IV} [151].

Others exogenous ligands, including fluoride, cyanide, azide, nitric oxide, carbon monoxide and hydrogen peroxide, presented different reactivity and spectroscopic effects on the interaction with the enzyme [89, 130, 157, 172, 173]. Indeed, some of those inhibitors bind irreversibly to the enzyme or chelate the copper atoms, as observed by Haltia and co-authors in the structures of N_2OR crystals treated with cyanide and hydrogen peroxide, in which a lower occupancy of the copper atoms of the "CuZ center" was reported [157]. The binding mode of the other exogenous ligands is not known, and it remains to be elucidated whether their binding induces conformational changes in the copper centers or in the enzyme. These studies can provide additional insights into the complex catalytic mechanism of this enzyme and clarify the substrate interaction with the enzyme, which will be discussed in the Chapter 6 of this thesis.

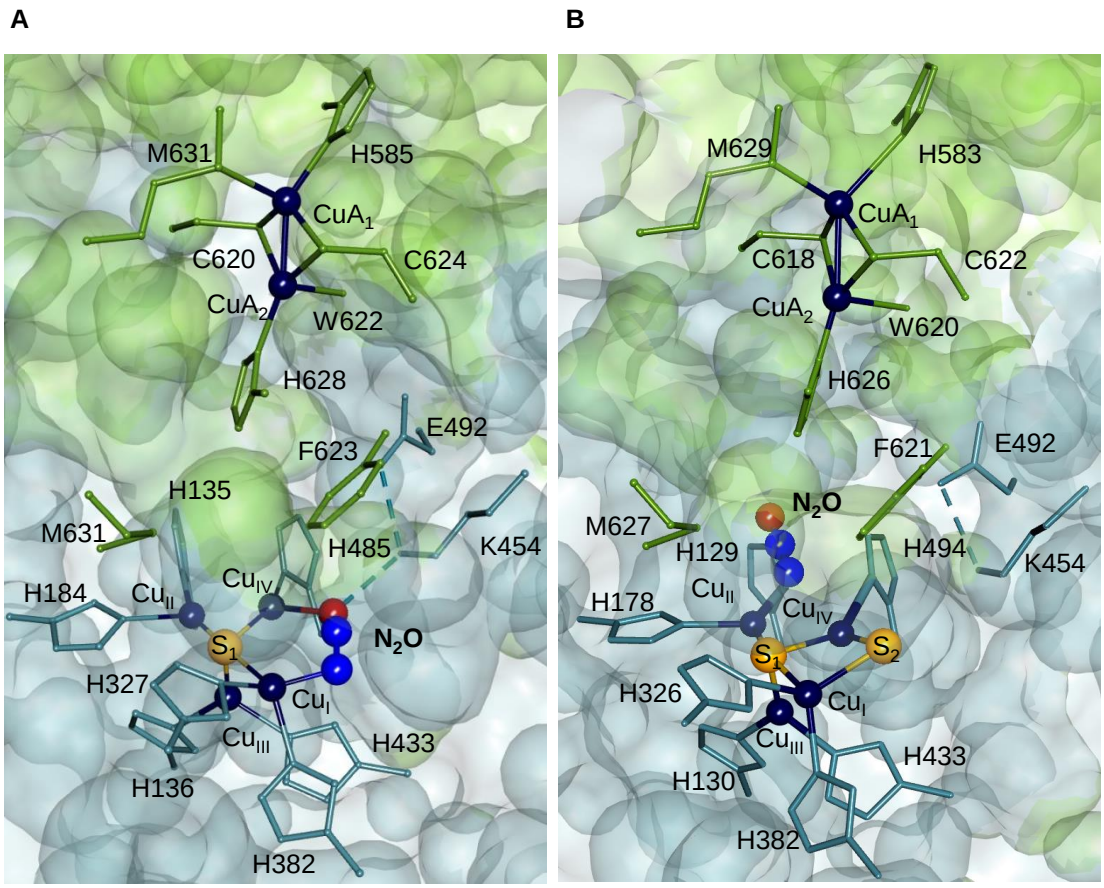

Figure 1.10 - Substrate binding mode in N_2OR. (A) The N_2O was modeled in the Cu_I-Cu_{IV} edge in a μ-1,3-bridging mode. The N_2O binding site was proposed for *A. cycloclastes* N_2OR structure, based on DFT calculations and spectroscopic features of the "CuZ center" as CuZ*(4Cu1S), in the [$4Cu^{1+}$] oxidation state. (B) The N_2O molecule is located between CuA and "CuZ" centers. *P. stutzeri* crystals of N_2OR, with the "CuZ center" as CuZ(4Cu2S), in the [$2Cu^{2+}$-$2Cu^{1+}$] oxidation state, were pressurized with N_2O. The surface at the dimer interface, as well as the relevant residues involved in the substrate binding mode are represented and colored according to the monomer by green and blue. The N_2O atoms are colored according to the element. The residues are numbered according to their primary structure. Figures were prepared using DS visualizer 4.5, using PDB ID: 2IWF (A) and 3SBR (B).

There is, to our knowledge, only one N_2OR structure crystallized in the presence of N_2O, solved for *P. stutzeri* N_2OR (at 2.24 Å resolution) after pressurization of anaerobically prepared purple crystals (Figure 1.10) [152]. In this preparation, CuA center is in the [$1Cu^{1.5+}$-$1Cu^{1.5+}$] oxidation state and "CuZ center" as CuZ(4Cu2S) is in the [$2Cu^{2+}$-$2Cu^{1+}$] oxidation state [152], a form of the enzyme that is not catalytically competent. In this structure, N_2O is not coordinated to any metal center, being located above the Cu_{II}-μ_4S-Cu_{IV} face in a linear mode, between both CuA and CuZ(4Cu2S), and not even close to the edge position of Cu_I-Cu_{IV} that in this case is occupied by a sulfur atom (Figure 1.10B) [152, 159]. Moreover, a hydrophobic channel for substrate access to this location was proposed and the reorientation of the N_2O molecule is envisaged through F621 and M627 residues (Figure 1.10) [152, 153]. The only significant difference between the *P. stutzeri* N_2OR structures in the

presence and absence of substrate is, as mentioned before, at the CuA center, with H583 imidazole ring being rotated and coordinating CuA_1 atom in the presence of N_2O [152].

For the catalysis to occur, electrons have to be transferred from CuA center to "CuZ center". Two possible intramolecular electron transfer routes, based on molecular docking simulations, have been proposed for *M. hydrocarbonoclasticus* N_2OR containing the catalytic center as CuZ*(4Cu1S) [154, 174] (Figure 1.10). In one pathway the electron would be transferred from W613 (W622 in *A. cycloclastes*, numbered according to primary sequence), coordinating CuA center, to the F614 (F623 in *A. cycloclastes*, numbered according to primary sequence) entering the catalytic center via the oxygen positioned in the Cu_I-Cu_{IV} edge. The other pathway would involve electron transfer from the CuA ligand H619 (H628 in *A. cycloclastes*) to M620 (M631 in *A. cycloclastes*), and subsequently to H178 (H184 in *A. cycloclastes*), which coordinates Cu_{II} of "CuZ center".

1.7 Specific activity and activation mechanism of N_2OR

The N_2OR specific activity is expressed in $\mu mol_{N2O}\ min^{-1}\ mg^{-1}{}_{N2OR}$ and can be determined spectrophotometrically or by gas chromatographic assays [175, 176]. In the spectrophotometric assay the rate of N_2O reduction is indirectly determined by following the oxidation of reduced viologen dyes at 600 nm, which can either be initiated upon addition of the enzyme or water saturated-N_2O to the reaction mixture, which contains the reduced viologens and N_2O or the enzyme, respectively [122, 175]. In alternative, the activity can be directly measured based on the substrate (N_2O) consumption and/or product (N_2) formation by gas chromatography [90, 176].

The rate of N_2O reduction by *P. stutzeri* crude cell extracts, determined using the spectrophotometric assay, ranged from 48 to 72 $\mu mol_{N2O}\ min^{-1}\ mg^{-1}{}_{N2OR}$ [90, 177]. Nevertheless, the activity of *P. stutzeri* N_2OR purified in the presence and absence of oxygen, measured *in vitro* using the spectrophotometric assay, is on average 1.8 and 4.3 $\mu mol_{N2O}\ min^{-1}\ mg^{-1}{}_{N2OR}$, respectively [90]. Intriguingly, none of the specific activities determined for the isolated enzyme, independently of the proportion between the two "CuZ center" forms, are in line with the activity values obtained for the crude extract, suggesting that those values corresponded to an unready state of the enzyme [133]. These specific activity values are in agreement with the ones measured for N_2ORs purified from *P. pantotrophus* [131], *Alcaligenes xylosoxidans* [92] and *P.aeruginosa* [119, 178], using methyl (MV) or benzyl viologen as electron donors (ranging from 1 to 10 $\mu mol_{N2O}\ min^{-1}\ mg^{-1}{}_{N2OR}$).

These spectrophotometric assays are far from being physiological, as the reduction potential of the electron donors used (methyl viologen, - 450 mV *vs* SHE, pH 7.0 and benzyl viologen, - 374 mV *vs* SHE, pH 7.0 [179]) are below of what is expected to be found in the periplasm of Gram-negative bacteria. Nevertheless, physiologically relevant electron donors have been tested and identified that are able to donate electrons to N_2OR in *in vitro* activity assays. However, even in the presence of

reduced native donors, hypothesized to induce conformational changes in N_2OR [120], the specific activities cannot explain the high N_2O-reduction rates attained when using either crude cell extracts or whole-cells [79, 90, 117, 120, 122]. Nonetheless, a large excess of electron donor protein over the enzyme (~26000-fold excess) was recently reported to substantially increase the activity of *A. cycloclastes* N_2OR [123], but no molecular explanation was provided nor similar observations have been reported for any other enzyme.

On the other hand, a high specific activity, of 160 μmol_{N2O} min^{-1} mg^{-1}_{N2OR}, was reported for the enzyme isolated from *W. succinogenes* (clade II N_2OR) [98], an indication that it does not require activation. This could be attributed, as mentioned before, to the fact of this enzyme being able to receive electrons directly *via* menaquinol [36], with the additional domain playing a role in the electron transfer pathway *via* CuA center to "CuZ center". In fact, clade I N_2ORs may require additional accessory proteins to attain such activity, possibly NosR, or may require the formation of a supra-complex as recently reported in *P. aeruginosa* [180]. Thus, what is clear is the requirement of a chemical activation step of the purified clade I N_2OR in order to reach its maximum activity [168, 181].

Enzyme activation has been proposed to be attained through two processes: prolonged incubation with reduced viologens or with an alkaline solution, though the activity values attained with this later process are not as high as the ones with the former [90, 168, 175].

The pH has a distinct effect on the enzyme activation and N_2O reduction (Table 1.4) [182]. In fact, alkaline activation followed by the activity assays at neutral pH seems to be divergent between the N_2ORs isolated from different species: ~ 1.5 fold increase, after 14 h at pH 9.0, for *P. pantotrophus* N_2OR with "CuZ center" as CuZ*(4Cu1S)/CuZ(4Cu2S) [94], ~ 1.3-1.4 fold increase, after 3 h at pH 10.0, for *A. xylosoxidans* N_2OR with "CuZ center" as CuZ(4Cu2S) [92], ~ 14 fold increase, after 16 h at pH 9.8, for *P. stutzeri* N_2OR with "CuZ center" as CuZ(4Cu2S) [90], or ~ 50-75 fold increase for *P. aeruginosa* N_2OR at pH 10 with "CuZ center" as CuZ(4Cu2S) [178]. Thus, when the enzyme, in particular with "CuZ center" mainly as CuZ(4Cu2S), is incubated at alkaline pH the specific activity increases more than when it is activated at neutral or more acidic pH, despite the heterogeneous increment in activity between species [182]. The exact molecular mechanism for the alkaline activation is unknown, but could be related with the deprotonation of a "CuZ center" nearby residue [182].

Incubation with a reduced viologen increases the activity in two orders of magnitude [168, 181]. Nevertheless, the activation of N_2OR is not only dependent on the incubation with a compound with a very low reduction potential but also on the type of reducing agent and on the incubation time with the reduced viologens: dithionite (with a reduction potential of - 471 mV *vs* SHE at pH 7.0 [183]), by itself does not activate N_2OR (with "CuZ center" in any of the two forms) [168, 181], while N_2OR with "CuZ center" as CuZ*(4Cu1S) after 3 h incubation in the presence of 100-fold excess of reduced methyl viologen attains maximum activity.

This activation process is related to the reduction of resting CuZ*(4Cu1S) (k ~ 1.2x10^{-3} s^{-1}, in the presence of reduced methyl viologen), in which CuZ*(4Cu1S) in the [1Cu^{2+}-3Cu^{1+}] oxidation state is reduced to [4Cu^{1+}] [168]. However, it is important to point out that this has a very slow reduction rate to be part of the catalytic cycle [160, 166]. The reduction process is marked by a decrease in the absorbance at 640 nm and can be followed by decay of the EPR signal intensity that is correlated with the reduction of the "CuZ center" as CuZ*(4Cu1S), in the [1Cu^{2+}-3Cu^{1+}], to the diamagnetic [4Cu^{1+}] state [168]. Upon decrease of the EPR signal, there is the concomitant increase in activity, suggesting that [4Cu^{1+}] state is the *in vitro* catalytic relevant oxidation state of CuZ*(4Cu1S) [168]. A pK_a of 9.0 ± 0.2 for the reduction process (from [1Cu^{2+}-3Cu^{1+}] to [4Cu^{1+}]) was determined by following the rate of EPR signal decay and assigned to a nearby lysine [161].

It is important to mention that the features of the visible spectrum of fully reduced N_2OR do not disappear completely, due to the presence of a small amount of N_2OR with "CuZ center" as CuZ(4Cu2S), since it is not possible to obtain an enzyme sample with a homogeneous form of "CuZ center", and CuZ(4Cu2S) is not fully reduced by reduced methyl viologen to the [4Cu^{1+}] oxidation state [160].

1.8 The catalytic competent forms

Two catalytic competent forms of the N_2OR are known so far: the fully reduced state of CuZ*(4Cu1S) and the CuZ^o intermediate species.

The fully reduced state of CuZ*(4Cu1S), [4Cu^{1+}], is obtained after prolonged exposure of N_2OR to an excess of reduced (methyl or benzyl) viologen, as mentioned above. In this state, due to the d^{10} configuration of the copper atoms, both MCD and EPR features are absent as this species is diamagnetic with no unpaired electrons (S = 0).

N_2OR in the active fully reduced state reacts with the substrate even after removal of reduced methyl viologen, demonstrated by the partial re-appearance of the visible and EPR spectral features and supported by GC-MS detection of the product (dinitrogen), when a ^{15}N labeled N_2O was used [181]. The spectroscopic evidences are the appearance of the CuA center features in the visible spectrum, at 480, 540 and 800 nm, and of a band at 640 nm, corresponding to the re-oxidation of the CuZ*(4Cu1S) to [1Cu^{2+}-3Cu^{1+}] oxidation state, which is associated with the re-emergence of a hyperfine pattern in the EPR spectrum, involving two electrons [181].

The kinetic parameters of N_2OR, as well as its pH dependence, have been investigated (Table 1.4) [119, 122, 182]. N_2ORs containing "CuZ center" mainly as CuZ*(4Cu1S) exposed to viologens by a prolonged period exhibited higher specific activities, as the case of *M. hydrocarbonoclasticus*, *A. cycloclastes* and *P.denitrificans*. High turnover numbers of 321 s^{-1} and 163 s^{-1} were obtained for *M. hydrocarbonoclasticus* N_2OR [122] and *A. cycloclastes* N_2OR [119], respectively, showing that [4Cu^{1+}] is kinetically competent in reducing N_2O (Table 1.4). The specific activity of *A. cycloclastes* N_2OR

is pH dependent, with two pK_a values of 6.8 and 9.8 [119]. In the case of *M. hydrocarbonoclasticus* N_2OR, the pH profile will be discussed in Chapter 4. In the presence of its physiological electron donor cytochrome c_{552}, the maximum activity is attained at lower pH values, with a pK_a of 8.3 [122]. The pH dependence of specific activity of *P. pantotrophus* N_2OR in the presence of mammalian cytochrome *c* exhibited, similarly to *M. hydrocarbonoclasticus* N_2OR, higher activities at lower pH values, with a maximum observed at pH ~ 5.6 [94].

The hypothesis that other oxidation states of N_2OR "CuZ center" are able to react with N_2O was recently investigated [160]. Despite the various oxidation states that N_2OR centers can adopt (Table 1.3), not all are catalytically competent. For instance, CuZ(4Cu2S) in the [$2Cu^{2+}$-$2Cu^{1+}$] state and resting CuZ*(4Cu1S) in the [$1Cu^{2+}$-$3Cu^{1+}$] state, do not react with N_2O even when CuA center is reduced (no spectroscopic changes were observed in the presence of N_2O) [160] .

On the other hand, N_2OR with "CuZ center" as CuZ(4Cu2S) in the [$1Cu^{2+}$-$3Cu^{1+}$] state and with CuA center reduced, slowly reacts with N_2O (k = 0.6 h^{-1}), as supported by MCD and resonance Raman studies [160]. In this reaction, both CuA and CuZ(4Cu2S) centers were re-oxidized to the [$1Cu^{1.5+}$-$1Cu^{1.5+}$] and [$2Cu^{2+}$-$2Cu^{1+}$], respectively, in a two-electron process [160]. However, such low turnover numbers suggests that CuZ(4Cu2S) in the [$1Cu^{2+}$-$3Cu^{1+}$] state is not relevant for the catalytic cycle and thus is unlikely to be the active form *in vivo* [133, 160], possibly having a role as a protective form of the enzyme when either the substrate or electrons are not available to complete the cycle. Moreover, specific activities of these forms are usually very low compared to the fully reduced CuZ*(4Cu1S) (Table 1.4).

Table 1.4 - Kinetic properties of clade I N_2OR from different bacteria. Adapted from [184].

Bacteria	"CuZ" main form	ED	K_m for ED (μM)	K_m for N_2O (μM)	K_{cat} (s^{-1})	Specific activity (U mg^{-1})	pH and pK_a	Ref.
M. hydrocarbonoclasticus	CuZ*	MV	12	14	321	157	8.0	122, 167
	CuZ*	c_{552}	50		4	1.8		122
P. stutzeri	CuZ*	BV				2		90
	CuZ	BV				4 60[b]	9.8	90
P. denitrificans	CuZ	BV	1	7		122		89
P. pantotrophus	CuZ	MV				3	8.0	131 94
	CuZ*	MV				9		131
	CuZ	cyt *c*	6			0.03	5.6	94
A. cycloclastes	CuZ*	MV	14	25	163	166	6.8[a] 9.8[a]	119, 123
	CuZ*	MV				87		95
	CuZ*	Paz	29	19	89	114		123
P. aeruginosa	CuZ	BV				0.5		178
		BV	4	2		27[c]		
R. sphaeroides	CuZ*	BV	26[d]			63[d]	9.0	185
Hyphomicrobium denitrificans	CuZ	BV				45[e], 29[f]	8.8	96
A. xyloxidans	CuZ	MV				6		92

Notes: The specific activities reported as U mg^{-1} are referred to μmol_{N2O} min^{-1} $mg_{N2OR}{}^{-1}$.
[a]Values for the pK_a; [b]Specific activity determined after base activation at pH 9.8; [c]Specific activity determined after base activation at pH 10; [d]Specific activity determined at pH 9.0; [e]N_2OR with CuA oxidized and CuZ(4Cu2S) oxidized; [f]N_2OR with CuA reduced and CuZ(4Cu2S) reduced;.
CuZ is CuZ(4Cu2S) and CuZ* is CuZ*(4Cu1S); ED – electron donor; c_{552} – cytochrome c_{552} ; cyt *c* – Horse heart cytochrome *c*; Paz – Pseudoazurin; MV – methyl viologen; BV – benzyl viologen.

In single turnover experiments, an intermediate species was identified and named CuZ^o [148]. This intermediate species was observed after addition of a stoichiometric amount of N_2O to N_2OR, with CuA center reduced and CuZ*(4Cu1S) in the [$4Cu^{1+}$] state, with a lower limit for this re-oxidation being determined to be 200 s^{-1}, which is compatible with the turnover numbers found for the enzyme [160]. This is an intermediate species, whose activity is of the same order of magnitude as N_2OR with CuZ*(4Cu1S) in the [$4Cu^{1+}$] state [148]. Thus, this is the first catalytically competent oxidized form of "CuZ center" to be described. CuZ^o slowly decays to the resting CuZ*(4Cu1S) (k_{decay} ~ $5x10^{-3}$ s^{-1}) in the absence of external electron donors and substrate [148], as observed in those

single turnover experiments: the decay in activity is concomitant with the decrease in the CuZº absorption band at 680 nm, and associated with the increase in the 640 nm band, characteristic of the resting CuZ*(4Cu1S) [148, 167].

CuZº visible spectrum is characterized by a strong absorption band at 680 nm ($\varepsilon \approx 2000\ M^{-1}\ cm^{-1}$, identified after subtraction of CuA and CuZ(4Cu2S) contributions) (Table 1.3) [167]. Simultaneous fitting of MCD and absorption spectra allowed the identification of six transitions assigned as μ_4S^{2-}→Cu CT transitions, His→Cu CT transitions and also d→d transitions [167]. Two of the three transitions assigned as μ_4S^{2-}→Cu CT transitions, showed different relative intensities compared to those observed for the resting CuZ*(4Cu1S) [162, 167]. Furthermore, in the CuZº spectrum the transition corresponding to the spin delocalization onto Cu_I is lower relative to the transition corresponding to the spin delocalization onto Cu_{IV}, as opposed to what was observed in the resting CuZ*(4Cu1S), suggesting a more homogeneous copper spin distribution between Cu_I and Cu_{IV} in CuZº [162, 167].

The X-band EPR spectrum exhibits similar characteristics (*g*-values) to those determined for the [$1Cu^{2+}$-$3Cu^{1+}$] state (S = 1/2) of resting CuZ*(4Cu1S) (Table 1.3) [148]. The axial signal with $g_{\parallel} = 2.177 > g_{\perp} = 2.05 > 2.0$ indicates that the spin resides in the Cu d_{x2-y2} orbitals [148, 167]. A 6-line hyperfine pattern was identified in the $g_{\parallel}$ region and simulated with two equal hyperfine constants ($A_{\parallel}$= 4.2 mT), indicative, contrary to what was observed in the resting CuZ*(4Cu1S), of an unpaired spin equally distributed over the two copper atoms, confirming the analysis of the absorption and MCD spectra presented before [167]. In the resonance Raman spectra, upon excitation at 676 nm, an intense vibration and a weak shoulder were identified at 426 and 413 cm^{-1}, respectively, and assigned to Cu-S stretching vibrations [167]. Moreover, the vibration at 413 cm^{-1} showed a 3 cm^{-1} shift in solvent O^{18} isotope-sensitive and also a 36 % increase in intensity, predicting a ligand with an oxygen atom in the Cu_I-Cu_{IV} edge [167].

Two computational models were hypothesized for CuZº in *M. hydrocarbonoclasticus* N_2OR, one with a H_2O edge ligand and another with a OH^- coordinated terminally to Cu_{IV} and hydrogen bonded to K447 [167]. The spectral features of CuZº are only reproduced by the model with a OH^- coordinated terminally to Cu_{IV} (1.93 Å) and stabilized by a H-bond to the protonated lysine, which in turn strongly interacts with the negatively charged E485 residue [167]. The involvement of the CuZº and other intermediate species in the catalytic cycle is part of this study and the achievements will be further discussed in Chapter 5.

1.9 Aims

The last reaction of denitrification pathway is catalyzed by N_2OR, which reduces nitrous oxide a potent greenhouse gas and ozone depletion substance, to dinitrogen [14, 15, 17]. The catalytic center of

the enzyme has a completely distinct nature being a sulfide-bridged tetranuclear copper center and thus it has been a major subject of research in the bioinorganic field in the last 35 years.

The aim of this work (covered in Chapters 3 and 4) was to understand the effect of environmental acidification on the denitrification pathway. Transcriptomic, proteomic, spectroscopic and structural studies had been conducted to provide clues to explain why at low pH the denitrification is impaired, but the N_2OR is isolated with its catalytic center as CuZ*(4Cu1S), which in turn presents high specific activity *in vitro*. Understanding the relation between the pH and the form of N_2OR isolated is of prime importance to explain the possible molecular mechanisms involved in maintaining the *in vivo* ability of cells to reduce nitrous oxide and to develop strategies to mitigate the emission of N_2O when these mechanisms are affected.

The second main objective was to clarify the catalytic mechanism of reduction of nitrous oxide (covered on Chapter 5). Spectroscopic studies were performed to identify and characterize the intermediate species involved in the catalytic cycle and to evaluate if these intermediates are catalytically competent species, which is essential to understand the mechanism of this challenging enzyme. In addition, electrochemical and potentiometric studies were performed to investigate the reduction potential of the metal centers of N_2OR and its pH dependence, which was important to better understand the reactivity of this enzyme. Moreover, the reactivity of N_2OR redox centers with inhibitors was evaluated to understand their effect on the centers and provide insights into the substrate binding mechanism to the catalytic “CuZ center” (covered on Chapter 6).

Chapter 2

Materials and Methods

2 Materials and Methods

2.1 Materials

The chemicals used in this work were bought from Sigma, Merck, Panreac, Riedel-de-Haën and Fluka, unless otherwise stated. All these reagents were acquired in their highest grade commercially available and used without further purification.

In the assays with N_2O, a saturated water solution (25 mM at 25 °C [175]) was obtained from a gas stock mixture 5 % Ar/ 95 % N_2O (Air liquid). NO-saturated water solution (95.5 µM at 20 °C [186]) were prepared from a gas mixture of 95 % He/ 5 % NO (Air liquid).

Solutions of sodium dithionite and potassium ferricyanide were prepared in 100 mM Tris-HCl pH 7.6, while sodium ascorbate solutions were prepared in deionized water.

2.2 Bioinformatic analysis

Bioinformatic tools were used to analyze the deposited genome sequence of *M. hydrocarbonoclasticus* ATCC49840 [187], with the accession number NC_017067 (NCBI database: https://www.ncbi.nlm.nih.gov) and search for homologous genes encoding the catalytic subunits of denitrification enzymes, as well as their accessory factors. Identification of putative gene functions was performed by Blast search (https://blast.ncbi.nlm.nih.gov/Blast.cgi). Gene organization between different microorganisms and the encoded proteins were compared by multiple sequence alignments, using Clustal W2 (http://www.ebi.ac.uk/Tools/msa/clustalw2/) [188].

Prediction of signal peptides (Sec and TAT) were obtained from PrediSi, a tool of PRODORIC database (http://www.prodoric.de/) [189] and Pred-TAT (http://www.compgen.org/tools/PRED-TAT) [190].

The Virtual Footprint of PRODORIC database [189] was used to predict the FNR binding boxes in the promotor regions. The 200 bp region upstream from the initiation codon of each promoter were analyzed to detect putative binding sites and their scores for FNR, NarL and IHF, using the position weight matrices of FNR and IHF from *Escherichia coli* K12 and NarL from *Pseudomonas aeruginosa* PAO1.

The coordinates of N_2OR structures from *M. hydrocarbonoclasticus* (1QNI), *P. denitrificans* (1FWX), *A. cycloclastes* (2IWF), *S. denitrificans* (5I5I) and *P. stutzeri* (3SBQ, 3SBP and 3SBR) were obtained from the RCSB Protein Data Bank (PDB) (https://www.rcsb.org).

Protonation/deprotonation of amino acids in the protein environment was predicted by DEPTH server (http://cospi.iiserpune.ac.in/depth/) [191], using the structure obtained by X-ray crystallography and also the deposited structure of N_2OR from *P. stutzeri* (PDB ID: 3SBQ).

2.3 *M. hydrocarbonoclasticus* growth conditions

M. hydrocarbonoclasticus 617 cells were grown in artificial seawater (ASW) liquid medium containing 1.17 % w/v NaCl, 0.075 % w/v KCl, 0.3 % w/v NH_4Cl, 1.23 % w/v $MgSO_4.7H_2O$, 0.61 % w/v Tris(hydroxymethyl)aminomethane, 0.1 % w/v yeast extract and 0.12 % w/w sodium lactate [192]. The pH of the medium was adjusted to 7.5, with 37 % w/w HCl or to pH 6.5 or 8.5 to study the pH effect in the denitrification. The medium was sterilized by autoclaving 20 min at 120 °C. Prior to inoculation, the medium was supplemented with sterilized (0.2 µm filters) solutions of K_2HPO_4 (18.6 mg L^{-1} of culture), $CaCl_2.2H_2O$ (147 g L^{-1} of culture), $FeSO_4.7H_2O$ (1 mg L^{-1} of culture) and a Starkey oligoelement solution [193] (1 mL L^{-1} of culture).

Cultures, maintained in ASW agar plates, were used to inoculate 5 mL ASW liquid medium and were grown aerobically at 30 °C for 24 h at 210 rpm. The grown cultures were transferred (as 10 % of total volume) for subsequent increasing volumes (50 mL and then 500 mL) of new ASW liquid medium prior to flasks (50 mL) and bioreactor (2, 5 or 10 L) inoculation.

2.3.1 Growth in the bioreactor

The 2, 5 or 10 L bioreactor (Sartorius), operated in a batch mode, was supplemented with grown culture (10 % of total volume), 0.75 % w/v sodium lactate and 10 mM sodium nitrate used as electron acceptor. A low aeration rate (0.2 vvm) was maintained during the growth and a constant stirring (150 rpm) was kept during 5 h, and then lowered to 50 rpm until the end of the growth (48 h). The pH of the growing cultures was continuously controlled and automatically adjusted to pH 6.5, 7.5 or 8.5 with 1 M HCl and 1 M NaOH. The growth at each pH was performed at least in triplicate. Bacterial growth in the bioreactor was monitored by collecting small aliquots, from which optical density at 600 nm (OD_{600nm}) was measured. These aliquots were also used to quantify the expression of the genes encoding the catalytic subunits of the denitrification enzymes, as well as to determine the nitrite and nitrate levels and for the activity assays (see below).

The purity of the culture was evaluated in an optical microscope at the end of each growth. After 48 h of growth, cells were harvested by centrifugation (Beckman Avanti J-26 XPI) at 7930 *g* for 15 min. The pellet was resuspended in 50 mM Tris-HCl pH 7.6 (in a proportion of 1 g cells mL^{-1} buffer) and degassed by argon bubbling prior to its storage at - 80 °C.

2.3.2 Growth in sealed serum flasks

The influence of pH was also analyzed in the absence of aeration using 100 mL serum flasks (pH 6.5 and 7.5), sealed with a rubber septum and aluminum caps containing 50 mL AWS liquid medium, supplemented as described above. The aerobically grown inoculum was transferred (10 % of total volume) with a syringe to the gas-tight flasks. Similar conditions to the bioreactor growth were used with the following modifications: there was no aeration during the growth and the

cultures were stirred in a shaker. Additionally, for the growths performed at pH 6.5, the pH was manually adjusted (pH variation between 6.5 and 6.9), while in the growths performed at pH 7.5, the pH was only monitored but not adjusted (pH variation between 7.30 and 7.65).

At each time-point, the cell densities were measured at 600 nm on a spectrophotometer (Shimadzu UV 160U), nitrate and nitrite were quantified and the rates of nitric and nitrous oxide reduction by the whole-cells were measured and analyzed (see below).

2.4 Nitrate and nitrite quantification

Nitrate and nitrite quantifications during the growth of *M. hydrocarbonoclasticus* were performed using the Nitrate/Nitrite Assay Kit (Sigma), according to the manufacturer's instructions. This method involves two separated reactions, one to detect nitrite and another for detection of both nitrate and nitrite [194]. For colorimetric detection of these metabolites, two standard curves were prepared, one with nitrate and other with nitrite, in a concentration range of 0 to 100 µM. The culture sample was centrifuged at 1000 *g* for 15 min, to remove the insoluble material and 100 µL of the remaining solution were disposed in a 96 well plate for nitrite detection. In parallel, for nitrate and nitrite detection, 10 µL of nitrate reductase together with 10 µL of the enzyme co-factors were added to 80 µL of culture solution. The plate was incubated at RT for 2 h and then 50 µL of Griess reagent A (sulfanilamide, prepared in acid solution) were added to each well followed by an incubation of 5 min. Lastly, 50 µL of Griess reagent B (1-naphthylethylenediamine, prepared in acid solution) were added to each well and incubated for 10 min, allowing the formation of a azo coupling between diazonium species. The absorbance was measured at 540 nm in a VersaMax ELISA Microplate Reader using the SoftMax Pro 6.4 software.

2.5 Nitric oxide and Nitrous oxide reduction by whole-cells

Whole-cell activity assays for nitric oxide and nitrous oxide reduction were performed inside an anaerobic chamber (MBraun) filled with argon gas (O_2 < 3 ppm).

Assays for nitric oxide reduction were performed with constant stirring, by adding 40 µL of *M. hydrocarbonoclasticus* cell suspension to a quartz cuvette already containing 120 µM methyl viologen and 60 µM sodium dithionite in 100 mM Tris-HCl pH 7.6 (in a final volume of 1 mL). The nitric oxide reduction assay was initiated with the addition of 100 µL NO-saturated water (to a final concentration of 9.6 µM).

A similar assay was prepared for nitrous oxide reduction assay, but with 100 µM methyl viologen and 50 µM sodium dithionite in 100 mM Tris-HCl pH 7.6 (in a final volume of 1 mL), with the reaction initiated immediately (also without any further incubation) with the addition of 50 µL N_2O-saturated water, to a final concentration of 1.25 mM (Figure 2.1). The assays were measured

spectrophotometrically, following the oxidation of reduced methyl viologen monitored at 600 nm in a diode array spectrophotometer (Agilent 8453).

The measured activity was indirectly calculated as micromoles of NO or N_2O reduced per minute per optical density ($\mu mol_{NO\ or\ N2O}\ min^{-1}\ cell^{-1}$) (see Section 2.5.1).

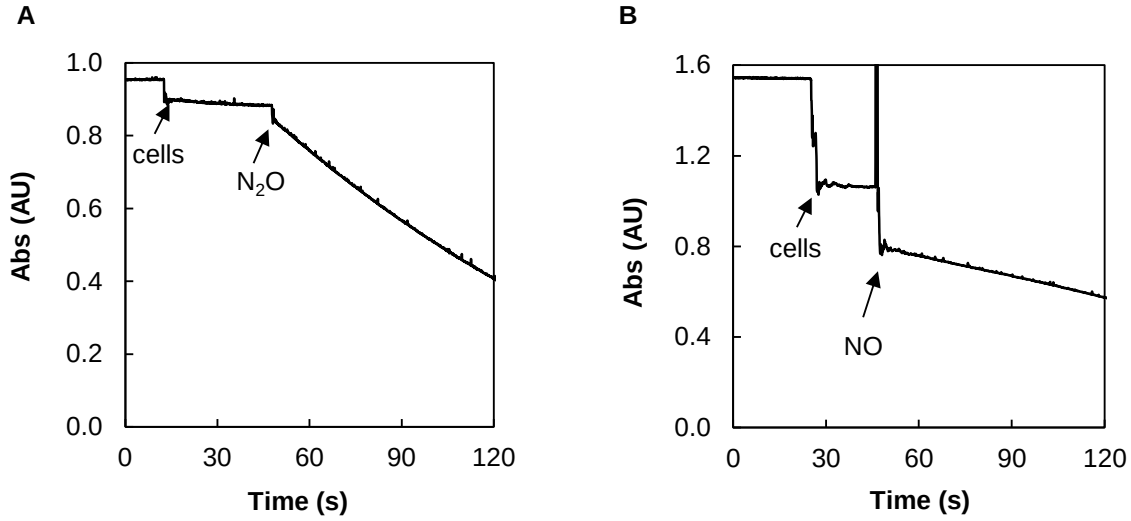

Figure 2.1 - Kinetic traces of N_2O and NO reduction assay by whole-cells, using methyl viologen as electron donor. In the assays, 40 µL of *M. hydrocarbonoclasticus* cell suspension (in a total volume of 1 mL) were added to a solution containing 100 µM (in the case of N_2O assay) or 120 µM (in the case of NO assay) of reduced methyl viologen in 100 mM Tris-HCl pH 7.6, followed by addition of (A) 1.25 mM N_2O-saturated water or (B) 9.6 µM NO-saturated water. The arrows indicate the addition point of cells and substrates.

2.5.1 Data analysis – NO and N_2O reduction by whole-cells

The rate of NO and N_2O reduction by whole-cells was indirectly measured through oxidation of methyl viologen. In the curve obtained, linear regressions were used to fit regions immediately before and after substrate addition. The slope of the fitting before substrate addition was subtracted to the slope obtained after substrate addition. The rates were determined taking into consideration the calculated slope and the extinction coefficient of methyl viologen (ε = 11.4 $mM^{-1}\ cm^{-1}$), determined at 600 nm [175]. We also consider that methyl viologen re-oxidation requires one electron while N_2O reduction involves two electrons and the reduction of two molecules of NO involves two electrons.

Note that in this assay, the subtraction of the slope prior to the addition of substrate is particularly important as other enzymes might also use the reduced methyl viologen, causing partial oxidation even before the addition of substrate.

As mention above, rates of NO and N_2O reduction were reported as micromoles of NO or N_2O reduced per minute per optical density ($\mu mol_{NO\ or\ N2O}\ min^{-1}\ cell^{-1}$).

2.5.2 Kinetic parameters for the N_2O reduction by whole-cells

The dependence of N_2O in the reduction rate by whole-cells was performed in a 1 mL quartz cuvette, containing 100 μM methyl viologen and 50 μM sodium dithionite in 100 mM Tris-HCl pH 7.6, to which 3 μL of cells was added (containing 0.09 mg of total protein), collected by centrifugation at the end of the growth performed at pH 7.5 in a bioreactor. The assay was initiated by the addition of 20, 40, 80, 120, 250 and 752 μM of N_2O-saturated water. Triplicates for each substrate concentration were performed. Activities were calculated as described above (see Section 2.5.1), but reported as μmol_{N2O} min^{-1} mg^{-1} of total protein (determined using the Pierce™ 660nm protein assay, Section 2.9.1). The parameters K_m and V_{max} were calculated by fitting the curve with Michaelis-Menten kinetics (Equation 2.1):

$$v = \frac{V_{max} \times [S]}{K_m + [S]} \quad (2.1)$$

2.6 Quantification of gene expression and cotranscriptional analysis of *nos* cluster

2.6.1 Nucleic acid extraction and cDNA generation

RNA, from samples of bioreactor cultures taken at different time-points, was isolated using the Isolate II RNA mini kit (Bioline), according to manufacturer's instructions. Genomic DNA contamination was removed by on-column digestion with DNase I, supplied with the kit. RNA yields were determined at 260 nm and purity was estimated by determining the A_{260nm}/A_{280nm} and A_{260nm}/A_{230nm} ratios. To generate cDNA, 500 ng of each RNA sample was reversely transcribed using the SensiFAST cDNA Synthesis Kit (Bioline), using the following conditions: 10 min at 25 °C, followed by 15 min at 42 °C and 5 min at 85 °C (for enzyme inactivation). cDNAs were diluted (1:100) and stored at - 80 °C until further use. DNA used in standard curves was extracted from a sample of the bioreactor culture taken during the exponential phase, using the Isolate II Genomic DNA Kit (Bioline), according to the manufacturer's instructions.

2.6.2 Quantitative Real-Time PCR

Expression of *M. hydrocarbonoclasticus* genes involved in the denitrification pathway - *narG*, *nirS*, *c-norB* (*MARHYR3054*), *q-norB* (*MARHY3014*), *nosZ*, *nosR*, *nosD*, *nosL*, *senC*, *MARHY1049*, *MARHY1380*, *MARHY1479* - was analyzed by quantitative real-time PCR (qPCR). Reactions were performed using SensiFAST™ SYBR No-ROX Kit (Bioline) with specific primers for each gene at 250 nM (Table 2.1) and 3 μL of cDNA. Gene expression levels were determined using the relative standard curve method [195], which uses standard curves to interpolate unknown quantity values from a sample. This was performed using DNA standard curves, as previously described [196]. Briefly, for each target, as well as for the control (16S rRNA), a standard curve was

generated using serial dilutions of genomic DNA. The amount of cDNA of each target and control gene, present in every sample, was determined from their respective DNA standard curve, through conversion of the obtained threshold cycle (C_t) value [195, 196]. Relative normalized expression values were then obtained by dividing the values for each target gene by the values for the control gene (*16S rRNA*). Several housekeeping genes that have been described for other bacteria as stable endogenous controls for quantitative gene expression were also tested (*gyrA*, *proC*, *recA*, *rpoD*, data not shown) [197-199], but did not provide stable results. Thus, the housekeeping 16S *rRNA* gene was used as endogenous control as its expression remained relatively stable, during the different growth phases (data not shown). This gene has been commonly used as the control gene for qPCR in many studies [200-202]. Primers were designed using Primer3 software [203] (Table 2). "No template" and "RT minus" (a reverse transcription reaction containing all reagents except the reverse transcriptase enzyme) controls were also included in every PCR assay. Reactions were run in duplicate in a Corbett Rotor-Gene instrument (Qiagen) using the following thermal cycling conditions: 95 °C for 5 min followed by 40 cycles of 95 °C for 15 s and 60 °C for 30 s. Analysis of melting curves generated by the stepwise increase of the temperature from 60 °C to 95 °C, were used to verify the specificity of the amplified products. Three biological replicates were analyzed but not at the exact same time points, thus a single representative experiment is shown (similar results were obtained for the other replicates).

Table 2.1 - Primers used for qPCR analysis of the denitrification genes in *M. hydrocarbonoclasticus*, and some of the accessory genes associated with N_2OR.

Gene	Primer	Sequence (5'-3')
narG	narG_F narG_R	ATCCACGCCCAGTTTCTC CCACCTCCTTCTTCTATGCTC
nirS	nirS_F nirS_R	GCGATGAAGTGTGGTTCTCT AACGATGGCGGATTTCTTGT
c-norB (*MARHY3054*)	norB2_F norB2_R	AGAAGCCCAGACCGAACT GCGAACACCCAGAACAGAAT
q-norB (*MARHY3014*)	norB_F norB_R	GCTGAATACGACACCCACTC CCAGGAAGCCATAAACACCA
nosZ	nosZ_F nosZ_R	CGGCAGGAAACGGTCTTT CTGATGGCAAATGGCTGGT
nosR	nosR_F nosR_R	ACAGAAGCCGAAGATGATGC TGTAAACCAGGAAGCCGTG
nosD	nosD_F nosD_R	GACTACCTGGGCTGGGAT TCGGTTCATAAGGCACATCG
nosL	nosL_F nosL_R	CTTTACCGAGCGAGAACAGA TGTCTTTGGTGGAGCAGAAT
senC	senC_F senC_R	CGAGGAAGGTGAGACGGT CCCACGAACACGAAGGTC
MARHY1049	1049_F 1049_R	GGTTGAGGGCGAGAAAGT CAGGTCTTCGGCACCATC
MARHY1380	1380_F 1380_R	GTGAATCTCTGGGGGTTTGG TTCATCGTCGGAGGGTATCT
MARHY1479	1479_F 1479_R	ATACTCCGACACGGCAATG TCATCAGCCCAGAACTCAAG
16S rRNA	16S_F 16S_R	CCACTACCCTCTACCACACT TAACCTGGGAACGGCATTT

2.6.3 Cotranscriptional analysis of *nosRZDFYL*

From a sample collected during the exponential phase of *M. hydrocarbonoclasticus* growing in a bioreactor performed at pH 7.5, 2 µg of total RNA were used to generate cDNA (as described in Section 2.6.1).

To determine if *nosRZDFYL* is composed of a single transcriptional unit, PCR reactions were performed using 6 µL of generated cDNA and NZYTaq DNA polymerase (Nzytech) with primers that would amplify regions between *nosR* and *nosZ* (nosR_F/nosZ_R), *nos*Z and *nosD* (nosZ_F/nosD_R) and *nosD* to *nosL* (nosD_F/nosL_R) (Table 2.1). Amplification products and also controls (genomic DNA and RT minus reaction) were analyzed in an agarose (1 %) gel electrophoresis, run at 100 V for 20 min and staining with SYBR® Safe solution (Invitrogen).

2.7 Proteomic analysis of membrane fractions

The *M. hydrocarbonoclasticus* cells were harvested from the growth performed at pH 6.5 and 7.5 in the bioreactor, diluted 5 times and homogenized in the presence of DNAse I endonuclease (Roche) and protease inhibitor cocktail (EDTA free cOmplete™ Protease Inhibitor, Roche). The cells were lysed in a french press (Thermo-FA-080A) at 1200 psi and then centrifuged (Beckman Avanti J-26 XPI) at 3000 *g* for 30 min at 4 °C. The cell debries were discarded and the supernatant was ultracentrifuged (Beckman Coulter Optima LE-80k centrifuge) at 185000 *g* for 1 h at 4 °C to separate the soluble and membrane fractions. The membrane fractions obtained from each growth were resuspended in 10 mM Tris-HCl pH 7.6.

2.7.1 Sample preparation for 2D gel

The membrane fractions (obtained from the growth performed at pH 6.5 and 7.5) were precipitated with trichloroacetic acid (TCA) in a 1:1 ratio followed by 30 min incubation on ice. Then, this sample was centrifuged (Hermle Z32HK) at 9290 *g* 15 min at 4 °C and the supernatant was discarded. The pellet was washed with ice-cold acetone and centrifuged again at 12850 *g* for 5 min at 4 °C to ensure that all TCA was removed. The supernatant was discarded and the pellet was left to dry.

The protein pellet was solubilized in a rehydration solution containing 7 M urea, 2 M thiourea, 2 % w/v CHAPS, 1 % v/v IPG buffer (GE), 0.002 % w/v bromophenol blue and 0.28 % w/v dithiothreitol (DTT). The total protein content was determined by the Pierce™ quantification kit (Thermo scientific) (see below, Section 2.9.1). The 7 cm imobiline dry strips (GE), with a pH range 3-10 non-linear or in the 4-7 range, were rehydrated with 80 μg of the solubilized protein sample for 16 h.

2.7.2 Two-Dimensional gel electrophoresis

An Ettan IPGphor 3 unit (GE) was used for the electric focusing. A four-step program (step 1 - 1 h and 30 min at 300 V, step 2 – 30 min in a voltage gradient up to 1000, step 3 – 1 h and 30 min in a voltage gradient up to 5000 V and step 4 - 1 h and 30 min at 5000 V) were run for 5 hours in a total of 12.8 kV. The strips were removed and equilibrated in two steps before the second dimension. An equilibrium solution containing 6 M urea, 0.05 M Tris-HCl pH 8.8, 30 % v/v glycerol, 2 % w/v SDS and 0.002 % w/v bromophenol blue was used in the first step with addition of 10 mg mL^{-1} DTT and shaked during 10 min followed by a similar second step containing 25 mg mL^{-1} iodoacetamide (Amersham) instead of DTT.

For the second-dimension, the equilibrated strip was applied on top of a 10 % SDS-PAGE. The gel was sealed with 1 % w/v agarose in the electrophoresis running buffer, containing 0.025 M Tris-HCl, 0.192 M glycine, 0.2 % w/v SDS and 0.02 % w/v bromophenol blue. The gel ran at a

constant voltage of 80 V for 15 min, followed by 150 V for 45 min. The gel staining was performed overnight with colloidal Coomassie blue solution containing 5 % w/v aluminium sulfate, 10 % v/v ethanol, 0.02 % w/v colloidal bromophenol blue G250 and 2 % v/v ortophosphoric acid. For distaining a solution of 10 % v/v ethanol and 2 % v/v ortophosphoric acid was used.

2.7.3 Gel analysis

Gels were digitalized in an ImageScanner (GE) and analyzed using the ImageMaster 7.0 software (GE). The spots were identified and compared between gels of the membrane fraction at different pH growth, in terms of matching (showing different relevant intensity) and differential spots.

2.8 Isolation of nitrous oxide reductase and its physiological redox partner

2.8.1 Nitrous oxide reductase

N_2OR was isolated in the presence or in the absence of oxygen (in an anoxic chamber, 2 % H_2 in Ar atmosphere, Coy Labs), since differences in the "CuZ center" content were attributed to prolonged exposure of the enzyme to oxygen [21, 24, 132].

Each purification step was monitored through UV-visible spectroscopy and by 12.5 % SDS-PAGE (staining with Coomassie blue and for heme proteins [204]) to evaluate N_2OR purity.

Spheroplasts were prepared with the cells collected from each bioreactor growth. To the cell suspension, under stirring, DNAse I (Roche) and protease inhibitors (EDTA free cOmplete™ Protease Inhibitor, Roche) were added followed by cold dH_2O (5 times over total cells volume). Then, EDTA was added (to a final concentration of 0.5 mM) and the suspension was incubated under stirring for 30 min at RT. Periplasmic and cytoplasmic fractions were separated by centrifugation at 32816 *g* for 1 h in a Beckman Coulter centrifuge (Avanti J-26 XPI). N_2OR was further isolated from the periplasmic fractions (Figure 2.2).

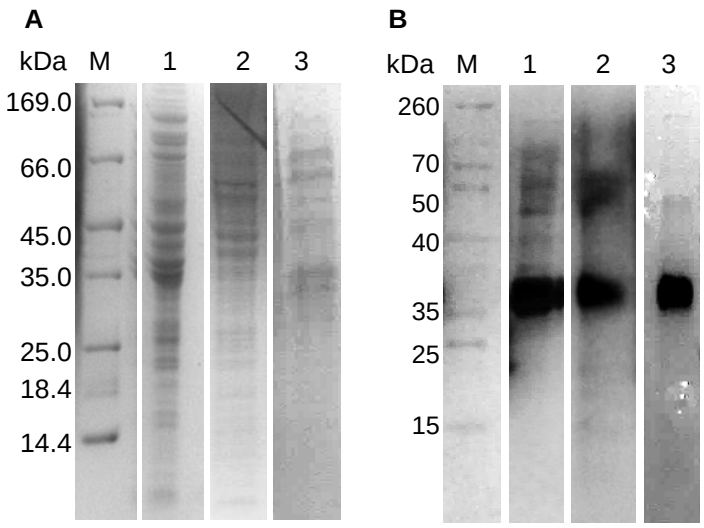

Figure 2.2 - SDS-PAGE (12.5 % polyacrylamide) analysis of periplasmic fractions obtained from *M. hydrocarbonoclasticus* growths in bioreactor at different pH values, Coomassie blue stained (A) and heme stained (B). Lanes M - marker, 1 – growth at pH 6.5, 2 – growth at pH 7.5, 3 – growth at pH 8.5. The gels were run for 1 h at 150 V.

The resulting periplasmic extract was loaded onto an anionic exchange DEAE FF column (Ø 2.6 cm x 14 cm, GE), previously equilibrated with 10 mM Tris-HCl pH 8.0. After washing out the unbound proteins, a linear gradient, from 0 to 300 mM NaCl in 10 mM Tris-HCl pH 8.0, was applied during 200 min at 3 mL min^{-1} to elute the bound proteins. The fractions containing N_2OR, eluted with approximately 200 mM NaCl, were combined and dialyzed overnight against 10 mM Tris-HCl pH 8.0 or diluted 10 times with 10 mM Tris-HCl pH 8.0 (dilution is used when the purification was performed under anoxic conditions). As second purification step, an anionic exchange Source 15Q chromatographic column (Ø 2.6 cm x 13 cm, GE) or as alternative a HitrapQ FF chromatographic column of similar dimensions was used, equilibrated with 10 mM Tris-HCl pH 8.0 at 2 mL min^{-1}. N_2OR was eluted with an increasing ionic strength step gradient, from 0 to 300 mM NaCl in 10 mM Tris-HCl pH 8.0 over 180 min. The N_2OR-containing fractions were combined and concentrated under argon atmosphere at 4 ºC, using a Vivacell (Sartorius) apparatus with a YM30 membrane. When necessary, an additional step was performed, in which the N_2OR fraction was loaded onto a Superdex 200 column (GE) equilibrated with 50 mM Tris-HCl pH 8.0, 150 mM NaCl. Purified N_2OR fractions were immediately frozen in liquid nitrogen in the form of little spheres and stored also in liquid nitrogen until further use. Analysis of the fractions obtained after each chromatographic step in a SDS-PAGE gel is exemplified in Figure 2.3.

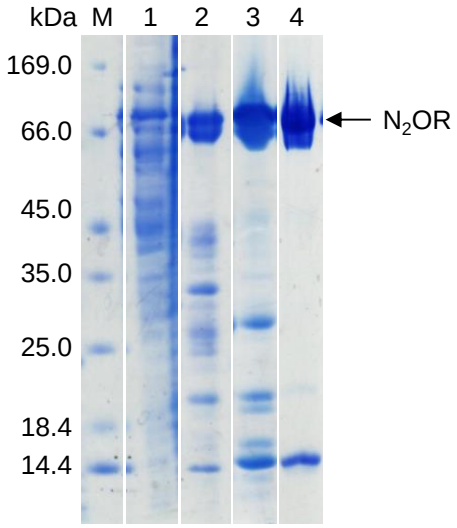

Figure 2.3 - SDS-PAGE (12.5 % polyacrylamide) of the fractions obtained after each chromatographic step of N_2OR purified under anoxic conditions, from a *M. hydrocarbonoclasticus* growth performed at pH 7.5. Lanes M - marker, 1 - periplasm, 2 – fraction after DEAE FF, 3 – fraction after Hitrap Q FF, 4 – fraction after Superdex 200. The gel ran for 1 h at 150 V and was stained with Coomassie blue.

2.8.2 Cytochrome c_{552}

Cytochrome c_{552}, present in the periplasm, has a pI near 7, and therefore lower affinity to an anionic exchange DEAE FF column equilibrated with 10 mM Tris-HCl pH 8.0, coming out in the flow-through. The unbound proteins from this column were collected and concentrated using a Vivacell (Sartorius) apparatus over a YM5 membrane, at 4 ºC under argon atmosphere. The concentrated fraction was loaded onto a Superdex 75 column (10/600 GL, GE) equilibrated with 50 mM Tris-HCl pH 7.6, 150 mM NaCl. The fractions of pure cytochrome c_{552} were combined based on a high purity ratio (Abs_{410nm}/Abs_{280nm}), above 5.8.

Pure fractions were loaded onto a PD-10 desalting column (GE) equilibrated with 20 mM Tris-HCl pH 7.6, for buffer exchange and then divided into small aliquots and stored at - 80 ºC. The concentration of cytochrome c_{552} was determined spectrophotometrically, based on the ascorbate reduced spectrum (Figure 2.4), using the extinction coefficient at 552 nm ($\varepsilon = 19.3\ mM^{-1}\ cm^{-1}$ [205]).

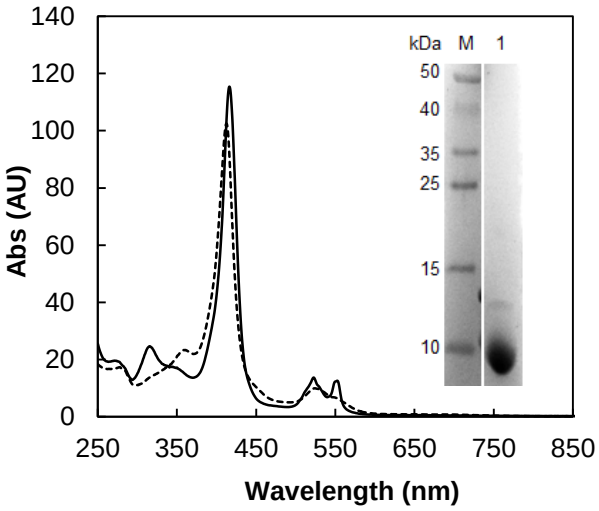

Figure 2.4 - UV-visible spectra of cytochrome c_{552} (3.6 µM) as prepared (dashed line) and reduced with sodium ascorbate (solid line). Insert: SDS-PAGE (12.5 % polyacrylamide) of the purified cytochrome c_{552} (lane 1), stained with Coomassie blue.

2.9 Analytic methods used in nitrous oxide reductase studies

2.9.1 Determination of total protein concentration

Total protein content was measured by the modified Lowry method [206] or when referred, by the Pierce™ 660nm protein assay reagent (Thermo Scientific).

Lowry method combines two reactions: the copper reduction ($Cu^{2+} \rightarrow Cu^{1+}$) by the protein at an alkaline pH (biuret reaction) and the formation of a complex between Cu^{1+} and the protein in the presence of Folin-Ciocalteau reagent, exhibiting an absorption maximum at 750 nm. Briefly, 100 µL of protein were incubated with 400 µL Biuret solution for 10 min and then, 3.5 mL of 2.3 % w/v sodium carbonate was added followed by 100 µL of Folin-Ciocalteau commercial solution. The mixture was incubated for 30 min and the absorbance measured at 750 nm in a spectrophotometer (Shimadzu UV-160A). Bovine serum albumin was use as standard, in a concentration range between 0 and 0.3 mg mL^{-1}.

Pierce™ 660nm protein assay reagent was used for samples containing reducing agents or to quantify samples with small volumes. This method consists in addition of 150 µL of Pierce™ reagent to a 10 µL of protein sample and bovine serum albumin standards (concentration range between 0 and 0.3 mg mL^{-1}) followed by incubation of the mixture for 5 min at RT. After that time, absorbance was measured at 600 nm in a nanodrop (Thermo Scientific).

2.9.2 Sulfide determination

Labile sulfur was determined aerobically based on methylene blue formed in the presence of S^{2-} [207]. In short, 100 µL of purified protein (8 µM), in 20 mM Tris-HCl pH 8, were incubated with 10 µL

of 50 mM N,N-dimethyl-p-phenylenediamine oxalate in 7.2 M HCl followed by addition of 10 µL of 100 mM $FeCl_3$ in 1.2 M HCl. The samples were incubated for 20 min to allow the formation of methylene blue and then centrifuged (5 min at 14000 *g*) to remove the precipitated protein. The methylene blue, formed in the presence of sulfide, was measured at 667 nm. A fresh solution of $Na_2S.9H_2O$ was used as standard (concentration range between 0 and 50 µM) and evaluated using the same protocol.

2.9.3 Copper quantification

Copper content was determined following a modified protocol of Hanna *et al.* [208]. In this method, the Cu (I) forms a complex with 2, 2'-biquinoline in an acetic acid medium.

A sample of 100 µL of N_2OR was mixed with 300 µL of 20 mM sodium ascorbate (freshly prepared in 100 mM potassium phosphate at pH 6.0) and incubated for 30 min at RT. Then, 600 µL of 2,2'-biquinoline solution (0.5 mg mL^{-1}), prepared in glacial acetic acid, was added. The samples were incubated for 10 min prior to the measurement of the absorbance at 546 nm. A solution of copper (II) acetate, prepared in deionized water, was used as standard for the construction of a calibration curve, between 0 and 24 µM and used to determine the copper concentration in N_2OR.

Copper content was also frequently determined by Inductively Coupled Plasma emission analysis (ICP) in a Jobin-Yvon (Ultima) instument. ICP 23multielements (Reagecom) standard were prepared in a concentration range of 0 to 3 ppm. ICP analysis was performed as an internal service in LAQV – Atomic emission spectroscopy, Faculty of Sciences and Technology – Nova University of Lisbon.

2.10 Spectroscopic methods

2.10.1 Visible spectroscopy

The visible spectra of different isolated forms of N_2OR from *M. hydrocarbonoclasticus* were recorded on a UV-1800 spectrophotometer (Shimadzu). Each purified N_2OR sample was reduced with either 100 mM sodium ascorbate, 200 mM sodium dithionite or oxidized with a solution of 10 mM potassium ferricyanide.

N_2OR concentration was recurrently determined spectrophotometrically, as it was rather difficult to have a pure protein sample (see Figure 2.3). Determination of the concentration was based on the extinction coefficient of the "CuZ center" of each sample, previously determined as 3.5 mM^{-1} cm^{-1} for CuZ*(4Cu1S) at 640 nm, in its sodium dithionite reduced form [91]. The extinction coefficient of a sample with 10 % of "CuZ center" as CuZ*(4Cu1S) was estimated in this work as 4.0 mM^{-1} cm^{-1}, at 670 nm also for the sodium dithionite reduced spectra. This estimate was based on the total protein content determined by modified Lowry method, and the copper content determined by

2, 2'-biquinoline method (see Section 2.9). Note that all values of N_2OR concentration along this thesis are referred to the monomeric form.

2.10.2 Electron Paramagnetic Resonance spectroscopy

EPR tubes containing N_2OR (~ 150 µL at 200 µM) purified from the *M. hydrocarbonoclasticus* growths performed at pH 6.5, 7.5 and 8.5 were incubated with 10 mM potassium ferricyanide, 100 mM sodium ascorbate, 500 mM sodium dithionite and methyl viologen under anaerobic conditions.

The EPR spectra of each sample were recorded on a X-band Bruker EMX spectrometer equipped with a rectangular cavity (model ER 4102T) and an Oxford Instruments continuous liquid helium flow cryostat, operating at 30 K. Experimental conditions were as follows: microwave frequency, 9.65 GHz; microwave power, 2 mW; gain, $1x10^5$.

2.10.2.1 Spin quantification

The spin of each sample was quantified relative to the sodium dithionite reduced sample, assuming a spin of 1 in that condition, as previously described in [91, 132].

Briefly, the area of each EPR spectra, obtained for the different oxidation states, was integrated (using the second derivative spectrum) and related to the integrated area of sodium dithionite reduced spectra of each preparation. In the dithionite reduced sample, CuA center is reduced being EPR silent, while the "CuZ center" is in the redox state [$1Cu^{2+}$-$3Cu^{1+}$] containing one unpaired electron and therefore we assume a total spin of 1 for this sample. Spin quantification of other redox forms were related to this sample.

As an example, a sample with 100 % of "CuZ center" as CuZ*(4Cu1S) has a total spin of 1 in its reduced form (with either sodium ascorbate or sodium dithionite), and a total spin of 2 in its fully oxidized state (CuA center and "CuZ center" having one unpaired electron each).

2.11 Steady-state kinetics

All the procedures to activate N_2OR and the N_2O reduction assays were performed inside an anaerobic chamber (MBraun) at RT and monitored by oxidation of the redox mediator present, using a TIDAS diode-array spectrophotometer.

2.11.1 Enzyme activation and activity assay in the presence of reduced methyl viologen

Initially, the effect of time of incubation with methyl viologen in the activation of N_2OR was tested. N_2OR (70 nM) was incubated for 600 min in the presence of 100 µM reduced MV in 100 mM Tris-HCl pH 7.6. During the incubation time, samples of 950 µL of the mixture were taken

and reacted with 1.25 mM N_2O in a stirring quartz cuvette. The oxidation of methyl viologen was followed at 600 nm as previously describe by Dell'Acqua *et al* [122].

In most of the assays performed, the maximum specific activity of N_2OR was observed after 3 h incubation (Figure 2.5). All the following activation assays were performed with at least 3 h incubation under these conditions.

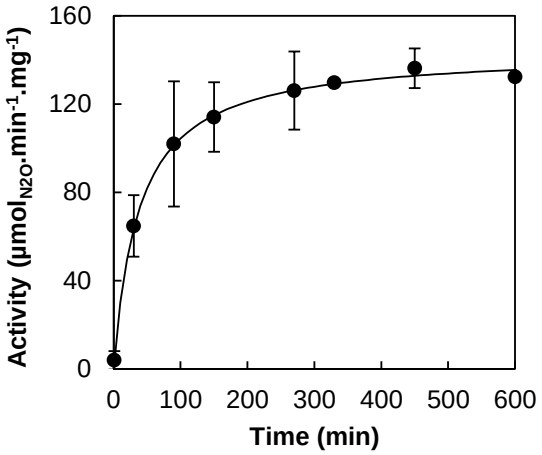

Figure 2.5 – Specific activity of N_2OR, with 65 % of "CuZ center" as CuZ*(4Cu1S), as a function of incubation time with reduced MV as electron donor. N_2OR (70 nM) from *M. hydrocarbonoclasticus* was incubated in the presence of 100 µM MV and 50 µM sodium dithionite in 100 mM Tris-HCl pH 7.6. Each reaction was initiated by the addition of 1.25 mM N_2O-saturated water and followed at 600 nm.

Therefore, in the activity assays, N_2OR (70 nM) was incubated in the presence of 100 µM reduced MV in 100 mM Tris-HCl pH 7.6 for 3 h. The reaction was initiated by the addition of 1.25 mM N_2O (Figure 2.6). An identical assay, but without pre-activation of the enzyme with MV, was also performed for the protein isolated from each batch (Figure 2.6).

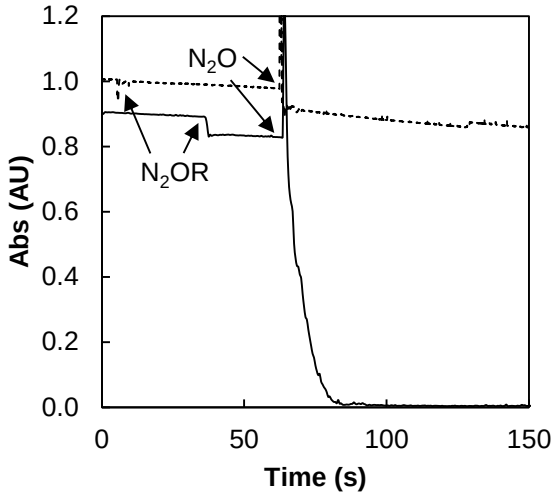

Figure 2.6 - Example of steady-state kinetic traces of N_2OR using reduced MV as electron, with its oxidation followed at 600 nm. The reactions were initiated by the addition of 1.25 mM N_2O-saturated water. The arrows indicate the addition point of N_2OR and N_2O. Kinetic traces with pre-activated N_2OR are represented by a solid line and traces with N_2OR without prior incubation by a dashed line.

Specific activity was indirectly calculated, because N_2O or N_2 are not measured, (see Section 2.11.4) and reported here as $\mu mol_{N2O}\ min^{-1}\ mg^{-1}{}_{N2OR}$.

The specific activity of the pre-activated enzyme (after 3 h incubation with reduced MV) was performed for each preparation and can be related with its percentage of CuZ*(4Cu1S). This relation was established through the combination of specific activity and EPR spin quantification (see section 2.10.2.1) of a sample containing the highest amount of CuZ*(4Cu1S) observed so far. Thus, this N_2OR sample with 100 % of "CuZ center" as CuZ*(4Cu1S) has a specific activity of ~ 200 $\mu mol_{N2O}\ min^{-1}\ mg^{-1}{}_{N2OR}$. Considering this relation, the percentage of CuZ*(4Cu1S) in other preparations was extrapolated from the specific activity calculated (see Section 2.11.4) and reported for each assay performed.

2.11.2 N_2OR activation

Activity assays of N_2OR with ascorbate or cytochrome c_{552} were performed in the absence of MV. In these assays, N_2OR (60 µM) were reduced with 100 equivalents of reduced MV in 100 mM Tris-HCl pH 7.6 for 3 h and desalted into 100 mM Tris-HCl pH 7.6 with a NAP-5 Sephadex G-25 column (GE).

2.11.3 Activity assay in the presence of cytochrome c_{552}

The N_2OR activity was also investigated in the presence of its physiological redox partner, cytochrome c_{552}. The reduction of cytochrome c_{552} (400 µM) was performed under the presence of oxygen incubating the protein with 5 mM sodium ascorbate for 5 min, followed by desalting in a PD-10 Sephadex G-25 column (GE) equilibrated with 100 mM Tris-HCl pH 7.6. Afterwards it was placed inside an anaerobic chamber. Concentration of the reduced cytochrome was determined spectrophotometrically as previously described in Section 2.8.2.

The activity assay was performed using a stirred cuvette already containing 10 µM cytochrome c_{552} in 100 mM Tris-HCl pH 7.6 and 1.25 mM N_2O-saturated water, and initiated by addition of 70 nM of pre-activated N_2OR, with 25 % or 90 % of "CuZ center" as CuZ*(4Cu1S) (Figure 2.7). The reaction progress was monitored at 552 nm and the activity determined (see Section 2.11.4).

Additionally, a non-activated 50 µM N_2OR, with 10 % of "CuZ center" as CuZ*(4Cu1S), was reduced with 5 mM sodium dithionite for 1 h and desalted using a NAP-5 Sephadex G-25 column (GE) equilibrated with 100 mM Tris-HCl pH 7.6. Dithionite reduced N_2OR (70 nM) was added to a stirring cuvette containing 7 µM cytochrome c_{552} and 1.25 mM N_2O. The reaction progress was monitored for 3 h at 552 nm and the activity determined (see Section 2.11.4). In the end of the assay, potassium ferricyanide was added to fully oxidize the cytochrome c_{552}.

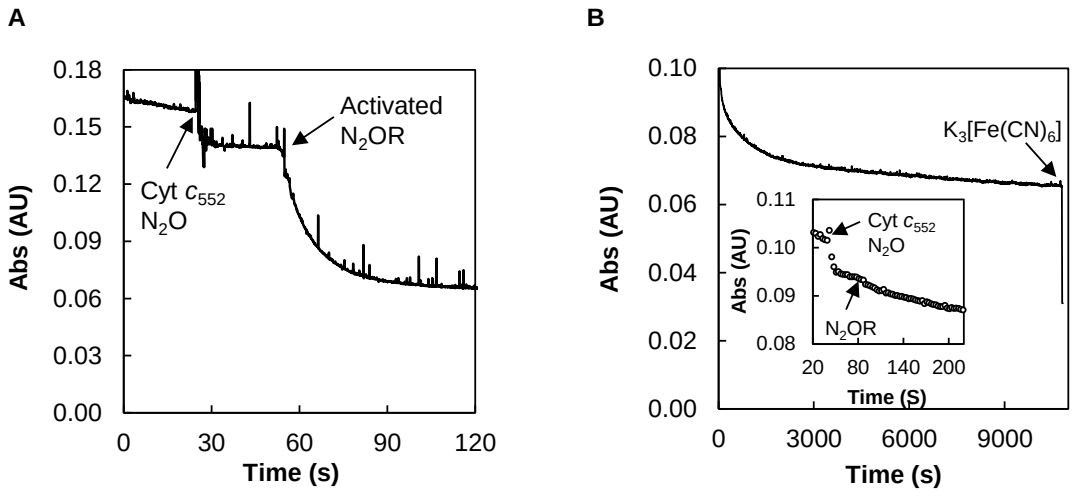

Figure 2.7 - Example of steady-state kinetic traces of N_2OR in the presence of physiological redox donor (cytochrome c_{552}), followed at 552 nm. (A) Activity assay initiated by 70 nM activated N_2OR, with 90 % of "CuZ center" as CuZ*(4Cu1S), in a cuvette containing 1.25 mM N_2O and 10 µM cytochrome c_{552}. (B) Activity assay initiated by dithionite-reduced N_2OR, with 10 % of "CuZ center" as CuZ*(4Cu1S) in a cuvette containing 1.25 mM N_2O and 7 µM cytochrome c_{552}. Insert: Absorbance in the initial seconds (20 - 220 s) evidencing the addition of N_2OR. The arrows indicate the addition of N_2OR, cytochrome c_{552} and N_2O.

2.11.4 Data analysis – Reduction rates of N_2O

Similarly to rates of N_2O reduction by whole-cells, specific activity of N_2OR is also indirectly measured through the oxidation of the reduced methyl viologen or cytochrome c_{552}. Curve progression immediately after the addition of substrate was analyzed and fitted with a linear regression, being the slope used for the calculation. Additionally, to calculate the rate of methyl viologen or cytochrome c_{552} re-oxidation it was necessary to consider its extinction coefficient, $\varepsilon = 11.4\ mM^{-1}\ cm^{-1}$, determined for methyl viologen at 600 nm [175] and $\varepsilon = 19.3\ mM^{-1}\ cm^{-1}$, determined for cytochrome c_{552} at 552 nm [205]. Note that both methyl viologen and cytochrome c_{552} required only one electron loss to become oxidized while one molecule of N_2O requires two electrons in its reduction and thus for the calculation of reduction rates of N_2O it was also necessary to take this into consideration. The oxidation rate of electron donors immediately prior to the substrate addition was taken into consideration for the calculation of the reduction rates of N_2O. Indeed, the slope immediately before the substrate addition was subtracted to the slope determined after the addition of substrate. This was particularly important in activity assays in which the reduction rates of substrate are small.

Afterwards these rates are divided by the amount of N_2OR used in the assay, and thus specific activity is reported as micromoles of N_2O reduced per minute per milligram of enzyme ($\mu mol_{N2O}\ min^{-1}\ mg^{-1}{}_{N2OR}$).

2.11.5 Effect of pH on the activation of the N_2OR

As-purified N_2OR (7 μM) from *M. hydrocarbonoclasticus*, with 40 % of "CuZ center" as CuZ*(4Cu1S) was incubated for 3 h with 10 mM methyl viologen and 5 mM DT in 100 mM of different buffer solutions: MES pH 5.5, MES pH 6.5, Tris-HCl pH 7.6, Tris-HCl pH 8.5, CHES pH 9.5, CHES 9.7 or CAPS pH 10.4.

In the activity assay, 10 μL of the activated mixture were added to a stirring 1 mL quartz cuvette containing 100 mM Tris-HCl pH 7.6 followed by addition of 1.25 mM N_2O. At least triplicate assays were performed. Specific activities were calculated as previously described (see Section 2.11.4) and reported to $\mu mol_{N2O}\ min^{-1}\ mg^{-1}{}_{N2OR}$.

Specific activity *vs* pH was fitted with an equation of a bell-shaped and two pK_a were determined (Equation 2.2):

$$\text{Activity} = \frac{\text{Activity}_{max}}{1+10^{(pKa1-pH)}+10^{(pH-pKa2)}} \quad (2.2)$$

The effect of activation by an alkaline buffer solution was examined by dialysis of 7 μM N_2OR with 20 % of "CuZ center" as CuZ*(4Cu1S) in 50 mM CHES pH 9.7 for 24 h at 4 ºC under anaerobic conditions. In parallel, a control assay was performed similarly using a dialysis buffer with 50 mM Tris-HCl pH 7.6.

Spectra were collected during the incubation time and at each time-point the specific activity was spectrophotometrically measured in a 1 mL quartz cuvette containing 100 mM Tris-HCl pH 7.6, 100 μM reduced methyl viologen, followed by addition of 1.25 mM N_2O, without prior incubation. The spectrum acquired after 24 h was oxidized with an aliquot of 10 mM potassium ferricyanide solution.

2.12 Time dependent kinetic assays of N_2OR

The following experiments were performed inside an anaerobic chamber (MBraun) at RT, except the direct reduction of oxidized N_2OR with sodium ascorbate (Section 2.12.1). All the time dependent reactions were followed by visible spectroscopy (between 350 – 900 nm), using a TIDAS diode-array spectrophotometer connected to optical fibers (inside the anaerobic chamber) or using a diode array spectrophotometer (Agilent 8453).

2.12.1 Direct reduction of oxidized N_2OR with sodium ascorbate

Different forms of N_2OR, with 80 % or 10 % of "CuZ center" as CuZ*(4Cu1S), were fully oxidized by addition of 10 mM potassium ferricyanide and desalted using a PD10 Sephadex G-25 column (GE) equilibrated with 100 mM potassium phosphate pH 7.6.

Fully oxidized 17 μM N_2ORs in 100 mM potassium phosphate pH 7.6 were reduced with 0.5 mM or 7.5 mM sodium ascorbate in a stirring 1 mL quartz cuvette. Spectra were recorded every second in a diode array spectrophotometer (Agilent 8453). In parallel, an identical experiment was performed in which reduction was followed after addition of 0.5 mM of sodium ascorbate and 5 μM of 2,3,5,6-tetramethyl-1,4-benzenediamine (DAD), which was prepared in 20 % ethanol.

2.12.2 CuZ^o formation and decay at different pH

N_2OR with 60 % of "CuZ center" as CuZ*(4Cu1S) was fully reduced (see Section 2.11.2) and desalted in a NAP-5 column to a buffer solution, containing 20 mM of MES, HEPES, CAPS and TAPS adjusted to pH 6.0, 7.6, 8.5, 9.0, 9.5, 9.7 or 10.0. The activated protein was quantified by the Pierce™ method (see Section 2.9.1).

Reaction of fully reduced N_2OR (~ 20 μM) with a stoichiometric amount of N_2O was used to form the CuZ^o species and the reaction was followed spectrophotometrically in a time dependent assay. The data were fitted to a one-phase exponential decay function.

Copper content of the enzyme before the activation and also after the assay was determined for the assay at pH 7.6, using the 2, 2'-biquinoline method (Section 2.9.3). The decay of the CuZ^o at pH 7.6 was followed by steady-state kinetics assays and the activity determined per total protein, determined by the Pierce method.

2.12.3 Formation of new intermediate species

In a typical assay of CuZ^o decay, performed in potassium phosphate buffer at pH 7.6, 22 μM fully reduced N_2OR, with 60 % of "CuZ center" as CuZ*(4Cu1S), was reacted with an approximately stoichiometric amount of N_2O and at the end of the reaction the sample was oxidized by addition of a small amount (~ 5 μL) of a solution of 10 mM potassium ferricyanide. Desalting of the oxidized sample was performed on a NAP-5 column (GE) equilibrated with 100 mM potassium phosphate pH 7.6, to remove the excess of potassium ferricyanide. The spectrum of desalted N_2OR was recorded and afterwards the sample was kept outside of the anaerobic chamber at 4 °C. The spectrum was recorded 3 days later (outside of the anaerobic chamber) in a UV-1800 spectrophotometer (Shimadzu). A similar assay was later performed, in which the spectra of oxidized N_2OR after desalting was monitored for 15 h inside the anaerobic chamber.

In a parallel assay, the reaction of 20 μM fully reduced N_2OR, with 80 % of "CuZ center" as CuZ*(4Cu1S), in the presence of sodium ascorbate (366-fold excess over the enzyme) without N_2O

was also monitored for 60 min. After this time, N_2OR was oxidized with a solution of 100 mM potassium ferricyanide, followed by reduction with 100 mM sodium ascorbate and after that with 100 mM sodium dithionite.

2.12.4 Reduction of CuZ° by sodium ascorbate

N_2OR with 60 % or 80 % of "CuZ center" as CuZ*(4Cu1S) was activated and used to form CuZ^o, in 100 mM phosphate pH 7.6, as described in Section 2.12.2. This reaction was performed as a control for the following assays. The reduction was monitored spectrophotometrically by visible spectroscopy for at least 1 h on a TIDAS diode-array spectrophotometer connected to optical fibers.

Two reduction assays of CuZ^o with ~ 400-fold or ~ 16-fold excess of sodium ascorbate over the enzyme were performed in 100 mM potassium phosphate pH 7.6. In the first assay, to a 1 mL stirring cuvette containing 20 μM fully reduced N_2OR, with 80 % of "CuZ center" as CuZ*(4Cu1S), 36 μM N_2O were added (time set to 0 s), followed by the addition of sodium ascorbate (366-fold excess over the enzyme) after 37 s. The second assay was identical, containing 30 μM N_2OR, with 60 % of "CuZ center" as CuZ*(4Cu1S), being initiated by the addition of 32 μM N_2O, followed by the 490 μM sodium ascorbate (~16-fold excess) after 30 s. Spectra were collected during 120 min in both assays and the absorbance at 482 and 683 nm were analyzed, normalized and fitted.

A parallel assay was performed, in which 30 μM fully reduced N_2OR, with 60 % of "CuZ center" as CuZ*(4Cu1S), was added to a 1 mL stirring cuvette containing already 200 μM N_2O and 10 mM sodium ascorbate in 100 mM phosphate pH 7.6. Spectra of the reaction were also recorded as in a time dependent assay.

Control experiments in the presence and absence of sodium ascorbate were performed.

2.12.4.1 Data analysis – normalization for kinetic fitting

Time dependent assays were normalized for the kinetic fittings. In the case of the assay with N_2OR mainly with CuZ(4Cu2S), this center was time dependent normalized at 550 nm, taking into consideration that 47 % of the total absorbance at this wavelength is due to the contribution of the CuA center (previously determined by the subtraction of an ascorbate reduced spectrum from a totally oxidized CuZ(4Cu2S) spectrum).

In the sample containing mainly CuZ*(4Cu1S), CuA was normalized at 482 nm, as no other features overlap at this wavelength. For CuZ*(4Cu1S) center, data was collected at 653 nm but at this wavelength CuA center contributes to the changes with time. Therefore, CuA center contribution at each time for the 653 nm features was subtracted based on the amount of CuA center present (35 %). The contribution of CuA center to the oxidized N_2OR spectra with 90 % of

"CuZ center" as CuZ*(4Cu1S) were obtained by subtracting the features of CuZ*(4Cu1S). Similarly, a contribution of the CuA center (50 %) to CuZ^o, at 683 nm, was also determined and considered in the fittings analysis.

The fit of the data was performed by the kinetic Tenua program using the experimental parameters determined. The correlation coefficient was determined by the least square method.

2.13 Crystallization and data collection

All the crystallization experiments were performed in an anaerobic chamber, 2 % H_2 in Ar atmosphere and < 1 ppm O_2 (Coy Labs).

N_2OR crystals were grown by the sitting-drop vapour diffusion method, using 1 µL protein sample (10 mg mL^{-1}), in different redox states, and an equal volume of reservoir solution (0.1 M Bicine pH 9.5, 18 % w/v PEG 4000, 10 % v/v isopropanol, 0.6 M NaCl and 0.01 M spermidine as addictive), similar to the conditions used by Brown *et al* [91, 125]. This condition was refined by gradients of NaCl (0.2 to 1 M) and isopropanol (5 to 25 %) concentrations, as well as pH of the buffer (from 8.0 to 9.5), though most of the crystals obtained were grown only with slight variations of the initial conditions. Nevertheless, spermidine was found not to be essential for the growth of the crystal. Purple and blue crystals were obtained after 3 - 4 days at 25 °C or 20 °C with a flower or diamond shape.

Attempts were made to crystallize different forms of the enzyme with 10 %, 50 % or 90 % of "CuZ center" as CuZ*(4Cu1S), as well as crystallization of different redox states by incubating N_2OR with sodium dithionite or reduced methyl viologen and also in the presence of ligands as iodide. Soaking experiments of N_2OR crystals by incubation with potassium iodide for 2 h and 4 h were also performed, however the data collected did not exhibit electron density for the presence of iodide. As most of the crystals obtained were small or the diffraction was not good, the microseed technique was used as an attempt to increase the number of crystals or improve their size. This technique uses a crystal seed for the growth of other crystals and was performed by adaptation of a protocol from Hampton research (seed Bead™ kit), based on [209]. The number of seeds was optimized by testing different dilution of the seed. The number of crystals and their size improved but a high resolution diffraction pattern was not obtained.

For data collection, N_2OR crystals were transferred to cryoprotectant solution (reservoir solution supplemented with 15 % v/v ethylene glycol) and flash-cooled in liquid nitrogen. X-ray diffraction data were collected on beam lines PXI and PXII at the Swiss Light Source, Paul Scherrer Institute, Switzerland. Crystallographic data collection for the higher diffractions obtained is shown (Table 2.2).

Table 2.2 - Crystallographic data collection of N_2OR from *M. hydrocarbonoclasticus.*

	Blue crystal 90 % as CuZ*(4Cu1S)	**Purple crystal 10 % as CuZ*(4Cu1S)**
Space group	$P6_1$	$P6_1$
Wavelength [Å]	1.000	1.000
Cell constants *a*, *b*, *c* [Å] α, β, γ [°]	211.3; 211.3; 164.5 90; 90; 120	210.5; 210.5; 165.1 90; 90; 120
Resolution limits [Å]	49.0 (2.4)	48.8 (1.9)
Completeness (%)	100.0 (99.9)	100.0 (99.9)
Unique reflections	162 407 (7998)	325 029 (2046)
Multiplicity (%)	21.2 (20.9)	20.8 (20.6)
R_{merge}	0.218 (1.266)	0.223 (3.444)
$R_{p.i.m.}$	0.048 (0.288)	0.050 (0.746)
Mean I/ σ(I)	14.1 (2.9)	13.8 (1.4)
Mosaicity	0.10	0.06

2.13.1 Structure and refinement

The datasets obtained were integrated and scaled by XDS [210] and AIMLESS [211] (CCP4: Supported program [212]). The structure was solved by molecular replacement, in MOLREP [213], using a refined model of a monomer of *M. hydrocarbonoclasticus* N_2OR. The models were manually rebuilded on coot software [214] and refined with REFMAC5 [215]. The final model was evaluated by MolProbity (http://molprobity.biochem.duke.edu/) [216].

2.14 Reduction potential

2.14.1 Potentiometric redox titration

All the redox titrations of N_2OR, were performed in an anaerobic chamber (MBraun) at 20 ± 2 ºC. The redox electrode (Crison), which combines a platinum wire and a reference Ag/AgCl electrode, was calibrated in 0.5 mM $NH_4Fe(SO_4)_2 \cdot 12H_2O$, 10 mM EDTA and 100 mM CH_3COONa at pH 5.0 by the addition of 10 and 15 µL of 100 mM $(NH_4)_2Fe(SO_4)_2 \cdot 6H_2O$. The potential measurements allowed the determination of a slope of + 59 mV and the difference between the measured and the expected potential (+ 108 mV *vs* SHE) was further used to correct all the potentials in the N_2OR redox titration.

Redox titration of N_2OR, with 15 % of "CuZ center" as CuZ*(4Cu1S), was performed in a stirring 3 mL cuvette containing 60 µM of fully oxidized N_2OR in 100 mM Tris-HCl pH 7.6 and 2 µM of each mediator (Table 2.3). Small volumes of sodium ascorbate and sodium dithionite (0.1 -100 mM) were added with a 10 µL Hamilton syringe in the reductive titration, and potassium ferricyanide (0.1 - 100 mM) was used for the oxidative direction. The reaction was followed spectrophotometrically (between 350 – 900 nm) and the potential (stabilized after each addition) was measured using a combined redox electrode.

Using the same protein batch (or equivalent percentage of CuZ*(4Cu1S), similar titrations were performed in the following buffer solutions: 100 mM MES buffer pH 6.5, 100 mM CHES buffer pH 9.0, 100 mM CAPS buffer adjusted to the pH values 10.2 and 10.4.

Redox titrations using the same procedure as described above were also performed for a sample with 50 % of "CuZ center" as CuZ*(4Cu1S) in 100 mM MES buffer pH 5.5 and 6.5, 100 mM Tris-HCl buffer pH 7.0 and 8.6, 100 mM CHES buffer pH 9.4 and 100 mM CAPS buffer pH 10.4.

Table 2.3 - Reduction potential of mediators used in the redox titration [217].

Mediator	**E (mV) at pH 7.0, 25 °C**
2,3,5,6-tetramethyl phenylenediamine	+ 260
1, 2- naphthoquinone-4-sulfonic acid	+ 210
1,2-naphthoquinone	+ 180
phenazine methasulfate	+ 80
resorufin	- 50
indigo carmim	- 111
2-hydroxy-1,4-naphthoquinone	- 145
methyl viologen	- 430

2.14.1.1 Data analysis

In this case, as both centers present different spectroscopic features, we consider CuA and CuZ(4Cu2S) as two independent centers, each having a one electron reduction.

The spectra obtained were corrected for the dilution and to the isosbestic point at 627 nm. The absorbance at 600 nm or at 800 nm was used to determine the % oxidized/reduced species and the data were simulated based on the Nernst equation (Equation 2.3):

$$E = E^0 + \frac{RT}{nF} \ln \frac{P_{ox}}{P_{red}} \quad (2.3)$$

Where, E is the electrode potential with reference to SHE, E^0 is the standard reduction potential of the redox couple, P_{ox} is the molar fraction of the population of the fully oxidized state while P_{red} is the population of fully reduced state, and thus $P_{ox} + P_{red} = 1$. R is the universal gas constant ($R = 8.31$ J K^{-1} mol^{-1}), T is the temperature in K (293.15 K), F is the Faraday constant (9.65×10^4 C mol^{-1}) and n is the number of electrons transferred.

For one electron reduction at 20 °C, Equation 2.3 is given by:

$$E = E_{m,7.6} + 58 \log_{10} \frac{P_{ox}}{P_{red}} \quad (2.4)$$

Where, $E_{m,7.6}$ is the reduction potential (mV) with reference to SHE at pH 7.6.

The reduction potential (mV) as a function of % oxidized/reduced species were simulated at each pH for both CuA and CuZ(4Cu2S) centers, using the Equation 2.5.

$$\%\frac{[ox]}{[red]} = \frac{10\text{^}\left(\frac{E-E_{m,7.6}}{58}\right)}{10\text{^}\left(\frac{E-E_{m,7.6}}{58}\right)+1} \times 100 \quad (2.5)$$

2.14.2 Electrochemistry

The experiments were conducted on an anaerobic chamber (O_2 < 4 ppm) at 20 ºC and all the solutions were prepared in deionized water. All the potentials are quoted against standard hydrogen electrode (SHE).

The electrochemical measurements, by cyclic voltammetry (CV) and differential pulse (DP) voltammetry, were performed with a μautolab and collected and analyzed in GPES software package (both from ECO chemie). A three-electrode configuration cell was used with an Ag/AgCl reference electrode (+ 208 mV *vs* SHE), a platinum wire as the counter electrode and a work electrode. For direct electrochemistry a carbon nanotube modified glassy carbon (GC) (BASi, ref. MF2012) with nominal radius = 0.15 mm, was used as the working electrode, while a gold electrode (BASi, ref. MF2014) with nominal radius = 0.15 mm was used for mediated electrochemical experiments.

2.14.2.1 Direct electrochemistry

Functionalization of Multi-walled carbon nanotubes

Multi-walled carbon nanotubes (MWCNTs) were purchased from Sigma and functionalized as described by Carvalho *et al* [218]. Shortly, 120 mg of MWCNTs were functionalized in 3 M HNO_3 for 24 h. The HNO_3 was removed by paper filtration and the nanotubes were washed with milli-Q water until the discarded water reaches pH ~ 7.0. The MWCNTs were dry at 80 °C for 24 h. The solid was dispersed in 1 % w/v dimethylformamide and sonicated for 3h.

Electrode preparation

Before each experiment the glassy carbon electrode surface was polished with 1 and 0.5 μm alumina slurry, sonicated for 5 minutes and rinsed with deionized water. The functionalized MWCNTs (7 μL) were deposited on the electrode surface and left to dry for 45 min at RT. Each electrode prepared with MWCNTs was immersed in the electrolyte and voltammograms at different scan rates were recorded prior to enzyme deposition. Then, a drop of the N_2OR solution

(10 µL) was applied on the surface of MWCNTs and left to dry for 45 min before electrode immersion in the electrolyte solution. Different forms of N_2OR were used and the exact percentage of CuZ*(4Cu1S) is described in the figures legends.

Activation of N_2OR (see Section 2.11.2) was performed for the turnover studies, using a preparation with 60 % of "CuZ center" as CuZ*(4Cu1S). Activated enzyme was desalted using a NAP-5 Sephadex G25 column (GE) equilibrated with 100 mM potassium phosphate pH 7.0 to remove the excess of reducing agents and then concentrated using a ultrafiltration micro concentrator (MWCO 30 kDa) (Sartorius) to a final concentration of 124 µM. A drop of N_2OR (4 µL) was immobilized on the GC electrode containing the MWCNTs, using the same procedure as before.

Electrochemical measurements

Most of the experiments were conducted using a 100 mM potassium phosphate pH 7.0 solution. In the pH dependence experiments, solutions containing 20 mM of MES, HEPES, CAPS and TAPS were adjusted to different pH values from 5.5 to 10.5.

The CV experiments were performed in a potential window between + 0.9 to – 0.5 V (*vs* SHE) and the scan rate (v) varied between 5 and 100 mV s^{-1}. DP voltammetry experiments were conducted in the same potential window as CV experiments, using a pulse width of 100 ms, a pulse amplitude of 50 mV and a step potential of 2 mV.

Turnover assays were also performed in 100 mM potassium phosphate pH 7.0 electrolyte solution. These assays were analyzed in the presence of increasing concentrations of N_2O up to 1.4 mM. Different electrode preparations using the same activated enzyme were used and the data obtained were analyzed and fitted with the Michaelis-Menten equation.

2.14.2.2 Mediated electrochemistry

Electrode preparation

Mediated electrochemistry of N_2OR in the presence of cytochrome c_{552} was previously reported [148] and a similar membrane electrode preparation was used in the present study. Before each experiment the electrode surface was polished with 1.0, 0.5 and 0.3 µm alumina slurries, sonicated for 5 minutes and rinsed with deionized water.

Then, a 4 µL drop of a mixture of N_2OR, with 60 % of "CuZ center" as CuZ*(4Cu1S), and cytochrome c_{552} (140 µM) in a 1:1 ratio was deposited. The membrane containing the solution was fixed with the O-ring in the gold electrode previously coated with 2 µL of neomycin (2 mM).

Electrochemical measurements

The cyclic voltammetry experiments were performed in 100 mM of potassium phosphate pH 7.0 as the supporting electrolyte previously equilibrated with the chamber atmosphere. CVs were recorded on a potential window between + 0.5 to – 0.1 V at a scan rate of 10 mV s^{-1}. Before substrate addition, ten scans were performed on the selected working window. A saturated concentration of N_2O was directly injected into the electrolyte with a syringe (to a final concentration of 2 mM). Controls in the absence of N_2OR or in the absence of cytochrome c_{552} were performed.

2.15 Exogenous ligand binding

All the sample preparation, titrations and kinetics assays were performed inside an anaerobic chamber (MBraun).

2.15.1 Titration of exogenous ligands with N_2OR

N_2OR with 10 % or 50 % of "CuZ center" as CuZ*(4Cu1S) were incubated for 5 min in the presence of an excess of potassium ferricyanide and also for 1 h in the presence of excess of sodium dithionite, in the case of 10 % CuZ*(4Cu1S). Samples were buffer exchanged to 100 mM Tris-HCl pH 7.6 using a NAP-5 Sephadex G-25 column (GE). These samples were used in the titration experiments with halides.

Fully oxidized N_2ORs (both forms previously prepared) were titrated with halides (F^-, Cl^-, Br^- and I^-) and also nitric oxide. Additionally, reduced N_2OR with 10 % as CuZ*(4Cu1S) form was also titrated with iodide and nitric oxide. The titration experiments were followed by visible spectroscopy in a TIDAS diode array spectrophotometer.

Experiments were conducted using a stirring cuvette containing 12 μM or 18 μM of N_2OR with 50 % or 10 % of "CuZ center" as CuZ*(4Cu1S), respectively, in 100 mM Tris-HCl pH 7.6. Small amounts of concentrated stock solutions of ligands (2 M NaCl, 1 M NaF, 1 M NaBr, 1 M KI, 95.5 μM NO) were added to the cuvette with a Hamilton syringe, until there were no spectral changes. Two similar experiments were performed in which 12 μM N_2OR, with 50 % of "CuZ center" as CuZ*(4Cu1S), were titrated with iodide in 20 mM of MES, HEPES, CAPS and TAPS adjusted to pH 6.0 and pH 9.0.

Another titration was performed in which reduced N_2OR (20 μM) with 10 % of "CuZ center" as CuZ*(4Cu1S) was titrated with iodide in 100 mM Tris-HCl pH 7.6.

All the spectra were corrected for the absorbance at 400 nm and the ligand-receptor binding equation was used to fit the curve of the difference spectra as function of ligand concentration (Equation 2.7).

$$B = \frac{B_{max} \times [L]}{K_d^{app} + [L]} \quad (2.7)$$

Where B_{max} is the maximum bound ligand-receptor complex, [L] is the free ligand concentration, K_d^{app} is the ligand concentration at which half of the receptor is bound.

2.15.2 Azide, cyanide, nitric oxide and iodide

Sample preparation

Oxidized N_2OR, with 65 % of "CuZ center" as CuZ*(4Cu1S) was incubated during 48 h in the presence of 5-fold excess of cyanide or 2.5-fold excess of nitric oxide, in 100 mM Tris-HCl pH 7.6. N_2OR was also incubated with 750-fold excess of azide in 100 mM Tris-HCl pH 7.6 but during 24 h. Additionally, fully oxidized N_2ORs with 10 % or 65 % of "CuZ center" as CuZ*(4Cu1S), 7 µM and 20 µM respectively, were incubated with 500-fold excess KI in 100 mM Tris-HCl pH 7.6 during 48 h. Incubations were kept under anoxic conditions at 4 °C.

Visible spectroscopy

The visible spectra of each of these ligand assays were collected on a Shimadzu UV-1800 spectrophotometer during the incubation period. After this period, each sample was divided, and part was oxidized with a solution of 10 mM potassium ferricyanide, while the other was reduced with a solution of 200 mM sodium dithionite. Each sample was three-times washed in 100 mM Tris-HCl pH 7.6, using a Vivaspin 500 (Sartorius, YM30) to remove the excess of reducing/oxidizing agents and the spectra of oxidized and reduced sample were recorded.

Protein concentration was determined by Lowry method [206] (detailed in Section 2.9.1) and the copper content was estimated based on 2,2'-biquinoline method [208] (as described in Section 2.9.3).

EPR spectroscopy

The effect of KI (500-fold excess over protein) on N_2OR, with 10 % of "CuZ center" as CuZ*(4Cu1S) (200 µM) or with 65 % of "CuZ center" as CuZ*(4Cu1S) (166 µM), was monitored over time by EPR spectroscopy, using the following experimental parameters: microwave frequency, 9.65 GHz; microwave power, 2 mW; gain, $1x10^5$; temperature, 30 K (see Section 2.10.2).

Steady-state kinetics

Specific activities of N_2OR in the presence of the ligand were monitored during the incubation period. In this assay, at each time-point a sample of N_2OR (70 nM) was incubated in the presence of reduced methyl viologen for 3 h for enzyme activation, followed by addition of N_2O to the assay [122] (as described in Section 2.11.1). At least triplicates of each assay were performed.

The concentration dependence of cyanide (175-fold excess, 1750-fold excess and 8750-fold excess), azide (7000-fold excess and 9350-fold excess) and iodide (0, 50, 250, 500, 1000, 2500 or 5000-fold excess) on N_2OR specific activity was determined during 24 h.

Differential scanning calorimetry

The thermal stability of N_2OR (20 μM), with 10 % and 50 % of "CuZ center" as CuZ*(4Cu1S), in the presence and absence of potassium iodide, was evaluated by differential scanning calorimetry using a nano DSC (TA instruments). The experiments were performed using 600 μL of 20 μM N_2OR in 100 mM HEPES pH 7.0. For the assays in the presence of ligand, each form of the enzyme was previously incubated with 500-fold excess of iodide for 48 h.

In these experiments, a baseline with the same buffer as the protein was performed between each N_2OR sample. The temperature scanning was performed with an increase of 1 °C per minute from 10 °C to 110 °C. Data were analyzed with NanoAnalyze software (TA instruments), being the profile normalized to the number of moles present in each assay and the baseline subtracted to the heat capacity profile. Then, data were simulated using a two state scaled model and the parameters melting temperature (T_m), calorimetric enthalpy (ΔH_{cal}) and van't Hoff enthalpy (ΔH_{vH}) were determined.

2.15.3 EGTA, Calcium and sulfide

Sample preparation

As-isolated N_2OR, with 50 % of "CuZ center" as CuZ*(4Cu1S) was incubated with 20-fold excess of EGTA in 100 mM CHES pH 9.0 during 6 h. The same enzyme preparation was also incubated with 156-fold excess of calcium chloride in 100 mM Tris-HCl pH 7.5 for 5 h.

Visible spectroscopy

The visible spectra of N_2OR incubated with EGTA or calcium chloride were collected on a TIDAS diode array spectrophotometer during the incubation period of each sample.

Steady-state kinetics

Specific activities, using 70 nM of protein incubated with EGTA, calcium or sodium sulfide (equimolar or 10-fold excess or 100-fold excess) were measured at different incubation times. The enzyme was activated in the presence of reduced methyl viologen for 3 h followed by N_2O reduction assay (as described in Section 2.11.1). In parallel, 70 nM of activated N_2OR were incubated with 100-fold excess of Na_2S for 1 h, followed by the N_2O reduction assays. All specific activities were performed in triplicate.

Chapter 3

The pH effect on the denitrification pathway of *Marinobacter hydrocarbonoclasticus*

Publications included in this Chapter:

Carreira, C.; Mestre, O.; Nunes R. F.; Moura, I., Pauleta, S. R. Genomic organization, gene expression and activity profile of *Marinobacter hydrocarbonoclasticus* denitrification enzymes, *FEMS Microbiology Ecology*. *Submitted*, **2017**.

Carreira, C.; Nunes R. F. ; Mestre, O. ; Moura, I., Pauleta, S. R. The pH effect on denitrification pathway of *Marinobacter hydrocarbonoclasticus* and nitrous oxide redictase. *In preparation*, **2017**.

Contributions to this Chapter:

The transcriptomic analysis was performed by Olga Mestre and part of nitrate/nitrite quantification, as well as some of the 2 L biorector growths were performed by Rute Nunes.

3 The pH effect on the denitrification pathway of *Marinobacter hydrocarbonoclasticus*

The nitrogenous compounds leached to costal seawaters and oceans, under low oxygen tensions, trigger the denitrification pathway [14, 15]. The incomplete denitrification caused by environmental factors, as deregulated pH, is one of the major contributors to the increase of atmospheric concentration of the long-lasting greenhouse gas N_2O.

In this work, *M. hydrocarbonoclasticus* 617, a denitrifier bacterium, is used as a model organism of a marine system to study the denitrification pathway. The pH effect (6.5, 7.5 and 8.5) on denitrification was analyzed in two types of experiments mimicking the surface and deeper waters in an aquatic system, represented by a batch system, using a bioreactor under microaerobic conditions and a closed system, using sealed serum flasks (anaerobic system after the initial oxygen consumption), respectively.

Moreover, N_2OR was isolated from growths performed in the bioreactor at each pH. Biochemical and spectroscopic characterization were performed for the three preparations of the enzyme. This study not only correlates the properties of all the known forms of the enzyme, but also a relation with the *in vivo* observations.

Our results provide clues to understand the mechanisms involved in N_2O release in soils and seawaters when a drop in pH occurs.

3.1 Genomic organization of denitrification genes

A search in the genome of *M. hydrocarbonoclasticus* ATCC 49840 showed that several genes encoding proteins involved in the different steps of the denitrification are clustered together comprising a genomic region of approximately 75 kb (Figure 3.1).

These genes include the *nosRZDFYL* gene cluster, containing the catalytic subunit of N_2OR, encoded by *nosZ* [20, 219]. Also present in this gene cluster is *nosR*, a gene encoding for a transmembrane protein, whose function remains unclear but seems to be important for *nosZ* transcription, as well as for enzyme full activity *in vivo* [79, 113]. The *nosD* gene encodes a protein that together with NosFY is proposed to form an ABC–transporter (NosDFY) and be involved in sulfur transport and in "CuZ center" assembly [80, 82], while *nosL* encodes a putative copper chaperone [24, 109].

Upstream the *nos* cluster is the *narLXKGHJV* cluster, (Figure 3.1) containing the genes *narG*, *narH* and *narV* (also designated as *narI*) that encode the α, β and γ subunits of NaR, respectively [219], being NarG the catalytic subunit of the enzyme. The *narJ* gene encodes a chaperone-like component involved in the maturation and assembly of the enzyme complex [38]. Upstream *narG*,

there are two genes *narXL*, that encode NarXL a two-component system involved in transcriptional regulation of genes in response to nitrate and/or nitrite [47, 219].

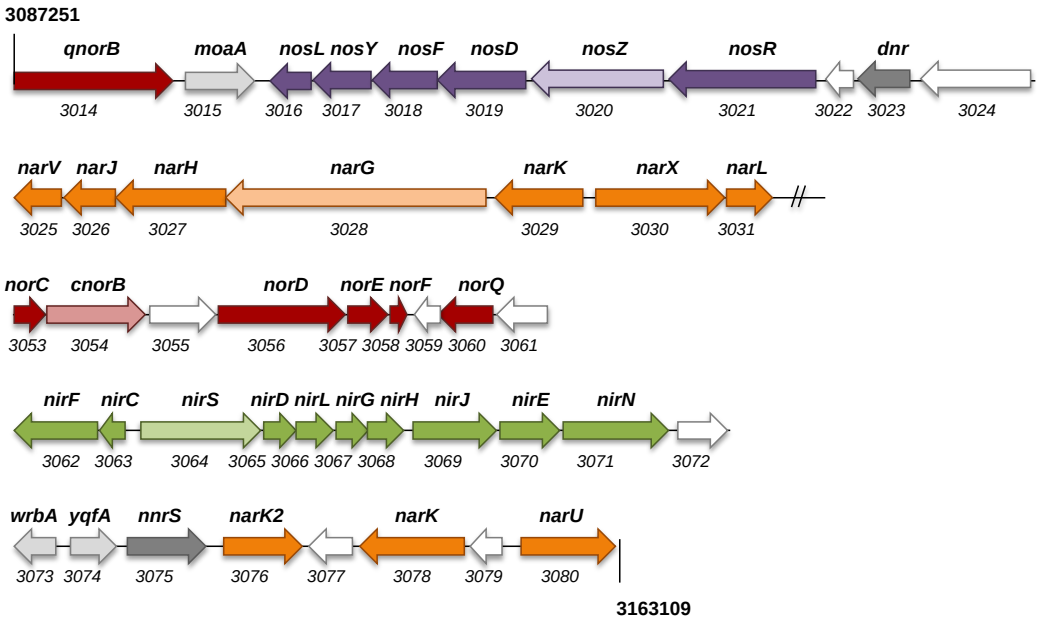

Figure 3.1 - Arrangement of denitrification genes in the genomic region 3087251-3163109 of *M. hydrocarbonoclasticus* ATCC 49840. Genes belonging to the nitrate reductase (*nar*), nitrite reductase (*nir*), nitric oxide reductase (*nor*) and nitrous oxide reductase (*nos*) clusters are colored in orange, green, red and purple, respectively. The catalytic subunit of each cluster is light colored. Unidentified genes are white colored and the *dnr* and *nnrS* regulator genes are colored in dark grey. The number below each gene is the *MARHY* gene identification. Our own *in silico* analysis indicates that *MARHY3057* and *MARHY3058* are putative *norE* and *norF* homologues, respectively. Arrows show the direction of transcription.

Three *narK* genes were identified. One is part of the *narLXKGHJV* cluster and other two were identified upstream in the genome (Figure 3.1), *MARHY3076*, annotated as *narK2*, and *MARHY3078*, annotated as *narK*. Homologues of NarK have been proposed to function either as nitrate/proton symporters that import nitrate into the cytoplasm, where it is reduced by nitrate reductase, or as nitrate/nitrite antiporters that transport nitrate into the cytoplasm and also nitrite into the periplasm to be either reduced by nitrite reductase or released into the extracellular environment [71, 72]. The mechanism of transport and specificity was clarified after the structure of the two transporters was solved, which were crystallized in the presence of nitrate or nitrite [220-222]. Additionally, *narU*, encoding in *E. coli* a nitrate/nitrite transporter [221, 223], is also annotated in the genome of *M. hydrocarbonoclasticus*. Multiple NarK-like transporters have also been identified in the genome of other bacteria, as in *P. aeruginosa* and *P. denitrificans* [71, 223, 224]. It is unclear why such an array of molecular systems would provide a significant benefit over a single transporter. It is possible that these are required in specific growth conditions, as observed in *E. coli* for NarU [223]. Further upstream in the genome, *norBC*, encoding the two subunits of the short-chain membrane-bound *c*-NOR were identified (Figure 3.1). NorB (MARHY3054) is the catalytic subunit, while NorC is a small membrane bound *c*-type cytochrome functioning as an electron

transfer subunit [219, 225]. The accessory genes *norQ* (*MARHY3060*, annotated in other organisms as *napH*) and *norD* (*MARHY3056*), together with two other ORFs (*MARHY3057* and *MARHY3058*) are located upstream the *norBC* operon, similarly to what is found in *P. denitrificans* genome [226]. Neither *norE* nor *norF* homologues were annotated in the genome of *M. hydrocarbonoclasticus.* However, a Blast search revealed that the translated sequence of *MARHY3057* shares 46 % sequence identity with *P. stutzeri* NorE (designated in that microorganism as NirQ), while MARHY3058 protein shares 53 % identity with *P. stutzeri* NirP (the NorF homologue in *Pseudomonas* species with 82 residues), even though in a very restricted region, covering only 49 % of the primary sequence. Indeed, this putative NorF (with 61 a.a.) is 40 % shorter than its homologues.

However, the analysis of the entire intergenic region between *MARHY3057* and *MARHY3058* identified a longer ORF encoding a protein with 79 residues that has 39 % primary sequence identity with *P. stutzeri* NirP. Therefore, we propose that NorF was misannotated in *M. hydrocarbonoclasticus* ATCC49840 genome, being encoded in the 3141724-3141963 genomic region rather than in the 3141778-3141963 region. NorE and NorF, are predicted to be membrane associated, though their exact function remains unknown [227]. It has been shown that NorEF are involved in denitrification as its inactivation slows nitrate reduction during denitrification, with accumulation of micromolar concentrations of nitric oxide [226, 227]. In contrast, *norQ* and *norD* are always found linked to or in the vicinity of *norBC* [225]. The encoded proteins are suggested to be involved in the maturation of NorBC in heme insertion, multisubunit assembly and/or insertion into the membrane [21, 225].

Curiously, a second *norB* gene (*MARHY3014*) also encoding a NOR, is annotated in *M. hydrocarbonoclasticus* genome, downstream the *nos* cluster and transcribed in the opposite direction (Figure 3.1). This NorB (MARHY3014) (471 a.a) shares only 24 % identity with the other NorB protein (MARHY3054), thought the alignment covered 75 % of the primary sequence. Indeed, NorB (MARHY3014) is composed of a single long-chain subunit being a *q*-NOR homologue (primary sequence identity with *Geobacter stearothermophilus q*-NOR is 37 %, with a 95 % coverage, and 25 % with *P. aeruginosa* large subunit NorB, but with only 60 % coverage). While *c*-NOR uses a *c*-type cytochrome as electron donor, *q*-NORs accept electrons from the quinone pool. The presence of two types of NOR in the same bacteria does not seem to be frequent [228, 229] and its biological relevance is unknown.

Upstream *nor* cluster, 10 genes involved in the nitrite reduction step of the denitrification pathway were found linked together, *nirFCSDLGHJEN*. Different genetic arrangements of *nir* genes have been identified in bacteria. *P. aeruginosa* presents the most similar genetic organization of the nitrite reductase cluster in comparison to the one of *M. hydrocarbonoclasticus* [46]. The only differences are in the *nirM* gene, encoding cytochrome c_{551}, which is absent in *M. hydrocarbonoclasticus nir* regulon and in *nirFC*, which are located upstream *nirS* and are

transcribed in the opposite direction. NirM is the electron donor of NiR in *P. aeruginosa*, while the cytochrome c_{552}, encoded by *MARHY3556*, was identified as the physiological electron donor of NiR (and also of NOR and N_2OR) in *M. hydrocarbonoclasticus* [230] and is distantly located in the genome.

The *nirS* gene encodes the cytochrome cd_1NiR, a homodimeric enzyme with *c*- and d_1-type hemes [231]. In recent years, it was identified that *nirDLGH* [232], *nirJ* [232], *nirE* [233, 234] and *nirN* [235] encode enzymes involved in the biosynthesis of heme d_1, all located in the cytoplasm, with the exception of NirN. NirF has been proposed to be a chaperone involved in the uptake and transport of heme d_1 precursor from the cytoplasm to NirN located in the periplasm. The exact role of NirC remains unknown, but has been shown to be essential for the synthesis of heme d_1 in *P. denitrificans* [236, 237]. NirC is predicted to be a periplasmic *c*-type cytochrome, playing a role in the biosynthesis of heme d_1 as an electron acceptor from NirN [233, 235].

A gene annotated as *nnrS*, was identified upstream *nir* cluster, which might be a membrane-bound NO sensor with a role in nitrosative stress, still poorly explored [238].

The denitrification pathway has been proposed to be regulated mainly by transcription regulators of the CRP/FNR family, FNR and DNR, that in *M. hydrocarbonoclasticus* are encoded by *MARHY0862* (FNR homologue) and *MARHY3023* (DNR homologue), with this later ORF being located upstream the *nos* gene cluster. FNR, that activates genes under oxygen-limiting conditions, is a homodimer containing a [4Fe-4S] cluster per protomer, which is sensitive to oxygen and to nitrosylation [239]. On the other hand, DNR senses N-oxides, in particular NO [240], through a heme [73].

These two transcription regulators bind specifically to consensus sequences of the type $TTGATN_4ATCAA$ (named FNR binding box). Thus, the promoter regions of the four gene clusters were analyzed to identify the presence of these binding boxes, up to 200 bp upstream their ATG site.

The most homologous consensus sequences were identified based on its score and distance to the ATG site (Figure 3.2, Supplementary information - S1). For most of the gene clusters, the putative binding regions are located around - 60 to - 90 bp, with the exception of *nirSDLGH* (- 161.5 bp) and *dnr* (- 121.5 bp). These distances agree well with the average location of these sites in the whole genome of *P. aeruginosa* [241] and also with the more common spacing locations observed for FNR in *E.coli*, which are usually centered at approximately - 41, - 61, - 71, - 82 and - 92 bp from the transcription initiation point [242]. Although these binding sites still need to be experimentally confirmed, the involvement of MARHY0862 (FNR homologue) and MARHY3023 (DNR homologue) in the regulation of the denitrification pathway will be discussed below.

In order, to distinguish which regulator is in control of each binding box and if these regulatory elements are in fact active, promotor activity analysis by fusing a *lacZ* reporter gene with each promotor would have to be further tested, together with DNA electrophoretic mobility shift assays (EMSA).

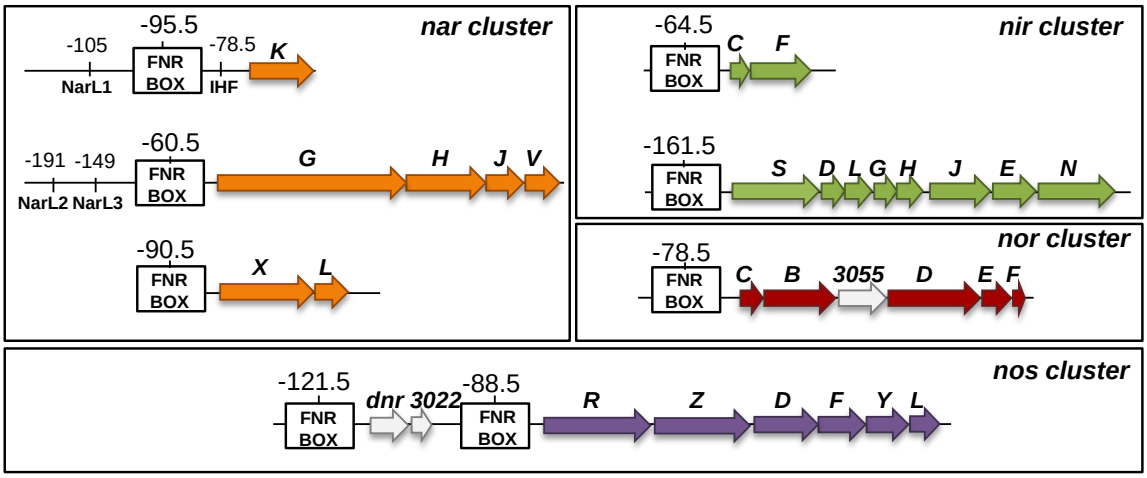

Figure 3.2 - Identification and analysis of putative FNR and NarL binding sites in nitrate reductase (*nar*), nitrite reductase (*nir*), nitric oxide reductase (*nor*) and nitrous oxide reductase (*nos*) gene clusters, involved in gene regulation. A putative FNR box was also identified upstream the *dnr* gene, located upstream *nos* gene cluster. The centered position of FNR, NarL and IHF sites relative to the ATG site is indicated. The matching of motifs with the consensus sequence and their scores are provided in Supplementary Information (S1).

In the case of *narGHJV* genes expression, two other regulators are usually associated, NarL and interaction with an integration host factor (IHF).

The NarXL system senses nitrate via NarX and responds to nitrate through NarL phosphorylation, activating the *nar* genes. NarL recognizes specific heptameric motifs (TACYYMT, being Y = T or C and M = C or A) located in the promoter regions of *nar* genes. Two potential sites (with high score to the ones identified in *P. aeruginosa* PAO1) were found in both *narK* and *narGHJV* (Figure 3.2, Supplementary Information S1). In the promoter region of *narK*, one NarL motif, NarL1 (TACCTCC), is centered at - 105 bp from the transcription initiation site, while in *narGHJV*, NarL2 (TGCTGCT) and NarL3 (TGCTTCT) sites, are centered at - 191 and - 149 bp, respectively (Figure 3.2). These motifs are oriented in the direction of *narGHJV* activation. Moreover, NarL is most probably not involved in regulation of *dnr* as no consensus sequences were identified upstream the FNR box, as opposite to what was described for *P. stutzeri* [243] *dnrE* and *P. aeruginosa* *dnr* [69] that carry the motifs and were shown to have a NarL-dependent transcription.

Between the NarL and FNR binding motifs is frequent to find motifs required for the binding of IHF, a heterodimer required for *nar* cluster induction [69, 244]. Our *in silico* analysis predicted a putative IHF binding site (CCCCAATGGTTTATAA) upstream *narK*, centered at position - 78.5 from the transcription initiation site, with a score of 83 % (Supplementary Information S1). Indeed, the motif is located downstream of *narK* predicted FNR box, but no other IHF binding motifs were detected in the promotor region of *narGHJV*. Nevertheless, a possible role of this protein in *nar* cluster induction cannot be ruled out.

3.2 *M. hydrocarbonoclasticus* growth in serum flasks: activity profile of enzymes of the denitrification pathway

M. hydrocarbonoclasticus was grown in AWS medium at pH 6.5 and 7.5 in sealed serum flasks (Figure 3.3). This close system mimics the deeper waters of aquatic systems as the oxygen tension is low.

In the initial 5 h, the cultures were stirred in an orbital shaker at 150 rpm and afterwards the stirring was reduced to 50 rpm. During the growths, pH was monitored, and in the case of pH 6.5 manually adjusted (pH varied between 6.5 and 6.9), while at pH 7.5 only minor variations were detected (pH varied between 7.3 and 7.7) and therefore at this pH the growth proceeded without pH adjustment.

Inspection of the growth curves indicates that the exponential phase started one hour after inoculation and had a duration of 5 h, with a rate of 0.19 ± 0.03 h^{-1} at pH 6.5 and 0.22 ± 0.02 h^{-1} at pH 7.5. After 5 h of growth, the time-point at which stirring was reduced, the growth enters in a stationary phase that lasts 50 h of growth. Furthermore, none of the growths showed a death phase.

During the growth, free nitrate and nitrite levels were quantified (as described in Materials and Methods, Section 2.4), which enabled us to monitor the activity of NaR and cd_1NiR, that catalyze the first and second steps of the denitrification pathway, respectively. Additionally the reduction rate of exogenous NO and N_2O by the whole-cells was determined at different times during the growth, as a way to identify when NOR and N_2OR were active in the cells.

The profile of denitrification metabolites shows that nitrate and nitrite were totally consumed in the growth performed in the serum flasks at pH 6.5 and 7.5, indicating that both enzymes, NaR and cd_1NiR, were active (Figure 3.3). As nitrite was consumed at both pH values, NO was most probably formed and acted as an inducer of the other denitrification enzymes.

Furthermore, metabolite concentration decreases faster at pH 7.5 comparatively to pH 6.5, suggesting that denitrification process is slower at more acidic pH (Figure 3.3).

The profile of the reduction rate of NO and N_2O by the whole-cells, grown at pH 7.5 in the serum flasks, shows maximum NO reduction rate at 3 h, when high levels of nitrite are still present in the medium, while the N_2O reduction was only observed after approximately 6 h of growth, indicating that both enzymes were active at pH 7.5 (Figure 3.3B). The ability of whole-cells to reduce these metabolites decreases towards the end of the growth.

On the other hand, the profile, obtained for *M. hydrocarbonoclasticus* grown at pH 6.5, showed very low rates of N_2O reduction, suggesting a lower expression of *nosZ* or that the form of N_2OR produced (a defeat at post-translational level) is not fully active (Figure 3.3A).

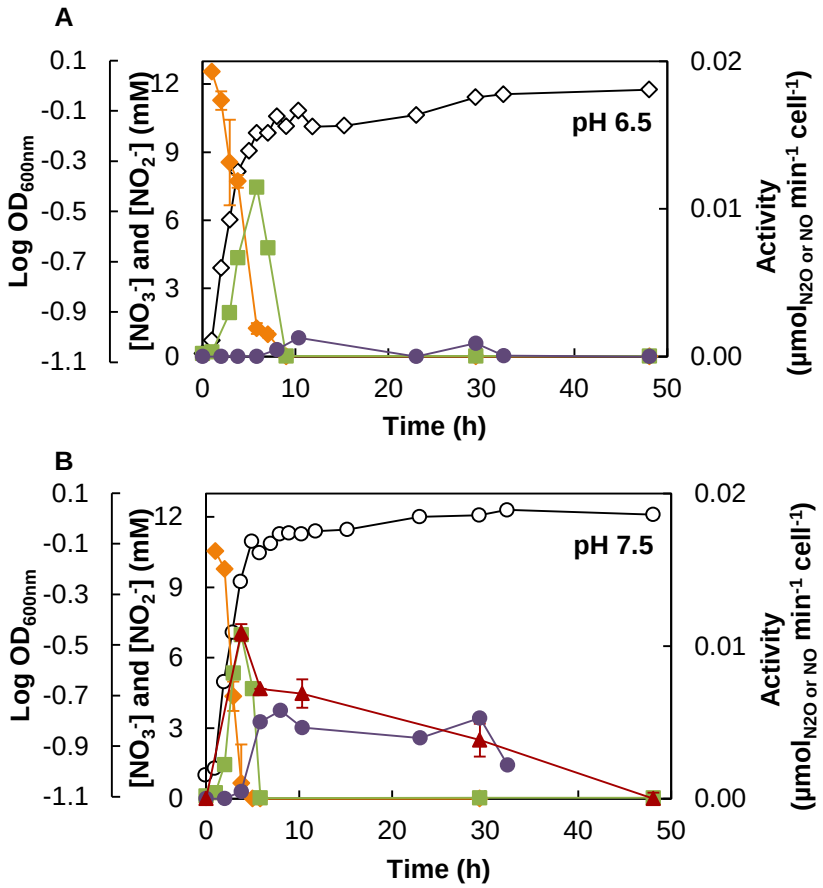

Figure 3.3 - *M. hydrocarbonoclasticus* growth curves in serum flasks under microaerobic conditions in the presence of nitrate and profile of denitrification metabolites and enzyme activities. In the upper panel (A), the growth curve (open diamonds) and the profile of metabolites and enzyme activities at pH 6.5 are presented. In the lower panel (B), the growth curve (open circles) and the profile of metabolites and enzyme activities at pH 7.5 are presented. Nitrate (orange diamonds) and nitrite (green squares) concentrations are reported in the primary axis and nitric oxide (red triangles), and nitrous oxide (purple circles) reduction by the whole-cells are represented in the secondary axis. The growth curves are represented as Log OD_{600nm} (open symbols). Nitric oxide reduction by the whole-cells was not determined in the growth performed at pH 6.5.

3.3 *M. hydrocarbonoclasticus* growth in a bioreactor under denitrifying conditions

A different type of growth, in a more controlled environment was also performed to investigate the effect of pH (6.5, 7.5 and 8.5) in the *M. hydrocarbonoclasticus* cultures. The growths were performed in a 2 L (5 L or 10 L for large scale protein production) bioreactor under microaerobic conditions (low aeration rate) and in the presence of nitrate (10 mM), to promote the denitrification (Figure 3.4) [21]. This type of growth is a model for denitrifying growth near the surface of an aquatic system.

At pH 7.5 and 8.5 the growth curves show the presence of a diauxic growth that occurs without any lag phase. The first phase at pH 7.5 lasts 5 h, while at pH 8.5 it has a slightly longer duration (approximately 7 h) but also a lower growth rate (Table 3.1). This phase is followed by a second phase that occurs until 28 h growth at pH 7.5 and until 23 h growth at pH 8.5, exhibiting similar

growth rates at both pH values (Table 3.1). After those times, both growths reached the stationary phase (Figure 3.4).

Moreover, for both pH values the O_2 levels rapidly decay and become negligible after 3 h until the end of the growth (Figure 3.4B). The lag phase was not observed in any of the replicated assays, indicating that there was no adaptation period or it was very small, and the death phase was not reached even after 48 h of growth, suggesting that the carbon source, lactate, had not been completely consumed. Similar diauxic growth has also been observed for *P. denitrificans* during anaerobic growth in the presence of 60 mM nitrate [245].

Despite the similar growth behavior at pH 7.5 and 8.5 a morphological change in *M. hydrocarbonoclasticus* cells was observed at pH 8.5. The cells lost their rod shape and became spherical (the same change in cell shape was observed when *M. hydrocarbonoclasticus* is plated onto a solid media at pH 8.5). Cells return to their usual rod shape when cultured again at pH 7.5, either in liquid or solid media. This cell shape change might be due to a reversible pH effect on the enzymes complexes involved in cell wall synthesis or in the cell wall assembly itself or it could also correspond to a modification on the membrane lipid content.

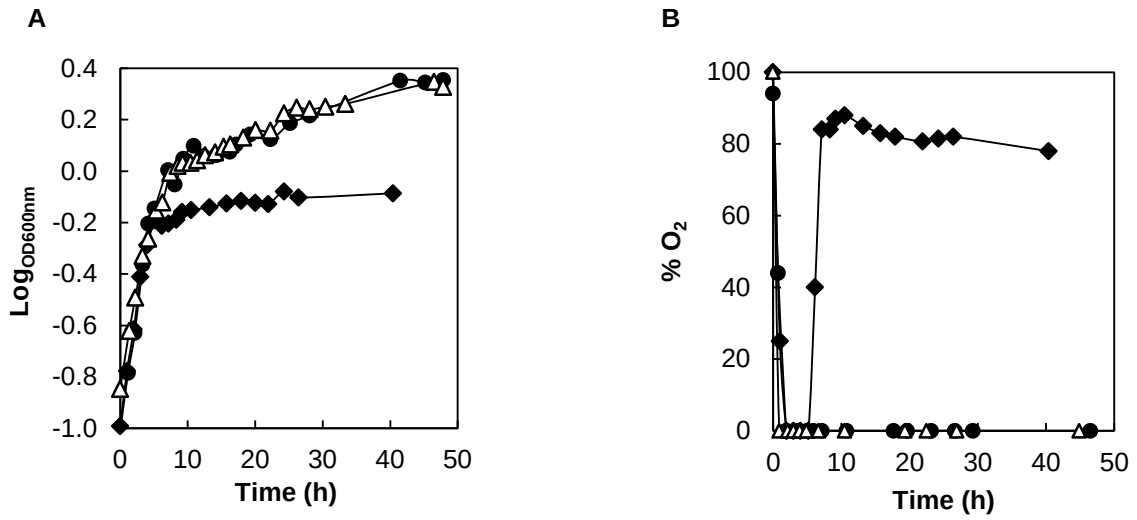

Figure 3.4 - Growths of *M. hydrocarbonoclasticus* in a 2 L bioreactor under microaerobic conditions at different pH values. Representative (A) growth profile and (B) oxygen profile measured during the growth. Growths were performed at pH 6.5 (filled diamonds), pH 7.5 (filled circles) and pH 8.5 (open triangles).

A different growth behavior was observed at pH 6.5 showing only two different phases, a short 4 h exponential phase with a growth rate of 0.164 ± 0.014 h^{-1}, followed by a long stationary phase (Figure 3.4, Table 3.1). Interestingly, at more acidic conditions the oxygen rapidly decays in the beginning of the exponential phase, similarly to the growth at other pH values, however an increase is observed after time-point 5 h, reaching levels around 90 % that remain high during the rest of the growth or in some growth replicas it decays, but only at the end of the growth. In fact, the increase of oxygen levels is simultaneous with the transition to the stationary phase, most probably due to

accumulation of toxic byproducts (see below), suggesting that *M. hydrocarbonoclasticus* growth ceases (OD_{600nm} = 0.64) at more acidic pH values leading to oxygen accumulation in the medium as the system is being continuously aerated.

Furthermore, the final OD_{600nm} is lower at pH 6.5 (OD_{600nm} = 0.82) than at pH 7.5 and 8.5 (OD_{600nm} = 2.11), corresponding to different cell mass yields (around 5 g L^{-1} growth to pH 6.5 *vs* around 8 g L^{-1} for the higher pH values).

Table 3.1 - Specific growth rates (μ) of *M. hydrocarbonoclasticus* cultures under denitrifying conditions at different pH in the bioreactor (microaerobic growth) and in the serum flasks (anaerobic growth). For the diauxic growths two specific growth rates were calculated.

pH	Microaerobic growth		Anaerobic growth
	$\mu_{first\ phase}$ (h^{-1})	$\mu_{second\ phase}$ (h^{-1})	μ (h^{-1})
6.5	0.164 ± 0.014	-	0.190 ± 0.030
7.5	0.173 ± 0.008	0.011 ± 0.001	0.220 ± 0.020
8.5	0.142 ± 0.008	0.012 ± 0.001	-

The growths performed in the bioreactor exhibited a different behavior from those performed in the serum flasks, as no diauxic growth was observed in the serum flasks. However, when comparing the specific growth rates, higher rates were observed for *M. hydrocarbonoclasticus* growth in the serum flasks at pH 6.5 and 7.5, and closer to the rate determined in the batch cultures at pH 7.5.

3.4 Gene expression during *M. hydrocarbonoclasticus* growth under denitrifying conditions

The expression of genes involved in the denitrification pathway during *M. hydrocarbonoclasticus* growth under denitrifying conditions at pH 6.5, 7.5 and 8.5 was analyzed by qPCR.

The *in silico* analysis of *M. hydrocarbonoclasticus* (ATCC 49840) genome indicated the presence of two *norB* genes (*MARHY3014* and *MARHY3054*), thus the expression of both genes was analyzed. The results showed that *norB_MARHY3054* (*c-norB*) gene appears to be the one transcribing an active nitric oxide reductase under the denitrifying conditions used, as no significant expression levels were obtained for *norB_MARHY3014* (*q-norB*) gene under these conditions (Figure 3.5). Therefore, *norB_MARHY3014* gene encoding a putative *q*-type NOR does not seem to be preferentially expressed during the denitrifying conditions tested here, and so its role in *M. hydrocarbonoclasticus* physiology remains unknown.

Expression profiles have shown that the maximum transcription levels of genes encoding the catalytic subunits of the denitrifying enzymes, *narG*, *nirS*, *c-norB* and *nosZ* occurs at the same time point (Figure 3.5).

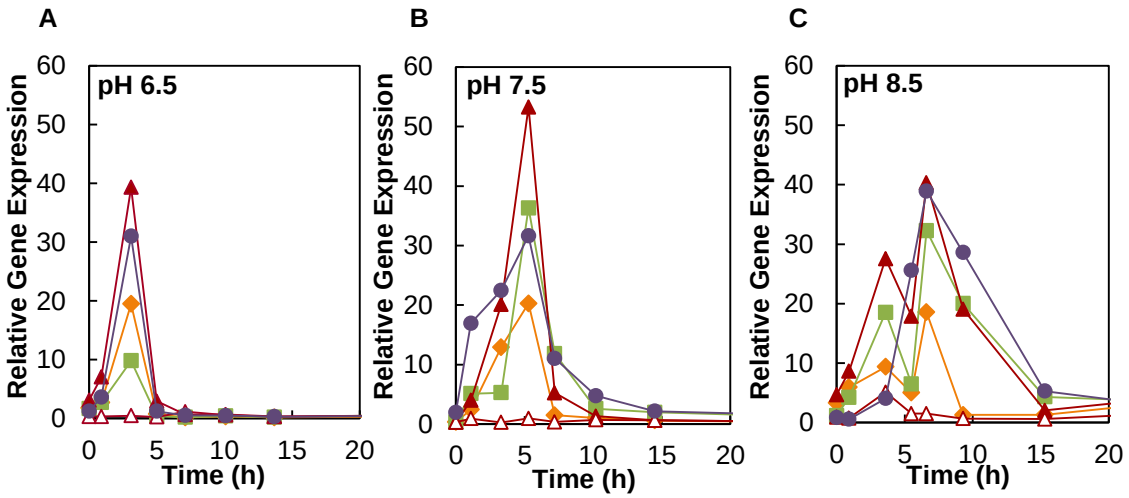

Figure 3.5 - Expression of *narG* (orange diamonds), *nirS* (green squares), *c-norB* (filled red triangles), *q-norB* (open red triangles) and *nosZ* (purple circles) encoding the catalytic domains of *M. hydrocarbonoclasticus* denitrification enzymes during 20 h for the growths performed at (A) pH 6.5, (B) pH 7.5 and (C) pH 8.5. Relative expression values were obtained by normalizing expression of each target gene relative to the control housekeeping gene 16S rRNA, as described in Materials and Methods (Section 2.6.2).

In *P. denitrificans*, *nosZ* and *narG* are expressed earlier than *nirS* [246]. This pattern of transcription was associated with oxygen removal that would trigger *narG* and *nosZ* transcription, while the onset of *nirS* (and most probably *norB*) transcription was associated with the increase in NO concentration that occurs afterwards [246]. In fact, more recent studies on this bacterium showed that *nosZ* is expressed earlier than both *nirS* and *norB* [247]. The simultaneous transcription of *narG*, *nirS*, *c-norB* and *nosZ* in *M. hydrocarbonoclasticus* suggests that a common signal(s) regulates the expression of these genes. Oxygen might have a role, as after 2-3 h of growth, it becomes negligible (Figure 3.4B).

The maximum levels of transcription occurred at time-point 3 h, 5 h and 7 h for pH 6.5, 7.5 and 8.5, respectively, which corresponds to the end of the exponential phase in each curve (Figure 3.4A). At this point, *narG* transcription levels are similar at the different pH values, but they are lower than the level of other genes encoding the catalytic subunits of the denitrification enzymes (Figure 3.5). Thus, additional regulatory mechanisms might be involved in the *nar* gene cluster expression. In fact, *M. hydrocarbonoclasticus nar* genes, similarly to what was observed in *P. stutzeri* [243] and *P. aeruginosa* [69], might be under the regulation of *narXL*, a two-component regulatory system that responds to nitrate, as NarL and also IHF DNA binding sites have been identified in the promoter region of *nar* gene cluster (Figure 3.2).

The gene expression profile in *M. hydrocarbonoclasticus* also showed that *nirS* expression is approximately 4-fold lower at pH 6.5 relative to pH 7.5 and 8.5 (Figure 3.5). Comparison of *nosZ/nirS* and *nosZ/norB* ratios at the maximum transcription points observed at each pH, shows

that *nosZ/nirS* is highly affected at pH 6.5, while no majors differences were observed in the *nosZ/norB* expression ratio at the different pH values tested, indicating that *nirS* is down-regulated at pH 6.5 (Figure 3.6). Furthermore, at pH 6.5 nitrite levels remained high (at around 6.5 mM) until the end of the growth (Figure 3.8). Interestingly, in *P. denitrificans* cultures grown at pH 6.0 nitrite accumulation in the medium was also observed, but in this case lower numbers of *norB*, *nosZ* and *nirS* transcripts (*narG* quantification was not reported), relative to growths performed at pH 7.0, were reported, although *nosZ/nirS* and *nosZ/norB* ratios were not significantly affected [247].

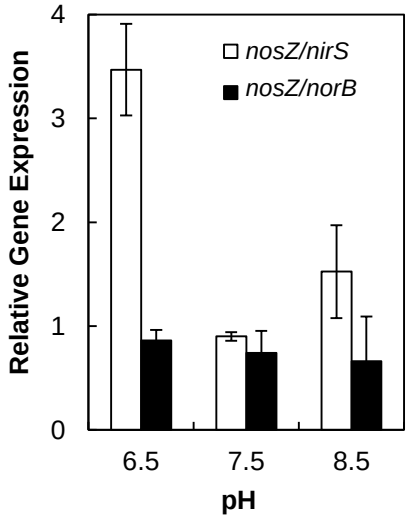

Figure 3.6 - Comparative gene expression of *nosZ/nirS* (white bars) and *nosZ/norB* (black bars) at pH 6.5, 7.5 and 8.5, at the time-point of maximum expression levels in the biological replicates. Relative expression values were obtained by normalizing expression of each target gene to the control housekeeping gene 16S rRNA.

3.5 Regulation of denitrification pathway in *M. hydrocarbonoclasticus* growth

In *M. hydrocarbonoclasticus*, the signals involved in the regulation of the denitrification genes have not been established. However, it is expected that the common effectors are oxygen and NO, as identified in other denitrifying bacteria [248], through FNR and DNR, respectively. In fact, given the pattern of transcription observed for the genes encoding the catalytic denitrifying subunit/domain, it can be postulated that oxygen and NO are also the main effectors in *M. hydrocarbonoclasticus*, and a putative regulatory network is presented (Figure 3.7).

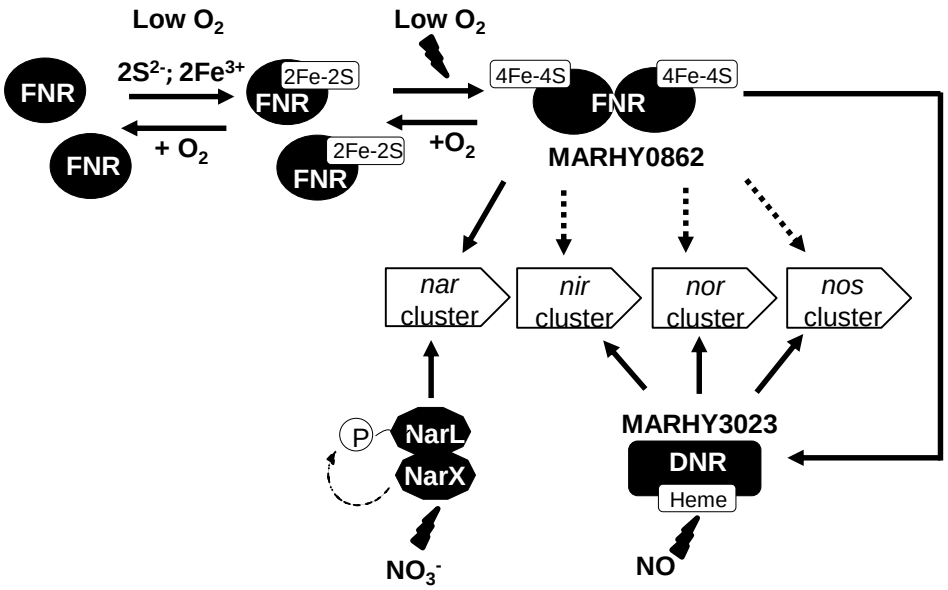

Figure 3.7 - Putative regulatory network controlling the denitrification genes in *M. hydrocarbonoclasticus*. The main signals involved in the regulation of *nar*, *nir*, *nor* and *nos* gene clusters are the low oxygen tensions, nitric oxide and nitrate. Two levels of regulation were postulated for *nar* cluster transcription through the FNR-like and the two-component system NarXL (histidine kinase and response regulator) in response to low oxygen and nitrate levels, respectively. The regulatory protein FNR is also involved in DNR activation. DNR responds to nitric oxide (first produced by the initial low levels of nitrite reductase) and regulates the expression of *nir*, *nor* and *nos* gene clusters. Our own bioinformatic analysis suggests that MARHY0862 and MARHY3023 are, respectively, the FNR and DNR homologues involved in regulation of the denitrification genes in *M. hydrocarbonoclasticus*. Dashed arrows indicate the putative but lower level of *nir*, *nor* and *nos* gene regulation by FNR.

Upon decrease of oxygen tension in the medium, FNR (MARHY0862) dimerize, becoming activated, and are able to bind specific DNA regions, activating the transcription of several genes required for the anaerobic metabolism, which include activation of *dnr* and *narGHJV*. In turn, due to the initial activity of cd_1NiR, from the initial low levels of *nirS* transcription, NO concentration will increase, and DNR (MARHY3023) will activate *nir*, *nor* and *nos* genes. In *P. aeruginosa* and *P. stutzeri*, DNR was also identified as having a NO-dependent response, being involved in the transcription of *nir*, *nor* and *nos* genes [31, 61, 249].

The existence of a cascade type regulation for these genes will prevent the accumulation of toxic products, such as NO. Although, FNR and DNR recognize the same promoter regions (as mentioned before), it has been shown that DNR is the specific regulator of denitrification [241]. The mechanism for the discrimination of these binding sites is still unknown, though nitrosylation of FNR could play a role, as when nitrosylated (which could occur above a certain NO level threshold), FNR reduces its binding affinity to the specific DNA regions. Moreover, as DNR lacks the cysteine motifs for Fe-S cluster formation and most probably senses NO through heme [73-75], it can still be active even if FNR is nitrosylated. This double regulatory mechanism will be important to avoid increasing release of toxic NO by cd_1NiR, together with down-regulation of *nir*, *nor* and

nos gene clusters, as with a second regulator, as DNR, denitrification can proceed by activating these genes clusters. On the other hand, *nar* genes would be regulated by low levels of oxygen and nitrate that activates their expression through the two-component system NarXL.

Although at pH 7.5, the expression of *nosZ* is higher after 1 h than the one of the other genes (Figure 3.5), this was not observed for the other pH values tested and thus *nosZ* may not be directly regulated by oxygen, contrary to other bacteria in which the earlier expression of *nosZ* suggested a direct regulation by oxygen levels [247]. This strengthens the hypothesis of *nosZ* being under DNR regulation.

3.6 Activity profile of denitrification pathway enzymes

In the case of *M. hydrocarbonoclasticus* growth performed in the bioreactor, the free nitrate and nitrite were also quantified during the time of the growth to monitor the activity of NaR and cd_1NiR (Figure 3.8). Reduction rate of nitric oxide and nitrous oxide by whole-cells was also determined at different time-points for the different pH values, similarly to the analysis performed for the growth in the serum flasks (Figure 3.8).

Common to all pH values, nitrate was totally consumed at the beginning of the growth, starting to be consumed in the second hour of the growth performed at pH 7.5 and 8.5, at the time-point at which oxygen level becomes negligible. However at pH 6.5, its consumption was slightly slower and only started after time-point 3 h (Figure 3.8). This is an indication that nitrate transport to the cytoplasm and NaR were active in the cells at that time point, independently of the growth pH. Indeed, at time-point 1 h, *narG* gene expression was already occurring at low levels, and thus it is likely that NaR was already active in the cells at that time (Figure 3.5). These results strengthen the hypothesis that nitrate and also a decrease on oxygen levels are the signals for the activation of *nar* genes transcription in *M. hydrocarbonoclasticus* (Figure 3.7).

The decrease in nitrate concentration was concomitant with the formation of nitrite, which reaches a maximum value close to the initial nitrate concentration.

In the growths performed at pH 7.5 and 8.5, the nitrite was completely consumed after approximately 8 h (during the initial stages of the second diauxic growth phase). This decrease in nitrite concentration can be attributed to the activity of cd_1NiR. In fact, the maximum nitrite concentration is achieved before maximal *nirS* expression. Considering that the decrease of nitrite concentration is due to cd_1NiR activity, as the denitrification pathway is active, the concomitant formation of nitric oxide is expected. The increasing concentration of NO will have a positive regulatory effect not only on *nirS* but also on *norB* and *nosZ* expression, as it was observed (Figure 3.5). This supports the hypothesis of NO being involved in the regulation of these genes through a DNR-type regulator (Figure 3.7).

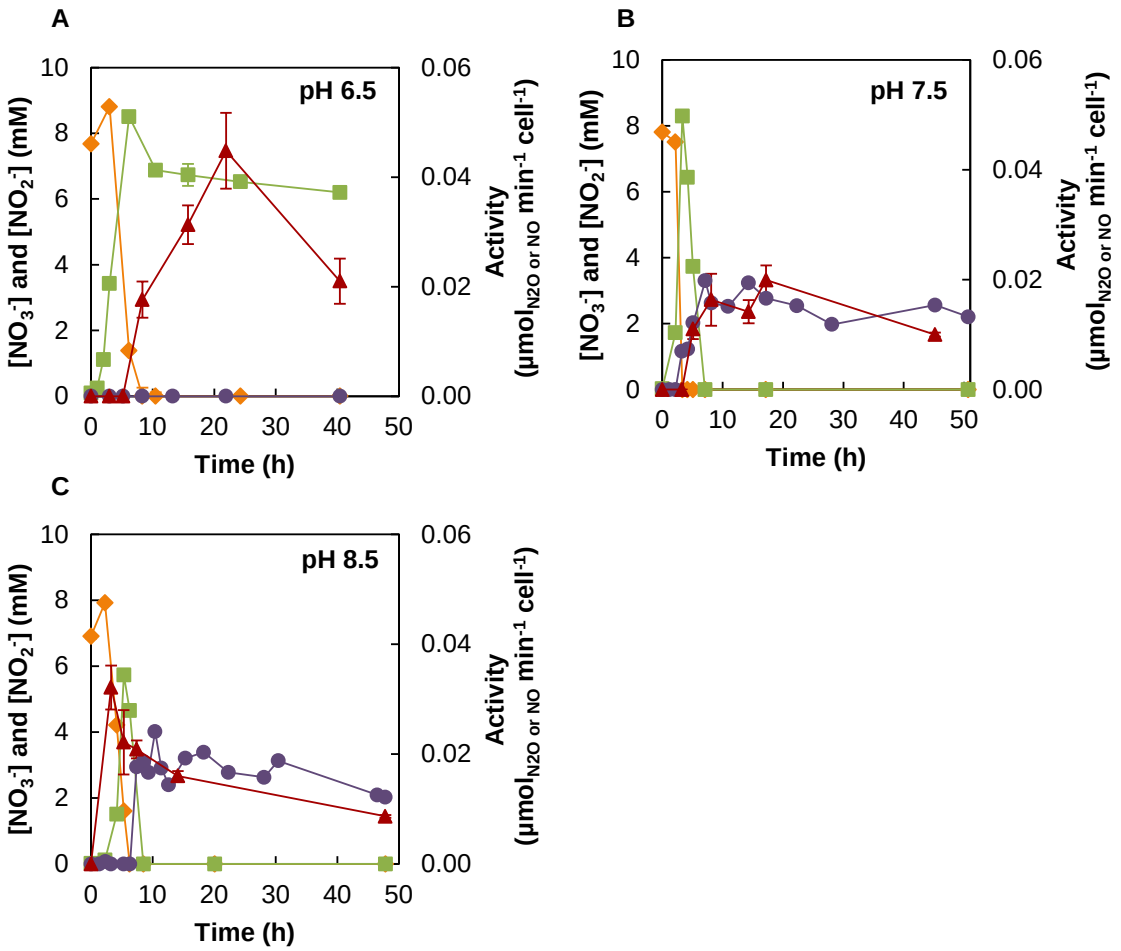

Figure 3.8 - Representative profile of *M. hydrocarbonoclasticus* denitrification metabolites and enzymatic activities at (A) pH 6.5, (B) pH 7.5 and (C) pH 8.5. Nitrate (orange diamonds) and nitrite (green squares) concentrations are represented in the primary axis and nitric oxide (red triangles), and nitrous oxide (purple circles) reduction by the whole-cells are represented in the secondary axis.

On the other hand, at pH 6.5 only 27 % of the total nitrite produced was consumed and thus high levels (6.2 mM) remained in the medium until the end of the growth (Figure 3.8A). Nitrite accumulation was also previously observed in different culture conditions of *P. denitrificans* grown at pH 6.0 and pH 6.8 [246, 247]. In fact, nitrite accumulation was also recently proposed to inhibit aerobic growth of *P.denitrificans* and it was linked to an increase of the expression of *fhp* gene (co-located with NsrR) encoding a flavohemoglobin hypothesized to potentially convert NO to nitrite or to N_2O [251].

As mentioned before, at pH 6.5 there are lower expression levels of *nirS* and thus lower levels of cd_1NiR in the cells would be expected, which was confirmed by electrophoretic studies (heme staining of SDS-PAGE) (Figure 3.9).

Even in *P. denitrificans* grown at suboptimal pH 6.8 and in which no differences in *nirS* expression was observed (relative to pH 7.5), lower NiR levels were immunochemically detected in the cells [246].

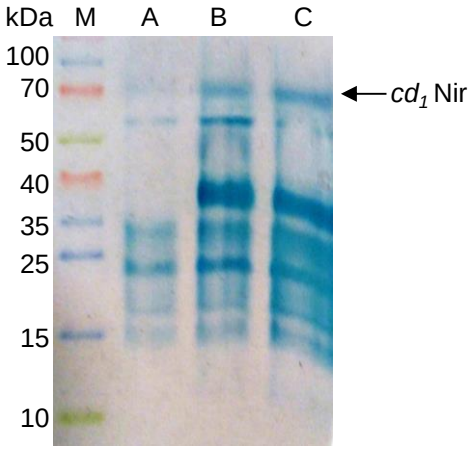

Figure 3.9 - Heme stained SDS-PAGE (12.5 % polyacrylamide gel) analysis of cells of *M. hydrocarbonoclasticus* grown in the bioreactor under microaerobic conditions in the presence of nitrate. Lanes A, B and C are the total extract obtained from the growth at pH 6.5, 7.5 and 8.5, respectively, normalized for an amount of cells (0.24 g cells mL^{-1}). The protein band corresponding to cd_1NiR is identified in the gel.

The observed nitrite accumulation in *M. hydrocarbonoclasticus* is correlated not only with the decrease in *nirS* expression, but also with a possible inactivation of the cd_1NiR by nitrous acid (HNO_2) that is formed (4.3 μM) under these conditions: the presence of nitrous acid might also be responsible for the growth arrest that is observed at pH 6.5. In fact, HNO_2 formation by denitrifying bacteria was previously observed in acidic cultures of *Pseudomonas fluorescens* and *P. denitrificans* upon nitrite accumulation [246, 250, 251]. Furthermore, HNO_2 dissociates into reactive species, such as nitric oxide and nitroxyl anion intermediates. Indeed, NO measurements in *P. denitrificans* cultures grown between pH 6 and 7.5 showed that NO accumulation is higher at more acidic pH values [252]. Thus, although cd_1NiR is inactivated at acidic pH, nitric oxide can be chemically formed explaining the NOR activity observed (Figure 3.8A).

The last two steps of the denitrification pathway are catalyzed by NOR and N_2OR, and thus the reduction rate of NO and N_2O was monitored indirectly through the oxidation of methyl viologen by the whole-cells (Figure 3.8). The results obtained show that the rates of NO and N_2O reduction were similar for the growth at pH 7.5 and 8.5, indicating that both NOR and N_2OR were active in the cells until the end of the growth, even if NO and N_2O are expected to be completely consumed earlier on [247]. Moreover, at these pH values, NOR is active in the cells before the completely consumption of nitrite, as at this point *c-norB* had already started to be transcribed.

The major difference between pH 7.5 and 8.5 is the time-point at which N_2OR becomes active, as at pH 7.5 cells are able to reduce N_2O at the time-point 3 h, while in the cells grown at pH 8.5 it was at 7 h. In fact, all our replicates of gene expression profile obtained at pH 7.5, show that at time-point 1 h *nosZ* had already started to be expressed at higher levels than the other genes and

earlier than its expression in any other pH (Figure 3.5). Furthermore, a delay between *nosZ* gene expression and the enzymatic activity at pH 7.5 was also observed and attributed to its complex maturation process, which involves several accessory factors. Thus, at pH 7.5, N_2OR is most probably ready to reduce N_2O as soon as this molecule is generated, explaining why both NOR and N_2OR were concomitantly active in the cells at this pH.

Therefore, since reduction of N_2O by the whole-cells was detected, it is plausible to argue that the four steps of the denitrification pathway are carried out at pH 7.5 and 8.5. On the other hand, at pH 6.5, NO might be chemically formed and most probably is reduced to N_2O, as the whole-cells are able to reduce exogenous NO, indicating that NOR is active in these cells. Although *c-norB* is concomitantly expressed with other genes at time-point 3 h and the timing of maximum transcription at pH 6.5 is earlier than at pH 7.5 and 8.5, the reduction of NO is observed only at time-point 8 h confirming that the denitrification process is slower at more acidic pH values.

On the other hand, the rate of N_2O reduction by the whole-cells is practically inexistent along the growth at pH 6.5 (Figure 3.8). Additionally, we also tested the reduction of exogenous N_2O by the whole-cells using a higher volume of cellular suspension (foreseeing that the N_2OR production could be lower). However, N_2O reduction was still not observed, an indication that N_2OR is not active in the cells grown under these conditions.

Gas measurements performed in *P. denitrificans* grown at low pH, showed accumulation of high levels of N_2O in the medium and a lower N_2 production that also started much later, compared to the growths at more neutral pH values [247]. These results evidenced a clear impair of denitrification at more acidic pH values, which corroborates our results on *M. hydrocarbonoclasticus*. This can explain the accumulation of N_2O when there is a drop of the pH in the environment (soil or water), as N_2OR is not active.

The inability of the cell suspension at pH 6.5 to reduce N_2O means that N_2OR is not present in an active form *in vivo*, which cannot be attributed to a deficient transcription of *nosZ* (Figure 3.5). Thus, to explain the absence of N_2O reduction by *M. hydrocarbonoclasticus* grown at pH 6.5 we investigated two possibilities (see Section 3.8):

i) effect of pH on the transcription of the accessory factors involved in the biosynthesis of N_2OR;

ii) effect of the pH on *M. hydrocarbonoclasticus* proteome.

3.7 Kinetic parameters for N_2O reduction by whole-cells

The N_2O reduction by whole-cells was also investigated for the collected cells from *M. hydrocarbonoclasticus* grown at pH 7.5 (48 h) and a hyperbolic behavior was observed (Figure 3.10). Note that activity is reported considering the total amount of protein, while in the previous assays the activity was reported considering the optical cell density.

In these conditions, *M. hydrocarbonoclasticus* cells exhibit a V_{max} of 2.2 ± 0.1 μmol_{N2O} min^{-1} mg^{-1} of total protein, for the reduction of N_2O and a K_m of 18 ± 5 µM. This K_m is in the same order of magnitude as the K_m of clade I *P. stutzeri* strain DCP-Os1 N_2OR (36 ± 9 µM) determined by N_2O consumption measurements, which are lower than those reported for whole-cells containing clade II N_2OR (1.0 ± 0.2 µM and 1.3 ± 0.4 µM, from *Dechloromonas denitrificans* strain ED-1 and *Anaeromyxobacter dehalogenans* strain 2CP-C, respectively) [99].

Furthermore, the K_m determined for N_2O reduction by *M. hydrocarbonoclasticus* whole-cells is similar to the value reported for the N_2O reduction by the *in vitro* activated N_2OR (K_m of 12 ± 4 µM) [122].

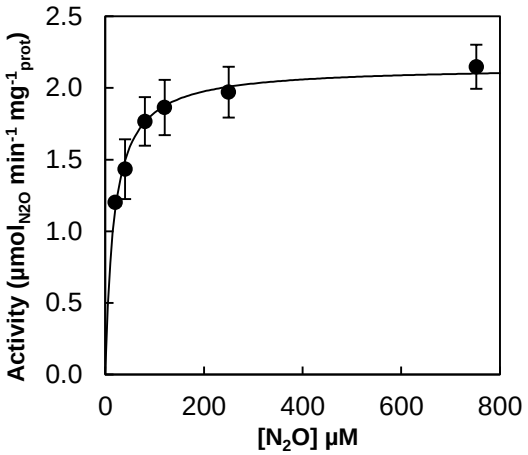

Figure 3.10 - Kinetic activity for the reduction of N_2O by the whole-cells of *M. hydrocarbonoclasticus* grown under microaerobic conditions in the presence of nitrate at pH 7.5. Assays were performed using methyl viologen as the electron donor and 20, 40, 80, 120, 250 and 750 µM N_2O-saturated water. Data were fitted to Michaelis-Menten equation, using a K_m of 18 ± 5 µM and V_{max} 2.2 ± 0.1 μmol_{N2O} min^{-1} mg^{-1} of total protein.

3.8 Why cells that grow at more acidic pH are not able to reduce N_2O?

3.8.1 Analysis of the expression levels of genes involved in the biosynthesis of N_2OR

The biosynthesis of N_2OR requires accessory proteins encoded by genes that are often part of the *nos* cluster. Thus, we investigated the transcriptional organization of *nos* cluster in *M. hydrocarbonoclasticus* using a sample collected from the growth performed in a bioreactor at pH 7.5. Our *in silico* analysis of *nos* cluster predicted that *nosRZDFYL* is most probably transcribed as a single transcriptional unit. To confirm our hypothesis primers were drawn for the PCR amplification of the intergenic regions. The size of the amplicons of cDNA samples corroborate with bioinformatic analysis (Figure 3.11). Thus, *nosRZDFYL* is transcribed into a single transcriptional unit and its organization is similar to that described for *P. aeruginosa nos* gene cluster [61].

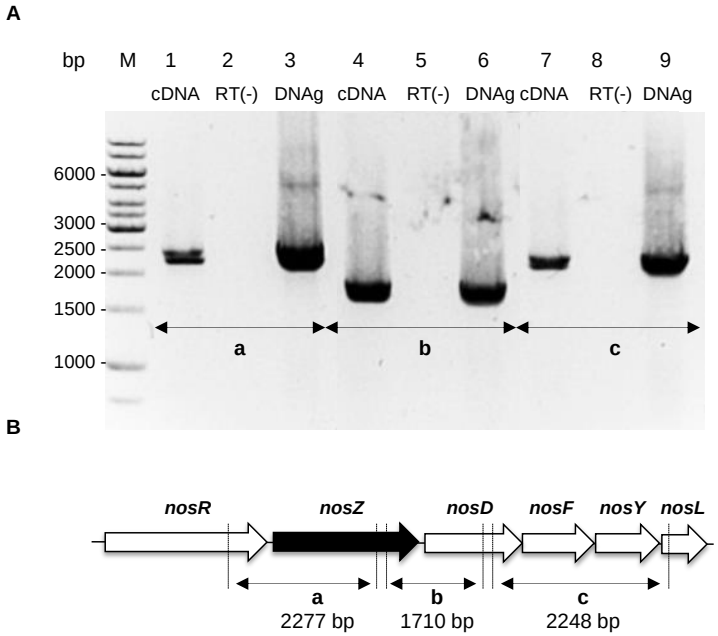

Figure 3.11 - Analysis of the transcriptional organization of *M. hydrocarbonoclasticus nos* gene cluster. (A) PCR products of intergenic regions between *nosR-nosZ* (a, lanes 1-3), *nosZ-nosD* (b, lanes 4-6) and *nosD-nosL* (c, lanes 7-9) using cDNA (lanes 1, 4, 7), RT (minus) control reaction (lanes 2, 5, 8) and genomic DNA (3, 6, 9). (B) Genomic organization of *nos* gene cluster in the genome of *M. hydrocarbonoclasticus*. The gene encoding for N_2OR is colored in black.

The expression of the accessory genes proposed to be involved in the assembly of the "CuZ center" or in maintaining N_2OR in an active state was examined as a function of pH (samples collected from growths performed in the bioreactors were used). These included not only *nosR*, *nosD*, but also two homologues of *nosX*, *MARHY1380* and *MARHY1479*, members of the *nosX*/*apbE* family (*nosX* is absent from *M. hydrocarbonoclasticus nos* cluster, but postulated to be essential for N_2OR activity [81]) (Figure 3.12).

The data indicates that *MARHY1380* is the *nosX* homologue in *M. hydrocarbonoclasticus*, as it presents higher expression levels than *MARHY1479* and its expression profile is similar to the one of the denitrifying genes (Figure 3.12).

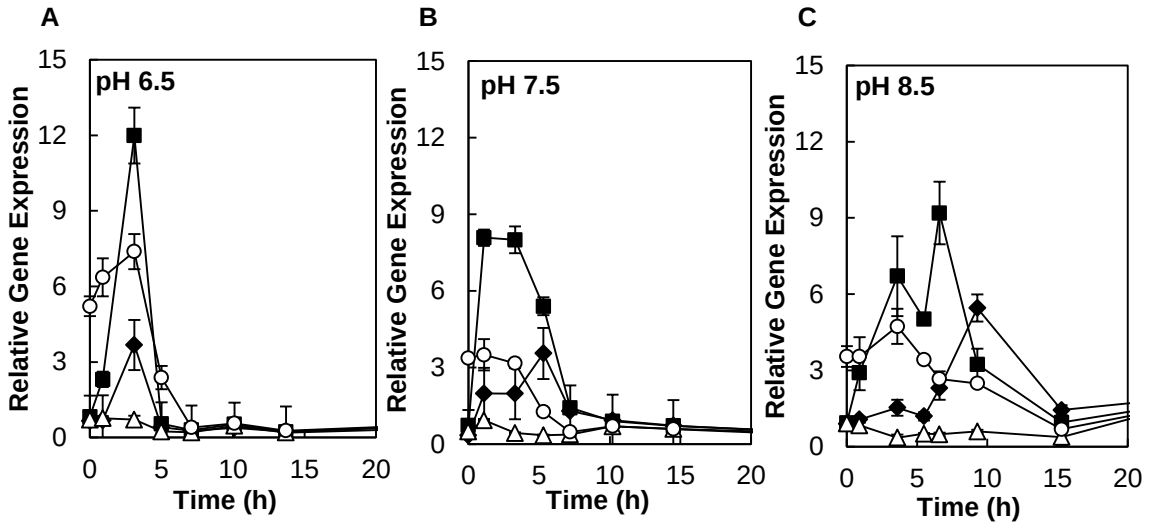

Figure 3.12 - Expression of *nosR* (filled diamonds), *nosD* (filled squares), *MARHY1380* (open circles) and *MARHY1479* (open triangles) encoding accessory proteins involved in biosynthesis of N_2OR from *M. hydrocarbonoclasticus* during 20 h, for the growths performed at (A) pH 6.5, (B) pH 7.5 and (C) pH 8.5. Relative expression values were obtained by normalizing expression of each target gene to the control housekeeping gene 16S rRNA, as described in Materials and Methods (Section 2.6.2).

Therefore, as observed in *P. stutzeri* the *nosX* homologue is remotely located in the genome downstream to the *nqr* operon [82, 86], and the same location was also identified for the *MARHY1380* in *M. hydrocarbonoclasticus*. Furthermore, the ApbE enzymes from *P. stutzeri* and *M. hydrocarbonoclasticus* were recently heterologously produced in *E. coli* and proposed to be the flavin donor protein of NosR [86].

The results presented in Figure 3.12 also indicate that no significant differences in the expression levels of the N_2OR accessory genes at different pH values are observe under the denitrifying conditions used (Figure 3.12). Moreover the maximum transcription levels of these genes occurred at the time-point at which *nosZ* gene expression is also maximal for pH 6.5 and 8.5. However at pH 7.5, these accessory genes are earlier expressed, being its maximum transcriptional level observed after 1 h. The expression of these genes in the beginning of the growth strengthens our hypothesis of earlier production of N_2OR at this pH (Figure 3.8B).

The mechanism of assembly of copper centers in N_2OR is not fully understood and in fact more than one mechanism might be involved in the insertion or maintenance of the centers in N_2OR [82]. We investigated if there is any down-regulation of genes at pH 6.5 that have been proposed to play a role in copper insertion in N_2OR from *M. hydrocarbonoclasticus*: *nosL*, *MARHY1049* and *senC* (Figure 3.13). In *M. hydrocarbonoclasticus*, *MARHY1049* encodes a conserved hypothetical protein of the periplasmic copper chaperone family, PCuAC, while the product of *senC* belongs to the SCO protein family implicated in the copper insertion in C*c*O [106-108].

The relative expression of *nosL* is similar between both pH and higher than *MARHY1049* and *senC* expression, as *nosL* is part of *nos* cluster and similar expression levels were observed for other

genes comprising the same cluster (Figure 3.12). However, in some organisms as *P. putida*, NosL has proven not to be essential for the synthesis of a functional N_2OR and the possibility of other candidates to insert the copper into "CuZ center" has been raised [82]. Recently, the products of *senC2*, *pcuC* and *Pden_4445* genes have been predicted to be involved in the copper assembly and maintenance of N_2OR from *P. denitrificans* [111].

Although both *MARHY1049* and *senC* have a lower expression when compared to *nosL*, no major differences were observed between pH 6.5 and 7.5 (Figure 3.13). These results corroborate later studies (see below) in which N_2OR isolated from the preparations obtained at different pH values presented a similar copper content. Therefore, copper insertion and expression of proteins involved in center assembly are most likely not being affected at pH 6.5.

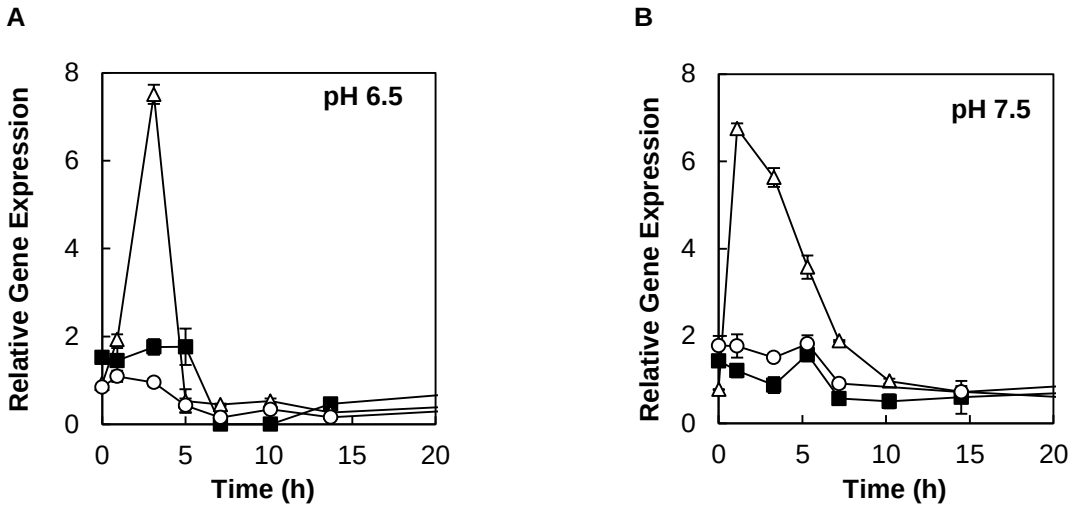

Figure 3.13 - Expression of *nosL* (open triangles), *senC* (open circles), *MARHY1049* (filled squares) encoding *M. hydrocarbonoclasticus* denitrification enzymes during 20 h for the growths performed at (A) pH 6.5 and (B) pH 7.5. Relative expression values were obtained by normalizing expression of each target gene to the control housekeeping gene 16S rRNA, as described in Materials and Methods (Section 2.6.2).

In conclusion, our data suggests that, even though there are differences between pH, no significant influence was observed on the transcriptional level of any gene associated with the maturation of N_2OR or in maintaining the active form of "CuZ center" *in vivo* that could explain the low N_2O reduction rates at pH 6.5.

3.8.2 Proteome of denitrifying *M. hydrocarbonoclasticus*

The effect on denitrification caused by acidic pH is recurrent and of prime importance. The regulatory mechanisms of pH in the periplasm are still poorly understood in Gram-negative bacteria, but a perturbation of pH in the growth medium is proposed to be reflected in the periplasm of *M. hydrocarbonoclasticus*, as its cell wall is permeable to ions [253-255]. On the contrary, the cytoplasm is most probably maintained at neutral pH, as it is capable of buffering itself and, in fact, protons are moved across de membrane generating an electrochemical gradient [253, 254].

Our results show that although the expression of *nosZ* and its accessory genes are not affected at pH 6.5, the N_2OR is inactive *in vivo*, most probably due to a post-transcriptional effect and thus we investigated the differences in proteins involved in the maturation of N_2OR, most of which are embedded or anchored to the membrane. In fact, recently it was reported that those proteins can form a supra-molecular complex in *P. aeruginosa* [180]. In this supra-molecular complex, integral membrane proteins of denitrification pathway (NarI, NorB, NorC and NosR) are associated with a complex array of other proteins (such as denitrifying enzymes, maturation factors, enzymes involved in the energy generation, as well as the systems associated to protein export) that together mediate the nitrate respirasome [180].

M. hydrocarbonoclasticus membrane proteome of denitrifying cells was analyzed by a 2D SDS-PAGE (based on pI and molecular mass). Differences in the proteome may reflect an alteration caused by pH, and further identification of these proteins by mass spectrometry (MS) can give a clue to explain the low N_2O reduction rate observed at pH 6.5.

The abundance of proteins is related to the growth phase wherein the cells are collected. Thus, we analyzed the cells in the stationary phase at the end of the growths (~ 48 h) performed at pH 6.5 and 7.5 in the bioreactor, under microaerobic conditions. Afterwards, the cells were lysed and ultracentrifuged to obtain the membrane fraction (the membranes were not washed to guarantee that the loosely-associate proteins were not removed) and analyzed by 2D separation. Preliminary electrophoretic maps (in the 3-10 pH range, data not shown) revealed that the protein spots were mostly acidic and thus imobiline strips in the 4-7 pH range were used in the assays.

Two biological replicates of membrane proteomes were obtained for each pH growth and representative gels are presented below (Figure 3.14). The 2D profiles maps show a relative good separation between the proteins. A clear proteome of membrane fractions is often challenging to obtain as these proteins are hydrophobic and prone to precipitation or aggregation and thus a proper solubilization is frequently required. In our case, an improvement in the profile maps was observed when the samples were treated with TCA.

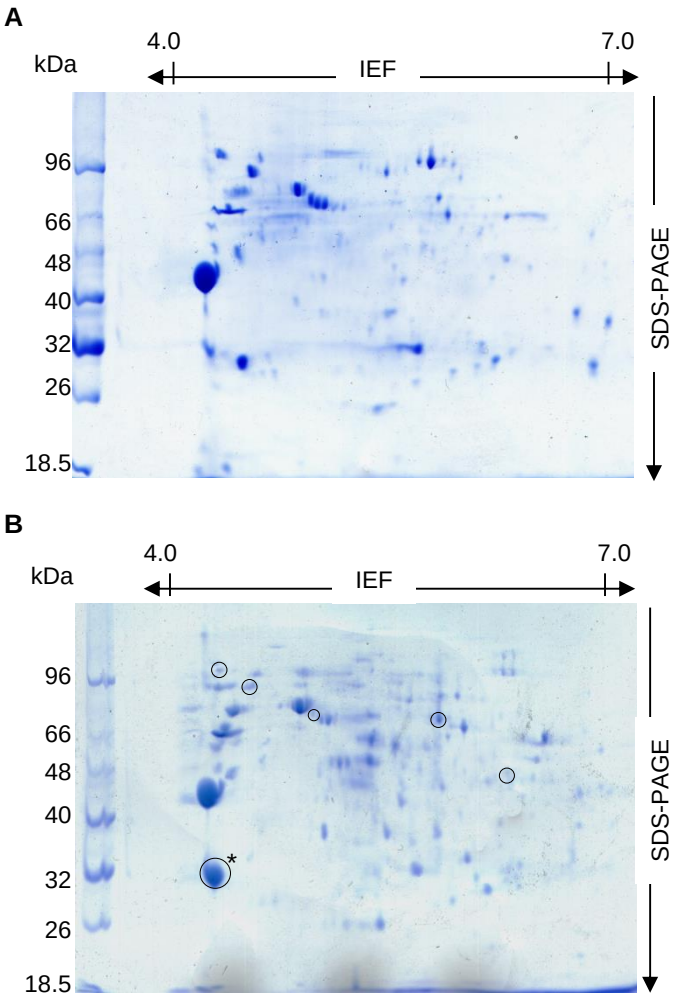

Figure 3.14 - 2D profile of the membrane fraction (80 µg) of *M. hydrocarbonoclasticus* cells grown under microaerobic conditions in the presence of nitrate (10 mM) at (A) pH 6.5 and (B) pH 7.5. Differential expression is indicated by black circles, being the spots selected based on a differential expression fold > 2 with p-values ≤ 0.05 between two biological replicates. For the 1st dimension the samples were applied on 7 cm IPG strips (pH range 4-7) and in the 2nd dimension the IPG strips were applied in a 10 % polyacrylamide SDS-PAGE, further stained with colloidal Coomassie blue. The spot identify by MS is marked with an asterisk.

The software ImageMaster 7.0 was used to identify a total number of 162 and 175 spots in two gels (two biological replicates) of the *M. hydrocarbonoclasticus* grown at pH 6.5. In the case of the growth performed at pH 7.5, 175 and 179 spots were identified in the gels of the biological replicates, indicative of a good reproducibility between growths performed at the same pH.

Although a low number of replicates were performed for each pH, a statistical analysis of the spots is presented in Table 3.2.

In the gels obtained from growth performed at pH 6.5, 79 % of spots matched with the ones of pH 7.5 membranes, suggesting that the expression of about 40 proteins was affected by pH (Table 3.2). In fact, most of the matched spots did not present a differential relative abundance, with only 6 showing a differential ratio higher than 2 and a statistically significant variation in expression

(although the low number of replicates). From the 6 identified spots, 4 are down-regulated in the growth performed at pH 6.5 (Table 3.2).

Differential proteins still need to be identified by MS, however considering the molecular mass and pI of the accessory proteins of N_2OR, most of the differential spots do not seem to correspond to these proteins (see Supplementary Information S2). In fact, we hypothesized that one of the differential spots (Figure 3.14B, the spot is marked with an asterisk) could correspond to the ApbE homologue given the *in silico* analysis, however further analysis of this spot by mass spectrometry identify a outer membrane protein (OmpW), from porin superfamily, with a molecular mass of 25 kDa and a pI of 4.3.

Thus, the synthesis of the accessory proteins may not be affected by pH or their amount is low and difficult to identify or are masked by others proteins with higher concentration.

Table 3.2 - Statistical analysis of spots from the 2D gel of the membrane fraction obtained from the growths performed at pH 6.5 and 7.5. Analysis was performed considering pH 7.5 grown as reference.

Spots	**pH 6.5**
Matches	138
Up-regulated	2
Down-regulated	4

3.9 Isolation and biochemical characterization of different forms of N_2OR

Little is known about the mechanism of N_2O reduction *in vivo*. However, it is now clear that a slightly acidification (pH 6.5) in the growth medium of *M. hydrocarbonoclastic*us is sufficient to affect N_2O reduction *in vivo*. Under these conditions N_2OR is inactive *in vivo*. Thus, the enzyme was isolated from cell extracts of *M. hydrocarbonoclasticus* grown in 10 L biofermenter at pH 6.5, 7.5 and 8.5.

Given the difficulty in controlling batch replicates, especially those performed at pH 6.5, we assured that the growths were similar, by measuring the OD_{600nm}, nitrate/nitrite concentrations, as well as the rate of NO and N_2O reduction by the whole-cells, at different time points, and only the ones with similar profiles were combine for protein purification.

Although the purification process of N_2OR from *M. hydrocarbonoclasticus* were previously described by Prudêncio *et al.* [91], some modifications were made (described in Section 2.8.1) since anoxic conditions had to be used to guarantee that the form of "CuZ center" was not altered during this process [21, 24, 132]. The isolated enzyme was biochemical and spectroscopic characterized (presented here), while their structural and electrochemical properties were further investigated (Chapter 4).

In parallel, the physiological electron donor of N_2OR, cytochrome c_{552}, was also purified to be used in kinetics and electrochemical studies. From now-on, N_2OR isolated from the growth performed at pH 6.5, 7.5 and 8.5 will be named $N_2OR_{6.5}$, $N_2OR_{7.5}$ and $N_2OR_{8.5}$, respectively, or designated by the form of the "CuZ center", either as CuZ*(4Cu1S) or as CuZ(4Cu2S). $N_2OR_{6.5}$ was most of the times purified under aerobic conditions, as the same form of the "CuZ center" is obtained in either the presence and absence of oxygen, while $N_2OR_{7.5}$ and $N_2OR_{8.5}$ were always purified under the absence of oxygen.

Additionally, these isolated N_2ORs were compared to the one obtained from an anaerobic growth, designated here as $Anaer_{7.5}$. $Anaer_{7.5}$ was isolated from a commercial growth of *M. hydrocarbonoclasticus* performed in a bioreactor (300 L) under strictly anaerobic conditions in the presence of nitrate [53].

The procedures used to isolate the protein in both growths, either in the presence or absence of oxygen, were similar and detailed in Chapter 2 (Section 2.8.1). The final N_2OR isolated from each growth was analyzed by SDS-PAGE, presented in Figure 3.15.

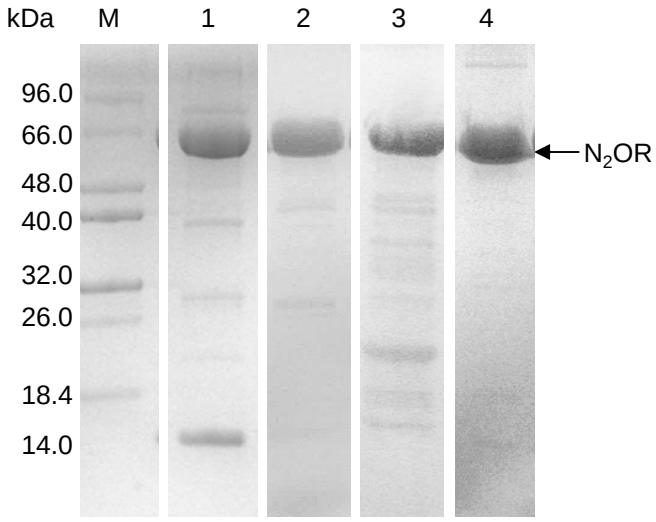

Figure 3.15 - Coomassie blue stained SDS-PAGE (12.5 % polyacrylamide) analysis of N_2OR purified from the growths performed in the bioreactor at different pH. Lanes M, 1, 2, 3 and 4 are the protein marker, $N_2OR_{pH6.5}$, $N_2OR_{pH7.5}$, $N_2OR_{pH8.5}$ and $Anaer_{7.5}$, respectively.

The yield of N_2OR obtained from each growth, copper and sulfur content were determined and compared (Table 3.3). The yield of N_2OR isolated from the periplasmic extract differ between preparations, with a higher yield of N_2OR per wet mass obtained for $N_2OR_{7.5}$, which is the optimum pH for the *M. hydrocarbonoclasticus* growth, while a three-fold lower yield was obtained for $N_2OR_{6.5}$ (Table 3.3). Due to the low purification yields obtained, especially for $N_2OR_{6.5}$, several batches were required to accomplish the spectroscopic and structural studies presented here.

Table 3.3 - Purification yield, copper and sulfur content of *M. hydrocarbonoclasticus* N_2OR isolated from the growths carried out at pH 6.5, 7.5 and 8.5 under microaerobic conditions and also at pH 7.5 under anaerobic conditions.

Sample	Yield ($mg_{N2OR}\ L^{-1}$)	Yield ($mg_{N2OR}\ g_{cell}^{-1}$)	Cu per N_2OR [a]	S per N_2OR [a]	Cu per S
$N_2OR_{6.5}$	0.5 ± 0.2	0.16 ± 0.02	3.6 ± 0.1	0.4 ± 0.1	8.4 ± 0.4
$N_2OR_{7.5}$	2.6 ± 0.4	0.5 ± 0.2	5.5 ± 0.4	1.7 ± 0.1	3.2 ± 0.3
$N_2OR_{8.5}$	1.1 [b]	0.27[b]	3.1 ± 0.2	ND	ND
$Anaer_{7.5}$ [c]	0.7 ± 0.3	0.6 ± 0.2	4.2 ± 0.1	1.3 ± 0.2	3.2 ± 0.4

Notes: [a]Considering N_2OR as monomeric; [b]N_2OR was purified from the growth performed at this pH only once; [c]Anaerobic growth performed at pH 7.5 in a 300 L reactor in the presence of nitrate. ND – not determined.

The amount of copper determined per $N_2OR_{7.5}$ (monomer) is close to the expected value (6 copper per monomer) and are in line with the values previously determined for N_2OR isolated from *M. hydrocarbonoclasticus* grown under anaerobic conditions, in which in some samples a fully copper occupancy is observed [91, 125], contrary to N_2OR purified from other microorganisms [90, 130]. $N_2OR_{6.5}$ and $N_2OR_{8.5}$ show a similar copper content, (Table 3.3), but lower than expected, possibly due to the presence of other proteins, decreasing the Cu/N_2OR ratio (Figure 3.15).

Comparison between the absorption ratio of as-isolated N_2OR at 280 nm and of potassium ferricyanide oxidized sample at 480 nm showed that the preparations followed the purity order: $N_2OR_{8.5}$ < $N_2OR_{6.5}$ < $N_2OR_{7.5}$ < $Anaer_{7.5}$. Corroborating this fact, $N_2OR_{8.5}$ is the least pure preparation, with a high content of hemic proteins that co-eluted with N_2OR in the anoxic purification (Figure 3.15). Therefore, a sample of $N_2OR_{8.5}$ was loaded onto a molecular exclusion column, performed rapidly in the presence of oxygen, to evaluate the Cu/N_2OR ratio. Removal of the contaminants improved the Cu/N_2OR ratio to 3.7 ± 0.1, however this value is still lower than expected, and thus the existence of apo-protein in both $N_2OR_{8.5}$ and $N_2OR_{6.5}$ cannot be completely excluded.

The content of labile sulfur in N_2OR was determined using the methylene blue method (described in Section 2.9.2) and related to the amount of copper and protein determined (Table 3.3). In the $N_2OR_{6.5}$ preparation, 0.4 ± 0.1 sulfur atoms were determined per protein monomer, while in the $N_2OR_{7.5}$, a higher ratio of 1.7 ± 0.1 was estimated. Moreover, as in the $N_2OR_{6.5}$ sample only approximately half of the expected copper atoms and half of expected sulfur were detected, a high Cu/S ratio was determined. This is most probably an error on the sulfur or protein quantification due to the low amount of protein obtained from the more acidic growth, and also because it was only possible to performed two replicates of sulfur quantification.

3.10 Spectroscopic characterization

The enzyme isolated from *M. hydrocarbonoclasticus* grown at pH 6.5, $N_2OR_{6.5}$, showed a visible spectrum different from that observed for both $N_2OR_{pH7.5}$ and $N_2OR_{pH8.5}$ (Figure 3.16).

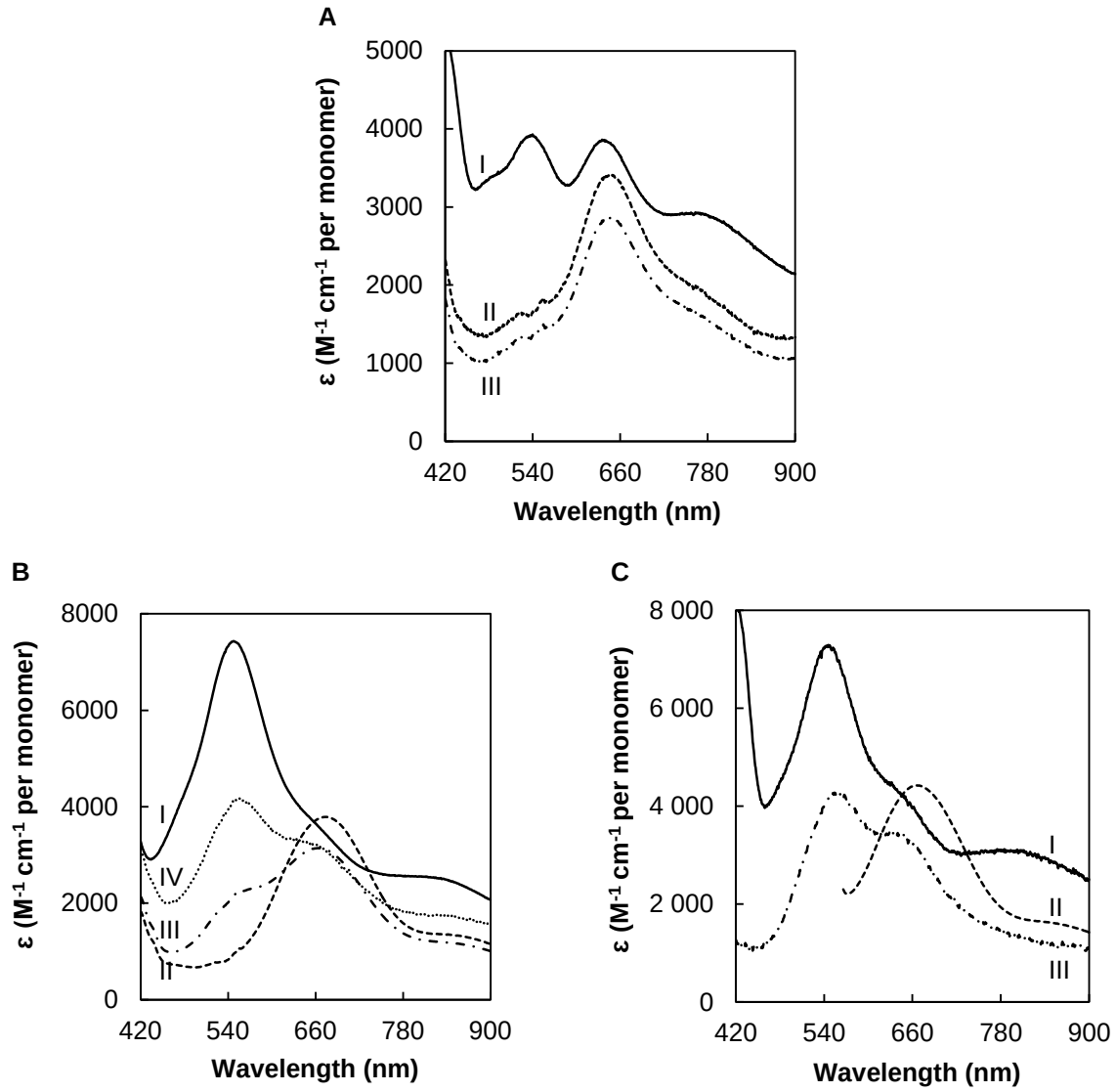

Figure 3.16 - Visible spectra of *M. hydrocarbonoclasticus* N_2OR isolated from cells grown at (A) pH 6.5, $N_2OR_{pH6.5}$, (B) pH 7.5, $N_2OR_{pH7.5}$ and (C) pH 8.5, $N_2OR_{pH8.5}$, in 100 mM Tris-HCl pH 7.6. In each panel is presented the spectra of potassium ferricyanide fully oxidized (I – solid line), sodium dithionite-reduced (II - dashed line), as-isolated (III – dashed-dotted line) and sodium ascorbate-reduced (IV – dotted line) states. In panel C, spectrum II is contaminated with cytochromes and thus this spectrum is only presented from 560 nm. Extinction coefficient is reported relative to the monomer.

The visible spectra of the as-isolated $N_2OR_{pH7.5}$ (and also $N_2OR_{pH8.5}$) show that both CuA and "CuZ" centers were obtained in the reduced state. Both centers were fully oxidized by addition of potassium ferricyanide, showing absorption bands at 480 nm, 540 nm and 800 nm and a shoulder at 640 nm (Figure 3.16B and C). Upon reduction of $N_2OR_{pH7.5}$ with sodium ascorbate, the CuA center is reduced not contributing to the spectra and the features of the "CuZ center" become

defined, with a maximum absorption band at 550 nm and a shoulder at 640 nm. In the sodium dithionite reduced form, $N_2OR_{pH7.5}$ and $N_2OR_{pH8.5}$ visible spectra exhibit a single absorption band at 670 nm, (Figure 3.16B and C).

The as-isolated $N_2OR_{pH6.5}$ exhibits a spectrum with maximum absorption band at 640 nm, characteristic of "CuZ center", while the CuA center is mainly reduced in the [Cu^{1+}-Cu^{1+}] state (Figure 3.16A). The spectrum in the presence of sodium ascorbate (data not show) and also sodium dithionite does not change significantly from that of the one in the as-isolated form. In fact, the band observed is sharper and at a different wavelength than the sodium dithionite reduced band observed in both $N_2OR_{pH7.5}$ and $N_2OR_{pH8.5}$ preparations. Upon oxidation with potassium ferricyanide, CuA center characteristic absorption bands are observed, at 480 nm, 540 nm and 800 nm, while the absorption band with a maximum at 640 nm does not change (Figure 3.16A).

Moreover, in the fully oxidized state of $N_2OR_{pH6.5}$, an absorbance 550/640 nm ratio of 1.0 - 1.2 was usually determined, while for the oxidized spectra of $N_2OR_{pH7.5}$ and $N_2OR_{pH8.5}$ the ratios were between 1.7 - 1.9, similar to anoxically purified N_2OR from a variety of microorganisms, in which the "CuZ center" was isolated as CuZ(4Cu2S) [89, 92, 131, 132].

Thus, N_2OR can be isolated with "CuZ center" in two different forms, depending on the pH at which the bacteria was grown, with $N_2OR_{pH7.5}$ and $N_2OR_{pH8.5}$ isolated with "CuZ center" mainly as CuZ(4Cu2S), while in $N_2OR_{pH6.5}$ as CuZ*(4Cu1S).

Additionally, when $N_2OR_{pH7.5}$ is purified in the presence of oxygen a different spectrum was obtained, consequence of the presence of a mixture of "CuZ center" forms, CuZ(4Cu2S) and CuZ*(4Cu1S), with CuZ*(4Cu1S) ranging between 40 % to 80 % (data not show). Thus, for $N_2OR_{pH7.5}$ and $N_2OR_{pH8.5}$ preparations, the anoxic isolation procedure was maintained in order to isolate the enzyme without perturbations caused by the presence of oxygen. On the contrary, the $N_2OR_{pH6.5}$ spectroscopic features are not altered if its isolation is performed in the presence of oxygen.

These two forms of the centers exhibit a variation on their sulfur content, which was previously addressed by spectroscopic and X-ray studies, and currently is well-known that "CuZ center" as CuZ*(4Cu1S) contains one sulfur atom per protein monomer, while the enzyme with CuZ(4Cu2S) has two [126, 143, 152, 158]. This explains the different values obtained for sulfur content in $N_2OR_{6.5}$ and $N_2OR_{7.5}$ preparations (Table 3.3). In addition, the fact that an enzyme preparation does not presented a form 100 % of "CuZ center" as CuZ(4Cu2S) will also affect the S/N_2OR and S/Cu ratio.

The X-band EPR spectra of the different N_2OR preparations ($N_2OR_{pH6.5}$, $N_2OR_{pH7.5}$ and $N_2OR_{pH8.5}$), were acquired at different oxidation states by selectively reducing the copper centers with sodium ascorbate, sodium dithionite or methyl viologen and also complete oxidation with potassium ferricyanide (Figure 3.17).

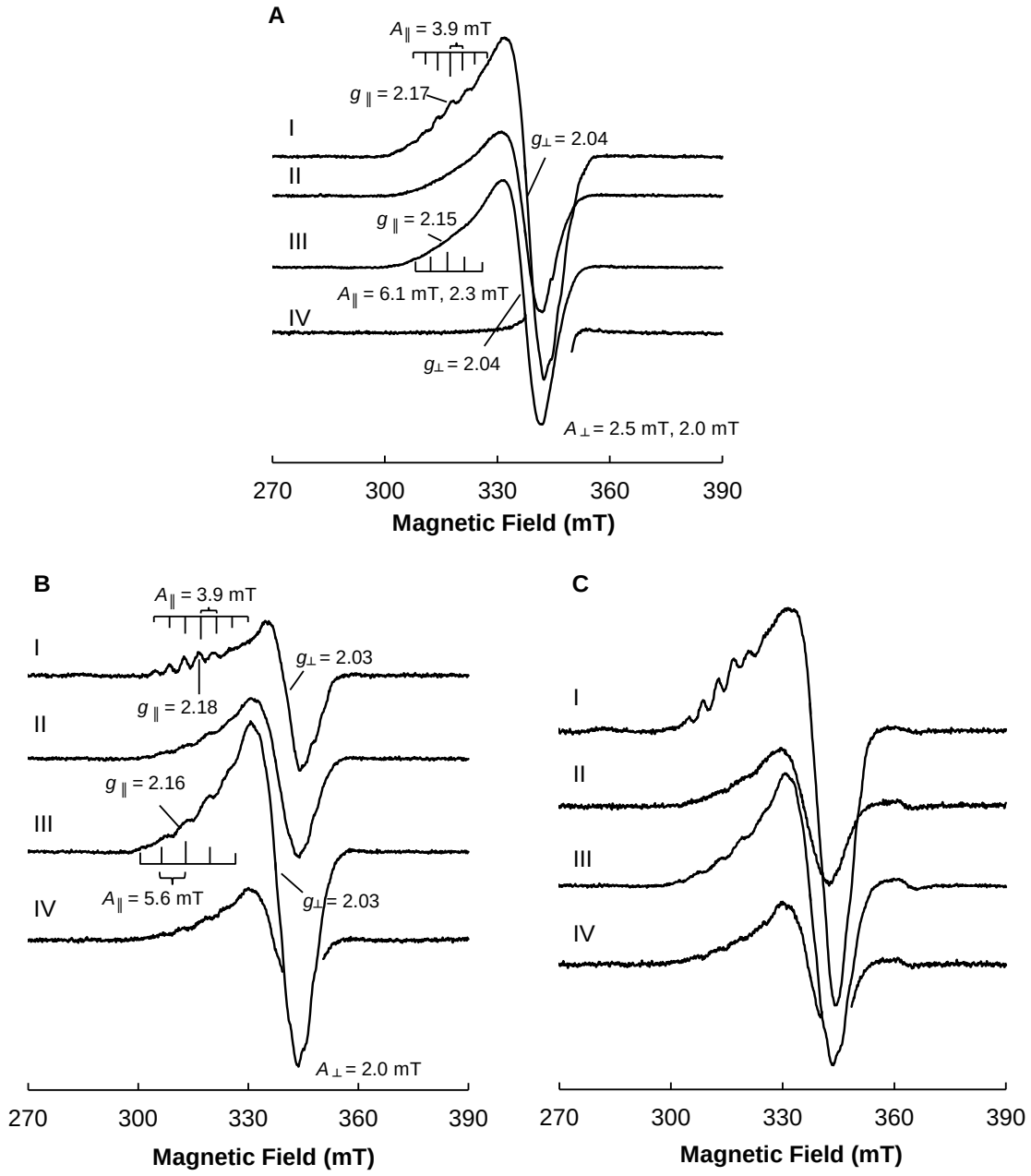

Figure 3.17 - X-band EPR spectra of *M. hydrocarbonoclasticus* N_2OR isolated from growths performed at different pH values: (A) $N_2OR_{pH6.5}$, (B) $N_2OR_{pH7.5}$ and (C) $N_2OR_{pH8.5}$. In each panel the spectra of oxidized (I), sodium ascorbate reduced (II), sodium dithionite reduced (III) and methyl viologen reduced (IV) are represented. The instrument settings for the acquisition were: microwave frequency, 9.65 GHz; microwave power, 2 mW; gain, $1x10^5$; temperature, 30 K. The contribution of methyl viologen radical in the spectra IV was removed.

The EPR spectrum of oxidized $N_2OR_{pH6.5}$ has an axial signal with $g_{\parallel}$ = 2.17 and $g_{\perp}$ = 2.04, and shows a low resolved pattern of seven hyperfine lines in the $A_{\parallel}$ region ($A_{\parallel}$ = 3.9 mT) (Figure 3.17A, Table 3.4). This pattern is explained by a delocalized electron (S = 1/2) between two coupled copper nuclei (I = 3/2), assigned to a mixed valence [$Cu^{1.5+}$-$Cu^{1.5+}$] state of CuA center. The broadening of the spectra is attributed to a delocalized electron on the CuZ*(4Cu1S), in the

[$1Cu^{2+}$-$3Cu^{1+}$] oxidation state, which is usually observed after reduction of CuA center with sodium ascorbate (Figure 3.17A – spectrum II), or sodium dithionite.

$N_2OR_{pH6.5}$ reduced with sodium dithionite also exhibits an axial EPR spectrum with broad lines not easily distinguished due to its low intensity (Figure 3.17A– spectrum III). Therefore, its simulation was only possible considering the existence of two $A_{\parallel}$ and two $A_{\perp}$ constants, which were previously reported by Ghosh *et al.*, (Table 3.4) [161]. The *g*-values determined, $g_{\parallel}$ = 2.15 and $g_{\perp}$ = 2.04, are similar to those previously reported [161]. This EPR signal is due to the CuZ*(4Cu1S), in the [$1Cu^{2+}$-$3Cu^{1+}$] oxidation state, similar to the features observed in the sodium ascorbate reduced spectrum (Figure 3.17A – spectrum II), as this center cannot be reduced by sodium dithionite. Nonetheless, this signal disappears upon prolonged incubation with reduced methyl viologen, indication of complete reduction of "CuZ center" to the [$4Cu^{1+}$] oxidation state, which is diamagnetic (Figure 3.17A– spectrum IV).

The features of the EPR of $N_2OR_{pH6.5}$ preparation are similar to the ones previously reported for *M. hydrocarbonoclasticus* N_2OR mainly with CuZ*(4Cu1S) [161]. These results strengthen the previous analysis of its visible spectra, indicating that "CuZ center" in $N_2OR_{pH6.5}$ is mainly as CuZ*(4Cu1S).

Table 3.4 - EPR parameters of $N_2OR_{pH6.5}$, $N_2OR_{pH7.5}$ and $N_2OR_{pH8.5}$, in different oxidation states used to simulate each EPR spectrum (simulated spectra are not shown).

Sample	Oxidation State	$g_{\parallel}$	$A_{\parallel}$ (mT)	$g_{\perp}$	$A_{\perp}$ (mT)
$N_2OR_{6.5}$	Oxidized	2.17	3.9	2.04	-
	DT-reduced	2.15	6.1, 2.3 [a]	2.04	2.5, 2.0 [a]
$N_2OR_{7.5}$	Oxidized	2.18	3.9	2.03	-
	DT-reduced	2.16	5.6 [b]	2.03	2.0 [b]
$N_2OR_{8.5}$	Oxidized	2.18	3.8	2.04	-
	DT-reduced	2.15	5.7 [b]	2.03	20 [b]

Notes: [a] Considering the same hyperfine coupling constants as Ghosh *et al.* [161], as it was not possible to simulate the second derivative spectrum; [b] Considering 3 identical hyperfine coupling constants.

In the case of oxidized $N_2OR_{pH7.5}$ sample, an axial signal is also observed with $g_{\parallel}$ = 2.18 and $g_{\perp}$ = 2.03 with a well resolved 7-line hyperfine coupling ($A_{\parallel}$ = 3.9 mT), in an intensity ratio 1:2:3:4:3:2:1, from the mixed valence CuA center contribution, due to the spin interaction with the two Cu nuclei (Figure 3.17B – spectrum I, Table 3.4). A well resolved 7-line pattern in N_2OR is generally observed when the only contribution to the spectra is the CuA center, suggesting that the form of "CuZ center" present in these samples is diamagnetic and in the [$2Cu^{2+}$-$2Cu^{1+}$] oxidation state.

In fact, upon CuA center reduction with sodium ascorbate an axial signal with low intensity is observed in the EPR spectrum of $N_2OR_{pH7.5}$. Interestingly, this is possibly due to the presence of a small contribution of CuZ*(4Cu1S) in the [$1Cu^{2+}$-$3Cu^{1+}$] oxidation state or by the fact that the

spectrum present in Figure 3.17B – spectrum II, was obtained by reduction of as-isolated N_2OR with sodium ascorbate, which was already in the [$1Cu^{2+}$-$3Cu^{1+}$] oxidation state (Figure 3.16B).

The sodium dithionite reduced spectra of $N_2OR_{pH7.5}$ exhibit an axial signal with 5-lines in the $g_{\parallel}$ region (Figure 3.17B). In fact, 10 lines were expected, although only the more intense ones were observed. This signal can be simulated with $g_{\parallel} = 2.16 > g_{\perp} = 2.03 > 2.0$ (Table 3.4). In order to accurately perform this simulation, three identical contributions of each hyperfine constants ($A_{\parallel} = 5.6$ mT and $A_{\perp} = 2.0$ mT) were required, indicating that the spin is delocalized over three multiple copper nuclei. This signal corresponds to the "CuZ center" in the [$1Cu^{2+}$-$3Cu^{1+}$] oxidation state and it exhibits different properties from the "CuZ center" in the same oxidation state in the $N_2OR_{pH6.5}$ [CuZ*(4Cu1S)].

Reduction of $N_2OR_{pH7.5}$ with reduced methyl viologen exhibit an EPR spectrum with an axial signal, similar to the sodium dithionite reduced spectra but with lower intensity, suggesting that methyl viologen cannot fully reduce this form of "CuZ center" to [$4Cu^{1+}$], as observed before in $N_2OR_{pH6.5}$. Previous spectroscopic studies reported that "CuZ center" as CuZ(4Cu2S) cannot be fully reduced with either sodium dithionite or reduced methyl viologen [160].

These results corroborate the visible spectra, suggesting that "CuZ center" in $N_2OR_{pH7.5}$ is mainly as CuZ(4Cu2S).

The EPR spectra of the different oxidation states of $N_2OR_{pH8.5}$ has similar features to the ones of $N_2OR_{pH7.5}$ EPR spectra, indicating that in this preparation "CuZ center" is also mainly as CuZ(4Cu2S), as mentioned before when its visible spectra were analyzed (Figure 3.17C).

The spin for the different oxidation states of each sample was quantified by integrating the signal given by the second derivative of the spectrum and are presented in Table 3.5.

Table 3.5 - EPR spin quantification of different forms of N_2OR isolated from the different growths.

Sample	Oxidized	As-isolated	Ascorbate reduced	Dithionite Reduced
$N_2OR_{6.5}$	1.8	1.1	1.0	1.0
$N_2OR_{7.5}$	0.6	1.0	0.3	1.0
$N_2OR_{8.5}$	1.3	0.6	0.7	1.0

Note: The spin of methyl viologen EPR signal is not considered, as the methyl viologen radical contributed to the spectra.

The spin quantification is based on the assumption that the sodium dithionite reduced sample has a total spin of 1 [91, 184]. In this state, CuA center is reduced (S = 0), EPR silent, while "CuZ center" is in the [$1Cu^{2+}$-$3Cu^{1+}$] oxidation state (either as CuZ*(4Cu1S) or CuZ(4Cu2S)), containing one unpaired electron (S = 1/2).

In the case of potassium ferricyanide oxidized spectrum, the total spin has a contribution of both CuZ*(4Cu1S) (S = 1/2) and CuA (S = 1/2) centers, since oxidized CuZ(4Cu2S) is EPR silent

(S = 0). Both CuZ*(4Cu1S) and CuA centers have one delocalized electron, having a total contribution of 2 spin/protein. Thus, in a fully oxidized N_2OR, with 100 % of "CuZ center" as CuZ*(4Cu1S) it is expected that the total spin would be 2. In fact, a spin of 1.8 was estimated for the fully oxidized $N_2OR_{pH6.5}$ (Table 3.5). In the presence of sodium ascorbate, CuA center is reduced and thus, the spin quantification is related only to "CuZ center". A spin of 1.0 was estimated for the sodium ascorbate reduced $N_2OR_{pH6.5}$ (Table 3.5). Given the spectroscopic features observed above, the "CuZ center" of $N_2OR_{pH6.5}$ is already in the resting CuZ*(4Cu1S) state being expected a spin close to 1. The spin quantification indicates that $N_2OR_{pH6.5}$ has 90 % of "CuZ center" as CuZ*(4Cu1S).

In the case of fully oxidized $N_2OR_{pH7.5}$ it is expected that the spin would be 1, however a lower spin was determined (Table 3.5), suggesting that either the sample is not fully oxidized or we can hypothesize that there was a problem with protein quantification.

Upon reduction with sodium ascorbate in a sample with ~ 100 % CuZ(4Cu2S), a spin near 0 would be expected. Under these conditions a spin of 0.3 was estimated for $N_2OR_{pH7.5}$, which can be explained either by the presence of some CuZ*(4Cu1S) in the sample, which is paramagnetic (S = 1/2), or that CuZ(4Cu2S) center is already in a reduced state, [$1Cu^{2+}$-$3Cu^{1+}$], even before the addition of sodium ascorbate. In fact, this latter explanation is reasonable as sodium ascorbate was added to the as-isolated sample and the visible spectra evidenced some reduction, which also corroborates the low spin quantification for the as-isolated form (Table 3.5, Figure 3.16). The spin of sodium ascorbate reduced sample, in particular $N_2OR_{pH7.5}$ would be accurately determined if the sodium ascorbate was added to the fully oxidized sample, and in that case we would be able to estimate the percentage of CuZ*(4Cu1S) present.

The $N_2OR_{pH8.5}$, spectroscopically identical to $N_2OR_{pH7.5}$, in the fully oxidized state, has a spin of 1.3, close to the expected value of CuA contribution (spin of 1), which can be justified by the presence of a percentage (~ 30 %) of CuZ*(4Cu1S) in the sample (Table 3.5).

The sample of $N_2OR_{pH8.5}$ reduced with sodium ascorbate has a spin quantification of 0.7, but the presence of CuZ(4Cu2S), in the [$1Cu^{2+}$-$3Cu^{1+}$] oxidation state, already in the as-isolated $N_2OR_{pH8.5}$ cannot be excluded (Supplementary Information S3). Similarly to $N_2OR_{pH7.5}$, ascorbate reduced sample was obtained by addition of sodium ascorbate to the as-isolated N_2OR. These results shown that although some CuZ*(4Cu1S) might be present in $N_2OR_{pH8.5}$, its quantification could not be accurately determined.

3.11 Kinetic studies

3.11.1 Activities of different forms of N_2OR

The activity of each N_2OR sample was determined in the presence of its physiological electron donor, cytochrome c_{552}, or using an artificial donor, methyl viologen, by a spectrophotometric assay [122] (Chapter 2, Section 2.11.3) and the results are presented in Table 3.6.

For all enzyme preparations, in the absence of pre-activation, specific activities lower than 1 $\mu mol_{N2O}\ min^{-1}\ mg^{-1}_{N2OR}$ were determined (Table 3.6). Thus, each of the purified N_2ORs was activated with reduced methyl viologen during 3 h prior to the assay (see Section 2.11.1). The $N_2OR_{pH6.5}$ preparation showed a specific activity (192 ± 14 $\mu mol_{N2O}\ min^{-1}\ mg^{-1}_{N2OR}$) higher than $N_2OR_{pH7.5}$ (51 ± 18 $\mu mol_{N2O}\ min^{-1}\ mg^{-1}_{N2OR}$) and $N_2OR_{pH8.5}$ (55 ± 5 $\mu mol_{N2O}\ min^{-1}\ mg^{-1}_{N2OR}$) preparations (Table 3.6). These results evidenced that an activation of the enzyme is required.

Since catalytic activities are directly proportional to the amount of "CuZ center" as CuZ*(4Cu1S) in the enzyme, the $N_2OR_{pH6.5}$ sample has a high percentage of CuZ*(4Cu1S), as reported before. In fact, considering that a sample with ~100 % CuZ*(4Cu1S) has a specific activity of 200 $\mu mol_{N2O}\ min^{-1}\ mg^{-1}_{N2OR}$, the percentage of CuZ*(4Cu1S) in each sample can be estimated [132, 168]. Therefore, $N_2OR_{pH6.5}$ has "CuZ center" mainly as CuZ*(4Cu1S), while the "CuZ center" of $N_2OR_{pH7.5}$ and $N_2OR_{pH8.5}$ have mainly "CuZ center" as CuZ(4Cu2S) (~75 %), with ~25 % of CuZ*(4Cu1S). Moreover, a similar content of CuZ*(4Cu1S) in $N_2OR_{pH6.5}$ was determined by EPR spin quantification (Table 3.5), corroborating the specific activities. In addition, these results corroborate well with the visible spectra of these samples (Figure 3.16).

Table 3.6 – Specific activities of *M. hydrocarbonoclasticus* N_2OR, isolated from the growth carried out at pH 6.5, 7.5 and 8.5, in the presence of physiological and artificial electron donors.

Sample	Methyl viologen (incubation 0 h) (U mg^{-1})	Methyl viologen (incubation 3 h) (U mg^{-1})	Cytochrome c_{552} [a] (U mg^{-1})	Cytochrome c_{552} [b] (U mg^{-1})
$N_2OR_{6.5}$	0.44 ± 0.04	192 ± 14	1.25 ± 0.07	-
$N_2OR_{7.5}$	0.30 ± 0.02	51 ± 18	-	0.004 ± 0.001
$N_2OR_{8.5}$	0.56 ± 0.04	55 ± 5	-	-

Notes: The specific activities reported as U mg^{-1} are referred to $\mu mol_{N2O}\ min^{-1}\ mg_{N2OR}{}^{-1}$; [a]The N_2OR:cytochrome c_{552} ratio of 1:140 was used in the assay and N_2OR was activated by reduced methyl viologen for 3 h. [b]The N_2OR:cytochrome c_{552} ratio of 1:100 were used in the assay

Additionally, the catalytic activity of all preparations was investigated in the presence of its putative physiological electron donor. A different assay allowing the separation of enzyme activity from the activation process was previously designed [122] (described in Section 2.11.3), in which the reducing agents were removed after complete reduction of the enzyme. This ensures that in the activity assay there is no interference of other electron donors.

A specific activity of 1.25 ± 0.07 $\mu mol_{N2O}\ min^{-1}\ mg^{-1}$, was determined for the fully reduced $N_2OR_{pH6.5}$, while $N_2OR_{pH7.5}$ reduced only with sodium dithionite has an activity of 0.004 ± 0.001 $\mu mol_{N2O}\ min^{-1}\ mg^{-1}$ (Table 3.6). Despite the lower activities observed in comparison with the artificial electron donor, these results demonstrate that the reduced form of CuZ*(4Cu1S) has a higher activity than the reduced CuZ(4Cu2S), when a relevant physiologic electron donor is used. Extrapolation of specific activities for a sample containing 100 % of "CuZ center" as

CuZ(4Cu2S) or 100 % as CuZ*(4Cu1S) are present in Table 3.7. Dithionite reduced samples were used to extrapolate the reactivity of 100 % CuZ(4Cu2S) using MV and cytochrome c_{552}, which showed very low specific activities.

Table 3.7 – Extrapolation of specific activities of *M. hydrocarbonoclasticus* N_2OR, for "CuZ center" as CuZ(4Cu2S) or CuZ*(4Cu1S), in the presence of physiological and artificial electron donors.

Sample	Methyl viologen (incubation 3 h) (U mg^{-1})	Cytochrome c_{552} (U mg^{-1})
100 % CuZ(4Cu2S)	0.17	0.0044
100 % CuZ*(4Cu1S)	200	1.4

Notes: The specific activities reported as U mg^{-1} are referred to μmol_{N2O} min^{-1} mg_{N2OR}^{-1}

In an attempt to understand the observed differences between *in vivo* and *in vitro* N_2O reduction, the rate of N_2O reduction was followed during the purification process. In this assay, a decrease in specific activity was observed when the periplasmic extract was separated from the remaining cellular fractions (cytoplasm and membranes), and thus an activation mechanism involving proteins of the separated cell fractions can be envisaged. Further incubation of periplasm with cytoplasm and membrane fraction (1 h or 5 h) did not reproduce the initial N_2O rates.

The differences observed in the activity between the proposed physiological and the artificial electron donors may be due to the internal electron flow. As methyl viologen is a small molecule it might donate electrons directly to both CuA and "CuZ" centers, while cytochrome c_{552} most probably transfers electrons through CuA center, as elucidated by docking studies [122, 154].

In fact, the catalytic activity *in vitro* is an antithesis of the *in vivo* process, as higher rates of N_2O reduction were observed for N_2OR purified from the growth at pH 6.5, when in fact the cells grown at this pH did not exhibit a measurable N_2O reduction rate. Indeed, in the whole-cells activity assay the cells were not previously incubated with methyl viologen, but even without pre-activation, the activity values observed *in vitro* do not justify the whole-cells activity or lack of it.

Activities in the presence of cytochrome c_{552} also do not justify the whole-cell activities, as $N_2OR_{pH6.5}$ presented higher catalytic activities compared to the other N_2ORs. On the other hand, $N_2OR_{pH7.5}$ (reduced with sodium dithionite to the [$1Cu^{2+}$-$3Cu^{1+}$] oxidation state) in the presence of cytochrome c_{552} gives the lowest activities which also cannot explain the whole-cells activity.

Many researchers state that in the periplasm space, such low reduction potentials are not attained and therefore the fully reduced CuZ*(4Cu1S) form of "CuZ center" cannot be the active form of the enzyme. However, it is clear that this form is the catalytic competent form *in vitro*, as no other oxidation state of this form or of the CuZ(4Cu2S) form was found to have high turnover numbers. Therefore, we hypothesized that CuZ(4Cu2S) might be a protective form of the enzyme, that is formed in the absence of electrons or substrate during purification process.

3.12 Conclusions

M. hydrocarbonoclasticus in one of the major bacteria that populates the oceans in the subtropical area and in the Mediterranean sea. Its genome presents all the genes encoding the catalytic subunits of enzymes responsible for each step of the denitrification pathway. These genes, as well as those encoding accessory factors, necessary for enzyme maturation, transcriptional regulators and substrate transporters, were found to be organized in a common *locus*. Genetic clustering of denitrification genes has been previously described for other bacteria, however, clustering of genes encoding the four denitrifying reductases as observed in *M. hydrocarbonoclasticus* seems to be less frequent [219, 256]. Such genomic arrangement of denitrification genes favors the hypothesis of the existence of "denitrification islands" that can be transferred horizontally across species [21].

Remarkably, this organism has genes that encode two different types of NORs, *q*-NOR and *c*-NOR, but under the denitrifying conditions used here only the later catalytic gene subunit is expressed at significant levels, and in fact this was the enzyme isolated from *M. hydrocarbonoclasticus* membrane extracts [257].

The two types of growth conditions tested here (using a bioreactor or sealed serum flasks) can be regarded as models of the metabolism occurring at two different sea depths. The growth in the bioreactor under microaerobic conditions would be a model for the layers close to the surface, while the growth in the sealed serum flasks a model for deeper sea layers.

For the growth performed in the bioreactor in the presence of nitrate, the genes encoding the catalytic subunits of denitrifying enzymes have a maximum expression level at the end of the first diauxic phase, which rapidly decreases to very low levels. A marked difference in gene expression is observed at more acidic pH, being the *nirS* expression 4-fold lower compared to pH 7.5 and 8.5.

We propose that the initial regulatory signal is oxygen, through a FNR-homologue transcriptional regulator (MARHY0862), which in turn activates the DNR-type transcription regulator (MARHY3023). This transcription regulator responds to NO, a secondary signal, formed by cd_1NiR, that will regulate the expression of *nir*, *nor* and *nos* gene clusters. The other secondary regulatory effector is nitrate, involved in the regulation of *nar* genes expression, through the two-component system NarXL.

Both type of growths performed showed differences in the by-products and enzyme activities profiles. Although nitrate consumption occurs in the early hours of the growth, nitrite is later consumed and in the case of the growth in the bioreactor at pH 6.5, nitrite levels remain high during all the growth. The low levels of cd_1Nir and its probable inactivation by nitrite accumulation in the growth media and consequent generation of nitrous acid are proposed to be the main causes of denitrification arrest at this pH.

The ability of cells to reduced nitric and nitrous oxide is also delayed in both types of growth, as accessory factors are required for the maturation of N_2OR (and also for cd_1Nir). Moreover, our data indicate that NOR is active until the end of the growth (48-50 h) in both types of growths and at the

different pH values. However, higher reduction rates of NO by the whole-cells were observed in the more acidic growth performed in the bioreactor, probably due to a down-regulated mechanism, as in this case NO is chemically produced. Despite the high NO reduction rates, N_2O reduction by whole-cells is practically inexistent, in the acidic growth. Nevertheless, a functional denitrification pathway in *M. hydrocarbonoclasticus* is observed from nitrate to dinitrogen gas in both growths performed at pH 7.5 and 8.5, while at pH 6.5, with only a drop of one pH unit from the optimal pH growth, the denitrification is impaired and not complete in this bacteria, and probably leads to N_2O release to atmosphere.

In fact, maintaining the enzyme active *in vivo* may require the presence of other proteins, such as NosR known as essential for N_2OR activity *in vivo* [82, 86].

In the present case, in order to seek for an explanation for the inability of the whole-cells (grown at acidic pH) to reduce N_2O, we investigated: i) the expression of genes involved in N_2O maturation; ii) the *M. hydrocarbonoclasticus* proteome profile and iii) the properties of N_2OR isolated from cells grown at different pH values.

Our data shows that the pH of the growth media does not have a clear influence in the transcription of any of the identified accessory genes of N_2OR. Advances in proteomics allowed the identification of 6 proteins with differential expression at pH 6.5, but a higher number of proteome replicates, as well as protein identification by MS are still required to identify any regulatory mechanism.

Different forms of N_2OR were isolated from a microaerobic growth of *M. hydrocarbonoclasticus* performed at different pH values. Understanding the properties of the different N_2OR forms is of prime importance as it might provide a clue to understand the relevant form of N_2OR *in vivo* and the molecular mechanisms that are affected at low pH.

Despite the low yields of protein obtained at pH 6.5, N_2OR was isolated, indicating that at least part of the protein was translocated to the periplasm.

Copper amount per protein is similar for both $N_2OR_{pH6.5}$ and $N_2OR_{pH8.5}$, which corroborates the unobserved differences in the expression of genes involved in copper assembly and that the mechanisms involved in copper center assembly may not be affected at this pH range.

The N_2OR isolated from different *M. hydrocarbonoclasticus* growth pH, exhibits different spectroscopic properties. From cells grown at pH 7.5 and 8.5, N_2OR was isolated with "CuZ center" mainly CuZ(4Cu2S), while from cells grown at pH 6.5, N_2OR was isolated with the "CuZ center" mainly as CuZ*(4Cu1S).

In addition, the specific activities determined for each of the activated enzymes was related with the amount of CuZ*(4Cu1S) center present in the isolated enzyme, which in its fully reduced state, $[4Cu^{1+}]$, has a higher turnover number, as previously reported in [132, 168]. In fact, upon activation with reduced methyl viologen, higher specific activities were determined for $N_2OR_{pH6.5}$ suggesting that this preparation has approximately 90 % of its active center as CuZ*(4Cu1S), which is in

agreement with the spin quantified by EPR and with its visible spectra. Lower activities were determined in the presence of its physiological electron donor, which are still higher for $N_2OR_{pH6.5}$. On the other hand, very low specific activities were determined without prior activation of the enzyme and no relationship between these activities and the forms of "CuZ center" of the enzyme was established, with the values calculated being in the same order of magnitude as those previously reported by Dell'Acqua *et al* [132].

In conclusion, we demonstrate that acidic pH affects the denitrification pathway in *M. hydrocarbonoclasticus* and although the mechanism involved in the loss of the ability of the cells to reduce N_2O is not fully understood, our results point to a possible mechanism:

i) at the post-translational level;

ii) enzyme transport to the periplasm by the Tat system;

iii) in maintaining N_2OR in an active form which is impaired at this moderately low pH.

Chapter 4

Characterization of different forms of N_2OR

The data present in this Chapter will be published in:

Carreira, C.; Pauleta, S. R.; Moura, I.; Dos Santos, M.M.C. Direct electrochemistry of nitrous oxide reductase from *Marinobacter hydrocarbonoclasticus* at a carbon nanotube modified glassy carbon electrode. *In preparation*, **2018**.

Pomowski, A.; Dell'Acqua, S.; Carreira, C.; Pauleta, S. R.; Moura, I; Einsle, O. High resoltution structure of the Cu_4S_2 center of nitrous oxide reductase from *Marinobacter hydrocarbonoclasticus*. *In preparation*, **2018**.

Contributions to this Chapter:

The crystallographic data acquisition and the structure solved by molecular replacement were performed by Anja Wüst, University of Freiburg, Germany. Cíntia Carreira performed refinement cycles on the structure.

4 Characterization of different forms of N_2OR

In this Chapter, the effect of pH on the activation of N_2OR is investigated for both forms of "CuZ center", CuZ(4Cu2S) and CuZ*(4Cu1S), through steady-state kinetics.

Structural differences between *M. hydrocarbonoclasticus* N_2OR, with 17 % and 90 % of "CuZ center" as CuZ*(4Cu1S), were analyzed by X-ray crystallography: the overall structures, as well as its redox centers are presented and discussed.

The complex redox behavior of the enzyme was examined by potentiometric redox titrations and direct electrochemistry. The reduction potentials of CuA and "CuZ" centers determined by these two techniques are compared, and the pH dependence of these values is reported and discussed here for the first time.

These studies were essential to better understand the catalytic mechanism of N_2OR.

4.1.1 Effect of pH on the activation of N_2OR

In order to address the pH effect on the activation of *M. hydrocarbonoclasticus* N_2OR and how it affects its specific activity, the enzyme was incubated with reduced methyl viologen at different pH values, and the N_2O reduction assay was performed at pH 7.6 (Figure 4.1). It is important to point out that the *in vitro* specific activity is proportional to the content in CuZ*(4Cu1S) of the sample, even when using an initial preparation with a high content in CuZ(4Cu2S), due to the low turnover number of this form of "CuZ center" (k_{cat} = 0.6 h^{-1}) [160].

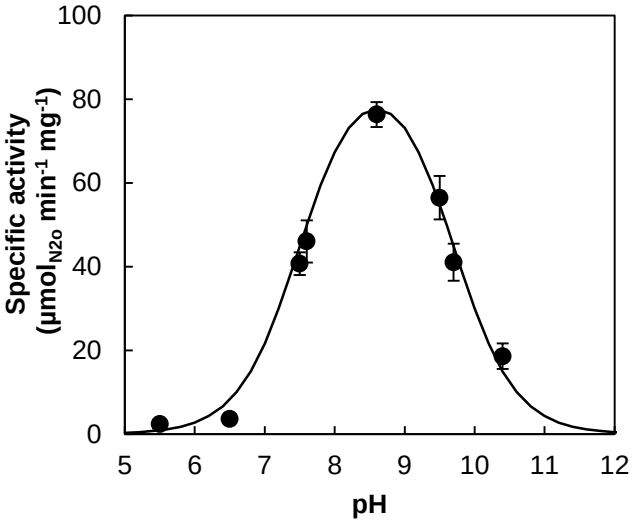

Figure 4.1 - Specific activity of N_2OR with 20 % of "CuZ center" as CuZ*(4Cu1S), activated for 3 h at different pH values at RT. Data were fitted with a bell-shaped curve, and pK_a values of 7.5 ± 0.2 and 9.7 ± 0.1, with optimum activation at pH ~ 8.5.

The results show that the optimum pH for activation of N_2OR is pH 8.5 and that higher pH does not seem to promote activation of the enzyme. Moreover, two apparent pK_a (7.5 ± 0.2 and 9.7 ± 0.1) were estimated (Figure 4.1).

The alkaline pK_a = 9.7 ± 0.1 can be attributed to the deprotonation of K447 (Figure 4.2). This residue has been proposed to be involved in the stabilization of an intermediate species in the enzyme turnover. In fact, a similar pK_a = 9.0 ± 0.2 has been estimated by the decay rate of the EPR signal intensity of CuZ*(4Cu1S) at different pH values, during reduction of this form of "CuZ center" to the fully reduced form [161]. When protonated, K447 is proposed to increase the reduction potential of this center, which is then easier to be reduced leading to higher reduction rates of CuZ*(4Cu1S) at lower pH values [161].

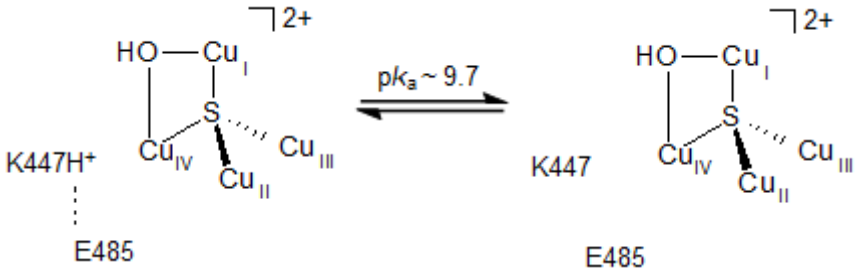

Figure 4.2 - Effect of pH on lysine residue (K447) in the vicinity of CuZ*(4Cu1S) center.

At more acidic pH values there is also a decrease in the specific activities, and the apparent pK_a = 7.5 ± 0.2 estimated is slightly higher than the one reported before (pK_a = 6.6) [122], though in both experiments few pH values were tested in the acidic and neutral range.

Activation profiles were previously reported for *A. cycloclastes* N_2OR with "CuZ center" mainly as CuZ*(4Cu1S), in which activation at more alkaline pH (pH = 9.4) presented higher specific activities relative to the activation at neutral or more acidic pH values [182], which does not seem to occur with *M. hydrocarbonoclasticus* N_2OR.

4.1.2 Effect of alkaline pH

Besides activation with prolonged incubation with reduced methyl viologen, N_2OR isolated from some microorganisms have been shown to be activated by prolonged incubation with an alkaline solution [90, 178]. This activation procedure seems to have a distinct effect on "CuZ center" as CuZ(4Cu2S), since the specific activity of enzyme preparations with "CuZ center" mainly as CuZ(4Cu2S) appears to increase without incubation with reduced methyl viologen, as the cases of *P. stutzeri* and *P. aeruginosa* [90, 178]. This effect is not so pronounced in a preparation with mainly CuZ*(4Cu1S) [90].

In order to further explore the effect of alkaline pH in the activation of *M. hydrocarbonoclasticus* N_2OR, with 20 % of "CuZ center" as CuZ*(4Cu1S), in a reduced state, the enzyme was dialyzed

against 50 mM CHES buffer pH 9.7 for 24 h. Specific activities were measured in 100 mM Tris-HCl pH 7.6 during the assay without prior incubation with reduced methyl viologen, and compared with a similar assay in which the same form of N_2OR was dialyzed against 50 mM Tris-HCl pH 7.6 (Figure 4.3).

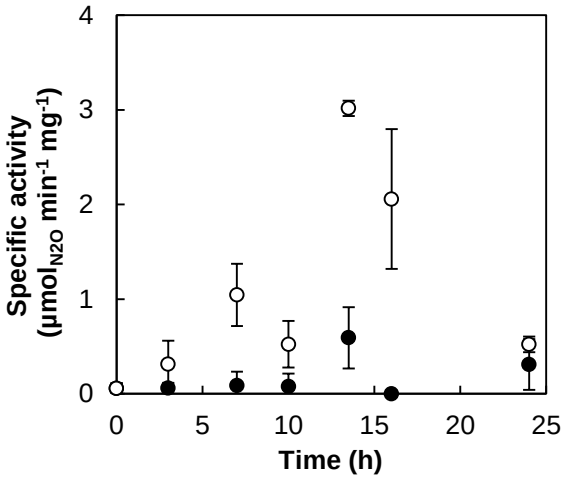

Figure 4.3 - Specific activity of N_2OR with 20 % of "CuZ center" as CuZ*(4Cu1S) during dialysis against 50 mM Tris-HCl 7.6 (filled circles) and 50 mM CHES pH 9.7 (open circles). The specific activities were measured at 0 h (without incubation with reduced methyl viologen) in 100 mM Tris-HCl pH 7.6.

Our results show an increase in the activity of the enzyme, relative to the control, when it is dialyzed in the presence of an alkaline solution, with a maximum at 14 h of incubation. However, this was only a 5-fold increase relative to the control (Figure 4.3). This increase is in line with that reported for *A. xylosoxidans* [92] and *P. pantotrophus* [94] N_2ORs, which also showed a slight increase in activity, 1.4-fold (at pH 10) and 0.5-fold (at pH 9), respectively. A pronounced increase in the activity was only reported for the cases of *P. stutzeri* [90] (by a 28-fold increase at pH 9.7), and *P. aeruginosa* [178] (by a 75-fold increase at pH 10).

In parallel, the visible spectra of N_2OR was monitored during the incubation and a shift in the absorption band with a maximum at 660 nm to 630 nm was observed suggesting conversion of CuZ(4Cu2S) into CuZ*(4Cu1S) (Figure 4.4A). We also observed a bleaching in the spectral features after 24 h of incubation.

Upon oxidation with potassium ferricyanide, the ratio Abs_{550nm}/Abs_{640nm} of the sample initially dialyzed at pH 9.7, changes from 2.1 to 1.6, indicating an increase of CuZ*(4Cu1S)/CuZ(4Cu2S) (Figure 4.4B). This small change in the main form can explain the observed activities, as activity is proportional to CuZ*(4Cu1S) content.

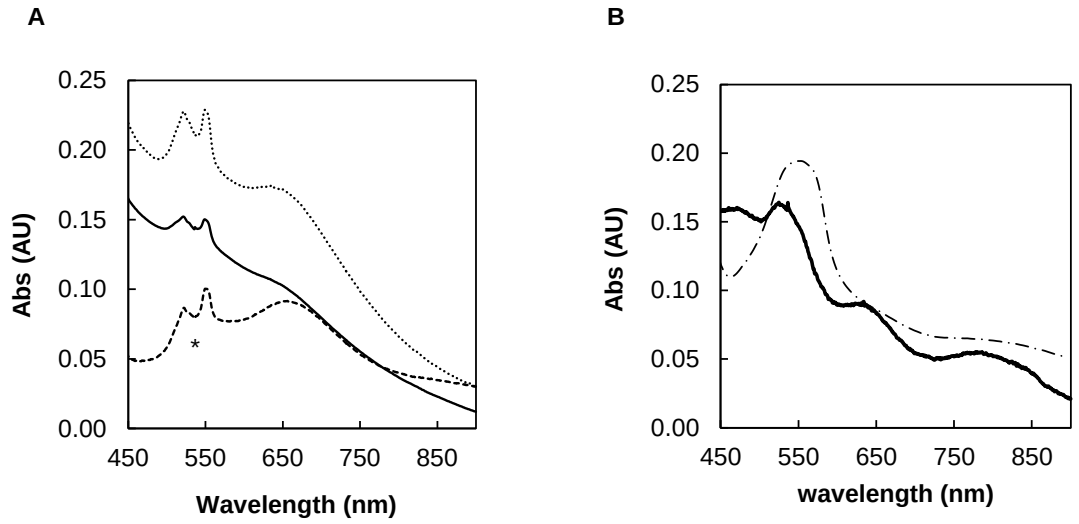

Figure 4.4 - Visible spectra of *M. hydrocarbonoclasticus* N_2OR with 20 % of "CuZ center" as CuZ*(4Cu1S). (A) As-isolated N_2OR, in [$1Cu^{2+}$-$3Cu^{1+}$] state, (dashed line) and dialyzed against 50 mM CHES pH 9.7, after 14 h (dotted line) and after 24 h (solid line). (B) Potassium ferricyanide oxidized spectra of N_2OR after 24 h of dialysis at pH 9.7 (solid bold line) and prior to the assay (dashed-dotted line) are represented. Absorbance was corrected to the total protein concentration. The asterisk indicates a small contamination with a cytochrome.

4.2 Three-dimensional structure of N_2OR with "CuZ center" in different forms

The structure of N_2OR isolated from different growth conditions (pH 6.5 and 7.5, respectively) of *M. hydrocarbonoclasticus*, was solved by X-ray crystallography.

Different forms of "CuZ center" have been crystallized in different redox states, with either CuZ(4Cu2S) as [$2Cu^{2+}$-$2Cu^{1+}$] or as [$1Cu^{2+}$-$3Cu^{1+}$] or with CuZ*(4Cu1S) either as [$1Cu^{2+}$-$3Cu^{1+}$] or [$4Cu^{1+}$] (see Material and Methods, Section 2.13). Good diffraction patterns were only obtained for N_2OR with either CuZ*(4Cu1S) or CuZ(4Cu2S) in the [$1Cu^{2+}$-$3Cu^{1+}$] oxidation state and also with reduced CuA center (Figure 4.5).

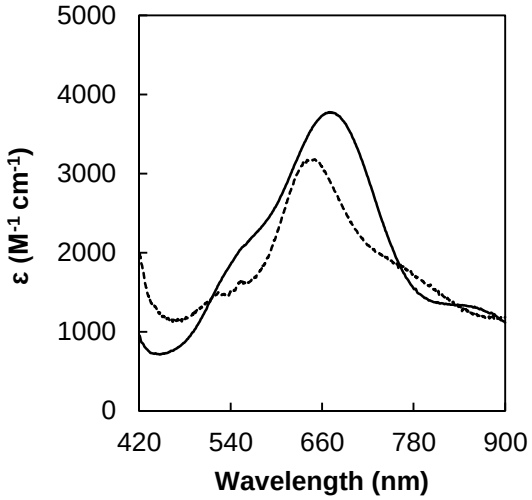

Figure 4.5 - Spectra of different forms of *M. hydrocarbonoclasticus* N_2OR used to produce crystals, being $N_2OR_{pH6.5,}$ with 90 % of "CuZ center" as CuZ*(4Cu1S) (dashed line) and $N_2OR_{pH7.5,}$ with 17 % of "CuZ center" as CuZ*(4Cu1S) (solid line), in 100 mM Tris-HCl pH 7.6.

Blue and purple crystals were obtained for $N_2OR_{pH6.5}$, with 90 % of "CuZ center" as CuZ*(4Cu1S), and $N_2OR_{pH7.5}$, as 17 % of "CuZ center" as CuZ*(4Cu1S), respectively, under anoxic conditions after 3 - 4 days, using the crystallization conditions previously reported by Prudêncio *et al.* [91] (Figure 4.6A and B). Most of the blue crystals have a flower shape, while purple crystals often have a diamond shape, even though flower shaped crystals have also been observed.

Better diffractions patterns were frequently observed for diamond shaped crystals of N_2OR with "CuZ center" as CuZ(4Cu2S) in the reduce state.

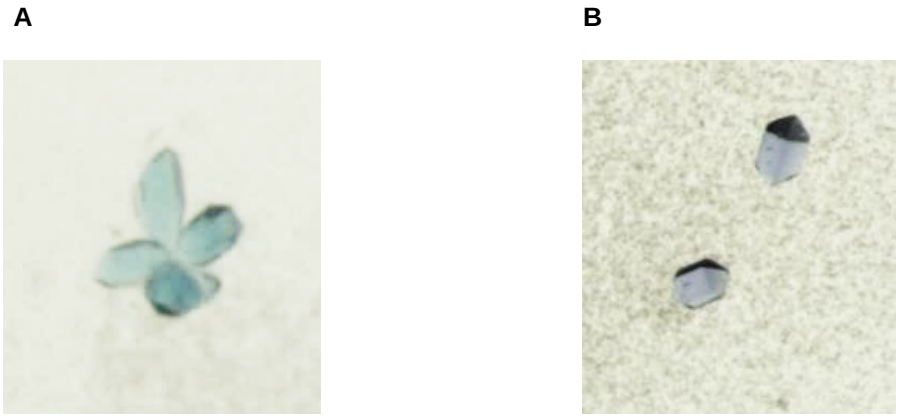

Figure 4.6 - Crystals of different forms of N_2OR from *M. hydrocarbonoclasticus*. (A) Blue crystals were obtained from the preparation with 90 % of "CuZ center" as CuZ*(4Cu1S), purified from a growth carried out at pH 6.5 and (B) purple crystals were obtained from a 17 % of "CuZ center" as CuZ*(4Cu1S) preparation purified from a growth performed at pH 7.5.

4.2.1 Overall structure and model quality

Only one structure of N_2OR from *M. hydrocarbonoclasticus* (solved at 2.4 Å) is deposited in PDB (PDB ID: 1QNI). This structure was obtained from blue crystals of the enzyme purified from a strictly anaerobic growth of this microorganism, in which N_2OR was isolated with "CuZ center" mainly as CuZ*(4Cu1S) [91, 125, 126].

In the present study, the best diffraction pattern was obtained at 2.4 Å and 1.9 Å for N_2OR with 90 % and 17 % of "CuZ center" as CuZ*(4Cu1S), respectively.

Both structures were solved by molecular replacement, with the monomer of the refined structure of *P. stutzeri* used as a starting model for both patterns.

Both crystals belong to the $P6_1$ space group and the asymmetric unit exhibits three homodimers, as also observed in the deposited structure of *M. hydrocarbonoclasticus* N_2OR [91, 125] (Figure 4.7). Two domains were identified in each monomer: a C-terminal domain with a cupredoxin fold, which holds the CuA center and an N-terminal domain with a β-propeller fold that holds the "CuZ center". Moreover, a head-to-tail geometry of the dimer is conserved in both structures, favoring the dimer functionality.

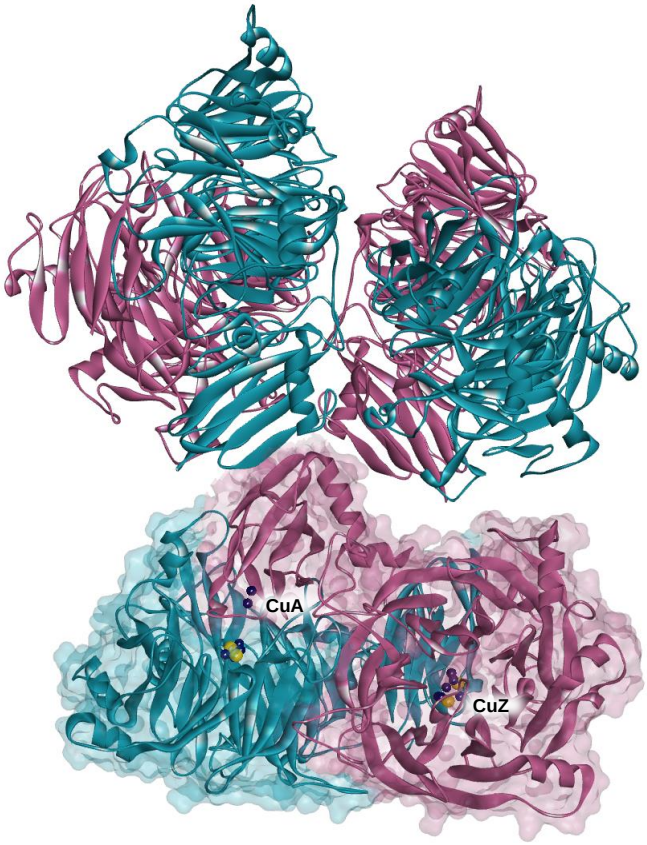

Figure 4.7 - Structure of asymmetric unit of the purple crystal. In each dimer, the monomers are differently colored. One of the dimer has the surface evidenced, as well as the CuA and CuZ(4Cu2S) centers, which are represented by spheres, being copper atoms represented by blue spheres and sulfur atoms represented by yellow spheres. CuA and "CuZ" centers of a monomer are identified. Figure was prepared with DS Visualizer 4.5.

Our main focus is the structure of N_2OR with "CuZ center" mainly as CuZ(4Cu2S), as in addition of being obtained at higher resolution, the structure of N_2OR with "CuZ center" as CuZ(4Cu2S) had not been reported for the enzyme isolated from *M. hydrocarbonoclasticus*.

The refinement statistics indicate that the final model has a good quality with a R_{factor} of 18 % (R_{free} of 23 %) for the sample with 17 % CuZ*(4Cu1S) (Table 4.1).

Based on the superposition of C^{α} of monomer structure of N_2OR from *M. hydrocarbonoclasticus* deposited coordinates (PDB ID: 1QNI), an overall r.m.s. (root mean square) deviation value of 0.307 Å (superposition of 572 atoms) was determined for the N_2OR with "CuZ center" mainly as CuZ(4Cu2S). Additionally, the superposition of 480 C^{α} between the monomer of N_2OR and the one of *P. stutzeri* (PDB ID: 3SBP), both crystallized with "CuZ center" mainly as CuZ(4Cu2S), also showed a small r.m.s. deviation value of 0.615 Å, as expected given the high identity (77 %) between their primary sequence (Figure 4.10).

Table 4.1 – Refinement statistics of the structure of *M. hydrocarbonoclasticus* N_2OR with 17 % of "CuZ center" as CuZ*(4Cu1S).

	Purple crystal
R_{factor} (%)	18
R_{free} (%)	23
no. atoms	
non-hydrogen atoms	27,932
solvent molecules	963
other heterogen atoms	15
r.m.s. deviations from ideal values	
bond lengths (Å)	0.02
bond angles (º)	1.87
overall *B*-factor (Å^2)	21.8
average *B*-factors (Å^2)	
protein main chain atoms	39.5
protein all atoms	35.6
solvent molecules	33.8

The quality of the model was evaluated by MolProbity [216], which indicates, based on the Ramachandran plot, that 94.2 % of the residues are in favored regions for $N_2OR_{pH7.5}$. The overall *B*-factor (also called temperature factor), which reflect the fluctuation of atoms from their mean position, was 21.8 Å^2 (Table 4.1). Indeed, two monomers of the asymmetric unit (molecules E and F) showed higher *B*-factors relative to the other monomers, as the amino acids on the surface of monomers E and F have a higher motion.

In both structures, two cations were consistently detected in each monomer. A calcium ion was observed in the N-terminal domain, while a second ion (modeled as K^+ or as Ca^{2+}) was found at the dimer interface (Figure 4.8). In the first reported structures these atoms were both modelled as calcium ions, however in *P. stutzeri* N_2OR [152] a calcium and a potassium ion were identified and more recently the structure of apo-N_2OR from *S. denitrificans* reconstituted with calcium suggested the binding of only one calcium ion per monomer [129].

The relevance of the second ion is not completely understood and in fact the flexibility of the enzyme to bind either K^+ or Ca^{2+} is somewhat interesting as the ion charge is different, yet both were modelled in the structures of N_2OR with "CuZ center" mainly CuZ(4Cu2S). The ligands of these ions are conserved between N_2ORs, with exception of a methionine, which in *M. hydrocarbonoclasticus* is a threonine residue (T265). The Ca^{2+} at the N-terminal domain is coordinated by two O_δ of E257, two O_γ of D271 and also by carboxylic oxygen atoms of T265 and Y254 (numbered according to *M. hydrocarbonoclasticus* N_2OR primary structure). The second ion (either a K^+ or Ca^{2+}) is coordinated to carboxylic oxygen atom of K447, two O_δ of E462 and four water molecules (Figure 4.8, Figure 4.10).

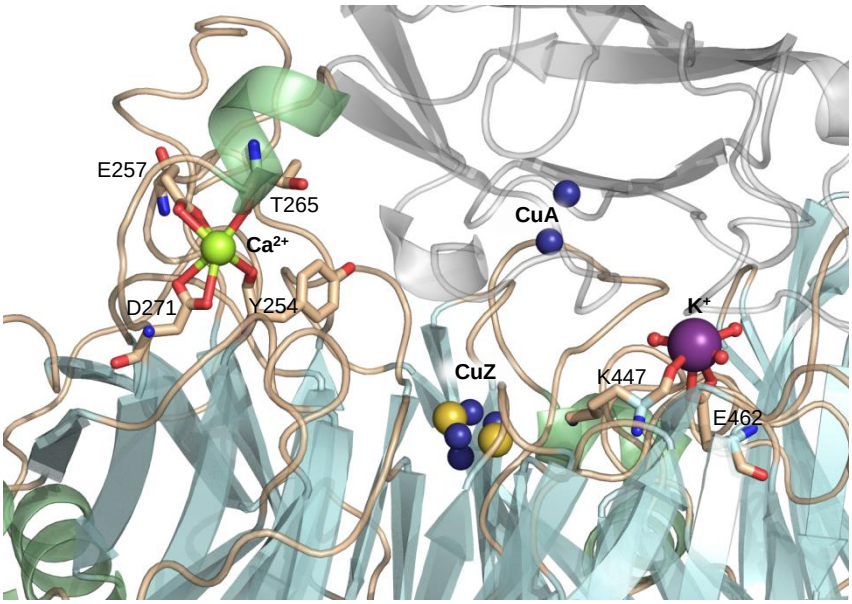

Figure 4.8 – Stereo representation of Ca^{2+} (green sphere) and K^+ (purple sphere) binding sites in the *M. hydrocarbonoclasticus* N_2OR structure obtained for the purple crystal at 1.9 Å. One monomer of N_2OR is colored according to the secondary structure, while the other is colored in grey. Copper and sulfur atoms are represented as blue and yellow spheres, respectively. The CuA center is part to the monomer colored in grey, while "CuZ center" belongs to the other monomer. Figure was prepared with Pymol.

Dimer interface region is also highly conserved between the structures, containing mainly non-polar residues favoring Van der Waals interactions, which are essential to stabilize the dimer, together with hydrogen bonds and the calcium ion [157].

The surface of N_2OR with "CuZ center" mainly as CuZ(4Cu2S) is mainly hydrophobic (Figure 4.9).

In fact, both CuA and "CuZ" centers have hydrophobic residues in their vicinity, being these the more hydrophobic regions of N_2OR surface (Figure 4.9B). This was expected, since previous studies have proposed that the nature of complex formed between cytochrome c_{552}, the putative physiologic electron donor, and *M. hydrocarbonoclasticus* N_2OR has a hydrophobic character, with the electron proposed to bind near the CuA center [122, 154].

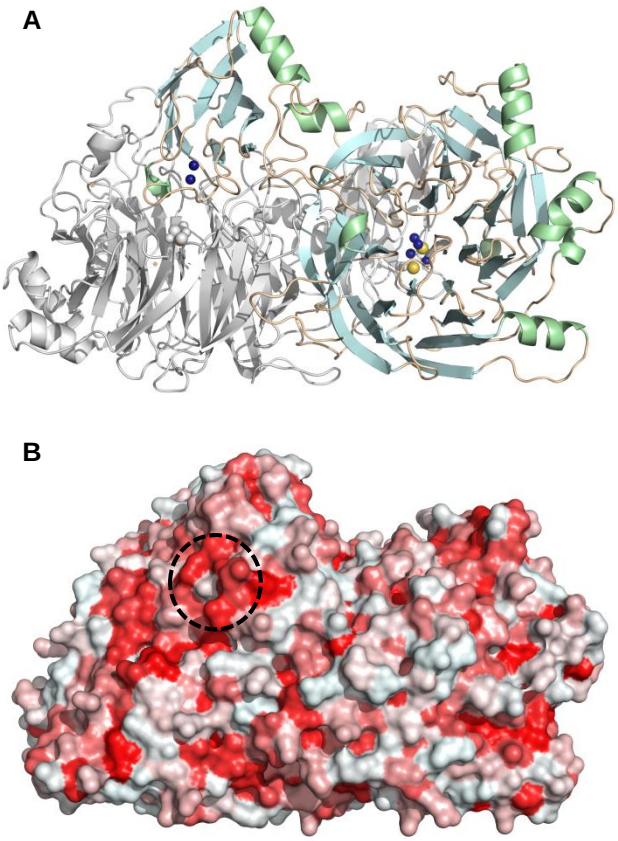

Figure 4.9 – Structure of purple crystal of *M. hydrocarbonoclasticus* N_2OR. (A) Representation of the backbone with one of the monomers highlighted, and colored according to the secondary structure. The CuA and CuZ(4Cu2S) centers are represented by spheres, being copper atoms represented by blue spheres and sulfur atoms represented by yellow spheres. (B) Surface is colored according to Eisenberg hydrophobicity scale (highly hydrophobic residues are colored in red). CuA center region is identified with a dashed circle. Figure was prepared with Pymol.

4.2.2 Structural features of CuA center

The binuclear CuA center, is located at the C-terminal domain and the residues involved in its coordination are strictly conserved between N_2ORs (Figure 4.10).

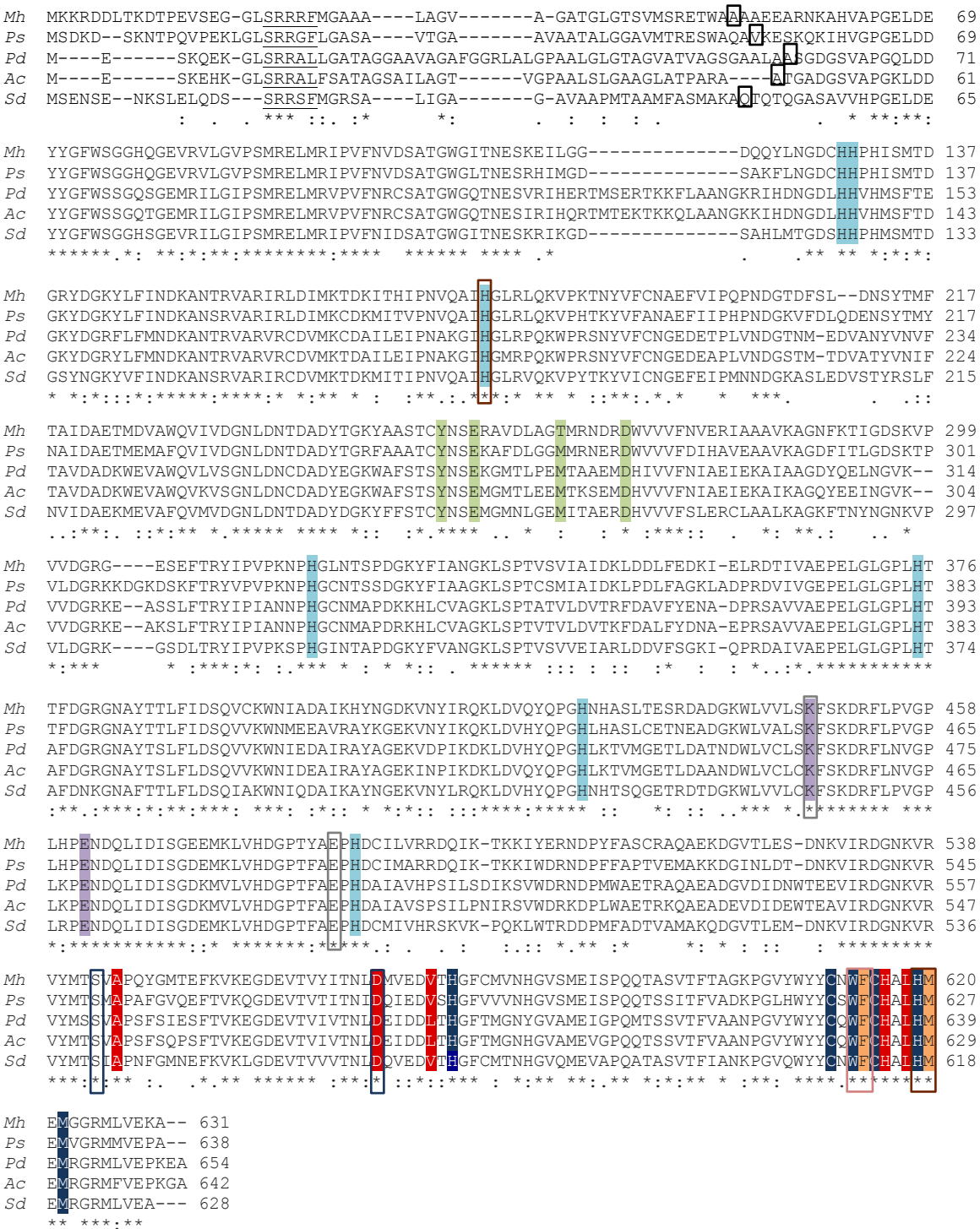

Figure 4.10 – Primary sequence alignment of N_2ORs whose structure have been deposited in the PDB. The conserved "CuZ" ligands are highlighted in light blue and the lysine and glutamate residues in the vicinity are identified by a grey box. CuA ligands are highlighted in dark blue and the residues coordinating the rotated histidine by a dark blue box. Residues postulated to be part of the intermolecular electron transfer are highlighted in red, and those of the intramolecular electron transfer are identified with a pink box (pathway 1) and with a brown box (pathway 2). Residues highlight at green and violet coordinate the calcium and the potassium ions, respectively. Residues highlight in orange are involved in re-orientation of N_2O molecule. The tat-motif is underlined and the start of mature proteins is identified with a black square. Bacterial species are identified by: *Mh – Marinobacter hydrocarbonoclasticus*, *Ps – Pseudomonas stutzeri*, *Pd – Paracoccus denitrificans*, *Ac – Achromobacter cycloclastes* and *Sd – Shewanella denitrificans*. Asterisks, colons or stops below the sequence indicate identity, high conservation or conservation of the amino acids, respectively.

In all monomers of the asymmetric unit of both structures, the copper atoms are coordinated to S_γ of C611 and C615, being CuA_1 also bound to $N_{\varepsilon 2}$ of H576 and a S_γ of M622, while CuA_2 is coordinated to the $N_{\varepsilon 2}$ atom of H619 and to the carbonyl group of W613.

Interestingly, none of the monomers of the asymmetric unit (in both structures) showed a flipped histidine residue (H576), even in the CuZ(4Cu2S) form, as opposite to most monomers of the asymmetric unit of *P. stutzeri* N_2OR without substrate, with "CuZ center" in this form [152]. Additionally, other crystal obtained from a different batch of *M. hydrocarbonoclasticus* N_2OR, with "CuZ center" mainly as CuZ(4Cu2S), solved at 2 Å resolution, also showed H576 coordinating CuA_1 in all monomers of the asymmetric unit.

Moreover, crystals of *M. hydrocarbonoclasticus* N_2OR, with 17 % of "CuZ center" as CuZ*(4Cu1S), were obtained from a preparation with CuA center reduced (Figure 4.6B), while the *P. stutzeri* N_2OR used in the crystallization appears to have been isolated with CuA center oxidized [152]. Thus and assuming that *P. stutzeri* N_2OR crystals did not undergo photoreduction, the switching mechanism might have a relation with the oxidation state of CuA center in the purple form, but parallel crystallization of oxidized and reduced CuA center are still needed to draw further conclusions. Although the causes of the histidine flip are not yet completely understood, the hypothesis of being a mechanism that is triggered by the presence of substrate cannot be excluded.

CuA center has a role in both inter- and intramolecular electron transfer, as it mediates the electron transfer from cytochrome c_{552} to the catalytic center of *M. hydrocarbonoclasticus* N_2OR [122, 154]. The residues A545, D569, V574, H616 and L618 are involved in the electron transfer from the heme group to the CuA center, while two pathways were proposed for electron transfer from CuA center to "CuZ center" [154]. In pathway one, the electrons are transferred from W613, which coordinates CuA_2, to F614 and then to the Cu_I-Cu_{IV} edge ligand (water derivative molecule of CuZ*(4Cu1S)) (Figure 4.10) [154]. In the pathway two proposed, the electrons are transfer from H619, which coordinates CuA_1, via M620 to H128, which coordinates the Cu_{II} atom in the "CuZ center" (Figure 4.10) [154]. Additionally, both S542 and D558 are also highly conserved, which were reported to establish hydrogen bonds with the flipped histidine of CuA center, in *P. stutzeri* N_2OR structure [152].

4.2.3 Structural features of "CuZ center"

The active site of the enzyme has a central location in the β-propeller folded N-terminal domain, which is accessible to the substrate through a channel that is extended to the surface (Figure 4.11) [151].

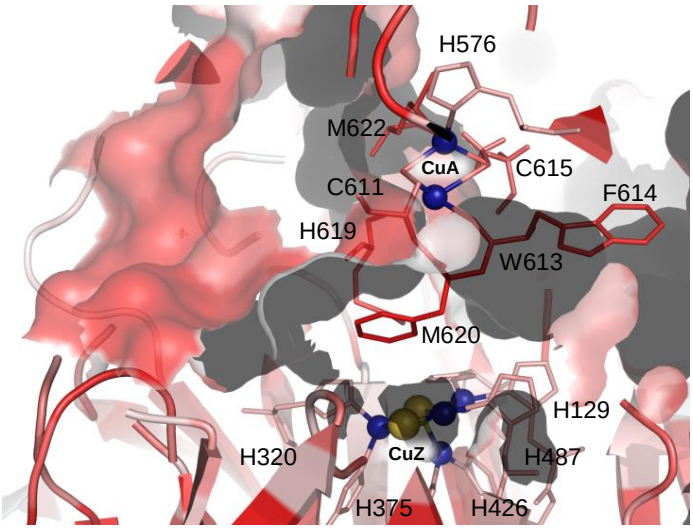

Figure 4.11 – Representation of the interface region between the functional dimer colored by Eisenberg hydrophobicity (the most hydrophobic residues are colored in red) in the structure of *M. hydrocarbonoclasticus* N_2OR with 17 % of "CuZ center" as CuZ*(4Cu1S). Hydrophobic residues in this region form a channel for the access of the substrate to the "CuZ center". The re-orientation of the N_2O molecule is through M620 and F614 residues. Figure was prepared with Pymol.

Despite the low copper quantification per protein frequently obtained in N_2OR isolated from some microorganisms [20], *M. hydrocarbonoclasticus* N_2OR is often isolated with ~ 10 Cu atoms per dimer, especially when grown at pH 7.5 in strictly anaerobic conditions (see Chapter 3, Table 3.3) [91].

In the structures of "CuZ center" of both forms, CuZ(4Cu2S) and CuZ*(4Cu1S), there is a clear electron density for the occupancy of the four copper atoms arranged in a distorted tetrahedron and a central labile sulfur atom, similar to other reported structures. The copper atoms in this center are coordinated by a total of seven histidine residues that are strictly conserved among the primary structures of N_2ORs (Figure 4.10).

In both cases, Cu_I, Cu_{II} and Cu_{III} are coordinate by two histidine residues (H375 and H320; H129 and H178; H426 and H130, respectively), while Cu_{IV} is coordinated by only one (H487).

Indeed, in the structural data obtained for N_2OR with 17 % of "CuZ center" as CuZ*(4Cu1S) no positive or negative electron density in the copper atoms was detected, suggesting a full occupancy for these atoms. In the case of N_2OR with 90 % of "CuZ center" as CuZ*(4Cu1S), a small positive density in the "CuZ center" was detected in some monomers, which might be due to a lower copper occupancy. In fact, a slightly decrease of the copper occupancy in "CuZ center" (from 1.0 to 0.8) in N_2OR with 90 % of "CuZ center" as CuZ*(4Cu1S), improved the fitting of the electron density.

In particular, a major difference between structures was detected regarding the edge ligand between Cu_I and Cu_{IV}, as expected by the different spectroscopic features described in Chapter 3 (Section 3.10).

Electron density maps generated with a sulfur atom as the edge ligand in the "CuZ center" structure obtained of N_2OR with 90 % of "CuZ center" as CuZ*(4Cu1S) shows negative difference electron

density at the sulfur atom, suggesting that the model should have an atom with fewer electrons (Figure 4.12A). In fact, an oxygen atom from a water-derived molecule, fits better at the edge ligand of the N_2OR with 90 % of "CuZ center" as CuZ*(4Cu1S), in accordance with the previously deposited structure of N_2OR from this organism (PDB ID: 1QNI) [126]. An approximately distance of 2.4 Å was calculated between the oxygen atom and both Cu_{IV} and Cu_I atoms.

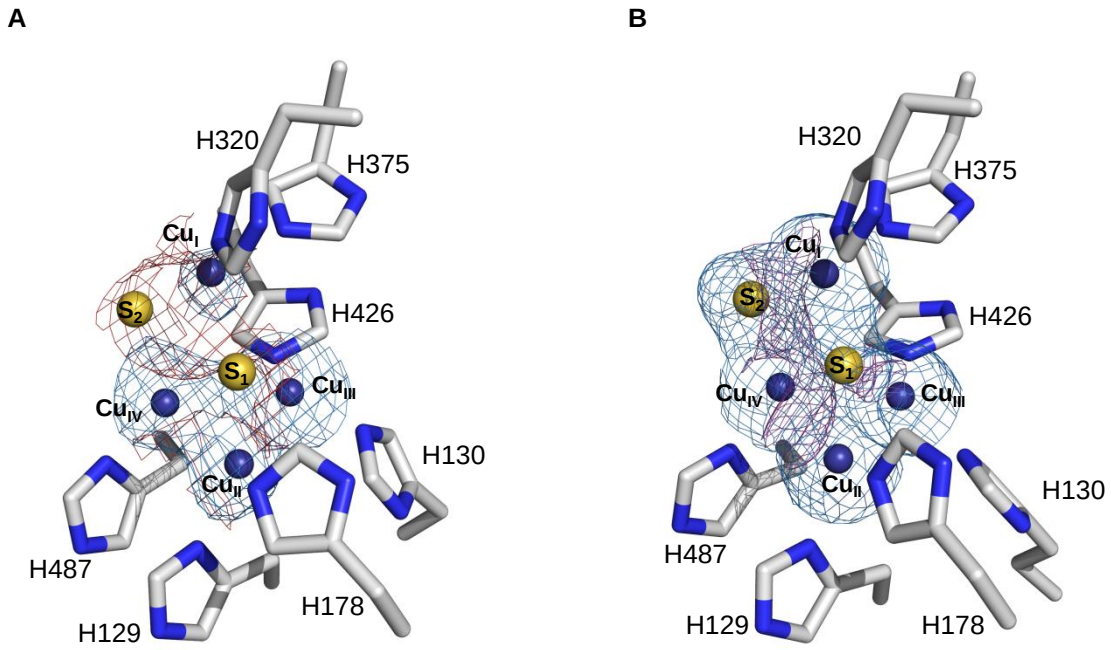

Figure 4.12 – Difference electron density maps for the "CuZ center" in a sample with 90 % of "CuZ center" as CuZ*(4Cu1S) (A) and 17 % of "CuZ center" as CuZ*(4Cu1S) (B). The coppers and sulfur atoms are represented by blue and yellow spheres, respectively. In panel (A) electron density map $2F_0$-F_c is contoured at 3.0 σ (blue) and the F_0-F_c electron density map calculated is contouring at -1.5 σ level (red). In panel (B) electron density map $2F_0$-F_c is contoured at 1.0 σ (blue) and the F_0-F_c electron density map calculated is contouring at 3.0 σ level (purple). F_0 and F_c are the observed and calculated structure factors, respectively. Difference electron density maps were generated by Fast Fourier Transform (CCP4: Supported program) and the figures were prepared with Pymol.

On the other hand, in the structure of N_2OR with 17 % of "CuZ center" as CuZ*(4Cu1S), the Cu_I-Cu_{IV} edge of "CuZ center" was modelled with a sulfur atom in all the monomers, which fits well with the electron density observed (Figure 4.12B). The sulfur atom is at approximately 2.4 Å from Cu_I and at a 2.5 Å from Cu_{IV}, in line with the distances reported for the second sulfur in *P. stutzeri* N_2OR [152].

This difference in the edge ligand corroborates the differences in the spectroscopic properties described before between $N_2OR_{pH6.5}$ and $N_2OR_{pH7.5}$ (Figure 4.5).

Although the three-dimensional structures of N_2OR with "CuZ center" as CuZ(4Cu2S), CuZ*(4Cu1S) and also of the apo-form have been reported [125, 126, 129, 151, 152, 157], there are still unanswered questions, such as the on/off mechanism of histidine in CuA center, the crystallization of the fully reduced CuZ*(4Cu1S) (which is the active form *in vitro*) or how inhibitors and

substrate bind to the different forms of the enzyme, since the only deposited structures of N_2OR pressurized with substrate has "CuZ center" as CuZ(4Cu2S), and both centers are in the fully oxidized state (a form of the enzyme known not to catalyze the reduction of N_2O) [152].

4.3 Redox behavior of the copper centers of *M. hydrocarbonoclasticus* N_2OR

4.3.1 Redox titration

Spectroscopic studies proved that both CuA and CuZ(4Cu2S) can be reversible reduced, contrary to CuZ*(4Cu1S), which can only be reduced after prolonged incubation in the presence of reduced methyl viologen. Although the two redox centers, CuA and CuZ(4Cu2S), are present, they behave independently in an oxidation/reduction process.

Potentiometric redox titrations were monitored by visible spectroscopy at two wavelengths, 660 nm and 800 nm, used to follow the reduction/oxidation events related to CuZ(4Cu2S) and CuA centers, respectively (Figure 4.13). In fact, CuA center is often monitored at 540 nm, as this band has higher intensity, however the oxidized CuZ(4Cu2S) center also contributes at 550 nm, masking CuA features. The absorbance at 480 nm was not used, as the sample in this experiment has a contamination with a cytochrome. In the case of CuZ(4Cu2S), absorbance was followed at the maximum absorption band of CuZ(4Cu2S) in the reduced state (660 nm), as at 550 nm there is higher contribution of CuA center.

The titrations were initiated with fully oxidized N_2OR, varying the potential from + 400 mV to - 200 mV (or to – 400 mV for pH higher than 10).

The spectroscopic data obtained show that both oxidative and reductive titration curves are superimposed for each of the centers at pH 7.6, with no evidence of hysteresis (Figure 4.13).

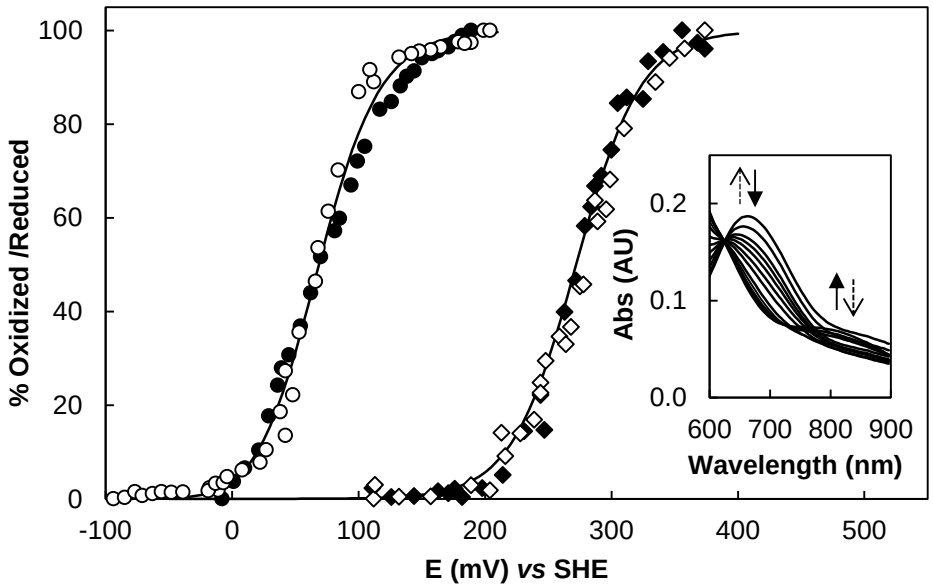

Figure 4.13 – Potentiometric redox titration of N_2OR, with 15 % of "CuZ center" as CuZ*(4Cu1S), performed at pH 7.6. The CuA (diamonds) and the CuZ(4Cu2S) (circles) centers were followed by visible spectroscopy at 800 and 660 nm, respectively. For both centers the absorbance was monitored in the reductive (filled symbols) and oxidative (open symbols) titration. The titration of each center was fitted to one-electron process using the Nernst equation, with a $E_{m,7.6}$ = + 272 ± 10 mV (*vs* SHE) for CuA center and a $E_{m,7.6}$ = + 65 ± 10 mV (*vs* SHE) for CuZ(4Cu2S) center. The insert is an example of the bands followed in the visible spectra, being the oxidation and reduction process represented by solid bold and dashed arrows, respectively.

The curves were fitted to Nernst equation of one-electron reduction for each center with reduction potentials of + 272 ± 10 mV and + 65 ± 10 mV, *vs* SHE, at pH 7.6. The more positive reduction potential was observed after addition of sodium ascorbate to the fully oxidized sample and is assigned to the $[1Cu^{1.5+}\text{-}1Cu^{1.5+}]/[1Cu^{1+}\text{-}1Cu^{1+}]$ redox couple of CuA center.

The reduction potential determined for CuA center is slightly higher than the value previously reported for *M. hydrocarbonoclasticus* N_2OR ($E_{m,7.6}$ = + 240 mV) in a preparation containing "CuZ center" mainly as CuZ*(4Cu1S), by potentiometric redox titration studies [148]. A similar value ($E_{m,7.5}$ = + 260 mV) was determined for this center in *P. pantotrophus* N_2OR [131]. Moreover, the reduction potential assigned to CuA center of C*c*O have also similar values, as is the case of *Thermus thermophiles* ($E_{m,6.5}$ = + 265 ± 10 mV) [258].

The lower reduction potential ($E_{m,7.6}$ = + 65 ± 10 mV) corresponds to the $[2Cu^{2+}\text{-}2Cu^{1+}]/[1Cu^{2+}\text{-}3Cu^{1+}]$ redox couple of CuZ(4Cu2S), in agreement with the value determined for this center in *P. pantotrophus* N_2OR ($E_{m,7.5}$ = + 60 mV) [131].

4.3.1.1 pH dependence

The pH dependence of the reduction potential of both CuA and CuZ(4Cu2S) centers was also investigated by potentiometry.

The reduction potential of CuA center was followed by visible spectroscopy at 480 nm at different pH values, ranging from 6.5 to 8.5, using a N_2OR sample with 50 % of "CuZ center" as CuZ*(4Cu1S). In most of the titrations performed, no significant hysteresis was observed between the oxidative and reductive curves suggesting that CuA center can be reversibly reduced at different pH values. The plot of the reduction potentials determined as a function of pH is presented (Figure 4.14).

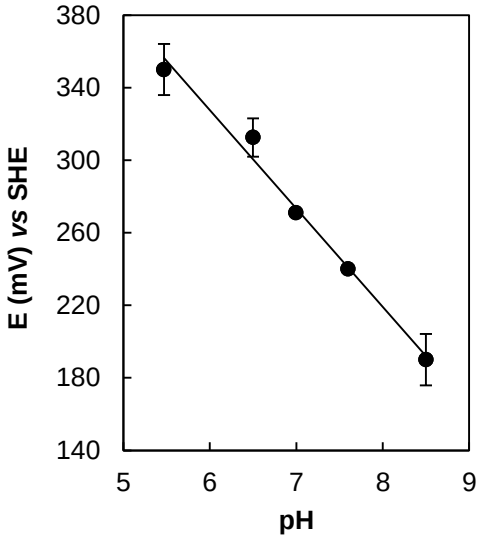

Figure 4.14 – pH dependence of the reduction potentials of CuA center at 20 °C. The potentiometric redox titrations were followed by visible spectroscopy at 480 nm in a N_2OR sample with 50 % of "CuZ center" as CuZ*(4Cu1S). Data obtained were fit (solid line) by a linear regression: $y = - 54.2x + 652.8$, $R^2 = 0.987$.

The reduction potential of CuA center varies linearly with pH (Figure 4.14). This relation has a slope of - 54 mV per pH unit, which is close to the - 58 mV per pH unit expected for a 1 H^+/e^- coupled process at 20 °C, indicating that under those conditions CuA center reduction is coupled to the binding of one proton. However, the spectrum of fully oxidized N_2OR at pH values between 5.5 and 8.1 did not show any differences in the CuA center absorption bands (data not show) [167], suggesting that in this pH range the protonation/deprotonation of side chains of residues directly coordinating the metal does not occur. Therefore, there must be another protonable residue close to CuA center that influences its reduction potential.

The pH dependence of CuA reduction potential and pH effect on the visible spectra have previously been reported for C*c*O from several microorganisms, such as *P. denitrificans* [259, 260] and *T. thermophiles* [259, 260], and also for the modified azurin [261]. In the case of the modified azurin a pK_a of 4.8 was estimated and a sharp variation of the potential with pH was reported [261], while in the native C*c*O from *T. thermophiles* ba_3 at pH between 4 - 7 low variations of CuA reduction potential were reported [262]. Indeed, the protein matrix must have a role in such variations of the reduction potential of CuA center with pH, which probably explains the different behavior observed for CuA center of N_2OR in comparison with other CuA centers.

Relative to "CuZ center", MCD and EPR spectroscopic studies showed the lack of pH dependence of CuZ(4Cu2S) spectroscopic features (between pH 6 and 10) [164]. Nonetheless, the pH dependence of its reduction potential has not been reported, and so potentiometric studies were performed between pH 6.5 and 10.4, at ~ 20 °C, using a N_2OR sample with 15 % of "CuZ center" as CuZ*(4Cu1S) (Figure 4.15, Table 4.2).

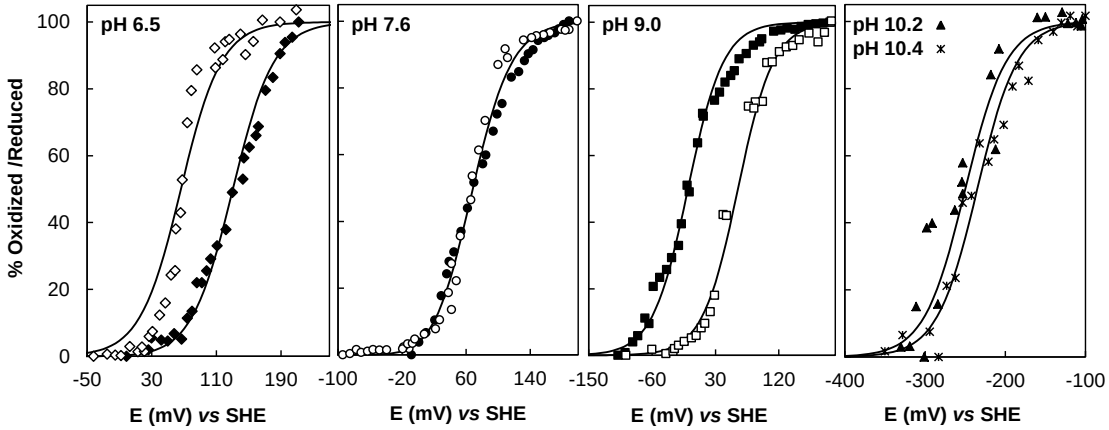

Figure 4.15 – pH dependence of the reduction potential of N_2OR, with 15 % of "CuZ center" as CuZ*(4Cu1S). Potentiometric redox titrations were performed at 20 °C followed by visible spectroscopy at 660 nm in the reductive (filled symbols) and the oxidative (open symbols) direction at pH 6.5 (diamonds), 7.6 (circles), 9.0 (squares), 10.2 (triangles) and 10.4 (crosses). The titration at each pH (indicated in each panel) was fitted to one-electron process using the Nernst equation. Titrations at pH 10.2 and 10.4 are only represented for the reductive direction. Note that the oxidative titration performed at pH 6.5 fits better for two electrons, most likely this is an artifact caused by an unreached equilibrium during the oxidation.

Table 4.2 – Oxidative and reductive reduction potentials of CuZ(4Cu2S) center of *M. hydrocarbonoclasticus* N_2OR at different pH values.

pH	**$E_{m,\ oxidative}$**	**$E_{m,\ reductive}$**
6.5	+ 66 ± 5 mV	+ 128 ± 5 mV
7.6	+ 63 ± 5 mV	+ 67 ± 5 mV
9.0	+ 60 ± 5 mV	- 9 ± 5 mV
10.2	-	- 250 ± 5 mV
10.4	ND	- 240 ± 5 mV

Note: ND – not determined

The redox titrations performed at pH 6.5 and pH 9.0 showed a hysteresis effect, which is a redox behavior different from the one observed for the potentiometric titration at pH 7.6 (Figure 4.15). Moreover, this hysteresis has a difference of *ca.* 60 mV between the reduction potential of the two directions (Figure 4.15, Table 4.2). This effect is most probably due to the pH dependence of the reductive titration.

The reductive titration, between pH 6.5 and 9.0, presents a decrease in the reduction potential as the proton concentration decreases in solution, which is characteristic of a pH-dependent system (Figure 4.15 and Supplementary Information S4 – Figures S4.2 and S4.3). Despite the few pH values tested, a strong effect of pH (- 55 mV per pH unit) was observed, which is consistent with the variation of - 58 mV per pH unit, characteristic of an oxidation-reduction process coupled with proton binding [263], suggesting that the one-electron reduction of CuZ(4Cu2S) is associated with the binding of one proton.

The reductive titration performed at high pH values (pH 10.2 and 10.4) exhibits also a Nernstian behavior, but falling below the trend line followed by the reduction potentials, due to some protein precipitation that starts to occur at these high pH values (Figure 4.15, Table 4.2). Additionally, this fact can also explain the difficulty in titrating CuZ(4Cu2S) in the oxidative direction at pH 10.2, making it impossible to fit the data.

Although more experimental data are required to completely understand this process, in order to find an explanation for the observation of hysteresis and that the reductive titration is pH dependent the following model was proposed for the reduction of CuZ(4Cu2S) (Figure 4.16). This mechanism involves two macroscopic oxidation states with four possible microstates, which are differently populated at the different pH values.

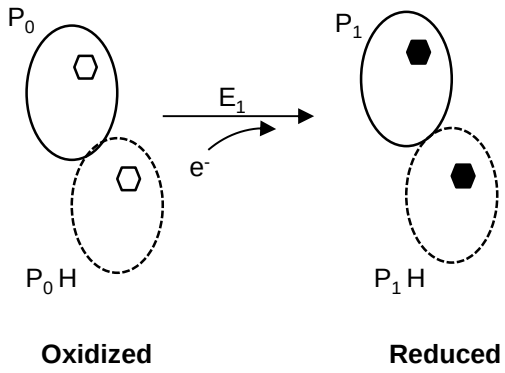

Figure 4.16 – Scheme illustrating the possible microstates of the CuZ(4Cu2S) center of *M. hydrocarbonoclasticus* N_2OR. The hexagons represent the CuZ(4Cu2S) center, which can be oxidized (open hexagons) or reduced (filled hexagons). The protonated (dashed circles) and deprotonated (solid circles) microstates are grouped according its oxidation potential, being P_0 and P_0H representing the oxidized and oxidized protonated microstates, and P_1 and P_1H representing the reduced and reduced protonated microstates, respectively.

Recent spectroscopic studies on the protonation states of CuZ(4Cu2S) have identified two pK_a values, a pK_a ~ 3 and a pK_a ~ 11, depending on the oxidation state of the "CuZ center" [164]. The pK_a ~ 11 was assigned to the thiolate edge ligand when the center is reduced, and the pK_a ~ 3 was predicted for the sulfide edge ligand in the oxidized form of the center. These pK_a values were used to estimate the different microstates according to the proposed model in Figure 4.16, at each studied pH (pH 6.5, 7.6 and 9.0). However, the profiles observed did not exhibit variations in the

molar ratios of the different microstates in this pH range, suggesting that the redox behavior observed cannot be explained by these pK_a values (Supplementary Information S4 – Figure S4.1), as differences in the experimental data were clearly observed.

However, there are other factors that can influence the reduction potential of a redox center, such as the protonation/deprotonation of residues side chains directly coordinating the metal ions, conformational changes of the redox centers, solvent effects and also electrostatic interactions in the proximity of the redox center [264].

In order to explain the experimental data, the X-ray structure of "CuZ center" was analyzed to identify the presence of ionizable residues in the vicinity of "CuZ center" that could influence the reduction potential of this center (Supplementary Information S4 – Figure S4.4). In fact, in the reduced state K447 might be involved in the stabilization of the thiolate edge ligand of CuZ(4Cu2S). Besides this residue, in the vicinity of "CuZ center" the only ionizable groups are the histidine side chains that coordinate the copper atoms of "CuZ center", and in fact its protonation might influence the reduction potential of "CuZ center". Considering that a pK_a = 9.2 has been attributed to K447 and that the pK_a of the histidine residues that coordinate the copper atoms of "CuZ center" was estimated by *in silico* analysis of its coordinates to be close to 6.0, these two pK_a values were used in the mathematic model to estimate the molar ratio of the different microstates during the titration at the different pH values (Supplementary Information S4 – Figure S4.3 and Equations S4.2 – S4.7). At pH 7.6, the deprotonated form (P_0) dominates the oxidized state, while the reduced state is dominated by the protonated form (P_1H). At this pH, we proposed an electron route from P_0 to P_1H, with a coupled transfer of electrons and protons.

On the contrary, at pH 6.5, a mixture of both microstates (P_0 and P_0H) is observed in the oxidized state while the reduced state is dominated by the protonated form (P_1H). A similar effect is observed at pH 9.0, in which in the reduced state there is a mixture of both microstates, while the oxidized form is dominated by the deprotonation one. This lack of dominance of a microstate on the titrations performed at these pH values (6.5 and 9.0), in either the oxidized or reduced state might explain the difficulty in the re-oxidative process of the redox titration: protonation of one or several of the histidine side chains that coordinate "CuZ center" leads to uncoordination of a copper atom (oxidized form) and the thiolate edge ligand of the reduced form is less stabilized by the deprotonation of K447 (reduced form).

4.3.2 Electrochemical behavior

The redox behavior of metal centers of N_2OR is complex and although it is now better understood after the potentiometric studies, the redox properties of the chemically inert CuZ*(4Cu1S) center are still a challenge. Understanding the mechanisms involved in the electron transfer and catalytic

process is crucial and thus electrochemical techniques, cyclic voltammetry and differential pulse voltammetry were used to further inspect the redox behavior of this enzyme.

Electrocatalytic reduction of N_2O by N_2OR was previously reported through mediated electron transfer by small electron shuttle proteins: cytochrome c_{552} using fully reduced *M. hydrocarbonoclasticus* N_2OR [148] and pseudoazurin acting as electron donor of *A. cycloclastes* N_2OR [123].

However, no direct electron transfer between the electrode and N_2OR has been reported so far.

We have used several approaches to promote the direct electron transfer using modified gold, graphite or carbon surfaces, as well as the use of different (charged) promoters, as polylysine and neomycin, but no electrochemical signals were observed. In addition, thin layer and membrane configuration were also tested, as well as electrochemistry in solution, but no differences from the blank voltammograms were detected. In fact, direct electrochemistry of N_2OR can be very challenging, as this is a large protein containing multiple redox centers in which the catalytic center is buried from the surface and thus a proper electron transfer pathway through CuA center to the "CuZ center" might be required.

Highly conductive and chemically stable materials with a large surface area can improve the immobilization process and also enhance the electron transfer, as is the case of carbon nanotubes (CNTs), which use has been notably growing in electrochemical and biochemical applications [265-267]. CNTs are composed of rolled graphene sheets forming tubes of small diameters (in the order of nanometers) and can be divided into single-walled carbon nanotubes (SWCNTs) or multi-walled carbon nanotubes (MWCNTs), with the later comprising several cylindrical-sheets with diameters of 2 – 100 nm [265].

MWCNTs properties and performance are related with the pre-treatment to which they are subjected. These pre-treatments are usually acidic (e.g. HNO_3 or H_2SO_4) and thermic, which remove impurities and confer an open-ended tube with functional groups, such as carboxylic acids, alcohols and quinones [218, 265, 268]. Further functionalization with other groups (such as thiols, amino acids, amides) can also be performed [268].

In this section, MWCNTs were used to investigate the direct electron transfer between the electrodes and N_2OR. MWCNTS were exposed to HNO_3 and also to a thermal treatment and then dispersed in DMF solution, to introduce oxide functional groups, able to interact with N_2OR. Moreover, electrocatalytic activity of N_2OR (without pre-activation) assisted by cytochrome c_{552}, was also investigated.

4.3.2.1 Direct electrochemistry

4.3.2.1.1 Non-turnover conditions

Cyclic voltammetry was first used to evaluate the non-turnover behavior of N_2OR in a 100 mM potassium phosphate buffer solution at pH 7.0.

Modification of glassy carbon (GC) surface with MWCNTs generates higher capacitive currents than those of bare GC. Similar currents were observed for different electrode modifications, indicating that MWCNTs layers are reproducible. Typically, a ratio between the electroactive and geometric area, A_{ele}/A_{geo} of ~ 110 was estimated between the capacitive current in the presence of MWCNTs and the bare GC electrode.

Initial cyclic voltammetric studies were conducted with a N_2OR preparation with 60 % of "CuZ center" as CuZ*(4Cu1S).

Direct electrochemistry of the enzyme was achieved with two signals identified in the voltammograms when N_2OR was deposited on the MWCNTs layer: a cathodic peak (Ep_c^I) with an anodic counterpart (Ep_a^I), denominated as signal I, and a second cathodic peak (Ep_c^{II}) at more negative potentials, with a less clear anodic counterpart, denominated as signal II (Figure 4.17). Note that in the absence of the enzyme, no new peaks were observed with continuous scans over the same potential window. Nevertheless, capacitive currents start to decrease after some time, possibly due to the loss of carbon nanotubes to the electrolyte.

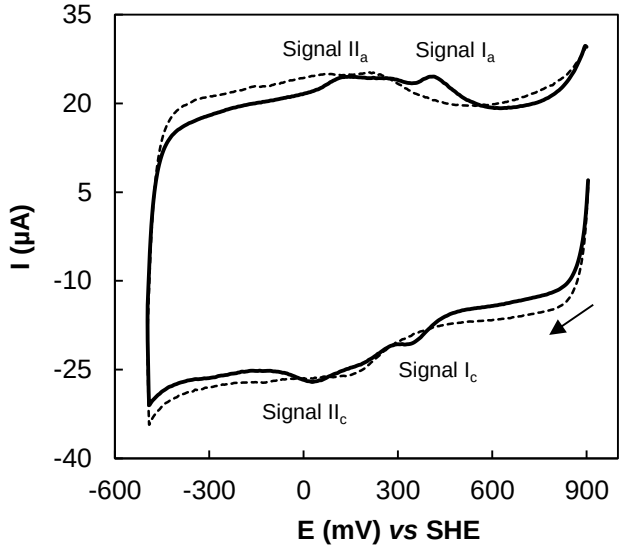

Figure 4.17 – Cyclic voltammograms of 200 µM of N_2OR with 60 % of "CuZ center" as CuZ*(4Cu1S), immobilized onto a MWCNTs layer coated on a glassy carbon electrode, in 100 mM potassium phosphate pH 7.0 at a scan rate of 10 mV s^{-1}. Dashed line represents the MWCNTs layer prior to enzyme immobilization and solid line voltammogram was obtained after N_2OR immobilization. The arrow represents the direction of the scan. Signal Ia and signal Ic, represents the anodic and cathodic peak of signal I and signal IIa and IIc represents the anodic and cathodic peak of signal II.

On the other hand, increasing the concentration of the enzyme deposited in the MWCNTs, higher

currents of the peaks were detected and therefore they can only be attributed to the direct electrochemical response of the enzyme.

The behavior of N_2OR on the modified GC electrode was evaluated by varying the scan rate (Figure 4.18).

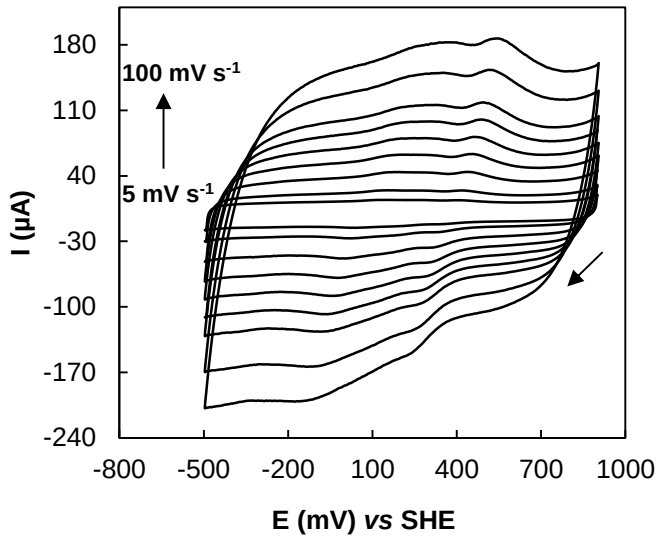

Figure 4.18 – Cyclic voltammograms ($5 \leq v \leq 100$ mV s^{-1}) of 200 µM of N_2OR with 60 % of "CuZ center" as CuZ*(4Cu1S), immobilized onto a MWCNTs layer (7 µL) coated on a glassy carbon electrode, in 100 mM potassium phosphate pH 7.0.

The peaks at high potentials (signal I), reveal a E°' = + 385 ± 5 mV (*vs* SHE), determined from the average of the anodic and cathodic peak potentials, $(Ep_c^I + Ep_a^I)/2$, at pH 7.0, given that this average remained almost constant in the scan range from 5 to 100 mV s^{-1}. On the other hand, the separation between the peak potential Ep_c^I and Ep_a^I increases with the scan rate (ΔE_p, varying from 40 mV at 5 mV s^{-1} to 308 mV at 100 mV s^{-1}). This increase of ΔE_p is characteristic of quasi-reversible processes, as opposite to reversible reactions, which are usually associated with none or very low separation of peaks potentials that remain constant with the scan rates [269].

The ratio of anodic and cathodic peaks currents (I_{pa}^I / I_{pc}^I) of signal I is close to 1, independently of the scan rate (Figure 4.19A). Two different behaviors of the peak currents with the scan rate were detected: in the range 5 to 50 mV s^{-1} a linear relation of the scan rate with the peak currents was observed indicative of diffusionless process; for scan rate higher than 50 mV s^{-1} a negative deviation of the linearity of peaks currents was observed due to the quasi-reversibility of the redox reaction.

Considering the width at half-height ($\Delta E_{p,1/2}$) of the peaks of signal I, which has a value of 100 ± 6 mV, indicates that it is a one-electron transfer reaction.

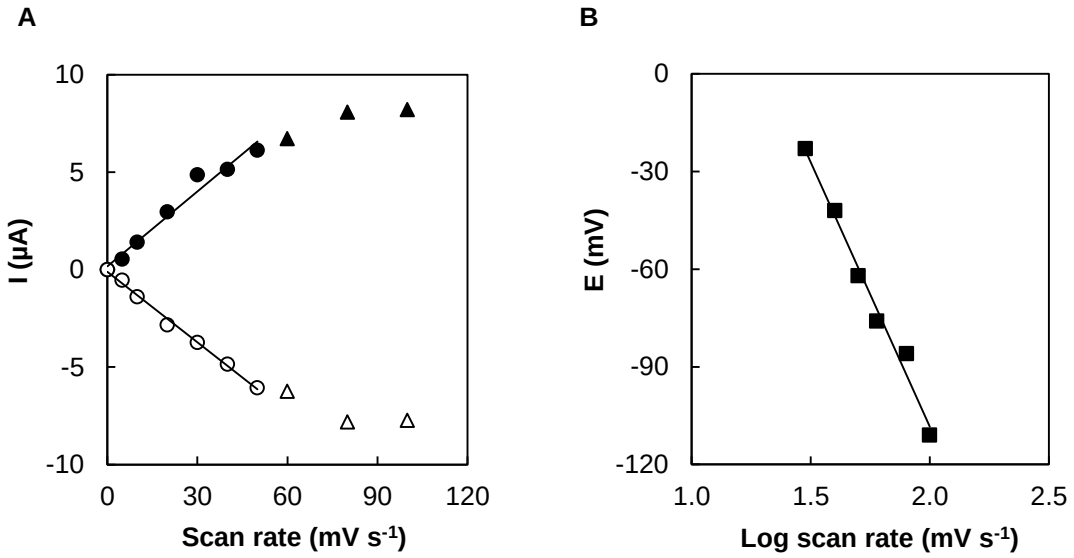

Figure 4.19 – Electrochemical behavior ($5 \leq v \leq 100$ mV s^{-1}) of 200 µM of N_2OR with 60 % of "CuZ center" as CuZ*(4Cu1S), immobilized onto a MWCNTs layer coated on a glassy carbon electrode, in 100 mM potassium phosphate pH 7.0. In panel (A) is presented the dependence of anodic (filled symbols) and cathodic (open symbols) peaks currents with the scan rate. Circles showed a linear dependence, with linear regressions: $y = 0.13x + 0.17$, $R^2 = 0.969$ and $y = 0.12x - 0.11$, $R^2 = 0.995$, for the anodic and cathodic peaks currents, respectively. Triangles show a different behavior. In panel (B) the potential of the cathodic counterpart of signal II is represent as a linear dependence with log of scan rate, for $v > 20$ mV s^{-1}. Linear regression: $y = 162.39x + 216.42$, $R^2 = 0.985$.

Signal I was assigned to CuA center of N_2OR, since the most positive reduction potential of the centers of N_2OR is related with CuA center redox process (E_m = + 240 mV at pH 7.6 [148]). The reduction potential determined by electrochemical methods here for signal I is deviated from the reduction potential previously reported and also from the potentiometric potential determined in this thesis, using a N_2OR sample with 10 % of "CuZ center" as CuZ*(4Cu1S), for which it was determined a E_m = + 272 mV ± 10 mV, at pH 7.6. This difference can be explained by the different pH of the electrolyte used in electrochemistry and the pH of buffer used in potentiometric redox titrations, as the reduction potential of CuA center is pH dependent (see below) and by the electrocatalytic effect of the MWCNTs in shifting the reduction potential to more positive values [218].

On the other hand, a broad signal, denominated as signal II, is observed at lower potentials, with an anodic counterpart not easy to distinguish as it shows very low currents and some overlapping with the MWCNTs signal. At low scan rates (≤ 20 mV s^{-1}) the anodic counterpart of the signal is identified, but with the increase of scan rate, the signal is no longer distinguishable.

The redox reaction responsible for signal II is not a reversible process, which is in accordance with the linear variation of cathodic potential with the log of the scan rate, for scan rates > 20 mV s^{-1} (Figure 4.19B). A reduction potential of + 70 ± 6 mV (*vs* SHE) at pH 7.0, was determined for signal IIc, from the average of cathodic (Ep_c^{I} = + 21 mV) and anodic peak potentials

(Ep_a^I = + 119 mV) at 10 mV s^{-1}. This signal is assigned to CuZ(4Cu2S), as a similar reduction potential was determined in a potentiometric titration at this pH.

Although signal II was assigned to CuZ(4Cu2S) based on the cathodic potential determined, "CuZ center" is a mixture of the two forms. Previous results suggested a different redox behavior associated to the two forms of the "CuZ center" and up-to-now the reduction potential of CuZ*(4Cu1S) is still unknown [148]. Thus, redox behavior of a N_2OR sample with 90 % of "CuZ center" as CuZ*(4Cu1S) was compared with others containing lower amounts of CuZ*(4Cu1S). Initially, cyclic voltammetry was used, but given the low faradaic currents associated to signal II, differential pulse voltammetry, a technique with higher sensitivity than CV, was used.

Typically, DP voltammograms obtained for both forms exhibit two main signals, identified as signal I and signal II at reduction potentials close to those observed by CV (Figure 4.20).

In some preparations, a small signal was detected at around - 250 mV. However due to the lack of reproducibility, and the fact that when observed it is lost after the first scan, it cannot be attributed to any metal center. Analysis of the intensities of peak currents of signal II were not conclusive since the protein concentration used in the different assays was not exactly the same.

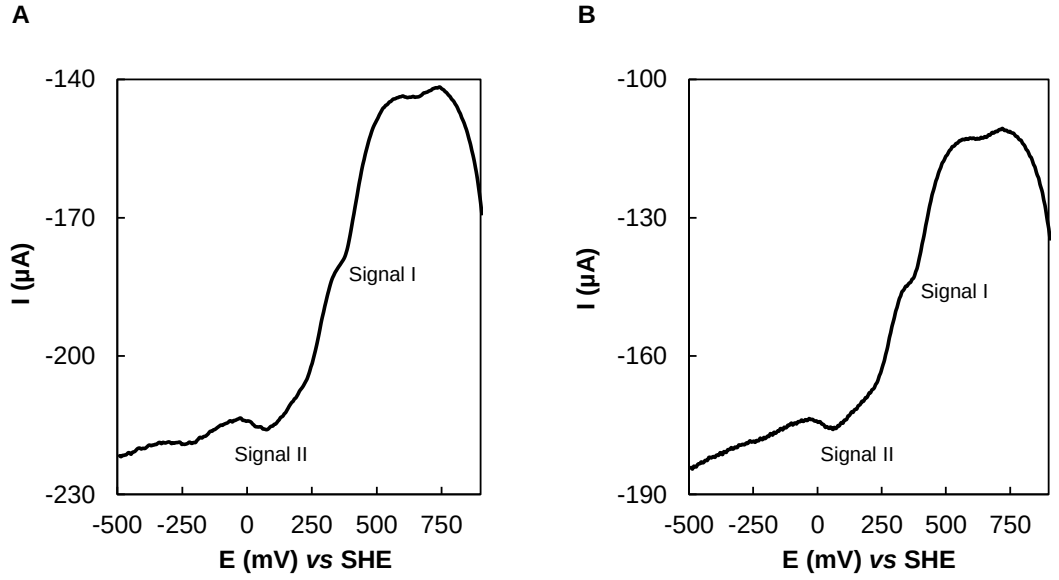

Figure 4.20 – Differential pulse voltammograms (t_p = 100 ms) of different forms of N_2OR immobilized onto a MWCNTs layer coated on a glassy carbon electrode, in 100 mM potassium phosphate pH 7.0. In panel (A) DP voltammogram was acquired for 174 µM of N_2OR with 90 % of "CuZ center" as CuZ*(4Cu1S) and in panel (B) DP voltammogram was acquired for 132 µM of N_2OR with 17 % of "CuZ center" as CuZ*(4Cu1S).

4.3.2.1.2 pH dependence

The pH effect on the reduction potential of N_2OR was analyzed by cyclic voltammetry and compared with the results obtained by potentiometry (Section 4.3.1). Independent assays were performed from pH 5.5 to 10.5 using two different N_2OR preparations: one with 90 % of "CuZ center" as CuZ*(4Cu1S) and another with 10 % of "CuZ center" as CuZ*(4Cu1S) (Figure 4.21).

The reduction potential of each signal was determined and plotted as a function of pH. Both signal I and signal II, independently of the percentage of CuZ*(4Cu1S) present in N_2OR preparation, show a similar behavior and the data were perfectly adjusted to a linear regression with a slope of *ca.* - 58 mV, indicating one electron transfer process coupled with one proton, in the pH range tested.

This redox behavior is similar to the behavior observed by potentiometry, as both evidenced a stoichiometric (1 H^+/ e^-) coupling of protonation to the reduction process. However, potentiometric experiments suggested the presence of apparent pK_{ox} and pK_{red}, in CuZ(4Cu2S) center, while such observation was not detected through electrochemistry. Thus, the possibility of an alteration on the enzyme deposited on the MWCNTs layer cannot be excluded.

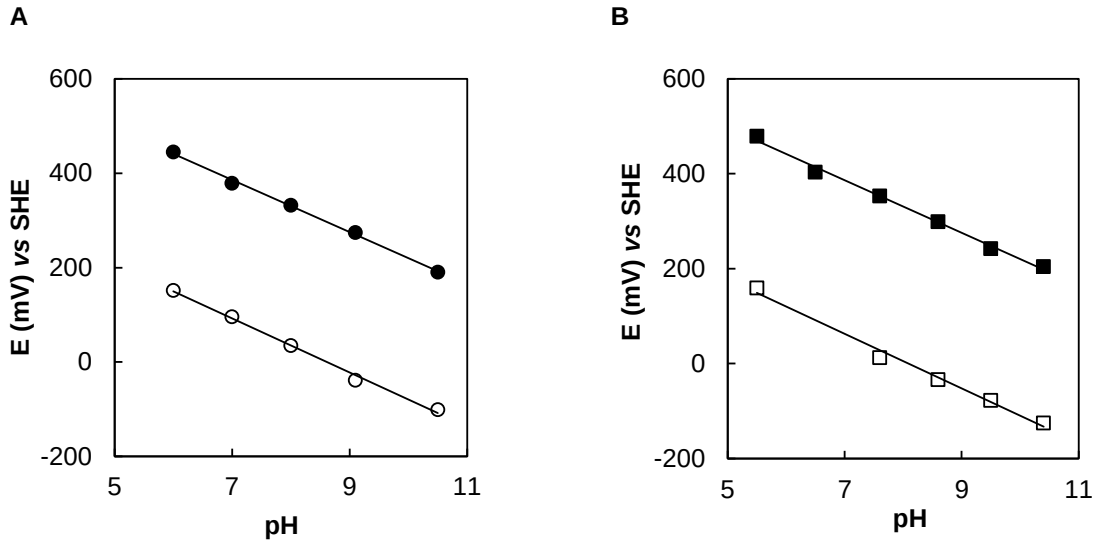

Figure 4.21 – Dependence of pH on the reduction potentials of signal I (filled symbols) and signal II (open symbols) of different forms of N_2OR observed by cyclic voltammetry at 20 mV s^{-1}. In panel (A) N_2OR with 90 % of "CuZ center" as CuZ*(4Cu1S) with signal I showing a linear regression y = -55.2x + 772.4, R^2 = 0.998 and signal II with a linear regression y = -57.4x + 494.3, R^2 = 0.995. In panel (B) a N_2OR sample with 10 % of "CuZ center" as CuZ*(4Cu1S) was used, being the linear regressions y = -55.4x + 773.9, R^2 = 0.995 and y = -57.4x + 464.7, R^2 = 0.991 determined for signal I and II, respectively.

4.3.2.1.3 Turnover conditions

The catalytic activity of the pre-activated N_2OR with 60 % of "CuZ center" as CuZ*(4Cu1S) was analyzed at pH 7.0 in the presence of N_2O. In some of the assays, a saturated concentration of N_2O was injected into the electrolyte to promote catalysis, but clear catalytic waves were not detected. However, catalysis (even if at low levels), was only detected when the enzyme was pre-activated in the presence of reduced methyl viologen (Figure 4.22). Upon substrate addition (varying between 0 and 1.4 mM), a sigmoidal wave develops around Ep_c^{II}. The peak current of each addition was measured at a potential of + 55 mV for different electrode preparations at a scan rate of 20 mV s^{-1}.

The catalytic currents (i_{cat}) measured were plotted as a function of N_2O concentration and fitted to Michaelis-Menten equation, with a K_m of 32 ± 9 µM and a i_{catmax} of 2.7 ± 0.2 µA. The K_m

determined is in the same order of magnitude as the K_m determined in the steady-state kinetics (K_m = 14 ± 3 µM) [122].

The turnover number (k_{cat}) can also be calculated from the catalytic current, and the charge (Q) associated with the non-turnover signal (since it is reproducible between preparations), according to Equation 4.1.

$$k_{cat} = \frac{i_{cat}}{Q} \tag{4.1}$$

The results obtained showed very low catalytic currents, and a k_{cat} value of 2.0 ± 0.3 s^{-1} was determined for pre-activated N_2OR, with 60 % of "CuZ center" as CuZ*(4Cu1S). This value is higher than the k_{cat} = 0.6 h^{-1}, determined for CuZ(4Cu2S) by kinetic studies [160], and thus activation of CuZ*(4Cu1S) form has to be considered, since no activation of N_2OR with mainly CuZ(4Cu2S) has been observed so far. In fact, previously reported potentiometric titration of fully reduced CuZ*(4Cu1S), [$4Cu^{1+}$], to the [$1Cu^{2+}$-$3Cu^{1+}$] oxidation state appears to have a reduction potential slightly higher than the one of CuZ(4Cu2S), although it could not correctly estimated as being an irreversible process [148]. Thus, in voltammetric experiments it is reasonable to proposed that the catalytic wave observed can be due to CuZ*(4Cu1S), since both "CuZ centers", CuZ(4Cu2S) and CuZ*(4Cu1S), might have relatively similar reduction potentials, and thus not be distinguishable by cyclic voltammetry under these conditions. The presence of the two signals might also explain the observation of a broad signal at + 55 mV.

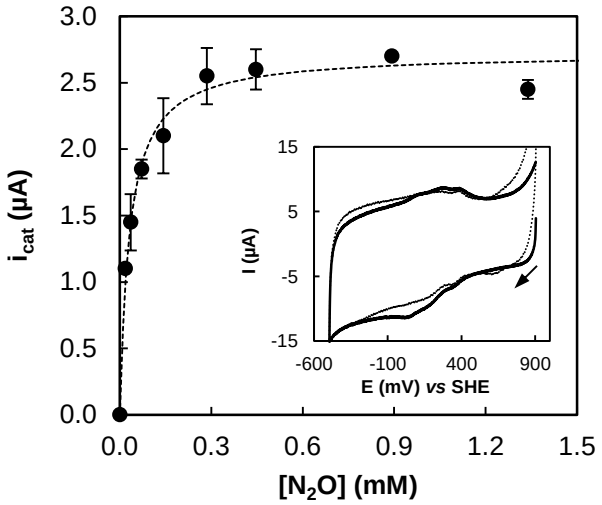

Figure 4.22 – Electrocatalytic peak current of activated N_2OR with 60 % of "CuZ center" as CuZ*(4Cu1S), in 100 mM potassium phosphate buffer pH 7.0. Different amounts of N_2O-saturated water were added to the electrolyte in a final concentration between 0 and 1.4 mM. Data were fitted to Michaelis-Menten equation, using K_m of 32 ± 9 µM and i_{catmax} of 2.7 ± 0.2 µA. Inset: cyclic voltammograms of activated N_2OR in the absence of substrate (dashed line) and in the presence of 0.45 mM of water-saturated N_2O (solid line) obtained at the scan rate of 20 mV s^{-1}.

4.3.2.2 Mediated electrochemistry

Previous studies performed in our laboratory proved that a mediated electrochemical catalysis of pre-activated *M. hydrocarbonoclasticus* N_2OR can be observed using the physiological electron donor, cytochrome c_{552} [148]. However, this assay requires prior activation of N_2OR by incubating the enzyme with reduced methyl viologen and up-to-date no *in vitro* catalytic response was observed for *M. hydrocarbonoclasticus* N_2OR in its as-isolated form. Interestingly, a similar assay with N_2OR from *A. cycloclastes* showed that the isolated N_2OR (without pre-activation) can catalyze the reduction of N_2O when the reaction is electrochemical mediated by pseudoazurin [123]. Considering the similarities between the reduction potential of these two mediators, pseudoazurin (+ 260 mV *vs* NHE, between pH 6.0 and 9.0 [123]) and cytochrome c_{552} (+ 245 mV *vs* SHE, at pH 7 [148]), we expected a similar behavior.

Therefore, the reaction of the electrocatalytic activation of as-isolated N_2OR with 60 % of "CuZ center" as CuZ*(4Cu1S), was investigated in the presence of cytochrome c_{552}. To perform this experiment a gold electrode coated with neomycin was used, containing both cytochrome c_{552} and N_2OR entrapped by a dialysis membrane. This configuration has the advantage of using small amounts of protein and also preventing its diffusion to the electrolyte [270].

Cyclic voltammograms obtained showed a well-defined reversible signal ($E^{o'}$ = + 245 ± 5 mV *vs* SHE, at pH 7.0), assigned to cytochrome c_{552}, but no changes in the voltammograms were initially detected upon substrate addition. Several attempts were made to observe a catalytic response without pre-activation, such as the use of different electrode configuration and variation of the ratios between N_2OR and cytochrome c_{552}, as well as low step potential and multiple oxidation and reduction cycles, in an attempt to activate N_2OR.

Low catalysis was always observed, through the development of a small waveform upon addition of a saturated concentration of N_2O to the electrolyte (Figure 4.23).

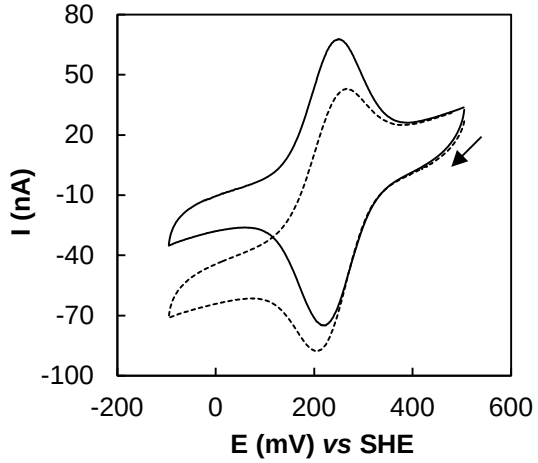

Figure 4.23 – Cyclic voltammograms of cytochrome c_{552} with as-isolated N_2OR with 60 % of "CuZ center" as CuZ*(4Cu1S), in 100 mM potassium phosphate buffer at pH 7.0, obtained at 10 mV s^{-1}. The voltammograms of cytochrome c_{552} (140 µM) in the presence of an equimolar ratio of N_2OR (solid line) and upon addition of 2 mM N_2O (dashed line) are presented. The arrow represents the direction of the scan.

This result shows lower catalysis than the catalysis in the presence of activated enzyme, reported by Dell' Acqua *et al* [148]. The mediated reaction observed is probably triggered by the electron transfer from the gold electrode to cytochrome c_{552} which, in turn, transfers electrons to N_2OR that is re-oxidized upon rapid reaction with N_2O (Figure 4.24).

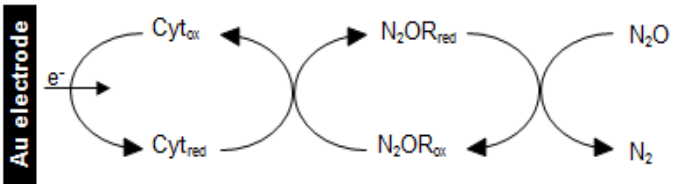

Figure 4.24 – Scheme for N_2OR mediated catalysis: cytochrome c_{552} is reduced by the gold electrode and rapidly oxidized by electron transfer to N_2OR, which in turn is re-oxidized by reduction of N_2O to N_2.

4.4 Conclusions

The pH dependence on the activation of the N_2OR is described here and showed that optimum activation occurs at pH 8.5. These assays evidenced that the turnover is affect not only by the pH of the kinetic assays, as previously reported [122, 161], but also by the pH used in the activation. We also demonstrate that prolong incubation of *M. hydrocarbonoclasticus* N_2OR, with "CuZ center" mainly as CuZ(4Cu2S), with an alkaline buffer solution does not increase significantly the activity of the enzyme.

Different forms of the enzyme were crystallized and the structure was solved by molecular replacement. The results obtained corroborate the spectroscopic differences observed between the two forms of the catalytic center. Comparison between both structures show that a second sulfur fits well in the Cu_I-Cu_{IV} edge of the CuZ(4Cu2S) center, as reported for the structure of the same form of the N_2OR isolated from *P. stutzeri* [152], while its occupancy is lower in the CuZ*(4Cu1S), and an oxygen from a water molecule fits better the electron density. In turn, the structure of CuA center is uniform between different monomers of the asymmetric unit and between both structures and no flip in the imidazole ring of H576 was detected.

Although the reduction potential of CuA center and CuZ(4Cu2S) has been previously reported [131, 148], a relation between the reduction potentials and the forms of the enzyme, as well as the pH effect on the reduction potential is reported here for the first time.

Potentiometric redox titration of CuA center evidenced an electron transfer process coupled with proton transfer.

The reduction potentials determined for CuZ(4Cu2S) at different pH values can be explained by two main behaviors: in the reductive direction the electron transfer process is coupled to a proton transfer and is pH dependent, while in the oxidative titration no dependence of potential with pH was evidenced, being assigned to an uncoupled electron transfer process. A pK_{red} of 9.2 is proposed and assigned to the nearby lysine residue (K447), in line with the spectroscopic studies reported for

N_2OR with "CuZ center" mainly as CuZ*(4Cu1S) [161], while a pK_{ox} of 6 is attributed to histidine side chains that coordinates the copper atoms of "CuZ center". The observed hysteresis may be due to the difficulty in stabilizing the reduced form of CuZ(4Cu2S) at higher pHs and by the protonation of the histidine side chain.

These results in combination with structural and spectroscopic data of different forms of N_2OR gave us some clues that can be useful to understand the mechanism involved in intra- and inter-molecular electron transfer.

The direct electrochemistry of N_2OR was reported for the first time, by immobilization of the enzyme on a modified MWCNTs GC electrode. Independently of the form of the enzyme, two distinct electrochemical signals were recurrently observed, one at higher potentials that present a quasi-reversible redox process assigned to CuA redox centers and a second signal at lower potential that shows an irreversible behavior for scan rates > 20 mV s^{-1} and was assigned to "CuZ center". Both signals show a similar pH dependence that indicates a one electron/one proton coupled process, as no pK_{ox} was identified in the pH range of 5.5. to 10.5.

Comparison of the two different forms of "CuZ center" was performed through DP voltammetry. Although no shift in the potentials of the peaks was observed for the existence of additional peaks, a difference in the intensity of faradaic currents cannot be ruled out.

The possibility of catalysis for each of the non-activated N_2OR forms was explored, but no catalytic wave was detected in the presence of the substrate. One the contrary, electrocatalytic response was measured for the pre-activated N_2OR and a K_m of 32 ± 9 µM was determined. When N_2OR was activated, a low catalytic activity (k_{cat} = 2.0 ± 0.3 s^{-1}) was observed, but higher than the catalytic turnover reported for CuZ(4Cu2S) by direct reaction of N_2OR with N_2O (k_{cat} = 0.6 h^{-1}), indicating that signal II might correspond to a small response of CuZ*(4Cu1S). In this case the possibility that both forms of "CuZ center" have a similar reduction potential is hypothesized.

The catalytic response of as-isolated N_2OR was also investigated using cytochrome c_{552} as electron donor by CV, using a gold electrode with a membrane configuration. Very low catalysis was observed and contrary to *A. cycloclastes* N_2OR, *M. hydrocarbonoclasticus* N_2OR requires activation to competently reduce N_2O in the presence of its physiological donor *in vitro*.

Chapter 5

Reactivity of N_2OR – Insights into the catalytic mechanism

The data presented in this Chapter was partially published in:

Johnston, E. M.; Carreira, C.; Dell'Acqua, S.; Ghosh, S.; Pauleta, S. R.; Moura, I.; Solomon, E. I., Spectroscopic Definition of the CuZo Intermediate in Turnover of Nitrous Oxide Reductase and Molecular Insight into the Catalytic Mechanism. *J. Am. Chem. Soc.* **2017,** *139*, 4462–4476. Doi: 10.1021/jacs.6b13225

5 Reactivity of N_2OR – Insights into the catalytic mechanism

The catalytic mechanism of N_2O reduction to molecular dinitrogen by N_2OR has been studied for several years. Kinetic, spectroscopic and structural studies were essential to distinguish the two forms of the catalytic center, CuZ*(4Cu1S) and CuZ(4Cu2S), as mentioned in the Chapter 3. Of these two forms, only CuZ*(4Cu1S) in its fully reduced state has been shown to be able to react with the substrate at a rate that explains the N_2O reduction by the whole-cells (Chapter 3).

Direct reaction of fully reduced CuZ*(4Cu1S) with stoichiometric amount of N_2O leads to the formation of an intermediate species CuZ° [148]. This is the first intermediate species proven to be competent in the rapid turnover, and whose nature will be addressed in this Chapter: rate dependence and the effect of pH on its formation and decay.

Furthermore, CuZ° reduction in the presence of sodium ascorbate, an artificial electron donor but whose reduction potential ($E^{o'}$ = + 60 mV *vs* SHE, at pH 7.0 [271]) is more in line with the reduction potential of the proposed physiological electron donor ($E^{o'}$ = + 245 ± 5 mV *vs* SHE, at pH 7.0), (when compared to methyl viologen, $E^{o'}$ = - 450 mV *vs* SHE, at pH 7.0 [179]), will be analyzed and compared with the reduction rate of CuZ*(4Cu1S) in the same conditions. This was essential to reveal the significance of this intermediate species in the catalytic mechanism. The existence of other intermediate species in the mechanism of N_2OR will also be addressed.

5.1 Reduction of N_2OR by sodium ascorbate: CuZ(4Cu2S) *vs* CuZ*(4Cu1S)

The reduction of CuA and "CuZ" centers in N_2OR from *M. hydrocarbonoclasticus* was investigated in the presence of 7.5 mM of sodium ascorbate (~ 400 fold-excess) during 800 s. In an enzyme preparation with 80 % of "CuZ center" as CuZ*(4Cu1S), a decrease in the absorption bands characteristic of CuA center was observed upon sodium ascorbate addition, contrary to the CuZ*(4Cu1S) features, that remain practically unchanged (Figure 5.1A). Normalized absorbance at 482 and 653 nm as a function of the time was fitted with a kinetic model involving three steps (Scheme 5.1).

Note that some considerations were performed to normalize the absorbance, since at 482 nm all the contributions are from CuA center, but at 653 nm there is also a contribution from CuA center, representing 35 % of the total contribution at this wavelength (see Section 2.12.4.1).

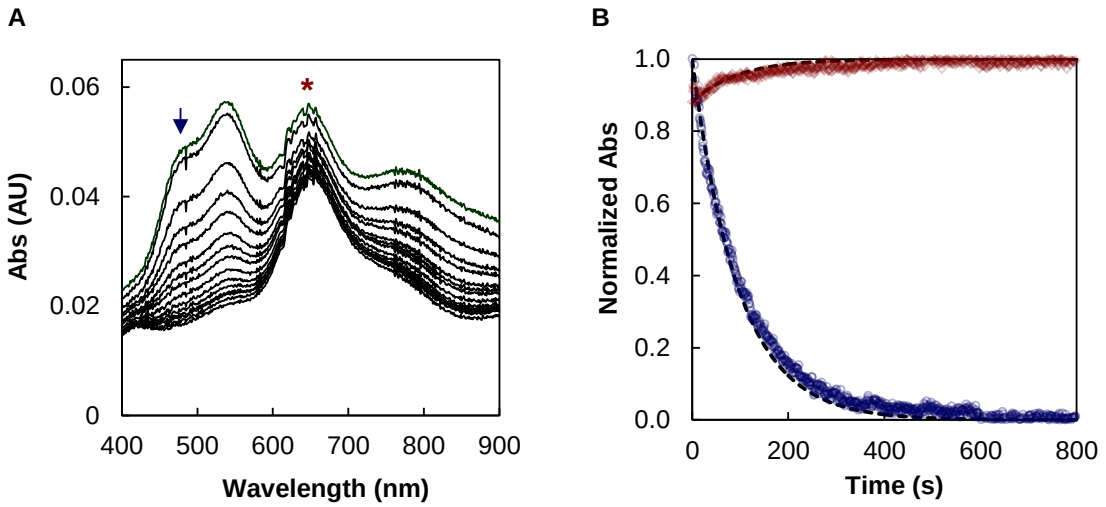

Figure 5.1 – Reduction of 16.5 µM N_2OR, with 80 % of "CuZ center" as CuZ*(4Cu1S), in the presence of 7.5 mM (~ 400 equivalents) sodium ascorbate. (A) Visible spectra during the reduction of oxidized N_2OR, by sodium ascorbate. Representation of spectra acquired every 1 min. The arrow represents the direction of the spectral changes at 482 nm and the asterisk represents the absorbance at 653 nm. (B) Time dependence of reduction of CuA center (blue) at 482 nm and CuZ*(4Cu1S) (red) at 653 nm. The absorbance was normalized and fitted (solid dashed line) using kinetics Tenua program with k_1 = k_2 = 1.4 M^{-1} s^{-1} and $k_{IET} < 1\times10^{-5}$ s^{-1}, R^2 = 0.993.

The model used to fit the data considers the following reactions:

1. Reduction of CuA and resting CuZ*(4Cu1S) centers in the presence of sodium ascorbate;

$$CuA_{[1Cu^{1.5+}-1Cu^{1.5+}]}CuZ^{*}{}_{[1Cu^{2+}-3Cu^{1+}]} + Asc \xrightarrow{k_1} CuA_{[1Cu^{1+}-1Cu^{1+}]}CuZ^{*}{}_{[1Cu^{2+}-3Cu^{1+}]}$$

2. The possibility of intramolecular electron transfer (IET) from reduced CuA center to the resting CuZ*(4Cu1S) center, which leads to oxidation of CuA and fully reduction of CuZ*(4Cu1S) centers;

$$CuA_{[1Cu^{1+}-1Cu^{1+}]}CuZ^{*}{}_{[1Cu^{2+}-3Cu^{1+}]} \xrightarrow{k_{IET}} CuA_{[1Cu^{1.5+}-1Cu^{1.5+}]}CuZ^{*}{}_{[4Cu^{1+}]}$$

3. Bimolecular reduction of oxidized CuA center;

$$CuA_{[1Cu^{1.5+}-1Cu^{1.5+}]}CuZ^{*}{}_{[4Cu^{1+}]} + Asc \xrightarrow{k_2 = k_1} CuA_{[1Cu^{1+}-1Cu^{1+}]}CuZ^{*}{}_{[4Cu^{1+}]}$$

Scheme 5.1 – Kinetic model used to fit the reduction of N_2OR, with "CuZ center" mainly as CuZ(4Cu2S), by sodium ascorbate.

Using this model, a bimolecular rate of 1.4 M^{-1} s^{-1} was estimated for CuA reduction (k_1 = k_2) (several fits performed exhibited a variation ranging between 1.2 and 1.4 M^{-1} s^{-1}), and an upper limit of the intramolecular electron transfer ($k_{IET} < 1\times10^{-5}$ s^{-1}) was estimated. In addition to the low k_{IET}, sodium ascorbate was also unable to directly reduce CuZ*(4Cu1S) and thus absorbance was almost constant throughout the time of the assay.

A comparative assay was performed in similar conditions, but using a N_2OR sample with 10 % of "CuZ center" as CuZ*(4Cu1S). Reduction with sodium ascorbate also showed mainly pronounced differences at the characteristic absorption bands of CuA center, while a decrease in the absorbance relative to CuZ(4Cu2S) center was not easily to identify due to the overlapping of the absorbance maxima of CuZ(4Cu2S) (550 nm) with that of CuA center (540 nm) (Figure 5.2). Indeed, to understand the contribution of CuZ(4Cu2S) to the CuA center at 482 nm, we normalized both the absorbance at 482 nm and 785 nm and both were simulated with the same $k_1 = k_2$, indicating that CuZ(4Cu2S) does not contribute to the absorbance at 482 nm.

In order to determine the CuZ(4Cu2S) reduction rate at 550 nm, we took into consideration the contribution of CuA center to this wavelength. This contribution was determined in a N_2OR sample with 10 % of "CuZ center" as CuZ*(4Cu1S) in which the sodium ascorbate spectrum was subtracted to a fully oxidized spectrum. The difference spectrum indicates that 41 % of the absorbance at 550 nm is a contribution from CuA center.

Therefore, normalized absorbance at 550 nm and 482 nm for CuZ(4Cu2S) and CuA centers, respectively, were fitted using similar kinetic models to those used for the bimolecular reduction of N_2OR with "CuZ center" mainly as CuZ*(4Cu1S) (Figure 5.2B, Scheme 5.2).

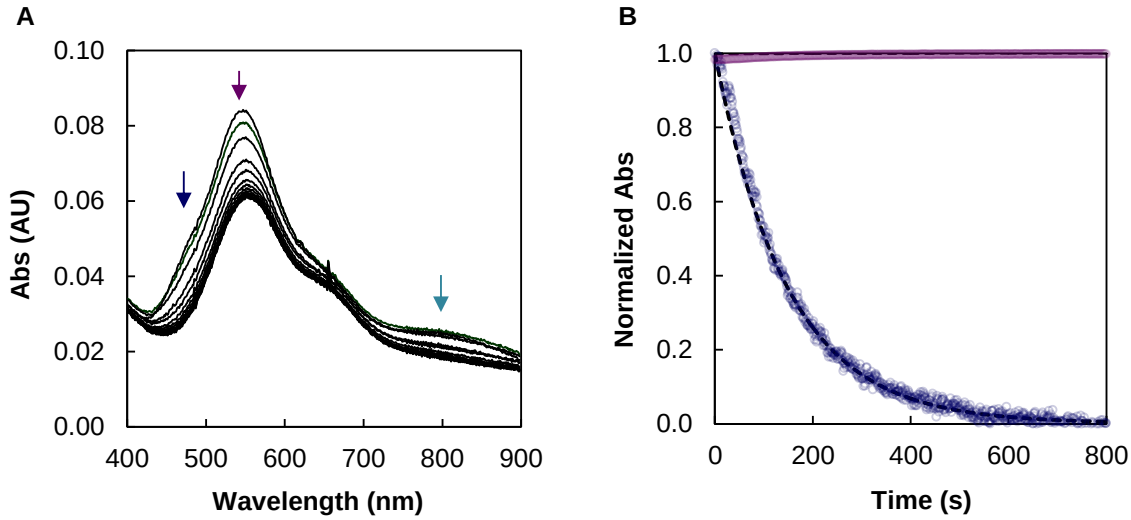

Figure 5.2 – Reduction of 17 µM N_2OR, with 10 % of "CuZ center" as CuZ*(4Cu1S) in the presence of 7.5 mM (~ 400 equivalents) sodium ascorbate. (A) Visible spectra during reduction of oxidized N_2OR, in the presence of sodium ascorbate, collected during 800 s. Representation of spectra acquired with 1 min intervals. The arrows indicate the direction of the changes in the spectra at 485 nm (dark blue), 550 nm (purple) and 785 nm (light blue). (B) Time dependence of reduction of CuA center (dark blue) and CuZ(4Cu2S) (purple). The absorbance was normalized and fitted (solid dashed line) using kinetics Tenua program with $k_1 = k_2 = 1\ M^{-1}\ s^{-1}$ and $k_{IET} < 1\times10^{-5}\ s^{-1}$, $R^2 = 0.914$. Normalized absorbance at 482 nm and 785 nm are fitted with similar parameters.

The bimolecular rates ($k_1 = k_2 = 1\ M^{-1}\ s^{-1}$) determined are similar to the bimolecular reduction of CuA center of N_2OR with mainly CuZ*(4Cu1S) ($k_1 = k_2 = 1.4\ M^{-1}\ s^{-1}$), indicating that the bimolecular reduction of CuA center is independent of the form of the catalytic center.

In these conditions, CuZ(4Cu2S) is not reduced in the presence of sodium ascorbate, as an upper limit of $k_{IET} < 1\times10^{-5}$ s^{-1} was estimated, similar to that observed for the enzyme preparation with "CuZ center" mainly as CuZ*(4Cu1S).

1. Reduction of CuA and CuZ(4Cu2S) centers in the presence of sodium ascorbate;

$$CuA_{[1Cu^{1.5+}-1Cu^{1.5+}]}CuZ_{[2Cu^{2+}-2Cu^{1+}]} + Asc \xrightarrow{k_1} CuA_{[1Cu^{1+}-1Cu^{1+}]}CuZ_{[2Cu^{2+}-2Cu^{1+}]}$$

2. The possibility of intramolecular electron transfer (IET) from reduced CuA center to the oxidized CuZ(4Cu2S) center, which leads to oxidation of CuA and reduction of CuZ (4Cu2S) centers;

$$CuA_{[1Cu^{1+}-1Cu^{1+}]}CuZ_{[2Cu^{2+}-2Cu^{1+}]} \xrightarrow{k_{IET}} CuA_{[1Cu^{1.5+}-1Cu^{1.5+}]}CuZ_{[1Cu^{2+}-3Cu^{1+}]}$$

3. Bimolecular reduction of oxidized CuA center;

$$CuA_{[1Cu^{1.5+}-1Cu^{1.5+}]}CuZ_{[1Cu^{2+}-3Cu^{1+}]} + Asc \xrightarrow{k_2 = k_1} CuA_{[1Cu^{1+}-1Cu^{1+}]}CuZ_{[1Cu^{2+}-3Cu^{1+}]}$$

Scheme 5.2 – Kinetic model used to fit the reduction of N_2OR, containing the "CuZ center" mainly as CuZ(4Cu2S), by sodium ascorbate.

The reduction of CuA center was also analyzed at 482 nm by 0.5 mM sodium ascorbate (25-fold excess) in the presence and absence of the artificial redox mediator DAD ($E^{o'}$ = + 260 mV, at pH 7.0 [217]).

Our results showed that using 0.5 mM sodium ascorbate to reduce CuA center in the absence of DAD, no plateau was observed within 800 s, indicating that reduction was not complete during that time period (Figure 5.3). The absorbance changes were fitted using the previous models and although the reaction was not finished, a rate of 6 M^{-1} s^{-1} (R^2 = 0.957) was determined. However, this rate can hold some variation if complete reduction was attained.

On the other hand, the time dependence of CuA center reduction in the presence of 5 µM DAD showed a plateau at 482 nm, indicating that CuA center reduction was complete. The kinetic traces were fitted using the previous model and a bimolecular rate of 28 M^{-1} s^{-1} (R^2 = 0.995) was calculated for CuA center reduction in a N_2OR sample with 60 % of "CuZ center" as CuZ*(4Cu1S).

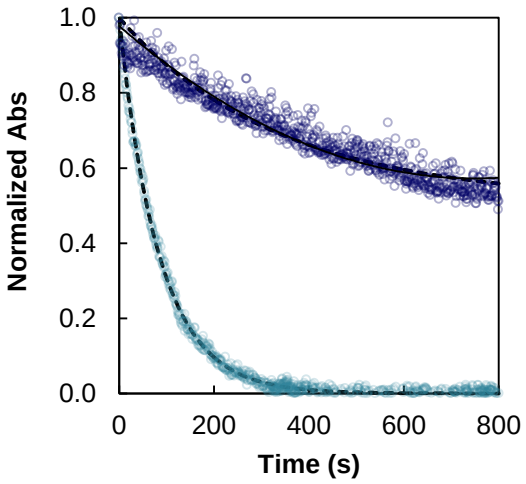

Figure 5.3 – Normalized time dependence of reduction of CuA center of 20 µM N_2OR with 60 % of "CuZ center" as CuZ*(4Cu1S) in the presence of 0.5 mM sodium ascorbate (dark blue) and in the presence of 5 µM DAD and 0.5 mM sodium ascorbate (light blue). Absorbance was determined at 482 nm. Kinetics were fitted using Tenua program, with $k_1 = k_2 = 6\ M^{-1}\ s^{-1}$ and $k_{IET} < 1\times10^{-6}\ s^{-1}$, $R^2 = 0.957$, for the assay performed in the absence of DAD, and $k_1 = k_2 = 28\ M^{-1}\ s^{-1}$ and $k_{IET} < 1\times10^{-5}\ s^{-1}$, $R^2 = 0.995$, when 5 µM DAD was added to the experiment.

The trend observed in the absence of DAD indicates that under the conditions used, CuA center cannot be fully reduced within 800 s. However, with the presence of an additional redox mediator CuA center was fully reduced in less than 500 s. The presence of DAD increases ~ 5 times the reduction rate of CuA center comparative to the same reaction in its absence. Similar behavior was observed in a sample with 10 % of "CuZ center" as CuZ*(4Cu1S).

Comparison between the IET rate of both assays, showed that under these conditions, the presence of DAD lowered by one order of magnitude the upper limit of this rate, suggesting that IET in the presence of DAD can be at least 10 times faster.

These results clearly showed that CuA center reduction by sodium ascorbate is independent of the "CuZ" form present in the enzyme, although its reduction was highly facilitated in the presence of a redox mediator with a reduction potential similar to cytochrome c_{552}.

5.2 Formation of CuZ° and its decay to a new intermediate species

In the presence of reduced methyl viologen, the resting CuZ*(4Cu1S), in the [$1Cu^{2+}$-$3Cu^{1+}$] state, can be fully reduce to [$4Cu^{1+}$], which upon stoichiometric addition of N_2O leads to the rapid formation of an intermediate species named CuZ° ($k_f = 200\ s^{-1}$) [160]. This species is characterized by the appearance of an absorption band at 680 nm ($\varepsilon = 2000\ M^{-1}\ cm^{-1}$, obtained after subtraction of oxidized CuA and CuZ(4Cu2S) contributions [167]) and by an axial EPR signal (S = 1/2), with $g_{\parallel} = 2.18$ and $g_{\perp} = 2.05$, showing a pattern of six distinguished hyperfine lines in the $g_{\parallel}$ region with $A_{\parallel} = 4.2$ mT, which corresponds to the [$1Cu^{2+}$-$3Cu^{1+}$] oxidation state [148].

The formation and decay of CuZ° was previously reported [148], and since this is an intermediate species, a decrease in the intensity of the absorbance band at 680 nm (k_{decay} = 5×10^{-3} s^{-1}) was observed, concomitant with the appearance of an absorption band at lower wavelength (640 nm) [148].

We have used a similar methodology to determine CuZ° decay rates on N_2OR samples with 60 % or 80 % of "CuZ center" as CuZ*(4Cu1S), which were also used in other studies reported in this thesis (Figure 5.4).

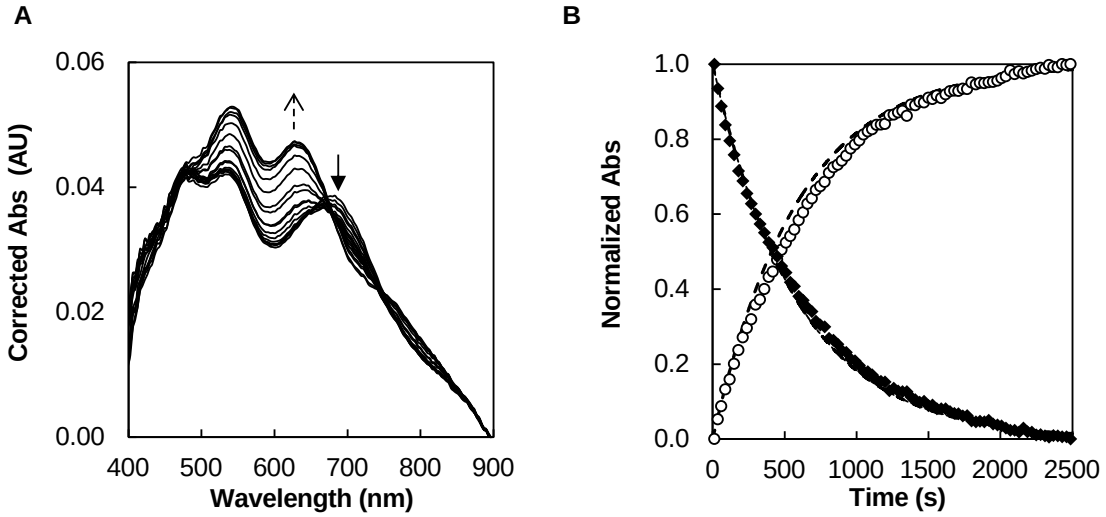

Figure 5.4 – CuZº formation and decay, obtained from 20 µM fully reduced N_2OR, with 60 % of "CuZ center" as CuZ*(4Cu1S), after reaction with 30.5 µM N_2O. (A) Visible spectra of CuZº decay (solid bold arrow) and formation of a new species at 617 nm (dashed arrow) during 2500 s of the reaction. The arrows indicate the direction of spectral changes. (B) Normalize time dependence at 683 nm (filled diamonds) and at 617 nm (open circles). The data were fitted (dashed black line) to a single exponential, using k_{decay} = 1.8 ×10^{-3} s^{-1}, R^2 = 0.985.

The first spectrum acquired 14 s after the addition of N_2O to the fully reduced form of the enzyme exhibits a band at 683 nm, characteristic of CuZ°, and also absorption bands at 480, 540 nm and 800 nm, corresponding to CuA center, though the absorption band at 800 nm is not so evident (Figure 5.4A).

The absorbance was monitored at 683 nm during 2500 s, showing a decay that can be fitted with a rate of 1.8×10^{-3} s^{-1}, lower than that previously reported (k_{decay} = 5×10^{-3} s^{-1}) [148], but still in the same order of magnitude (Figure 5.4B). Indeed, within our six replicas, CuZ° formed from N_2OR either as 60 % or 80 % of "CuZ center" as CuZ*(4Cu1S), decayed with minor variations (1.5×10^{-3} s^{-1} - 2.1×10^{-3} s^{-1}). The estimated value (k_{decay} = 1.8×10^{-3} s^{-1}) will be the one used in the kinetic models developed latter in this Chapter. In addition, it seems that CuZ° decay rate does not depend on the % of CuZ(4Cu2S) present.

The CuZº decay is associated to a decrease in activity over time. A maximum activity (157 µmol$_{N2O}$ min^{-1} mg^{-1} of total protein) was determined for the fully reduced form of N_2OR with 60 % of "CuZ center" as CuZ*(4Cu1S) and a rapid decrease over time was observed after N_2O

addition, with only 0.7 % of the observed initial activity (1.1 μmol_{N2O} min^{-1} mg^{-1} of total protein) remaining after 3000 s. These results are in accordance with similar observations reported by Dell'Acqua *et al* [148].

The major difference between the results obtained and the ones previously reported [148], lies in the second phase of the reaction, i.e. the increasing absorbance at 617 nm that is concomitant with CuZ^o 680 nm absorption band disappearance, which we believe to be the formation of a different intermediate species, never reported before, and whose features will be described and discussed below.

5.3 Formation of a new intermediate species (CuZ')

The formation of a new intermediate species, named here as CuZ', was first observed during the decay of CuZ°, as a species that has a maximum absorption band at 617 nm. In order to further understand the formation of this new intermediate species, changes in wavelength of the maximum absorption band of the "CuZ center" (between 610 and 690 nm), as well as the corresponding absorbance were monitored during 2500 s, after formation of CuZ° (Figure 5.5).

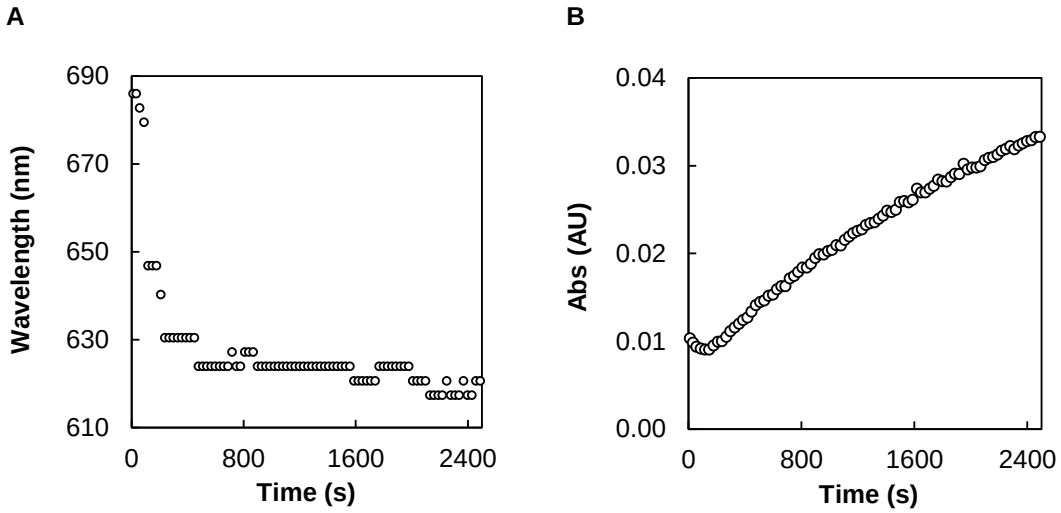

Figure 5.5 – Changes at the maximum absorption band of "CuZ center" after formation of CuZ° (reaction of 22 µM N_2OR, with 60 % of "CuZ center" as CuZ*(4Cu1S), with 24 µM N_2O). (A) Variation of the maximum wavelength (610 – 690 nm) over 2500 s reaction. (B) Plot of the maximum absorption observed in the visible spectra over 2500 s reaction. These values corresponded to the absorbance observed for each of the wavelengths showed in A. Reaction performed in 100 mM potassium phosphate at pH 7.6.

For the initial period of 240 s major shifts in the wavelength of the maximum absorption band were observed, with a shift to 630 nm due to the decay of CuZ^o, as previously mentioned, while in the remaining time only slight variations between 623 and 617 nm were observed (Figure 5.5A). The intensity of the maximum absorption increases over time and in fact no plateau was detected during the 2500 s, thought the wavelength of the absorption band was practically unchanged at that time

(Figure 5.5B). These results demonstrate that formation of the CuZ' intermediate species occurs at a very slow rate.

Characterization of CuZ' intermediate species was performed by visible spectroscopy, in which the oxidation of this species was monitored.

After 2500 s of CuZ° formation, CuZ' intermediate species is observed, evidenced by the appearance of the absorption band at 617 nm (Figure 5.6A). Upon potassium ferricyanide oxidation, absorption bands at 400, 540, 617 and 800 nm were observed. Contributions at 550 nm can be attributed to the oxidation of CuZ(4Cu2S), as the initial sample used had 40 % of "CuZ center" as CuZ(4Cu2S), while the observation of an absorption band at 617 nm suggests that CuZ' intermediate species does not change its oxidation state (Figure 5.6A). Moreover, comparison of this spectrum with the one of oxidized N_2OR prior to the experiment shows distinct characteristics, which indicates that CuZ' is different from CuZ(4Cu2S) and CuZ*(4Cu1S) (Figure 5.6B).

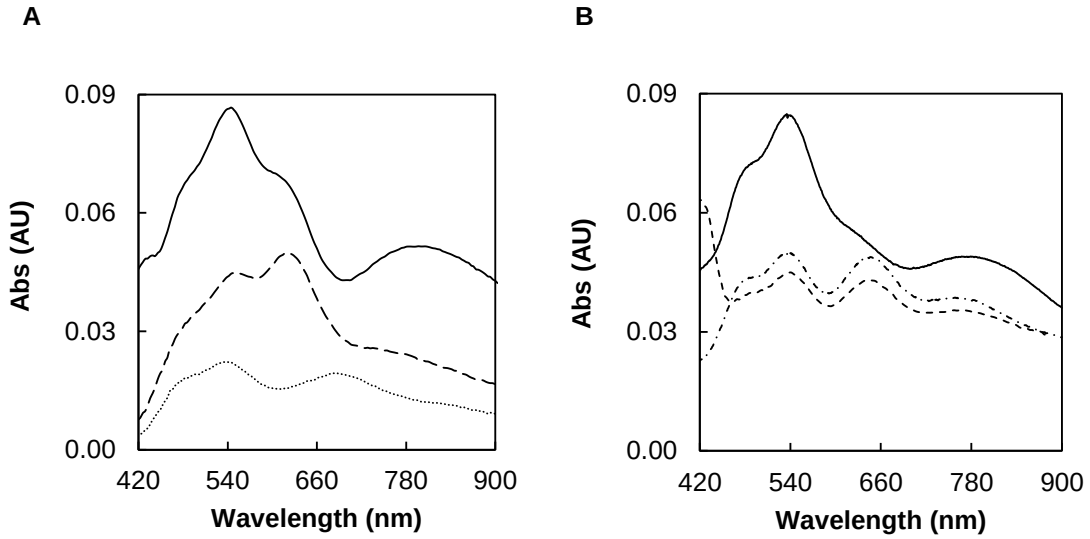

Figure 5.6 – Reactivity of 22 µM fully reduced N_2OR, with 60 % of "CuZ center" as CuZ*(4Cu1S), with 24 µM N_2O for 2500 s followed by oxidation with potassium ferricyanide. (A) Visible spectrum of CuZº collected after 14 s (dotted line) and after 2500 s of the addition of N_2O (long dashed line) and potassium ferricyanide oxidation (solid line) at the end of the reaction. (B) Visible spectrum of oxidation (solid line) at the end of reaction (another preparation similar as solid line spectra showed in A), the same oxidized spectrum but recorded after 3 days of oxygen exposure (dashed-dotted line) and the oxidized spectrum of N_2OR prior to the experiment (dashed line) are presented.

After removal of the oxidizing agent, this sample containing CuZ' was kept aerobically at 4 °C for 3 days under an atmosphere containing O_2. The visible spectrum was acquired, and different spectrum was observed which is superimposable with the spectrum of oxidized N_2OR prior to the experiment. This suggests a change in CuZ' intermediate species leading to the re-establishment of the resting CuZ*(4Cu1S) form.

In order to understand the spectral changes observed, we performed a similar experiment inside the anaerobic chamber at which the sample was oxidized, desalted to remove the excess of potassium ferricyanide and afterwards the spectra was monitored for 15 h. Within that time frame, no changes

were detected in the visible spectrum, suggesting that the decay of this species is slower than expected or it requires the presence of oxygen to restore the spectral features of CuZ*(4Cu1S) center.

Our results recurrently indicate the formation of this CuZ' intermediate species, differing from the behavior observed in previous studies, in which CuZ^o decay was concomitant with the re-establishment of CuZ*(4Cu1S) features at 640 nm, with no shifts on the wavelength or on the intensity of the band [148].

In order to understand if the formation of this CuZ' species is triggered by N_2O addition, we performed a control reaction, in which sodium ascorbate (~ 400 equivalents) were added to the fully reduced CuZ*(4Cu1S), without addition of N_2O (Figure 5.7). Fully reduced spectra collected at 0 s exhibits a maximum at 660 nm, due to the presence of 20 % of "CuZ center" as CuZ(4Cu2S), in a [$1Cu^{2+}$-$3Cu^{1+}$] oxidation state, that cannot be fully reduced to the [$4Cu^{1+}$] oxidation state. The spectrum acquired after 2500 s did not show any difference, as expected, since no substrate was added to the fully reduced enzyme.

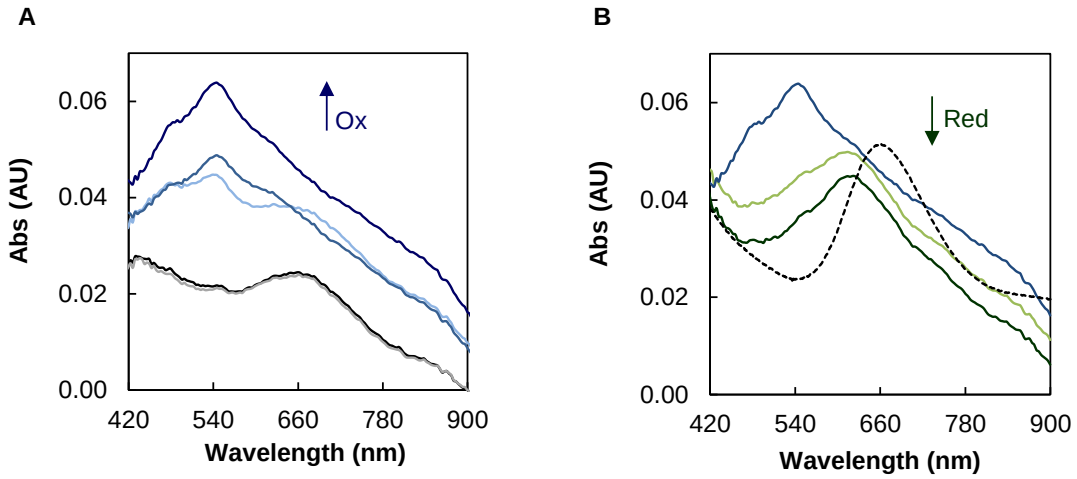

Figure 5.7 – Visible spectra of 20 µM fully reduced N_2OR, with 80 % of "CuZ center" as CuZ*(4Cu1S), over 2500 s in the presence of sodium ascorbate (~ 400 fold excess). (A) The fully reduced spectra of N_2OR after 0 s and 2500 s are presented in grey and black, respectively. Oxidation with increasing concentrations of potassium ferricyanide after 2500 s is represented by blue gradient color, being the darker spectra the one with highest concentration of potassium ferricyanide. (B) The spectra of oxidized, sodium ascorbate reduced and sodium dithionite reduced are colored in blue, light green and dark green, respectively. The spectrum of CuZ*(4Cu1S) reduced with dithionite was provided for comparison, represented by black dashed line. The arrows indicate the direction of spectra with increasing concentration of reducing agents. Ox – oxidation, Red - reduction.

Upon addition of increasing concentrations of potassium ferricyanide, oxidation of CuA center was observed, as well as the presence of a shoulder at 617 nm, similar to the CuZ' intermediate previously observed (Figure 5.7A). On the other hand, reduction of this oxidized sample with increasing concentrations of sodium ascorbate and then sodium dithionite caused reduction of the CuA center, but no changes in the absorption band at 617 nm were observed.

This assay proved that the second phase of the reactivity observed before was due to the formation of a CuZ' intermediate species and not caused by the presence of small amount of oxygen, as no changes in the fully reduced CuZ*(4Cu1S) were observed during 2500 s. Moreover, this intermediate species is not exclusively formed in the presence of substrate, but most likely is due to a secondary reaction observed when the fully reduced CuZ*(4Cu1S) is oxidized.

5.4 Effect of pH on CuZ^o decay

The pH dependence of the formation and decay of CuZ^o was investigated between pH 6.0 and pH 10.0, using a sample of N_2OR with 60 % of "CuZ center" as CuZ*(4Cu1S).

In each assay N_2OR was incubated with reduced methyl viologen at pH 7.6 for 3 h, and desalted into an universal buffer at different pH values (see Material and Methods, Section 2.12.2). CuZ^o was formed by addition of a stoichiometric amount of N_2O. Visible spectra was collected during 2500 s for each pH and variation at 683 nm was normalized and fitted to determine the decay rates of CuZ^o at each pH.

The formation of CuZ^o was consistently observed in the pH range 6.0 to 9.5, by the emergence of a strong absorption band with a maximum at 683 nm. Although we cannot accurately determine the rate of the CuZ^o formation for each pH, as this process occurs in the order of milliseconds, we compared the spectra obtained 14 s after the addition of N_2O at each pH (Figure 5.8). No major differences in the spectral features were detected (for CuZ° formed between pH 6.0 and pH 9.5), but at higher pH values (pH 9.7 and pH 10), the formation of this band was practically unobserved (Figure 5.8 – blue line).

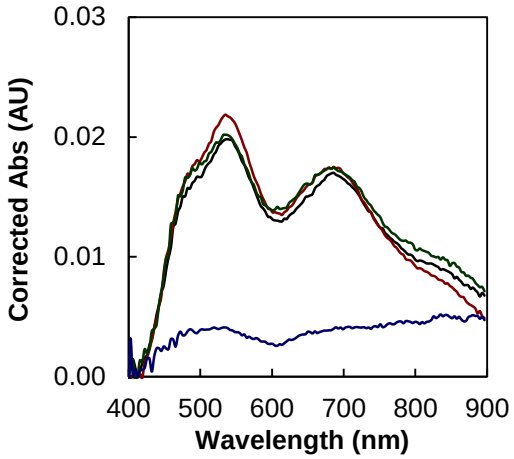

Figure 5.8 – Spectra 14 s after formation of CuZ° at pH 6.0 (red), 7.6 (black), 8.5 (green) and 9.7 (blue). Absorbance was subtracted to the amount of CuZ(4Cu2S) present in each sample.

CuZ^o decay rates did not evidence any relevant difference between pH 6.0 and pH 9.5, suggesting that CuZ^o decay is not pH dependent in this pH range (Table 5.1). At high pH values, the rates of

CuZ^o decay could not be determined as the model used in the other fits cannot be adjusted to the experimental data (data displayed in Supplementary information S5 - Figure S5.1).

These results suggested that CuZ^o at pH > 9.5 might not be formed at all. This can be explained by the deprotonation of K447 and E485, as both were reported to be involved in the stabilization of CuZ^o and also of the intermediate species prior to its formation ("intermediate 2" of the catalytic cycle, Figure 5.9) [167].

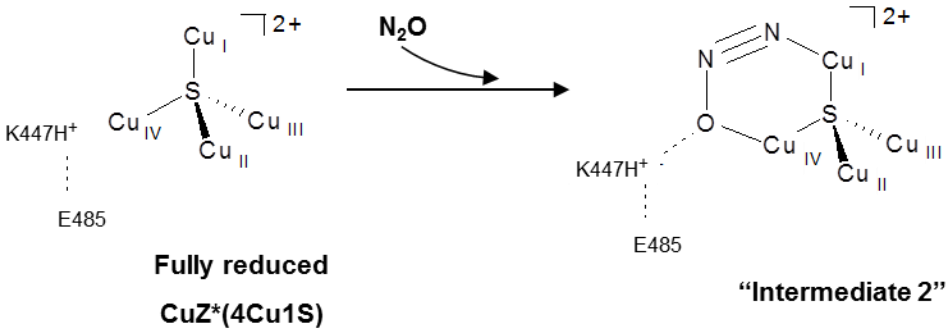

Figure 5.9 – Reaction of fully reduced N_2OR with stoichiometric amount of N_2O and formation of "intermediate 2" of the catalytic cycle.

In the "intermediate 2" species, N_2O is bound to Cu_I by the N atom and to Cu_{IV} by the O atom and stabilized by H-bound to K447, which in turn is also H-bound to E485, in the second sphere coordination. A pK_a ~ 9.7 was assigned to the lysine residue (K447) by steady-state kinetics studies (Section 4.1.1), which is similar to the value (pK_a ~ 9.2) previously attributed to this residue by Ghosh *et al* [168]. Moreover, the pK_a of K447 and E485 was predicted based on the coordinates of N_2OR from *M. hydrocarbonoclasticus* (PDB ID: 1QNI) to be 9.4 and 10.2, respectively. The reduced formation of CuZ° at higher pH can be explained by the destabilization of "intermediate 2" at pH values higher than 9.5.

Table 5.1 – Comparison of rates determined for CuZº decay and for CuZ' intermediate formation for N_2OR with 60 % of "CuZ center" as CuZ*(4Cu1S) with stoichiometric amount of N_2O at different pH values. Fittings of CuZº decay are presented in Supplementary Information (S5).

pH	CuZº decay rate	CuZ' formation rate
6.0	1.3×10^{-3} s^{-1}	$(1.4 \pm 0.2) \times10^{-3}$ s^{-1}
7.6	1.5×10^{-3} s^{-1}	$(1.5 \pm 0.04) \times10^{-3}$ s^{-1}
8.5	1.5×10^{-3} s^{-1}	$(1.6 \pm 0.07) \times10^{-3}$ s^{-1}
9.5	1.4×10^{-3} s^{-1}	$(1.0 \pm 0.1) \times10^{-3}$ s^{-1}
9.7	-	$(1.1\pm 0.1) \times10^{-3}$ s^{-1}
10	-	$(1.4 \pm 0.05) \times10^{-3}$ s^{-1}

In the second reactivity phase, identical features to those reported before were observed (Figure 5.6A). This phase, characterized by the increasing intensity of absorbance, showed an absorption band at 623 nm, which shifts to near 617 nm over time, even at high pH (Figure 5.10). Although the collected spectra showed different ratios between the absorption at 540 nm and 617 nm at the end of the reaction, no dependence of this ratio was observed with pH.

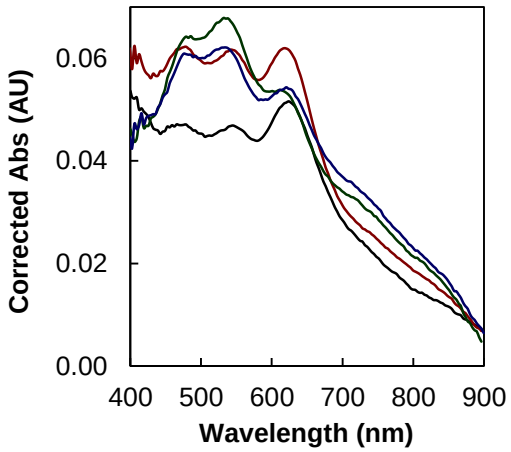

Figure 5.10 – Spectra 2500 s after CuZ° formation at pH 6.0 (red), 7.6 (black), 8.5 (green) and 9.7 (blue). Spectra were corrected for the total amount of protein by Pierce 660nm protein assay.

As observed before, this CuZ' intermediate species is formed in the absence of N_2O, when fully reduced N_2OR is oxidized (e.g. by potassium ferricyanide). Moreover, CuZ' can also be formed during the catalytic cycle from the fully reduced CuZ*(4Cu1S) [$4Cu^{1+}$] when N_2O becomes limited in the reaction. In this case as the enzyme already performed catalysis it is probably difficult to maintain a fully reduced state, since there is no methyl viologen in solution, even if sodium ascorbate is present, its potential is probably not enough to keep CuZ*(4Cu1S) [$4Cu^{1+}$] in this fully reduced state (Figure 5.11). N_2OR with CuZ' has the "CuZ center" in the [$1Cu^{2+}$-$3Cu^{1+}$] oxidation

state and CuA center in either oxidized or reduced form (if sodium ascorbate is in excess), which is quite similar to the oxidation state of "CuZ center" in N_2OR as CuZ^o or CuZ*(4Cu1S). The nature of the edge ligand in the CuZ' is probably different from the one in "CuZ center" as CuZ*(4Cu1S), giving the spectral differences. Moreover, we hypothesize that at pH > 9.7, there is no formation of CuZ°, although CuZ' can still be formed as this is a secondary reaction involving the oxidation of fully reduced CuZ*(4Cu1S) [$4Cu^{1+}$].

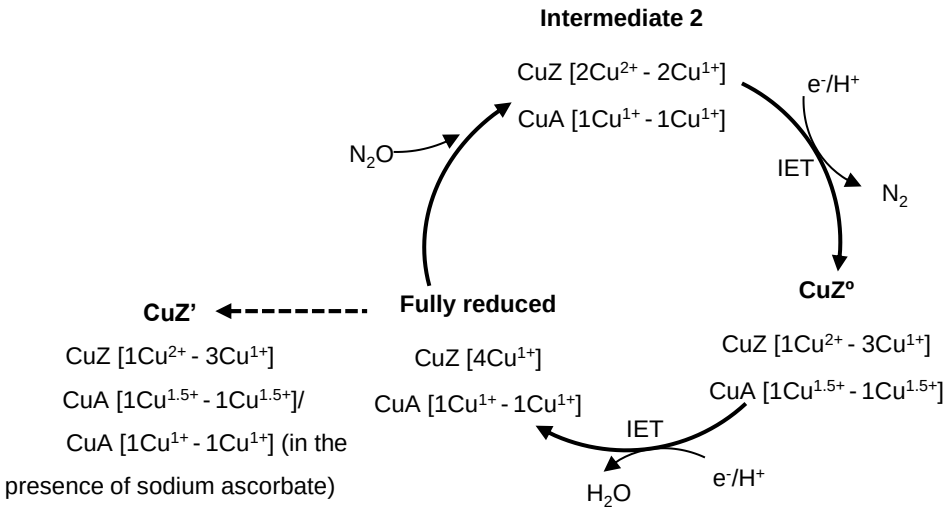

Figure 5.11 – Pathways of CuZ' formation and mechanism of N_2O reduction. CuZ' can be obtained by oxidation of fully reduced N_2OR or by decay of intermediate CuZ°.

As the formation of the new intermediate species occurs at different pH values, even if CuZ^o was not previously formed, we determined the rates of the formation of this CuZ' species (Table 5.1, Figure 5.12). The formation of this intermediate species was observed by the continuous increase in the absorbance at 617 nm during around 1500 s after which a plateau was reached, for most pH values (pH 6.0, 7.6 and 8.5) assayed. Rates of formation of the CuZ' intermediate species were determined through the fitting of the normalized data (Figure 5.12).

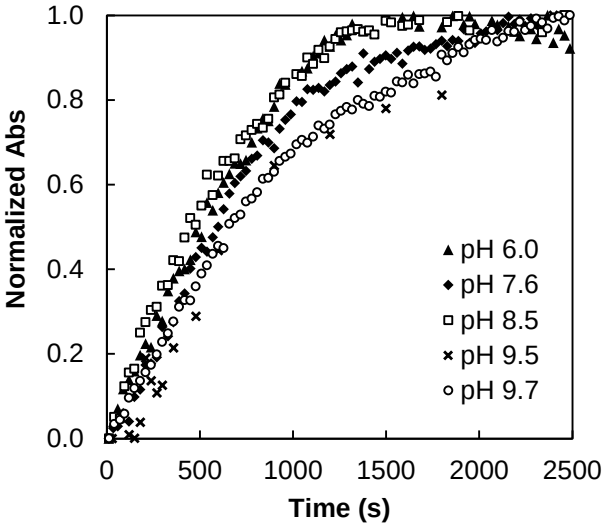

Figure 5.12 – Normalized time dependence of the absorbance at 617 nm, at pH 6.0 (filled triangles), 7.6 (filled diamonds), pH 8.5 (open squares), pH 9.5 (crosses) and pH 9.7 (open circles).

The rates of CuZ' formation were very small, when compared to the ones of CuZº formation. Yet, these rates are similar as the ones of the CuZº decay at the different pH values.

The profile and rates for each pH suggest that formation of CuZ' intermediate species is not pH dependent, at least in between pH 6 and pH 10.

5.5 Reduction of CuZº by sodium ascorbate

At this point it is clear that CuZº is involved in the rapid turnover of the enzyme, as the CuZ° decay is concomitant with the decay of N_2OR activity [148]. In order to study the involvement of CuZº in the catalytic cycle it was necessary to prove that CuZº can be re-reduced to [$4Cu^{1+}$] oxidation state, and thus continue the catalytic cycle. Therefore, an electron donor had to be chosen, the obvious choice would be cytochrome c_{552}, however due to the different molar extinction coefficient in the 400 - 800 nm region between the two proteins, the data analysis would be difficult, and therefore sodium ascorbate was used. Sodium ascorbate has a reduction potential of + 60 mV *vs* SHE, at pH 7.0 [271] and can be seen as a more physiologically relevant electron donor than methyl viologen (E°' = - 450 mV *vs* SHE, at pH 7.0 [179]), as such a low potential is not expected to be attained under physiologic conditions.

In order, to analyze the reduction of CuZº in the catalytic cycle, sodium ascorbate was added 37 s after N_2O, ensuring that CuZº was formed. Time dependence spectra of the reduction of CuZº were monitored for at least 1 h and the changes in the absorption bands were analyzed.

The reduction of CuZº upon addition of ~ 400 fold-excess of sodium ascorbate was examined (Figure 5.13), showing two distinct phases. In the first phase (0 – 800 s), CuZº maximum absorption at 683 nm shifts to 640 nm and a decrease in the intensity of CuA center bands at 482,

540 and 800 nm was detected (Figure 5.13A). The second phase of reactivity, started after 800 s and is characterized by an increase in the absorption features at 620 nm (Figure 5.13B).

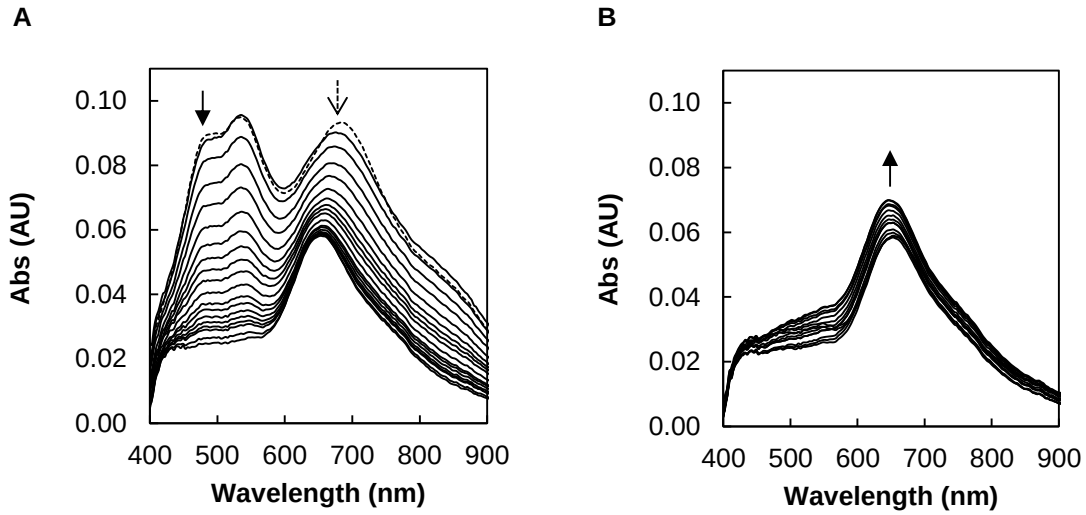

Figure 5.13 – Reduction of CuZ° (formed by reaction of 20 µM fully reduced N_2OR, with 80 % of "CuZ center" as CuZ*(4Cu1S), with 36 µM N_2O) in the presence of 7.3 mM (~ 400 equivalents) sodium ascorbate, added 37 s after N_2O addition. (A) Visible spectra of reduction of CuZ° in the first reactivity phase. Representation of spectra acquired every 0.5 min. The spectrum of N_2OR as CuZ° collected 14 s after N_2O addition is represented by a dashed line and the arrows indicate the direction of the spectra at 482 nm (solid bold arrow) and 683 nm (dashed arrow). (B) Visible spectra during the second reactivity phase represented every 5 min up to 1 h reaction. The arrow indicates the direction of the spectra at 620 nm.

The first phase undoubtedly indicates that reduction of the CuZ° occurs upon sodium ascorbate addition, being both CuA and CuZ° centers reduced within 800 s. Two main hypotheses can be used to explain the behavior observed, either CuZ° was rapidly reduced via electron transfer from CuA (IET), or CuZ° was directly reduced by sodium ascorbate and this reduction occurred at a similar rate as CuA center reduction. Both hypotheses were analyzed through kinetic models (Scheme 5.3 and Scheme 5.4) and the models were used to generate the fits of the normalized experimental data. Note that in these hypothesis the formation of CuZ' is not considered.

Considering the hypothesis of an IET, a seven step model was developed (Scheme 5.3):

1. Oxidized CuA center is reduced by sodium ascorbate in a bimolecular reaction;

$$CuA_{[1Cu^{1.5+}-1Cu^{1.5+}]}CuZ^{0}_{[1Cu^{2+}-3Cu^{1+}]} + Asc \xrightarrow{k_{red1}} CuA_{[1Cu^{1+}-1Cu^{1+}]}CuZ^{0}_{[1Cu^{2+}-3Cu^{1+}]}$$

2. IET from CuA to CuZ°;

$$CuA_{[1Cu^{1+}-1Cu^{1+}]}CuZ^{0}_{[1Cu^{2+}-3Cu^{1+}]} \xrightarrow{k_{IET}} CuA_{[1Cu^{1.5+}-1Cu^{1.5+}]}CuZ^{*}_{[4Cu^{1+}]}$$

3. IET from CuZº to CuA (we considered a possible reversibility of reaction 2.);

$$CuA_{[1Cu^{1.5+}-1Cu^{1.5+}]}CuZ^{*}_{[4Cu^{1+}]} \xrightarrow{k_{-IET}} CuA_{[1Cu^{1+}-1Cu^{1+}]}CuZ^{0}_{[1Cu^{2+}-3Cu^{1+}]}$$

4. Oxidized CuA center is reduced by sodium ascorbate in a bimolecular reaction in the presence of CuZ*(4Cu1S) in fully reduced state;

$$CuA_{[1Cu^{1.5+}-1Cu^{1.5+}]}CuZ^{*}_{[4Cu^{1+}]} + Asc \xrightarrow{k_{red2}} CuA_{[1Cu^{1+}-1Cu^{1+}]}CuZ^{*}_{[4Cu^{1+}]}$$

5. CuZº decays to CuZ*(4Cu1S), in the presence of oxidized CuA, which was previously determined to occur with a rate of 1.8×10^{-3} s^{-1} (see Section 5.2);

$$CuA_{[1Cu^{1.5+}-1Cu^{1.5+}]}CuZ^{0}_{[1Cu^{2+}-3Cu^{1+}]} \xrightarrow{k_{decay}} CuA_{[1Cu^{1.5+}-1Cu^{1.5+}]}CuZ^{*}_{[1Cu^{2+}-3Cu^{1+}]}$$

6. CuZº decays to CuZ*(4Cu1S), in the presence of reduced CuA (CuZº is unlikely unaffected by the difference in the redox state of CuA center);

$$CuA_{[1Cu^{1+}-1Cu^{1+}]}CuZ^{0}_{[1Cu^{2+}-3Cu^{1+}]} \xrightarrow{k_{decay}} CuA_{[1Cu^{1+}-1Cu^{1+}]}CuZ^{*}_{[1Cu^{2+}-3Cu^{1+}]}$$

7. Bimolecular reduction of CuA center by sodium ascorbate in the presence of CuZ*(4Cu1S), previously determined to have a value of 1.4 M^{-1} s^{-1} (see Section 5.1);

$$CuA_{[1Cu^{1.5+}-1Cu^{1.5+}]}CuZ^{*}_{[1Cu^{2+}-3Cu^{1+}]} + Asc \xrightarrow{k_{red3}} CuA_{[1Cu^{1+}-1Cu^{1+}]}CuZ^{*}_{[1Cu^{2+}-3Cu^{1+}]}$$

Scheme 5.3 – Kinetic model used to fit the reduction of CuZº via intermolecular electron transfer from CuA center. This model does not considers CuZ' formation. It is assumed that CuZ° decays to CuZ*(4Cu1S).

Another model can also be hypothesized considering the direct reduction of CuZº by sodium ascorbate, which involves seven steps (Scheme 5.4):

1. Bimolecular reduction of oxidized CuA center by sodium ascorbate in the presence of CuZº;

$$CuA_{[1Cu^{1.5+}-1Cu^{1.5+}]}CuZ^{0}_{[1Cu^{2+}-3Cu^{1+}]} + Asc \xrightarrow{k_{red1}} CuA_{[1Cu^{1+}-1Cu^{1+}]}CuZ^{0}_{[1Cu^{2+}-3Cu^{1+}]}$$

2. Bimolecular reduction of CuZº intermediate by sodium ascorbate in the presence of oxidized CuA center;

$$CuA_{[1Cu^{1.5+}-1Cu^{1.5+}]}CuZ^{0}_{[1Cu^{2+}-3Cu^{1+}]} + Asc \xrightarrow{k_{z^0}} CuA_{[1Cu^{1.5+}-1Cu^{1.5+}]}CuZ^{*}_{[4Cu^{1+}]}$$

3. Bimolecular reduction of CuZº intermediate by sodium ascorbate in the presence of reduced CuA center;

$$CuA_{[1Cu^{1+}-1Cu^{1+}]}CuZ^{0}_{[1Cu^{2+}-3Cu^{1+}]} + Asc \xrightarrow{k_{z^0}} CuA_{[1Cu^{1+}-1Cu^{1+}]}CuZ^{*}_{[4Cu^{1+}]}$$

4. Bimolecular reduction of oxidized CuA center by sodium ascorbate in the presence of fully reduced CuZ*(4Cu1S);

$$CuA_{[1Cu^{1.5+}-1Cu^{1.5+}]}CuZ^{*}_{[4Cu^{1+}]} + Asc \xrightarrow{k_{red2}} CuA_{[1Cu^{1+}-1Cu^{1+}]}CuZ^{*}_{[4Cu^{1+}]}$$

5. Decay of CuZº to CuZ*(4Cu1S) in the presence of oxidized CuA center, which was previously determined to occur with a rate of 1.8×10^{-3} s^{-1} (see Section 5.2);

$$CuA_{[1Cu^{1.5+}-1Cu^{1.5+}]}CuZ^{0}_{[1Cu^{2+}-3Cu^{1+}]} \xrightarrow{k_{decay}} CuA_{[1Cu^{1.5+}-1Cu^{1.5+}]}CuZ^{*}_{[1Cu^{2+}-3Cu^{1+}]}$$

6. Decay of CuZº to CuZ*(4Cu1S) in the presence of reduced CuA center;

$$CuA_{[1Cu^{1+}-1Cu^{1+}]}CuZ^{0}_{[1Cu^{2+}-3Cu^{1+}]} \xrightarrow{k_{decay}} CuA_{[1Cu^{1+}-1Cu^{1+}]}CuZ^{*}_{[1Cu^{2+}-3Cu^{1+}]}$$

7. Bimolecular reduction of oxidized CuA center by sodium ascorbate in the presence of CuZ*(4Cu1S), previously determined to have a value of 1.4 M^{-1} s^{-1} (see Section 5.1).

$$CuA_{[1Cu^{1.5+}-1Cu^{1.5+}]}CuZ^{*}_{[1Cu^{2+}-3Cu^{1+}]} + Asc \xrightarrow{k_{red3}} CuA_{[1Cu^{1+}-1Cu^{1+}]}CuZ^{*}_{[1Cu^{2+}-3Cu^{1+}]}$$

Scheme 5.4 – Kinetic model used to fit the reduction of CuZº directly via sodium ascorbate. This model does not considers CuZ' formation. It is assumed that CuZ° decays to CuZ*(4Cu1S).

In fact, some reactions are common to both models, being the main difference in steps 2 and 3, which involve the reduction of CuZº. As we have already shown (in Section 5.1), CuA reduction is independent of "CuZ center", as similar rates were determined for N_2OR with either 80 % or 10 % of "CuZ center" as CuZ*(4Cu1S). Thus, we considered a rate of 1.4 M^{-1} s^{-1} for the reactions 1, 4 and 7 ($k_{red1} = k_{red2} = k_{red3}$) in both models. Based on this evidence, we assumed that the same is valid for CuZº, i.e., the rate of CuZº decay to CuZ*(4Cu1S) is independent of the reduction of the CuA center, and in fact, this rate (k_{decay}) was previously determined to be 1.8×10^{-3} s^{-1} (Section 5.2).
Thus, the experimental data was fitted with both models using kinetics Tenua program. For the kinetic IET model, the best fit were obtained with a k_{IET} = 0.1 s^{-1} and k_{IET} /k_{-IET} = 1.1 s^{-1}, while the best fit for the direct CuZº reduction by sodium ascorbate were observed when k_{Z^o} = 0.6 M^{-1} s^{-1} was used (Figure 5.14).

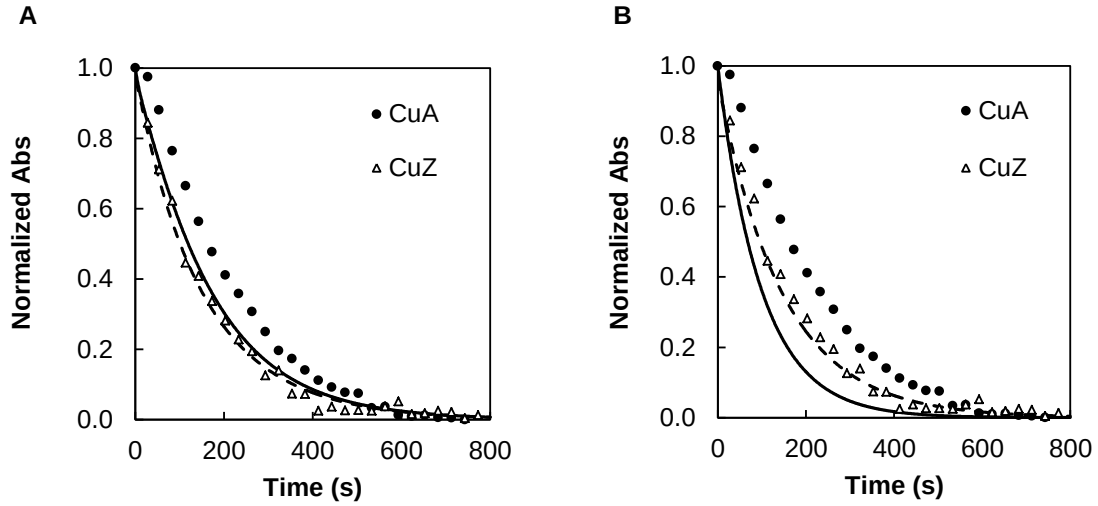

Figure 5.14 – Reduction of CuZº, obtained when 20 µM fully reduced N_2OR with 80 % of "CuZ center" as CuZ*(4Cu1S) reacted with 36 µM N_2O, in the presence of 7.3 mM (~ 400 equivalents) sodium ascorbate, added 37 s after N_2O addition. Normalized time dependence of CuA center reduction at 482 nm (filled circles) and CuZº reduction at 683 nm (open triangles): (A) Fit for an IET kinetic model, using $k_{red1} = k_{red2} = k_{red3} = 1.4\ M^{-1}\ s^{-1}$; $k_{decay} = 1.8\times10^{-3}\ s^{-1}$; $k_{IET} = 0.1\ s^{-1}$ and $k_{IET}/k_{-IET} = 1.1$; $R^2 = 0.983$. (B) Fit for the direct reduction of CuZº by sodium ascorbate, using $k_{red1} = k_{red2} = k_{red3} = 1.4\ M^{-1}\ s^{-1}$; $k_{decay} = k_{decay} = 1.8\times10^{-3}\ s^{-1}$; $k_{Z^o} = 0.6\ M^{-1}\ s^{-1}$; $R^2 = 0.952$. Note that correlation coefficients were determined for the CuZº fitting. Fit of CuA center reduction is represented by solid line and the CuZº reduction is represented by dashed line.

The results obtained demonstrate that experimental data is better fitted by a kinetic IET model ($R^2 = 0.983$). In this model the reduction of CuA center seems slightly faster than the experimental reduction observed, since the decay of the absorbance correspondent to CuA center is not well fitted in the model using those parameters. However, a much higher difference was observed when the experimental data was fitted with the kinetic model for the direct reduction of CuZº by sodium ascorbate ($R^2 = 0.952$).

In order to optimize the fittings of both models, the rate of bimolecular reduction of CuA center in the presence of CuZº was varied from the experimentally determined rate of bimolecular reduction of CuA center in the presence of CuZ*(4Cu1S). Variations within this rate were performed to improve the fitting and therefore new kinetic parameters were generated (Figure 5.15).

In the kinetic IET model, no major dissimilarities were observed if k_{IET} was maintained > $0.1\ s^{-1}$, as long as the equilibrium constant ($K_{IET} = k_{IET}/k_{-IET} = 2.5$) was also maintained. This allowed defining a k_{IET} of $0.1\ s^{-1}$ as the lower limit of the intramolecular electron transfer. The CuA center was better fitted when k_{red1} decreases *ca.* 35 % from $1.4\ M^{-1}\ s^{-1}$ to $0.9\ M^{-1}\ s^{-1}$. In fact, this change is reasonable as is in close proximity to the bimolecular rate of CuA reduction by sodium ascorbate experimentally determined in the N_2OR sample with 10 % of "CuZ center" as CuZ*(4Cu1S) (Figure 5.2).

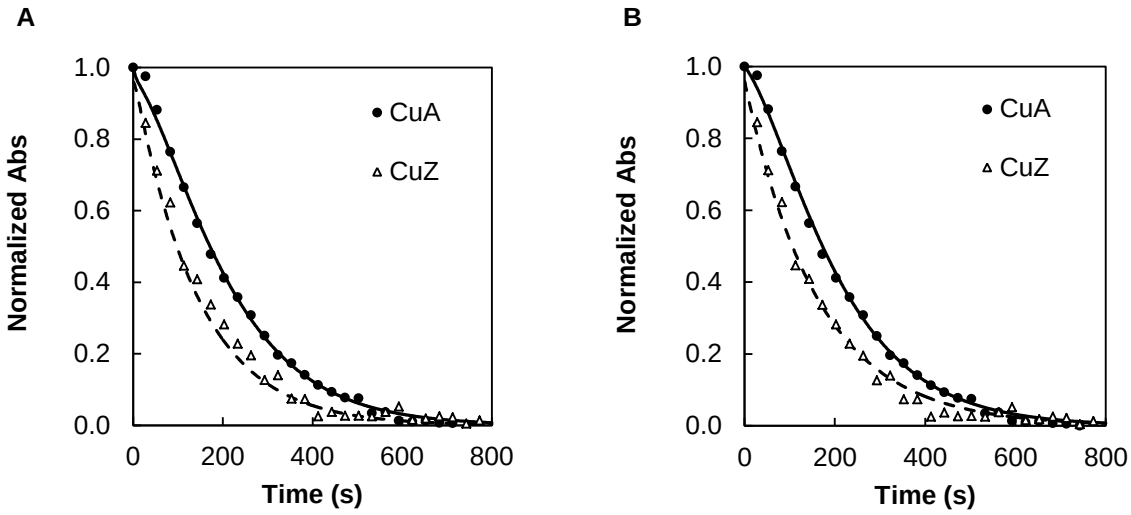

Figure 5.15 – Fitting of the reduction of CuA center (filled circles) and CuZ^o (open triangles) in a reaction of 20 µM N_2OR with 80 % of "CuZ center" as CuZ*(4Cu1S) with 36 µM N_2O, by sodium ascorbate (7.3 mM). The absorbance was normalized and fitted for CuA center at 482 nm (solid line) and CuZ^o at 683 nm (dashed line) with the two models described, using kinetics Tenua program. (A) Fit for an IET kinetic model, using k_{red1} = 0.9 M^{-1} s^{-1}; k_{red2} = k_{red3} = 1.4 M^{-1} s^{-1}; k_{decay} = 1.8×10^{-3} s^{-1}; k_{IET} = 0.1 s^{-1} and k_{IET}/k_{-IET} = 2.5; R^2 = 0.998. (B) Fit for the direct reduction of CuZ^o by sodium ascorbate, using k_{red1} = 0.17 M^{-1} s^{-1}; k_{red2} = k_{red3} = 1.4 M^{-1} s^{-1}; k_{decay} = k_{decay} = 1.8×10^{-3} s^{-1}; k_{Z^o} = 0.6 M^{-1} s^{-1}; R^2 = 0.993.

On the other hand, to improve the fitting of the direct CuZ^o reduction by sodium ascorbate, a drastic change in the k_{red1} (k_{red1} = 0.17 M^{-1} s^{-1}) had to be performed, (R^2 = 0.993), which is no longer in the same order of magnitude as before. By opposition to the IET model, this variation is not plausible since CuZ^o and CuZ*(4Cu1S) differ only in the edge hydroxide ligand, being the edge ligand of CuZ^o at ~ 7 Å away from the CuA center, and therefore the k_{red1} is not justified. In addition, the direct reduction of CuA center by sodium ascorbate seems to occur at a similar rate in N_2OR samples with different forms of "CuZ center". These results point out that CuZ^o reduction occurs via intramolecular electron transfer through CuA center and the kinetic model of the different intervening species generated over time is presented in Figure 5.16.

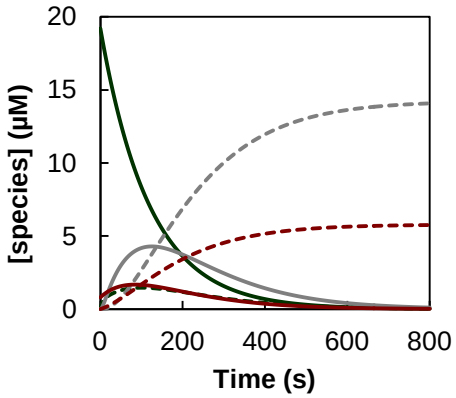

Figure 5.16 – Kinetic model of the CuZº reduction by IET through CuA center using the Scheme 5.3. Each line represents a different species, being those containing the CuA center oxidized represented by solid lines and those with the CuA center reduced by dashed lines. The "CuZ center" as CuZº, fully reduced form and resting state are colored by green, grey and red, respectively. The model was generated in the kinetics Tenua software using the following kinetic parameters: k_{red1} = 0.9 M^{-1} s^{-1}; k_{red2} = k_{red3} = 1.4 M^{-1} s^{-1}; k_{decay} = 1.8×10^{-3} s^{-1}; k_{IET} = 0.1 s^{-1} and k_{IET}/k_{-IET} = 2.5; [N_2OR] = 20 μM; [Asc] = 7.29 mM.

As the model shows, in the presence of excess of sodium ascorbate the CuZº is reduced to the fully reduced form, through electron transfer from CuA center. During this time period only 5 μM of resting CuZ*(4Cu1S) was formed (Figure 5.16).

Similarly, CuZº reduction was also investigated in the presence of a lower excess of sodium ascorbate (~ 16 fold-excess) during 3000 s (Figure 5.17). In this case CuZº was obtained from fully reduced N_2OR, with 60 % of "CuZ center" as CuZ*(4Cu1S). Two reactivity phases were also observed in the visible spectra (Figure 5.17A).

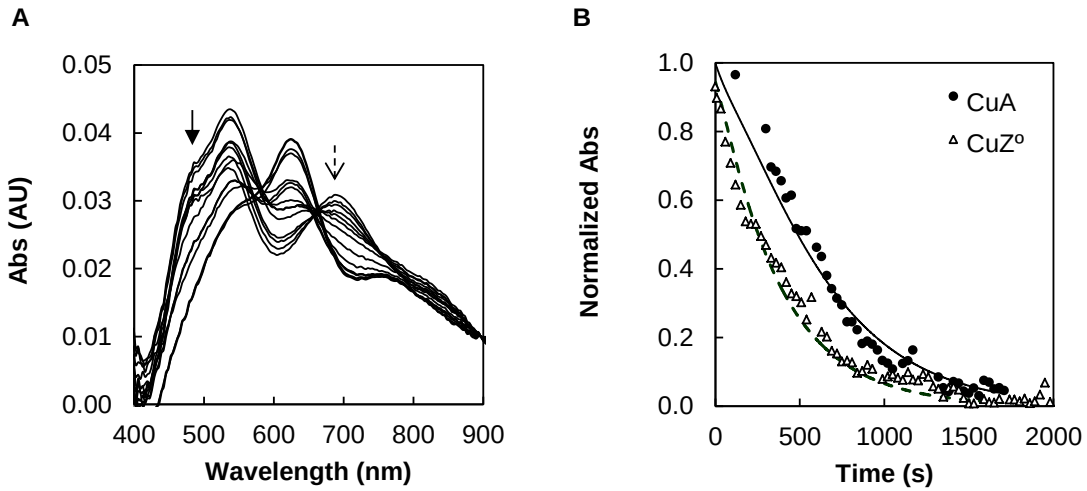

Figure 5.17 – Reduction of CuZº, obtained when 30 μM fully reduced N_2OR with 60 % of "CuZ center" as CuZ*(4Cu1S) reacted with 32 μM N_2O, by 490 μM (~ 16 equivalents) sodium ascorbate, added 30 s after N_2O addition. (A) Visible spectra of reduction of CuZº and CuA during 3000 s. The arrows indicated the direction on spectra changes with time, at 482 nm (solid bold arrow) and 683 nm (dashed arrow). (B) Fitting adjustment of reduction of CuA center (filled circles and solid line) and CuZº (open triangles and dashed line) for an IET kinetic model, using k_{red1} = 3 M^{-1} s^{-1}; k_{red2} = k_{red3} = 6 M^{-1} s^{-1}; k_{decay} = 1.8×10^{-3} s^{-1}; k_{IET} = 0.01 s^{-1} and k_{IET}/k_{-IET} = 2.5; R^2 = 0.998. Note that correlation coefficients were determined for the CuZº fitting.

The analysis of the spectra of the first phase showed that CuA center is not fully reduced within 800 s due to the lower amount of sodium ascorbate. In fact, this was also observed in the reduction study of oxidized N_2OR, with 80 % of "CuZ center" as CuZ*(4Cu1S), in the presence of sodium ascorbate under similar conditions (Section 5.1). Thus, the reduction of CuZ^o in this experiment was analyzed during 2000 s, guaranteeing that at that point both CuA and CuZ^o centers were completely reduced.

CuA and CuZ^o reduction, followed at 482 and 683 nm, respectively, were normalized within that time period and fitted using the kinetic model that considers the direct reduction of CuZ^o via IET from CuA (Scheme 5.3, Figure 5.17B). In order to properly fit the data, we first assumed that bimolecular reduction (reactions 1, 4 and 7) of this model occurs at the same rate as CuA reduction in the presence of CuZ*(4Cu1S), observed in similar conditions (Section 5.1), being $k_{red1} = k_{red2} = k_{red3} = 6\ M^{-1}\ s^{-1}$, initially used. However, as this rate was determined from an incomplete reduction of CuA center, a variation in this rate is expected and was tested during the fitting.

Resembling the previous fitting, changing the rate of k_{red1} to half of its initially value ($k_{red1} = 3\ M^{-1}\ s^{-1}$) provides a better fit, as it was observed a faster reduction of CuA center. On the other hand, the best fit was observed with a $k_{IET} = 0.01\ s^{-1}$ but as before $k_{IET}\ /k_{-IET} = 2.5$ was maintained.

The CuA center fit is not as good in this case as before, because the experimental data collected during the initial seconds showed same oscillations in absorbance. Despite this, the best fit was provided by IET model corroborating the results observed with large excess of sodium ascorbate. These results also supports our previous suggestion of an IET rate 10^4 faster that the IET from CuA center to resting CuZ*(4Cu1S) center.

Another experiment was prepared by adding the fully reduced N_2OR with 60 % of "CuZ center" as CuZ*(4Cu1S) to a solution containing a large excess of sodium ascorbate (~ 330 fold-excess) and N_2O (~ 7 fold-excess) over the enzyme (Figure 5.18A). Although some features of CuA center oxidation were observed in the first acquired spectrum indicating the formation of CuZ^o, CuA center was rapidly reduced. Indeed, a band with absorption maximum at 640 nm was observed approximately 400 s after the addition of N_2OR. Moreover, following the absorbance in the remaining time (during 3000 s), no shifts of the maximum absorption band at 640 nm were detected and no increase of absorption features at 620 nm were also observed (Figure 5.18B).

These results showed that under these conditions no formation of the CuZ' intermediate was observed and CuZ^o decays directly to resting CuZ*(4Cu1S) during the time of the assay. This suggests that decay to CuZ' occurs when N_2O is absent.

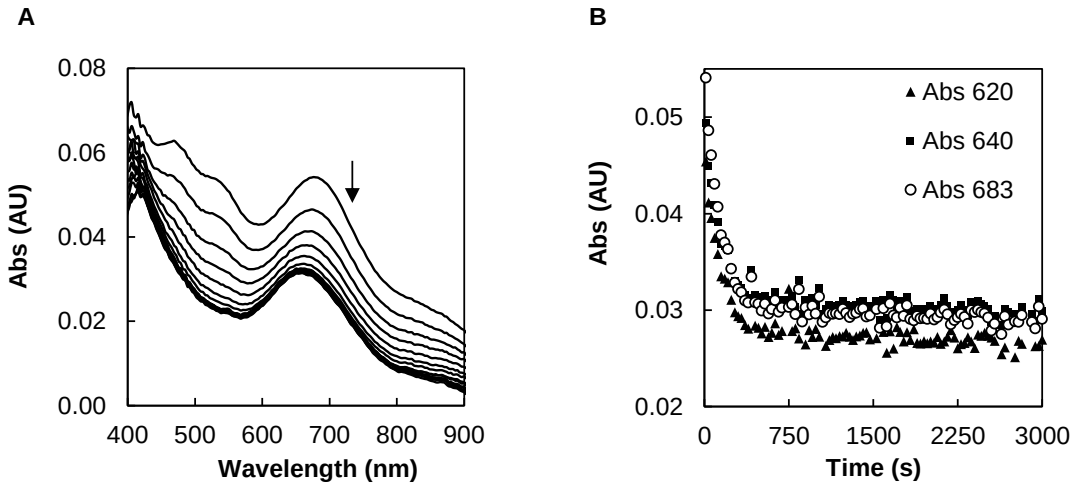

Figure 5.18 – Reaction of 30 µM fully reduced N_2OR, with 60 % of "CuZ center" as CuZ*(4Cu1S), with 10 mM of sodium ascorbate (~ 330 fold-excess) and 200 µM N_2O. (A) Visible spectra acquired during 3000 s. The arrow indicated the direction of changes over time. (B) Time dependence absorbance of CuZº at 683 nm (open circles), CuZ*(4Cu1S) at 640 nm (filled squares) and CuZ' intermediate at 620 nm (filled triangles).

5.6 Catalytic cycle

In light of our current knowledge, the activation and the catalytic mechanism of CuZ*(4Cu1S) of N_2OR from *M. hydrocarbonoclasticus* is presented in Figure 5.19.

Steady-state kinetics studies evidenced a rapid catalytic turnover (k_{cat} ~ 320 s^{-1}) [122], which implies that intermediate species involved in the catalysis of N_2O reduction must be rapidly reduced. Therefore, resting CuZ*(4Cu1S) cannot be part of the catalytic mechanism as this species exhibit a slow reduction (k = 1.2 × 10^{-3} s^{-1}, pH 7.3) [168], that is only observed in the presence of prolonged incubation with reduced methyl viologen.

During the *in vitro* activation of the enzyme, CuZ*(4Cu1S) is fully reduced to the [$4Cu^{1+}$] oxidation state (Intermediate 1). This well characterized form is competent in reacting with N_2O. The terminal N atom of the N_2O molecule binds to Cu_I, in a linear configuration [167]. The N-O bond cleavage is initiated with an elongation of the N-O bond, which induces a rearrangement of its structure, leading to the coordination of the oxygen atom to the Cu_{IV} atom, establishing a µ-1,3-N_2O coordination mode in a 139º angle [168, 272], with the oxygen forming a H-bond with the protonated K447 ("Intermediate 2").

The release of N_2 requires two electrons and one proton transfer, in a process involving all the copper atoms of "CuZ center" [167]. Indeed, one electron transferred *via* Cu_{IV}, is required for the N-O bond cleavage, followed by a proton transfer from K447 to the oxygen atom, resulting in an alteration of Cu_{IV} coordination to an OH. This ligand triggers the second electron transfer to disrupt the Cu_I-NO bond, resulting in N_2 release [167]. The lysine K447 becomes re-protonated by a proton from the solvent. CuZº species (intermediate 3) is formed after the coupled e^-/H^+ transfer from CuA center. This intermediate species has a hydroxide ligand coordinated to Cu_{IV}, which is stabilized

through H-bridging to K447. A second coordination sphere is involved in stabilization of CuZº species by the formation of another H-bond between K447 and E485 [167].

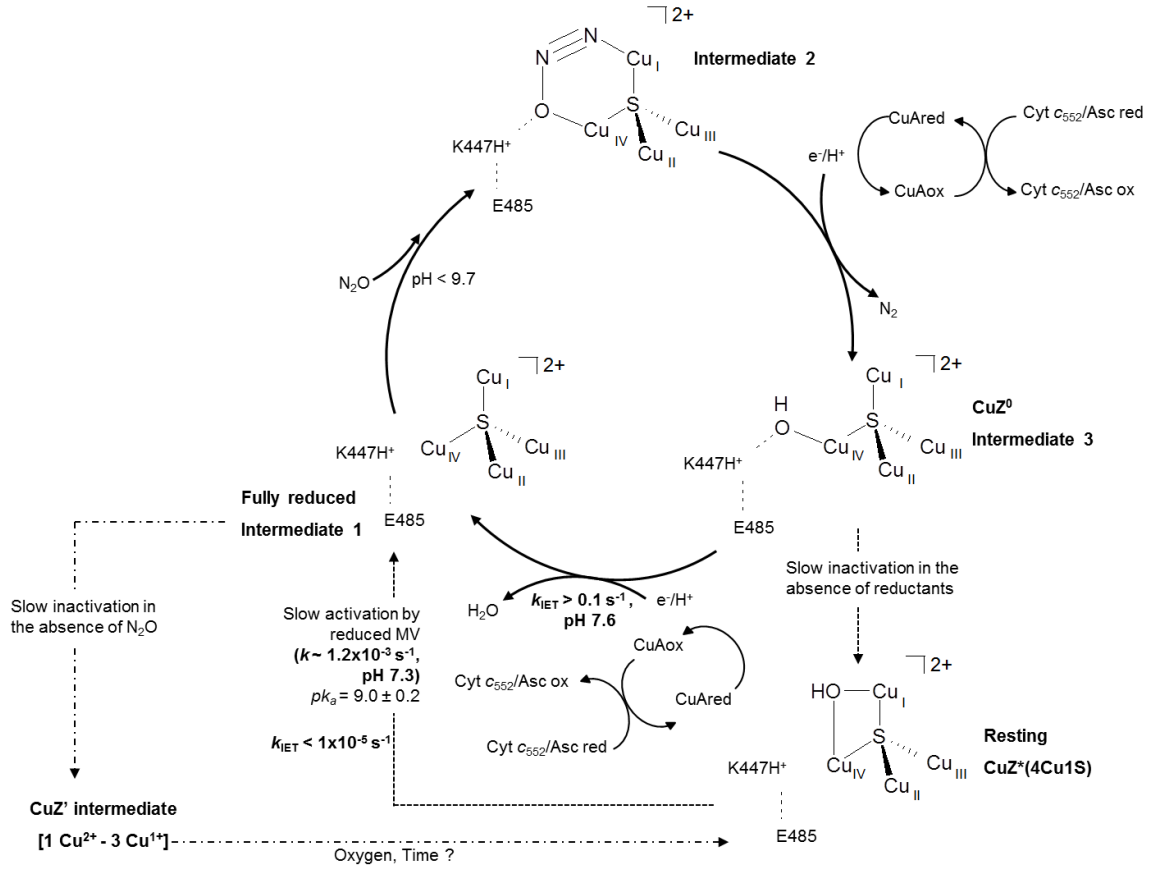

Figure 5.19 – Mechanism of activation and proposed catalytic cycle of N_2OR from *M. hydrocarbonoclasticus* with "CuZ center" as CuZ*(4Cu1S).

The catalytic cycle is completed through the reduction of CuZº by a rapid intramolecular electron transfer (k_{IET} > 0.1 s^{-1}, K_{IET} = 2.5) *via* CuA center, possibly reduced by cytochrome c_{552} since it was proved above that this center is reduced by a physiological relevant donor, sodium ascorbate.

In the absence of an external electron donor, the H-bond of CuZº to K447 is disrupted and an alteration of coordination of the active site occurs. In these conditions, the hydroxide ligand rearranges, most likely resulting in resting CuZ*(4Cu1S).

On the other hand, the formation of another intermediate CuZ' is observed, which is not part of the catalytic cycle. In this intermediate species "CuZ center" is in the [$1Cu^{2+}$-$3Cu^{1+}$] oxidation state, and is most likely formed from the oxidation of fully reduced CuZ*(4Cu1S) in the absence of substrate. Moreover, we propose here, that CuZ' slowly decays to the resting CuZ*(4Cu1S), which has a hydroxide ligand in the edge position between Cu_I-Cu_{IV}.

5.7 Conclusions

In this Chapter new insights into the reactivity of N_2OR, mainly with "CuZ center" in the CuZ*(4Cu1S) form, with N_2O were established and the catalytic mechanism was revisited in light of the current knowledge.

Since cytochrome c_{552} is able to donate electrons to CuA center of *M. hydrocarbonoclasticus* N_2OR, with "CuZ center" as CuZ*(4Cu1S), a kinetic study of direct electron transfer would be of outmost importance. However, due to the overlap of the absorption bands it would be difficult to follow this reaction. Thus, direct electron transfer was investigated in the presence of sodium ascorbate, an artificial electron donor (see below).

Reduction assays of the oxidized N_2OR in the presence of sodium ascorbate showed that CuA center can be easily reduced by this reducing agent and its reduction is independent of the form of the catalytic center, as the decay of CuA center in preparations containing different forms of "CuZ center" occurs at a similar rate. When DAD is present in the assay, it promotes a rapid electron transfer and the bimolecular reduction rate of CuA center becomes ~5-fold faster.

Regarding "CuZ center", under the concentration of sodium ascorbate used (~ 400 fold-excess over protein) the reduction of CuZ*(4Cu1S) was negligible, similarly to CuZ(4Cu2S) center.

The reaction of the fully reduced N_2OR in the presence of N_2O was previously investigated and the formation of an intermediate species, CuZ^o, was reported [148]. The formation of CuZ^o intermediate species was clearly evidenced in our studies and the decay rates observed were in the same order of magnitude as those previously reported by Dell'Acqua *et al* [148]. However, the second phase of the reactivity was quite different.

In here, evidences for the formation of CuZ' species were presented for the first time.

Like CuZ*(4Cu1S), CuZ' intermediate species is also redox inert but exhibits a maximum absorption at 617 nm. Further analysis showed that this new intermediate species might not be part of the catalytic cycle, as it was also observed upon oxidation of fully reduced CuZ*(4Cu1S) and this species does not present a high catalytic activity. Although further investigations are still needed, we consider in here the possibility of a very slow decay of this species to resting CuZ*(4Cu1S) in the presence of oxygen.

On the other hand, when a higher amount of N_2O was used relative to the enzyme, no shifts in the maximum absorption band relative to typical CuZ*(4Cu1S) features were detected. This is also supported by the addition of the enzyme to a large excess of N_2O, in which no CuZ' intermediate species was formed. Based on these observations, we envisaged the formation of an intermediate species, CuZ', linked to the absence of N_2O, while in the presence of excess of substrate and absence of reductants the CuZ° decays directly to the resting CuZ*(4Cu1S) form.

The pH dependence studies of the formation and decay of CuZ^o intermediate suggest that formation of CuZ^o does not occurs at pH values above pH 9.5 being attributed to the deprotonation of K447

and E485. These results corroborate the nature of "intermediate 2" and CuZ^o species, which we recently addressed by spectroscopic techniques and DFT calculations [167]. No effect of pH on the formation of the new intermediate species was observed, which we hypothesized to be a structural rearrangement of the CuZ*(4Cu1S) not perturbed by the deprotonation of the nearby lysine K447.

Although neither CuZ*(4Cu1S) nor CuZ(4Cu2S) centers were reduced in the presence of sodium ascorbate, the reduction of the catalytic competent CuZ^o intermediate was investigated in the presence of sodium ascorbate. Our results evidenced that CuZ^o is reduced by sodium ascorbate and the kinetic models developed strongly suggest that this intermediate species is reduced via intramolecular electron transfer through CuA center, being unlikely the direct reduction of the CuZ^o by sodium ascorbate. Furthermore, using low or large excess of sodium ascorbate over the enzyme, the rate of CuZ^o reduction through CuA center is 10^4 faster than the reduction of CuZ*(4Cu1S) through CuA center.

The reduction of CuZ^o with a physiological relevant reducing agent suggests that CuZ^o intermediate species is the oxidized form of the center in the catalytic cycle that can be rapidly reduced to the fully reduced state, closing the cycle. This competent intermediate species is of high importance as it can have a role in the *in vivo* catalysis. The other intermediate species remains to be isolated and characterized due to its short life time.

In conclusion, the catalytic cycle of N_2OR with "CuZ center" as CuZ*(4Cu1S) is now better understood. Substrate is able to react with the fully reduced CuZ*(4Cu1S) producing the CuZ^o intermediate species. In turn, CuZ^o in the presence of electrons, can be fully reduced to [$4Cu^{1+}$], by IET through CuA center, closing the catalytic cycle. In the absence of substrate, but when electrons are present, an intermediate non-catalytic species is formed, which we hypothesized to decay to the resting CuZ*(4Cu1S), although the conditions of this decay are still unclear.

Chapter 6

Interaction of exogenous ligands with nitrous oxide reductase

6 Interaction of exogenous ligands with nitrous oxide reductase

In this Chapter, we investigate the interaction of different exogenous ligands (cyanide, azide, nitric oxide and halides) with *M. hydrocarbonoclasticus* N_2OR, with "CuZ center" in two different forms, in order to identify their mode of action and the inhibition mechanism. Although the interaction of some of these ligands with N_2OR has been previously described [89, 130, 172, 173], at that time the existence of two different forms of the N_2OR active site was not known. Therefore, a thorough study is justified.

Here, we will compare the effect of ligands and identify whether they bind to CuA or "CuZ" centers, with the latter either as CuZ*(4Cu1S) or CuZ(4Cu2S), using UV-visible and EPR spectroscopies; their effect in the specific activity of N_2OR; and also the effect of iodide in the stability of N_2OR, using differential scanning calorimetry.

Analysis of these data can clarify the interaction of the substrate with the two forms of the "CuZ center".

6.1 Interaction of halides with different forms of N_2OR

Copper-containing proteins, especially those with mononuclear and binuclear copper sites, such as tyrosinase and hemocyanin, are well-known for their reactivity with small exogenous ligands, such as halides [146, 273, 274]. These ligands may interact differently with different forms and oxidation states of N_2OR, and thus we investigated the interaction of the halides with various enzymatic preparations.

Interaction of fluoride, chloride, bromide and iodide with the oxidized N_2OR, with 50 % of "CuZ center" as CuZ*(4Cu1S), was investigated (Figure 6.1). In these experiments, N_2OR was anaerobically titrated with increasing concentrations of each of these ligands and the changes were monitored by visible spectroscopy.

The results obtained show that addition of bromide between 0 and 218 mM, causes only a slight increase in the absorbance of all the visible spectra, suggesting that interaction of this ligand with this form of the enzyme probably does not occur (Figure 6.1C). On the contrary, fluoride, chloride and iodide, when added in a similar concentration range as bromide, gave rise to higher perturbations on the visible spectra.

Fluoride was the only halide tested that produced a decrease in the intensity of N_2OR absorption bands, with apparent perturbation of the CuZ*(4Cu1S) center upon increase of its concentration (Figure 6.1A). Although the formation of new species by visible spectroscopy was not evident, the reduction of CuA center was observed with increasing concentrations of fluoride.

Chloride seems to interact with CuZ*(4Cu1S), as it was observed an increase of absorbance at 640 nm (Figure 6.1B).

In the case of iodide, a larger effect was observed at the CuZ*(4Cu1S) center, with an increase in the absorbance at 640 nm, accompanied by an increase in intensity of the absorption band at 750 nm. These changes have been previously attributed to the formation of a blue adduct [151] (Figure 6.1D).

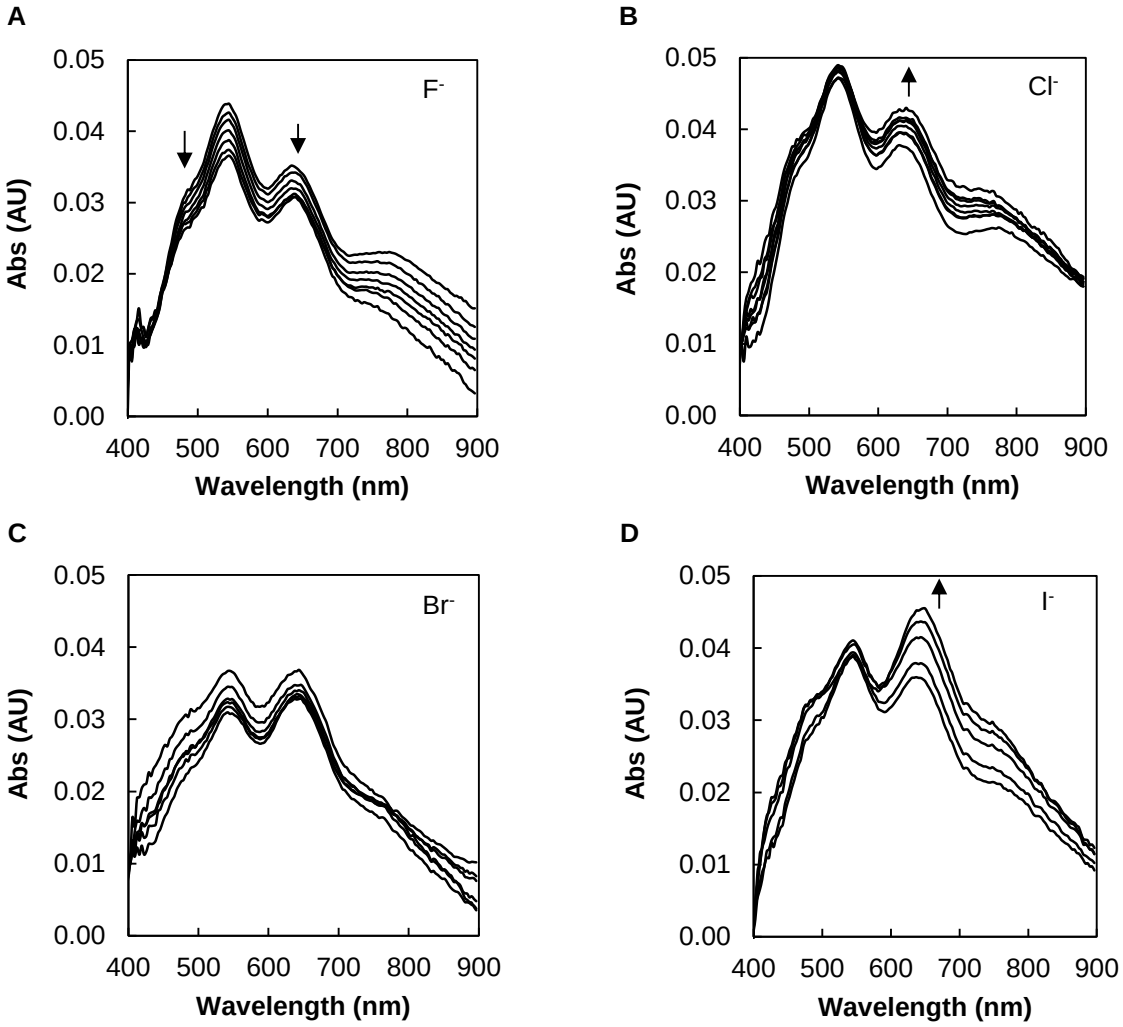

Figure 6.1 – Effect of halides in the visible spectra of 12 µM oxidized N_2OR with 50 % of "CuZ center" as CuZ*(4Cu1S), in 100 mM Tris-HCl, pH 7.6. (A) Addition of increasing concentrations of sodium fluoride, from 0 to 204 mM. (B) Addition of increasing concentrations of sodium chloride, from 0 to 224 mM. (C) Addition of increasing concentrations of sodium bromide, from 0 to 218 mM. (D) Addition of increasing concentrations of potassium iodide, from 0 to 219 mM. The arrows indicate the direction of the spectral changes. Spectra were corrected for the absorbance at 402 nm.

Although perturbations were detected in the absorption bands of CuA center, with increasing concentrations of fluoride and bromide, this is probably related with an effect on the "CuZ center" thought a partial reduction of CuA center may also occur. In fact, CuA center does not have free positions for ligand binding (unless His576 is flipped away from the CuA_1), and therefore formation of a metal-ligand complex is unlikely. Indeed, to our knowledge, there were no reports of CuA center being perturbed by the binding of halides.

The binding affinity of each halide to the tetranuclear site CuZ*(4Cu1S) was also estimated by titration assays. From the halides tested, bromide showed almost no differences in the absorbance at 640 nm and therefore we have to consider that bromide does not interact with CuZ*(4Cu1S), at least up to 10000-fold excess relative to the protein, as mentioned. In the case of fluoride, although a decrease in absorbance was noticed at 640 nm, upon subtraction of the contribution of CuA center to this wavelength, the variations observed were irrelevant.

On the contrary, titrations performed with chloride and iodide exhibited differences in the absorbance at 640 nm with increasing ligand concentrations. Apparent dissociation constants of 34 ± 2 mM and 40 ± 2 mM were estimated for chloride and iodide, respectively, for their binding to CuZ*(4Cu1S) (Figure 6.2). Chloride exhibits a higher affinity for CuZ*(4Cu1S), relative to the other halides, and thus the strength of the binding follows the order: $Br^- \sim F^- < I^- < Cl^-$. Indeed, chloride has a small size compared to iodide, possibly facilitating its binding. Nevertheless, the only known structure reported with a halide directly bound to "CuZ center" is the iodide-inhibited N_2OR from *A. cycloclastes*, in which iodide is bound to the edge between Cu_I-Cu_{IV} [151]. Although we cannot infer the binding position of the other halides by these experiments, similar variations of the N_2OR spectra in the presence of chloride and iodide were observed and therefore the possibility of these ions having the same mode of action cannot be excluded.

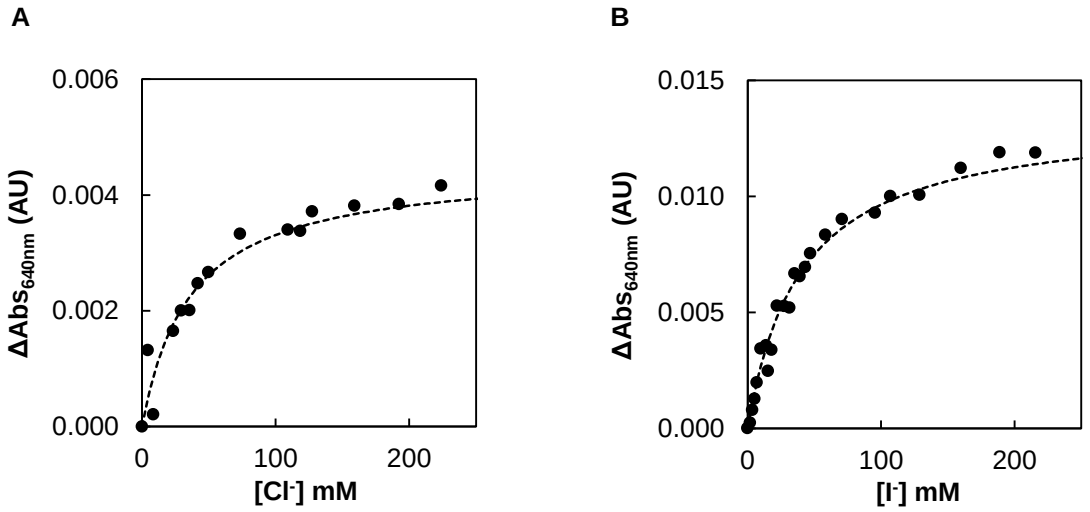

Figure 6.2 – Variation of the absorbance at 640 nm upon addition of (A) chloride and (B) iodide to N_2OR with 50 % of "CuZ center" as CuZ*(4Cu1S), at pH 7.6. Data were fitted to one binding site equation with a K_d^{app} of 34 ± 2 mM and 40 ± 2 mM, for the binding of chloride and iodide, respectively.

We also studied the iodide binding to N_2OR, with 50 % of "CuZ center" as CuZ*(4Cu1S), at pH 6.0 and 9.0. Moreover, as this is a mixture of 50 % CuZ*(4Cu1S), effects on the other form of "CuZ center" might occur and will also be analyzed.

The titrations performed at pH 6.0 and 9.0 showed similar changes in the visible spectra as the ones observed before in the titration at pH 7.6, indicating that iodide is able to bind CuZ*(4Cu1S) at

least between pH 6.0 and 9.0 (Figure 6.3). The apparent dissociation constant seems to be affected by pH, as a K_d^{app} of 24 ± 2 mM and 49 ± 3 mM were estimated for pH 6.0 and pH 9.0, respectively, demonstrating that the affinity is higher at lower pH. This might also explain why we were not able to observe iodide binding in the crystallographic studies, as crystallizations were performed at pH 9.5.

Furthermore, in the presence of 200 mM of iodide, a decrease in the intensity of the absorption band at 550 nm was also observed at different pH values, while the spectroscopic features of CuA center do not seem to be highly affected, an indication that iodide can also interact with CuZ(4Cu2S).

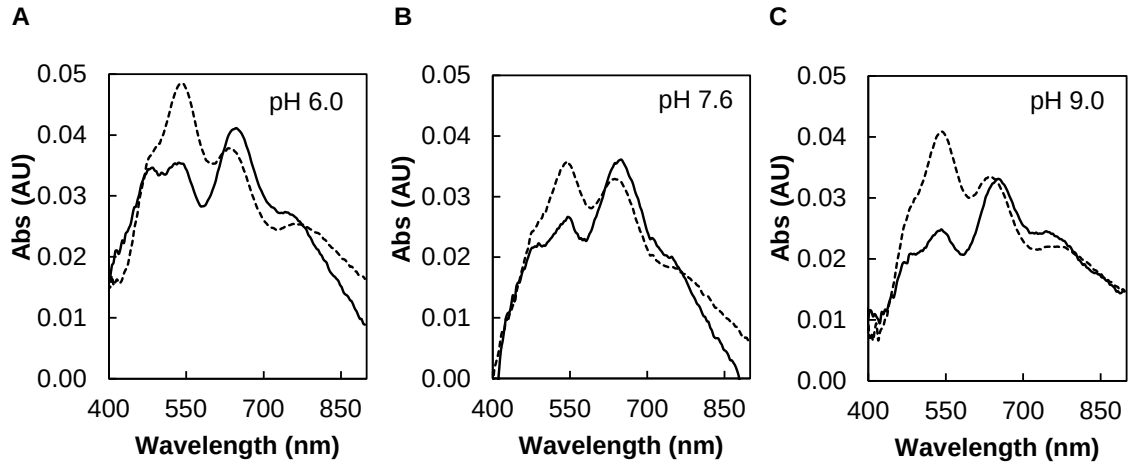

Figure 6.3 – Effect of pH on the iodide binding to 12 µM oxidized N_2OR with "CuZ center" as 50 % CuZ*(4Cu1S): (A) pH 6.0, (B) pH 7.6 and (C) pH 9.0. The spectra with 0 mM (dashed line) and 200 mM (solid line) are represented for each pH. Spectra were corrected to 399 nm.

Interaction of halides with N_2OR, with 10 % of "CuZ center" as CuZ*(4Cu1S), was also investigated, as in this form there is no overlap of the CuZ*(4Cu1S) features (Figure 6.4).

In the oxidized state of CuZ(4Cu2S), the absorbance at 550 nm decreases with ligand addition, except with fluoride, whose effect on the enzyme is almost inexistent (Figure 6.4A). This observation is in accordance with similar studies on *P. stutzeri* N_2OR, with "CuZ center" mainly as CuZ(4Cu2S), in which fluoride, even in large excess over the protein did not produce any major perturbations in the visible and EPR spectra of the enzyme [275].

On the other hand, the band at 550 nm decreases upon addition of chloride, bromide and iodide, but a large excess of ligand was necessary, to observe perturbations in the visible spectra in the 400 - 900 nm region.

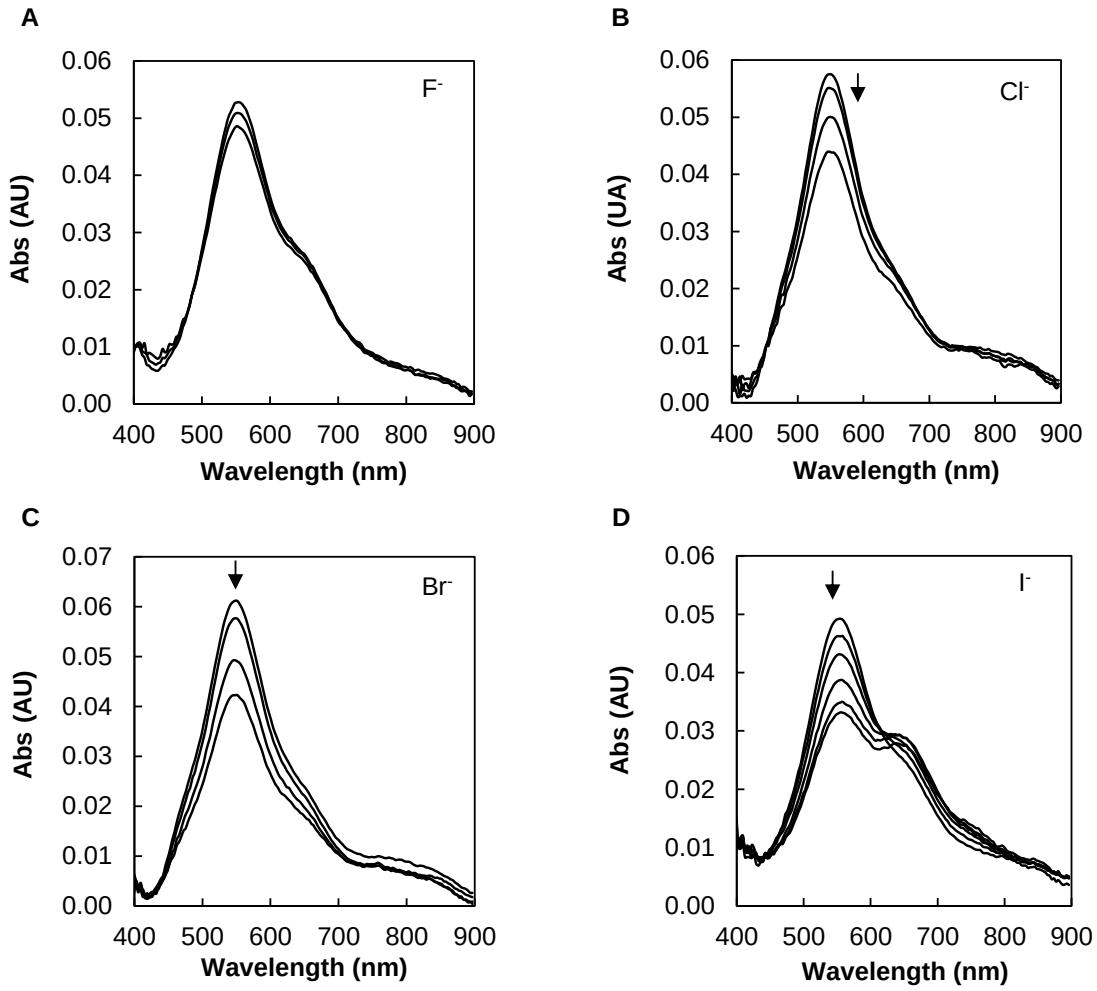

Figure 6.4 – Effect of halides on the visible spectra of 18 µM oxidized N_2OR with 10 % of "CuZ center" as CuZ*(4Cu1S), in 100 mM Tris-HCl, pH 7.6. (A) Addition of increasing concentrations of sodium fluoride, from 0 to 235 mM. (B) Addition of increasing concentrations of sodium chloride, from 0 to 600 mM. (C) Addition of increasing concentrations of sodium bromide, from 0 to 322 mM. (D) Addition of increasing concentrations of potassium iodide, from 0 to 300 mM. The arrows indicate the direction of absorbance changes with ligand additions.

Additions of chloride caused perturbations in the spectra, mainly observed between 450 - 650 nm, as observed in the difference spectra (Figure 6.5A). These changes seem to be associated with a non-specific binding, as the absorbance changes were proportional to the concentration of the ligand and up to 600 mM of chloride no plateau in the binding curve was observed (Figure 6.5B). Moreover, changes observed in the presence of chloride are similar to those previously reported for the titration of oxidized CuZ(4Cu2S) from *P. stutzeri* N_2OR (0.08 mM) with concentrations up to 366 mM of chloride (although there are differences in the N_2OR:NaCl ratio) [172].

In the case of bromide a large decrease in the absorbance was detected at 550 nm, but only for concentrations up to 250 mM and no new features were observed (Figure 6.4C).

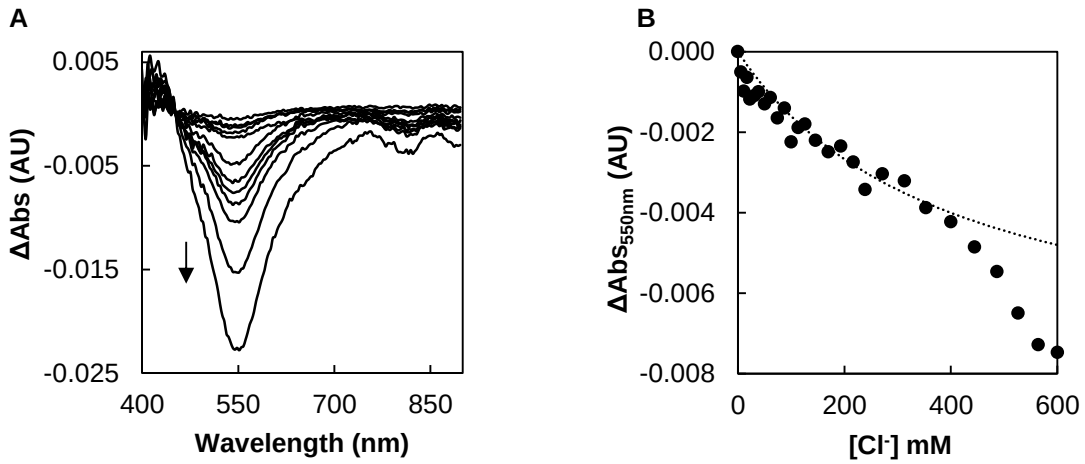

Figure 6.5 – Effect of chloride on the oxidized N_2OR (18 µM) with 10 % of "CuZ center" as CuZ*(4Cu1S) at pH 7.6. (A) Difference spectra during the titration with chloride (0 – 600 mM). The arrows indicate the changes with chloride additions. (B) Dependence of variation on the absorbance at 550 nm. Data cannot be fitted to a one binding site equation (dotted line).

On the other hand, iodide exhibited a different and stronger effect in the visible spectra, characterized by the emergence of a new band. In order to better understand these perturbations the difference spectra is presented (Figure 6.6A). Besides the observed differences at 550 nm, there is the emergence of a new band at 645 nm and with subsequent additions of iodide a shoulder at 750 nm is also observed. Interestingly, the decrease of the maximum absorbance at 550 nm is simultaneous with the increase of absorbance at 640 nm and thus a possible conversion of CuZ(4Cu2S) into CuZ*(4Cu1S) is hypothesized.

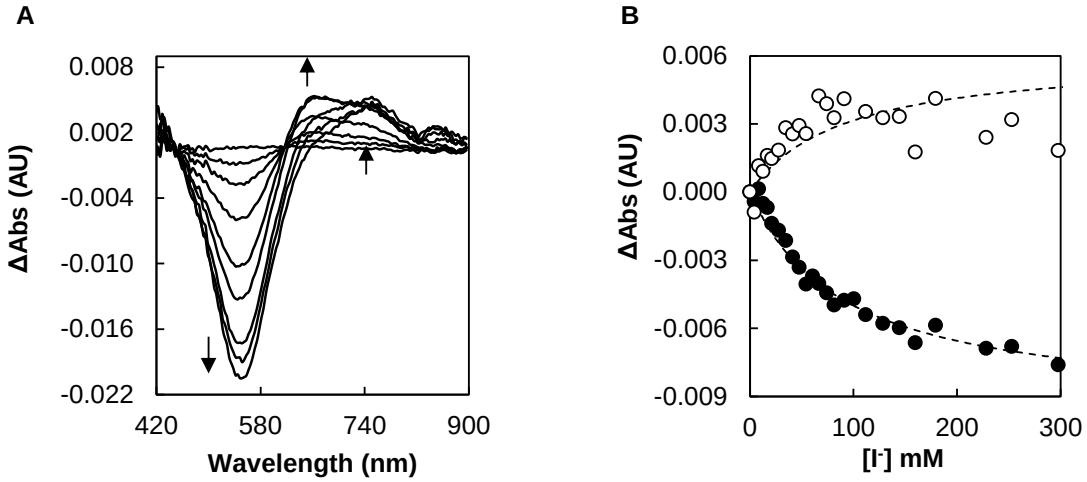

Figure 6.6 – Effect of iodide on the oxidized N_2OR (18 µM), with 10 % of "CuZ center" as CuZ*(4Cu1S), at pH 7.6. (A) Difference spectra during the titration with iodide (0 to 300 mM). The arrows indicate the direction of absorbance changes with iodide additions. (B) Dependence of variation on the absorbance at 550 nm (filled circles) and at 640 nm (open circles). Data were fitted to a one binding site equation with a K_d^{app} of 90 ± 4 mM.

Furthermore, the absorption band at 750 nm was only observed at concentrations of iodide higher than 297 mM and might be related with a ligand-to-metal charge transfer. Note that such concentrations where not tested in the titration described before using a N_2OR sample with 50 % of "CuZ center" as CuZ*(4Cu1S) and therefore we cannot consider that this band is exclusive of CuZ(4Cu2S) (see below).

Since in the previous titrations of N_2OR with "CuZ center" as CuZ*(4Cu1S), CuA center did not exhibit any perturbation upon addition of iodide, we calculated the apparent dissociation constant at 550 and 640 nm, without subtracting the CuA center contribution. Fitting the data to one binding site, a K_d^{app} of 90 ± 4 mM was estimated, indicating a lower affinity of the iodide for the CuZ(4Cu2S) relative to the CuZ*(4Cu1S) form (Figure 6.6B, Table 6.1).

As ligand affinity could vary with the oxidation state of the copper atoms, we also performed a titration of N_2OR, containing CuZ(4Cu2S) in the reduced state, with iodide (Figure 6.7). In this case, there were no contribution of the CuA center to the spectrum and N_2OR visible spectrum exhibits a maximum at 660 nm, which decreases with iodide additions. The apparent dissociation constant estimated at this wavelength was obtained by fitting the data to one binding site equation and has a value of 20 ± 2 mM.

The binding of iodide to different forms and redox states of the enzyme, suggests that this ion has higher affinity to the reduced CuZ(4Cu2S), relative to the oxidized state of this center.

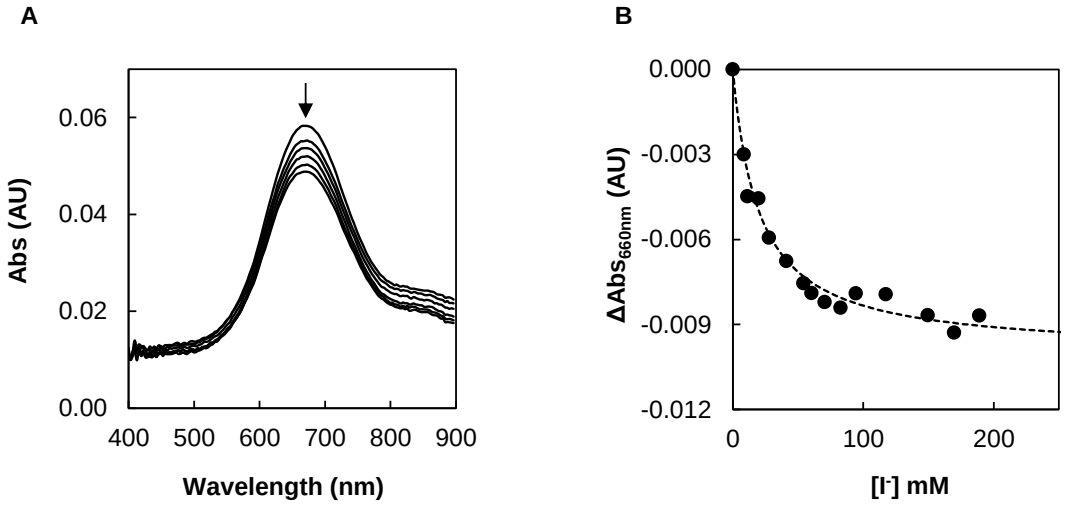

Figure 6.7 – Effect of iodide in the visible spectra of 20 µM reduced N_2OR, with 10 % of "CuZ center" as CuZ*(4Cu1S), at pH 7.6. The arrow indicates the direction of the absorbance changes with iodide in the range 0 to 190 mM. (B) Dependence of the variation on the absorbance at 660 nm with iodide concentration. Data were fitted to a one binding site equation with a K_d^{app} of 20 ± 2 mM.

From the halides tested, iodide produced the most interesting effect, as perturbations are observed in the two forms of the catalytic center (Table 6.1). The affinity of iodide at pH 7.6 follows the order: reduced CuZ(4Cu2S) > CuZ*(4Cu1S) > oxidized CuZ(4Cu2S). Thus, the binding of the iodide to the enzyme was investigated in more detail.

Table 6.1 – Parameters (ΔAbs_{max} and K_d^{app}) used in the fitting of each ligand with the different forms of the "CuZ center" of N_2OR.

"CuZ center"	**Cl^- (mM)**		**I^- (mM)**	
	ΔAbs_{max} (AU)	**K_d^{app} (mM)**	**ΔAbs_{max} (AU)**	**K_d^{app} (mM)**
Resting CuZ*(4Cu1S) (Abs 640 nm)	0.005	34 ± 2, at pH 7.6	0.014	24 ± 2, at pH 6.0
			0.008	40 ± 2, at pH 7.6
			0.008	49 ± 3, at pH 9.0
Oxidized CuZ(4Cu2S) (Abs 550 nm)	-	-	0.010	90 ± 4, at pH 7.6
Reduced CuZ(4Cu2S) (Abs 660 nm)	-	-	0.010	20 ± 2, at pH 7.6

6.2 Effect of iodide binding to different forms of N_2OR

6.2.1 Spectroscopic and steady-state kinetics studies

In order to understand the effect of iodide on the different forms of the "CuZ center" of *M. hydrocarbonoclasticus* N_2OR, an enzyme preparation with 65 % of "CuZ center" as CuZ*(4Cu1S) was incubated with 500-fold excess of iodide, under anaerobic conditions for 48 h (Figure 6.8A). During this period, a macroscopic change of the color of N_2OR from pink to blue was observed upon iodide exposure.

Larger spectroscopic changes occurred during the initial 7 h, in which the intensity of the characteristic bands of CuA center was perturbed. Differences in the CuZ*(4Cu1S) were practically not detected in this 7 h period.

Spectra collected after 24 and 48 h showed a complete bleaching of the CuA features, while at 640 nm, there was a small increase in the absorbance and the formation of a small shoulder at 750 nm (Figure 6.8). These are characteristics of the formation of a blue adduct, upon binding of iodide to the Cu_I-Cu_{IV} edge of the CuZ*(4Cu1S) center as reported for *A. cycloclastes* N_2OR [151].

In this titration it was observed some differences relative to the iodide titration of N_2OR with 50 % of "CuZ center" as CuZ*(4Cu1S) (Figure 6.1D), which are attributed to the incubation period in the presence of iodide.

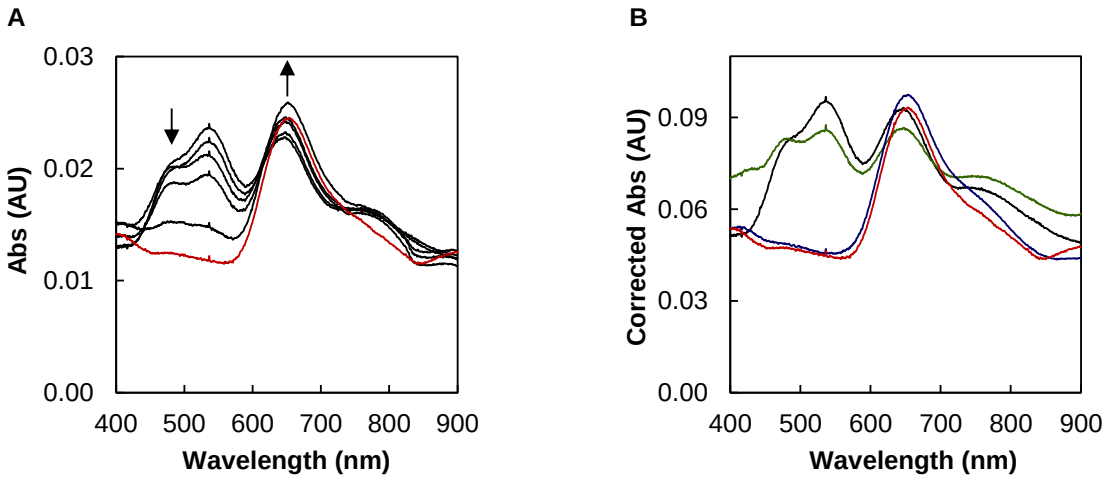

Figure 6.8 – Effect of iodide (500-fold excess) on the visible spectra of 7 µM oxidized N_2OR, with 65 % of "CuZ center" as CuZ*(4Cu1S), at pH 7.6. (A) Spectra of oxidized N_2OR after 0, 1, 5, 7, 24 and 48 h incubation with iodide. (B) The visible spectra of oxidized N_2OR (t = 0, black), after 48 h incubation with iodide (red), sodium dithionite reduction of inhibited N_2OR (blue) and oxidation of inhibited N_2OR (green) are represented. Absorbance was corrected based on the concentration of protein by modified Lowry method. The arrows indicate spectral changes with the incubation time.

The oxidized/reduced spectra of I-N_2OR adduct formed after 48 h incubation is presented in Figure 6.8B. Upon oxidation, characteristics of the CuA center are re-established, demonstrating that exposure of N_2OR to iodide simply leads to the reduction of CuA center.

In the reduced spectrum a shoulder at 750 nm can be observed. Moreover, the absorption maximum at 640 nm of the species formed did not shift upon oxidation or reduction, indicating that even if I^- is binding at the Cu_I-Cu_{IV} edge, this form of "CuZ center" remains redox inert.

The amount of copper atoms per protein was estimated before (6.9 ± 0.4) and after 48 h incubation with iodide (6.6 ± 0.5). These results indicate that no copper was lost during incubation with iodide.

Exposure of reduced N_2OR with 10 % of "CuZ center" as CuZ*(4Cu1S) to 500-fold excess of iodide also induced the formation of the iodide adduct, marked by a shift of the maximum absorbance at 660 nm to 645 nm, concomitantly with the emergence of a shoulder at 750 nm (Figure 6.9A). Upon oxidation with potassium ferricyanide, the spectrum of the I-N_2OR complex shows additional features of oxidized CuA center, but the features of the oxidized CuZ(4Cu2S) were no longer observed (Figure 6.9B). In addition, reduction of the I-N_2OR complex with dithionite did not re-establish the initial spectrum, as the maximum absorption band is still observed at 645 nm.

In fact, the spectra obtained after 48 h incubation with iodide and also the oxidized I-N_2OR complex are identical to that of N_2OR with "CuZ center" mainly as CuZ*(4Cu1S), suggesting that iodide might be binding to the same position as when the "CuZ center" is in the [$1Cu^{2+}$ - $3Cu^{1+}$] oxidation state, independently of the form of the "CuZ center".

Moreover, a copper/protein ratio of 9.0 ± 0.2 was determined for the iodide-incubated sample, which is identical to the ratio determined for the as-isolated enzyme (8.9 ± 0.4), indicating that iodide binding to this form of the enzyme also does not cause loss of copper.

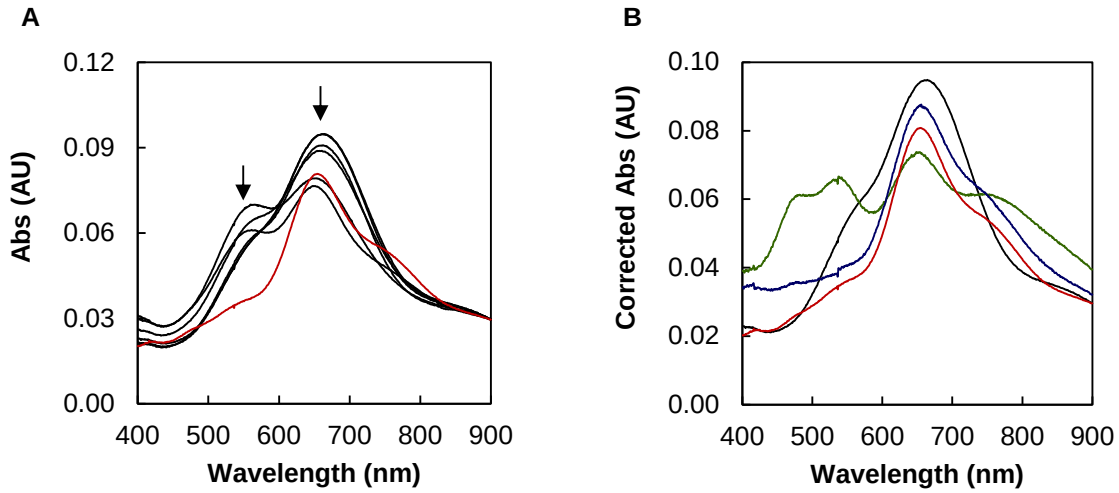

Figure 6.9 – Effect of iodide (500-fold excess) on the visible spectra of 20 µM oxidized N_2OR, with 10 % of "CuZ center" as CuZ*(4Cu1S). (A) Spectra of reduced N_2OR after 0, 1, 3, 5, 8, 20, 24 and 48 h incubation with iodide. (B) The visible spectra of oxidized N_2OR, (black), iodide incubated after 48 h (red), sodium dithionite reduction of inhibited N_2OR (blue) and oxidation of inhibited N_2OR (green) are represented. Corrected absorbance is based on the concentration of protein by modified Lowry method. The arrows indicate spectral changes with the incubation time.

The effect of 500-fold excess of iodide on the oxidized N_2OR, with 10 % of "CuZ center" as CuZ*(4Cu1S) was also monitored during 48 h and the changes were similar to those observed in the titration (Figure 6.10). During this incubation period there was a decrease of absorbance at 550 nm with concomitant increased of absorbance at 640 nm.

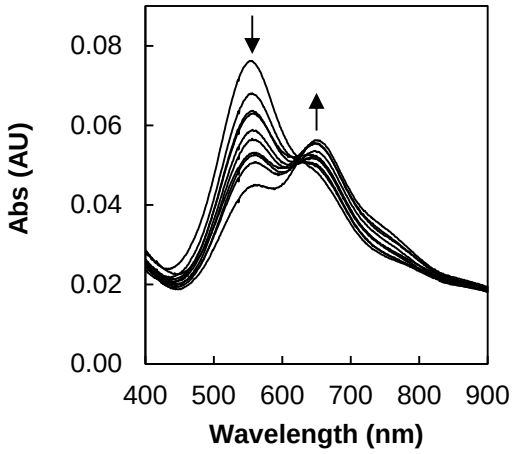

Figure 6.10 – Effect of iodide (500-fold excess), after 0, 1, 3, 5, 8, 20, 28 and 48 h incubation, on the visible spectra of 16 µM oxidized N_2OR, with 10 % of "CuZ center" as CuZ*(4Cu1S), at pH 7.6. The arrows indicate spectral changes with the incubation time.

The spectrum obtained after 48 h incubation is similar to the one reported for oxidized *P. stutzeri* N_2OR, with mainly CuZ(4Cu2S), after being incubated with 200 equivalents of KI during 36 h [275, 276]. Indeed, in the experiment performed with *P. stutzeri* N_2OR, a band at 632 nm was reported after 36 h incubation, which did not change even in the presence of a strong oxidizing agent [275, 276].

The complexes formed between iodide and the enzyme with different forms of "CuZ center" after 48 h were also analyzed by X-band EPR (Figure 6.11).

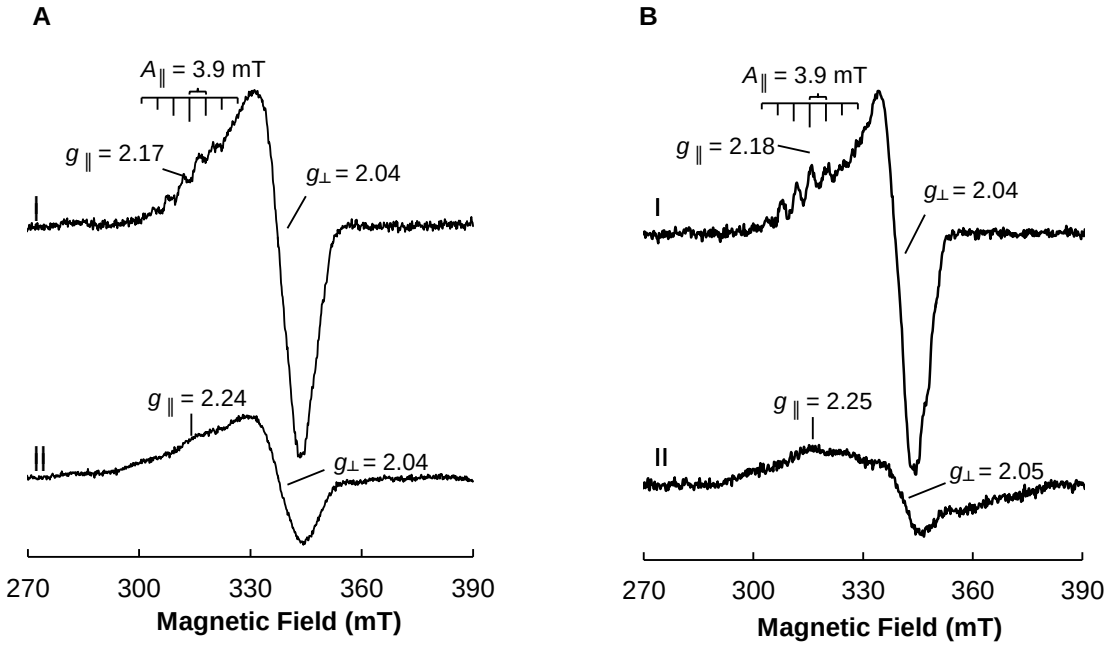

Figure 6.11 – X-band EPR spectra of iodide-N_2OR complex. (A) Spectra of 166 µM N_2OR with 65 % of "CuZ center" as CuZ*(4Cu1S) and (B) spectra of 200 µM N_2OR with 10 % of "CuZ center" as CuZ*(4Cu1S) are represented. In each panel, oxidized N_2OR and iodide incubated N_2OR (500-fold excess, incubated for 48 h) are numbered by I and II, respectively. Experimental settings: microwave frequency, 9.65 GHz; microwave power, 2 mW; gain, 1×10^5; temperature, 30 K.

The EPR spectrum of N_2OR with mainly "CuZ center" as CuZ*(4Cu1S) has an axial signal with a 7-line hyperfine pattern, characteristic of the presence of oxidized CuA center (Figure 6.11A). After N_2OR exposure to iodide for 48 h, the EPR spectrum of this sample still exhibits an axial signal, with $g_{\parallel}$ = 2.24 and $g_{\perp}$ = 2.04, but with broad features (Figure 6.11A).

In the case of oxidized N_2OR with 10 % of "CuZ center" as CuZ*(4Cu1S) and before incubation with iodide, an axial signal is observed in the EPR spectrum also with 7 hyperfine lines. Upon incubation with iodide during 48 h, the 7-line hyperfine structure disapears, and a broad and low resolved pattern is observed, which seems to be different from the one observed for the complex formed with N_2OR mainly as CuZ*(4Cu1S), but the signal is still axial, with $g_{\parallel}$ = 2.25, $g_{\perp}$ = 2.05 (Figure 6.11B).

Since iodide was shown to bind at the Cu_I-Cu_{IV} edge of CuZ*(4Cu1S) [151], and given the nuclei spin of 5/2 of iodide each of the copper lines can be divided into 6 lines undistinguished in this conditions, hampering the simulation of this spectrum.

In order to understand the changes caused by iodide, a spin quantification was performed. In a sample containing 100 % of "CuZ center" as CuZ*(4Cu1S) in its fully oxidized state it is expected a spin of 2, as both CuA (S = 1/2) and CuZ*(4Cu1S) centers (S = 1/2) are paramagnetic. On the other hand, fully oxidized CuZ(4Cu2S) is diamagnetic and does not contribute to the spin quantification. Therefore, the expected spin of the oxidized samples were estimated based on the percentage of CuZ*(4Cu1S) calculated by its specific activity. The spin quantification of I-N_2OR complexes were determined by integration of the area of each spectrum and related to the area of the spectrum of the respective oxidized N_2OR (Table 6.2).

Table 6.2 – EPR spin quantification of I-N_2OR complexes formed.

Sample	**Oxidized** [a]	**I-N_2OR**
65 % CuZ*(4Cu1S)	1.7	1.3
10 % CuZ*(4Cu1S)	1.1	0.9

Note: [a]expected spin given the percentage of CuZ*(4Cu1S) determined by its specific activity.

In the case of N_2OR with 65 % of "CuZ center" as CuZ*(4Cu1S), a spin of 1.3 was estimated upon iodide incubation, indicating that there was some reduction of the copper centers (oxidized sample has a spin of 1.7), similarly to that observed in the visible spectrum (Figure 6.8A), specially reduction of CuA center.

The N_2OR with 10 % of "CuZ center" as CuZ*(4Cu1S) in the fully oxidized state has a spin of 1.1 which decreases to 0.9 upon iodide incubation. Despite the small difference observed in the spin quantification, we can not conclude on the reduction of CuA center by the analysis of this result itself. In fact, given the reduction power of iodide, if reduction of both CuA and CuZ(4Cu2S) occurs, a spin of 1 would still be expected as CuZ(4Cu2S) in its reduced state is paramagnetic (S = 1/2).

EPR spectra upon iodide binding are still paramagnetic and the signals observed are different from the typical ones observed for N_2OR, in the [$1Cu^{2+}$-$3Cu^{1+}$] oxidation state, in the absence of iodide indicating that a complex is formed between N_2OR and this exogenous ligand.

The effect of iodide on the enzymatic activity was analyzed by steady-state kinetics during the incubation with iodide (Figure 6.12). At each time-point, a small sample of I-N_2OR was taken and incubated for 3 h in the presence of reduced methyl viologen and afterwards N_2O was added to start the assay. Surprisingly, the N_2OR with 50 % of "CuZ center" as CuZ*(4Cu1S) incubated with 500-fold excess iodide did not show a decrease in the activity (Figure 6.12A). Similarly, the

activity assays performed with a preparation with 10 % of "CuZ center" as CuZ*(4Cu1S) also showed an almost constant specific activity during the incubation with iodide.

In order to understand if the iodide does not really affect the specific activity of the enzyme, a N_2OR preparation with 65 % of "CuZ center" as CuZ*(4Cu1S) was incubated in the presence of KI (between 0 to 352 µM) for 24 h and then incubated 3 h with reduced methyl viologen before substrate addition. Our results showed that even in the presence of 5000-fold excess of iodide relative to the enzyme (352 µM of KI), no changes in the activity were observed (Figure 6.12B).

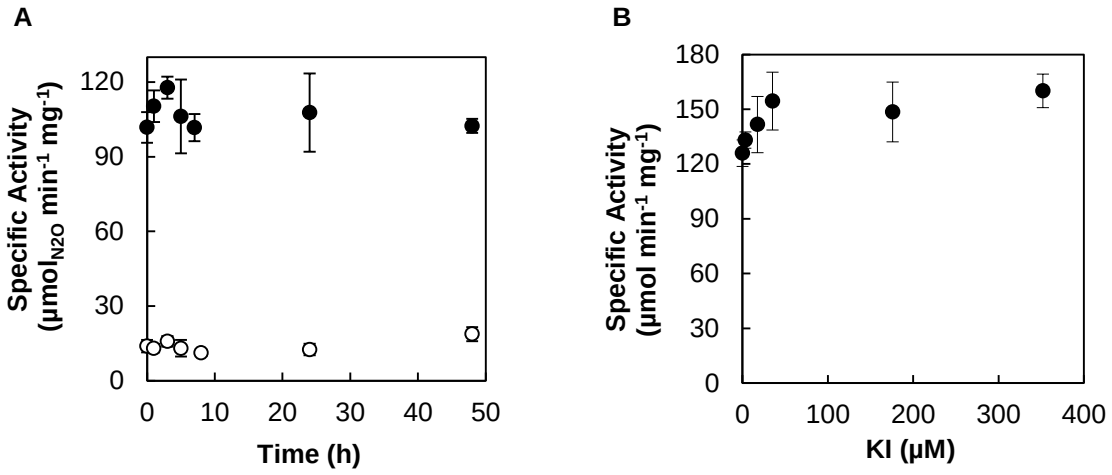

Figure 6.12 – Effect of iodide on the enzymatic activity of N_2OR. (A) The specific activity of 70 nM N_2OR, with 50 % of "CuZ center" as CuZ*(4Cu1S) (filled circles) and as 10 % of "CuZ center" as CuZ*(4Cu1S) (open circles) was measured at different incubation times with the ligand (500-fold excess). (B) Assays were performed with 70 nM of N_2OR, with 65 % of "CuZ center" as CuZ*(4Cu1S), incubated 24 h in the presence of 0, 3.5, 17.6, 35.2, 176 and 352 µM of KI (final concentrations in the activity assay).

6.2.2 Thermal stability of different forms of N_2OR in the presence and absence of iodide

The thermal stability of different forms of "CuZ center" was studied in absence and presence of iodide by differential scanning calorimetry (DSC) (Figure 6.13).

The asymmetric thermograms of N_2OR, with "CuZ center" as 10 % and 50 % CuZ*(4Cu1S), obtained in the absence of iodide, presents some differences between them (Figure 6.13A and C). Nevertheless, both thermograms displayed two broad endothermic peaks, each one fitted to a non two-state transition model. Similar melting temperatures (T_m) were observed for both "CuZ center" forms, with values of 51 ºC and 58 ºC, determined for the first and second transition, respectively (Figure 6.13A and C, parameters in Table 6.3).

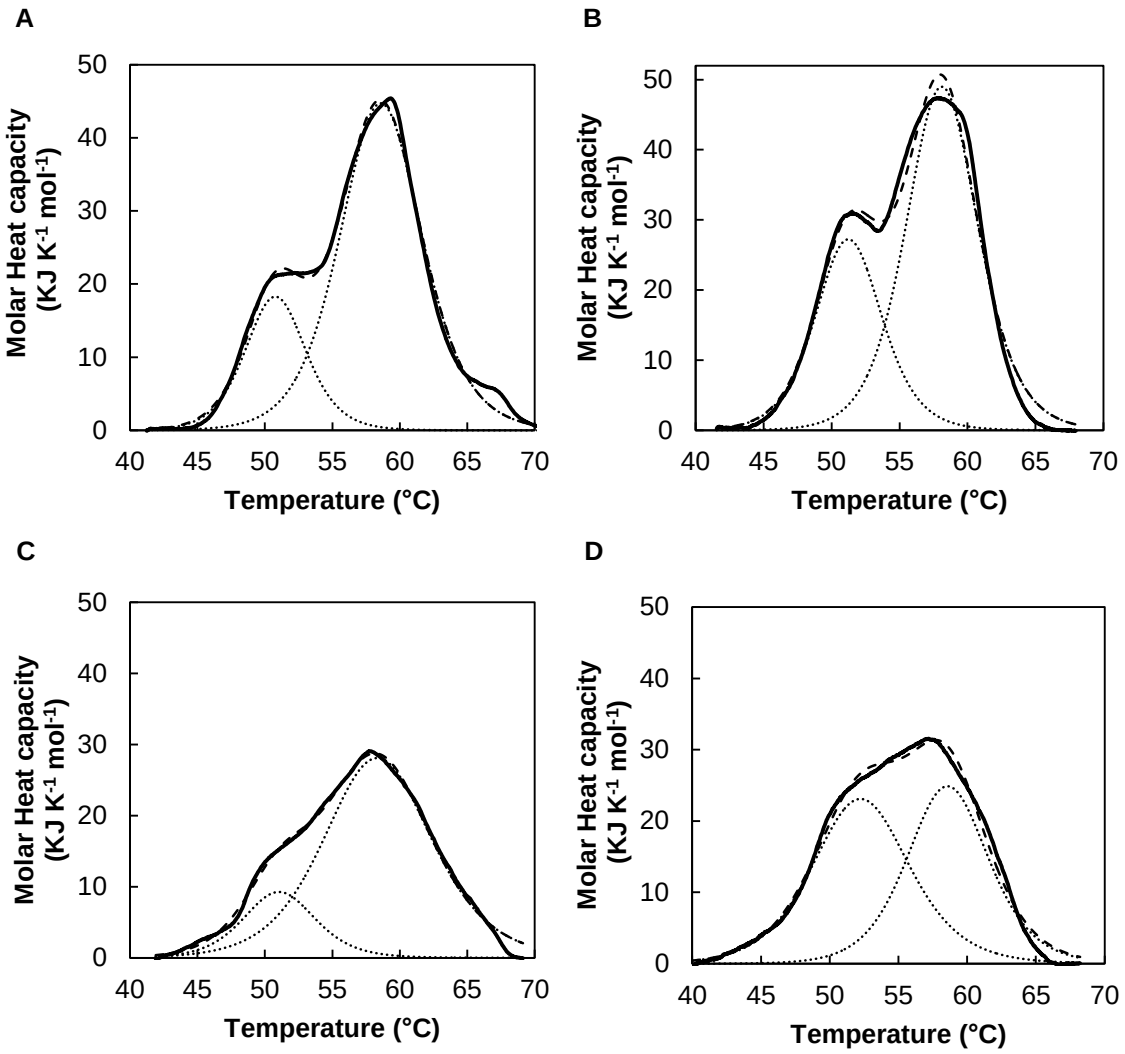

Figure 6.13 – Molar heat capacity profiles of different forms of N_2OR. N_2OR (20 μM), with 50 % of "CuZ center" as CuZ*(4Cu1S) in the absence (A) and presence (B) of KI. N_2OR (20 μM), with 10 % of "CuZ center" as CuZ*(4Cu1S) in the absence (C) and presence (D) of KI. Samples were prepared in 100 mM HEPES, pH 7.0. The sample prepared in the presence of the ligand was incubated with 500 equivalents of KI for 48 h at 4 °C. The thermograms were baseline corrected and normalized for concentration (solid line). The simulations fitting the data are represented by a dashed line which is the sum of two independent models represented by dotted lines.

Van't Hoff enthalpies (ΔH_{vH}), which are given by the shape of the transition curve, were identical for the first transition of different forms of N_2OR, while the second transition was quite dissimilar between these forms, being necessary a higher energy to disrupt the structure of the second species of N_2OR 50 % CuZ*(4Cu1S) compared to 10 % CuZ*(4Cu1S) form. It should be noted that in the sample with 10 % of "CuZ center" as CuZ*(4Cu1S), the fitting in the maximum of the second transition would probably give a more accurate model if we used a temperature limit, as it is possible that the thermogram is distorted by the aggregation that occurs at higher temperatures. But we fitted this thermogram using the same model as the others to be able to compare samples.

On the other hand, calorimetric enthalpies (ΔH_{cal}) were determined based on the total area of the thermogram peaks. Although comparison between ΔH_{cal} and ΔH_{vH} can give valuable information about the unfolding, in the case of N_2OR it is not so simple as this enzyme is a dimer. In fact, asymmetric thermograms are often associated to the unfolding of domains or subunits on proteins [277], thus, further studies are needed to access structural information.

The unfolding process is irreversible as precipitation after unfolding was detected in all the profiles near 83 ºC, being confirmed in the end of each experiment by visual inspection. Furthermore, the unfolding process of N_2OR most likely leads to the loss of its copper atoms, making the refolding process impossible.

These denaturation temperatures and shape of thermograms are in line with the apo-form of *S. denitrificans* N_2OR, in which a T_m of 54 ºC was reported by differential scanning fluorimetry [129], although an increase of T_m for the holo-protein would be expected. In fact, N_2OR from *S. denitrificans* has 68 % primary sequence identity with *M. hydrocarbonoclasticus* N_2OR and some differences in the T_m may occur.

The T_m was practically unaffected by the presence of iodide, indicating that ligand binding did not stabilize or destabilize the protein (Figure 6.13B and D, parameters in Table 6.3). In fact, for N_2OR with either form of "CuZ center", the presence of iodide does not change the main transitions. In addition, the calorimetric enthalpies did not change significantly in the presence of ligand.

The enthalpy of unfolding, in turn, seemed similar between the 1st and the 2nd transition in the iodide complex with N_2OR with 50 % of "CuZ center" as CuZ*(4Cu1S), while in the complex with 10 % of "CuZ center" as CuZ*(4Cu1S) the enthalpies between transitions were more dissimilar.

Table 6.3 – Parameters of the stability of different forms of N_2OR and the effect of iodide.

CuZ form	Ligand	ΔH_{cal} (KJ mol^{-1})	T_m (ºC)		ΔH_{vH} (KJ mol^{-1})	
			1st transition	2nd transition	1st transition	2nd transition
CuZ*(4Cu1S)	-	469.9	51.4	58.5	429.9	562.3
CuZ*(4Cu1S)	I^-	442.5	51.1	58.2	531.5	527.2
CuZ (4Cu2S)	-	342.3	51.3	58.2	440.8	370.0
CuZ (4Cu2S)	I^-	351.0	52.3	58.6	349.4	473.4

Notes: Enzyme was incubated with iodide for 48 h prior to the experiment. ΔH_{cal} – calorimetric enthalpy; ΔH_{vH} – van't Hoff enthalpy.

Given the results obtained, we propose a possible binding mode of iodide to the active center of N_2OR.

Spectroscopically, the formation of a metal-ligand complex in both forms was evidenced, but its thermostability was not affected. The crystallographic structure obtained in the presence of iodide showed an iodide atom bound to the Cu_I-Cu_{IV} edge at the CuZ*(4Cu1S) center [151]. However, in the

CuZ(4Cu2S), this edge is occupied by a sulfur atom, hampering the binding of other molecules to this site. Considering that iodide bound to the two forms of "CuZ center" has similar spectroscopic properties (at least when "CuZ center" is in the [$1Cu^{2+}$-$3Cu^{1+}$] oxidation state, in particular upon oxidation and reduction of I-N_2OR complex formed), we propose that iodide binds to both centers in a similar way. Moreover, we hypothesize that there is a displacement of the thiolate ligand upon iodide binding, though the catalytic activity of the inhibited form is not affected.

6.3 Effect of cyanide and azide on N_2OR

The binding of cyanide or azide, which are known to interact with copper centers, was investigated on N_2OR with 60 % of "CuZ center" as CuZ*(4Cu1S), by visible spectroscopy and steady-state kinetics in a time dependent assay.

Addition of 5-fold excess of cyanide to the oxidized N_2OR was monitored over 48 h under anaerobic conditions. A decrease in the intensity of the spectral features was observed during the incubation time in the region 400 – 900 nm (Figure 6.14A). After 48 h, we investigated the effect of this ligand on N_2OR and the reversibility of the spectral changes caused by cyanide incubation, through the oxidation and reduction of the inhibited sample (Figure 6.14B). Spectra were recorded after removal of excess of cyanide, oxidizing/reducing agents and unbound copper ions. Oxidation of the inhibited N_2OR did not completely re-establish the initial spectrum of the enzyme. In fact, the oxidized spectrum indicates that CuA features were only partially restored. On the other hand, the reduced spectrum, presented an intense absorption band with a maximum at 645 nm and a shoulder at 760 nm. These results suggest the formation of a new species at the active site that was not observed in the oxidized spectra. Besides the alteration of the "CuZ center", cyanide also caused copper depletion (from 6.9 ± 0.4 to 3.1 ± 0.1), with a loss of ~ 55 % of copper relative to initial sample, that might be related to the loss of "CuZ center".

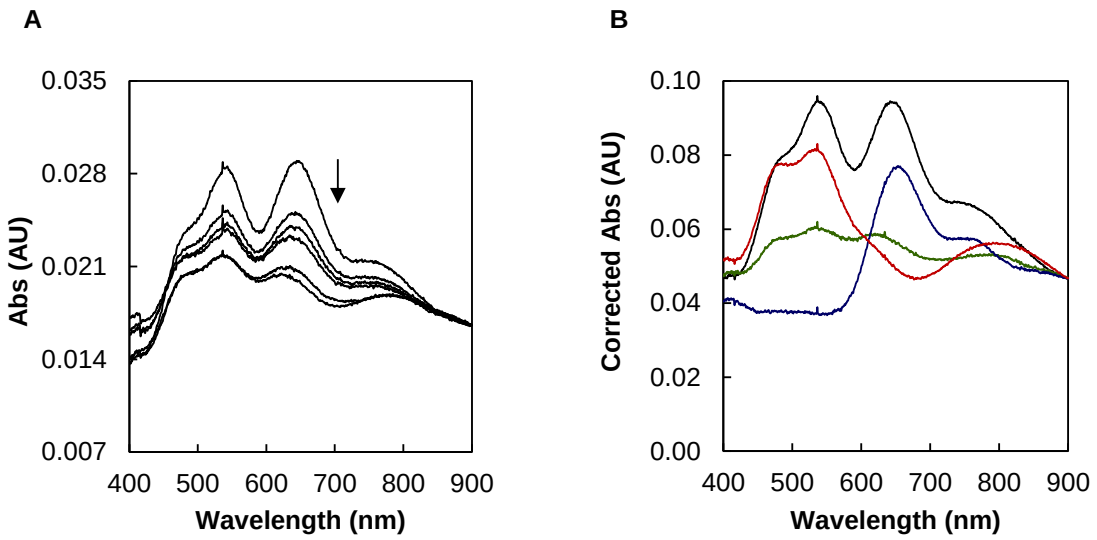

Figure 6.14 – Effect of cyanide (5-fold excess) on the visible spectra of N_2OR, with 65 % of "CuZ center" as CuZ*(4Cu1S). (A) N_2OR (7 µM) spectra recorded after 0, 0.25, 0.5, 1, 18, and 24 h during incubation. (B) The visible spectra of purified N_2OR (black), cyanide-incubated during 48 h (green), sodium dithionite reduction inhibited N_2OR (blue) and oxidation of inhibited N_2OR (red) are represented. The absorbance was corrected between samples based on the concentration of protein by modified Lowry method. The arrow represents the spectral changes with time.

A similar assay was performed with sodium azide (~ 700-fold excess) over 24 h, which showed identical changes to those observed in N_2OR incubated with sodium cyanide (Figure 6.15).

The recorded spectra showed a decrease in the intensity of the bands in the visible region but no new features were observed, contrary to earlier studies in which the addition of varying amounts of azide to N_2OR with mainly CuZ*(4Cu1S) center showed the formation of a new band at 375 nm, possibly due to N_3^-→Cu(II) LMCT transition, besides the bleaching in the visible region [172].

Moreover, ~ 33 % of the initial copper (from 6.9 ± 0.4 to 4.6 ± 0.3) was washed-out and the re-oxidized sample showed an increase in the ratio of A_{480}/A_{640} from 1.1 to 1.3. The results indicate that N_3^-, like CN^-, causes the destruction of "CuZ center".

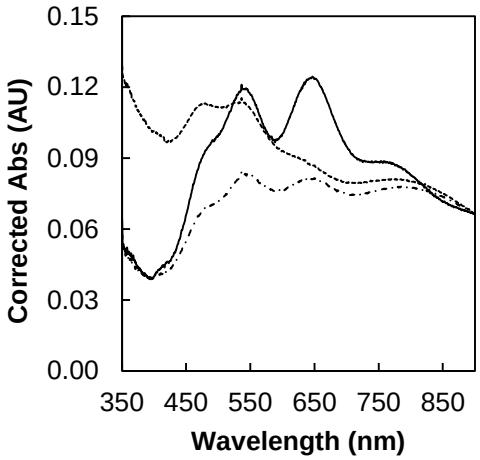

Figure 6.15 – Effect of azide (700-fold excess) on the visible spectra of 7 µM N_2OR, with 65 % as CuZ*(4Cu1S). The visible spectra of purified N_2OR (back line), azide incubated N_2OR after 24 h (dashed-dotted line) and oxidation of inhibited N_2OR (dashed line) are represented. The absorbance was corrected for the concentration of protein determined by modified Lowry method.

The effect of both ligands on the enzymatic activity was studied by steady-state kinetics at different incubation times (Figure 6.16A). Before incubation, a maximum specific activity of 128 ± 13 μmol_{N2O} min^{-1} $mg^{-1}{}_{N2OR}$ was determined. Subsequent decay of the activity with respect to the initial value was observed at different times of incubation. In the case of cyanide, no major differences were detected between 24 h and 48 h, suggesting that for the cyanide concentration used, a maximum decay of 60 % relative to the initial value was obtained after 24 h.

On the other hand, the azide, although used in large excess relative to N_2OR, exhibited only 30 % decrease of the activity relative to the initial value. Fitting of the data, using a one-phase exponential decay, enabled the estimation of an inactivation rate of N_2OR of 0.4 h^{-1} for azide, while a two-phase exponential decay was the best fit for the cyanide concentration used with two rate constants of 0.1 and 1.1 h^{-1} (Figure 6.16A).

The influence of ligand concentration on the enzymatic activity was also evaluated. In the presence of cyanide, enzymatic activity was almost undetected for a N_2OR:NaCN ratio of ~ 1:24, while in the case of azide all the concentrations tested displayed activity, but a decrease in the specific activity was observed with the increase of ligand concentration (Figure 6.16B).

These results point out that cyanide is a potent inhibitor of N_2OR, since low concentrations were used and a higher decay in the activity was observed. Furthermore, as both N_3^- and CN^-, were proven to promote copper loss, these are cases of irreversible inhibition, with the decrease of activity being due to the loss of the catalytic center.

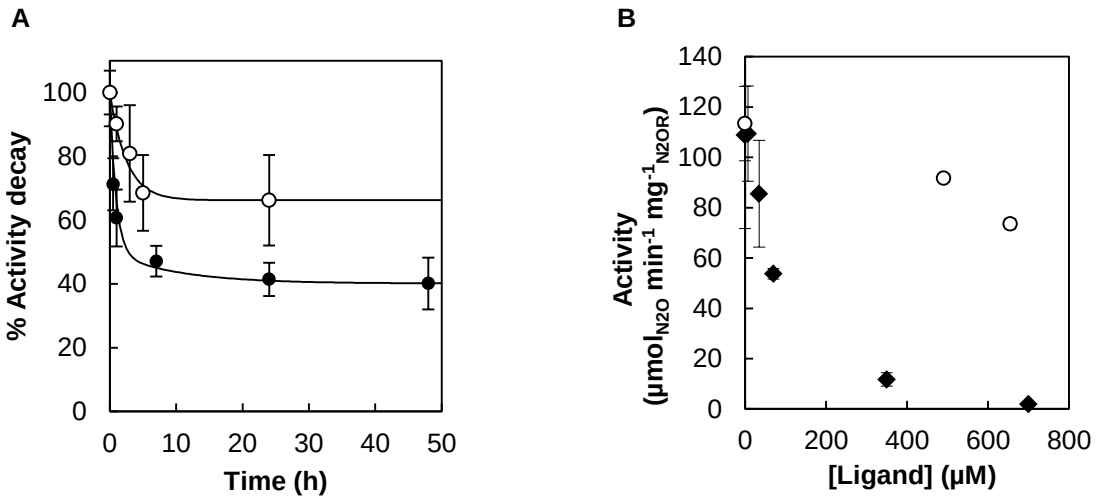

Figure 6.16 – Effect of azide (open circles) and cyanide (filled circles) on the enzymatic activity of N_2OR, with 65 % of "CuZ center" as CuZ*(4Cu1S). (A) The rate of decay of activity was measured as a function of time after addition of ligands. The azide data were best fitted to a one-phase exponential decay function with a rate constant k = 0.4 h^{-1} and cyanide data were best fitted to a two-phase exponential decay function, with two rate constants k_1 = 0.1 h^{-1} and k_2 = 1.1 h^{-1}. (B) Incubation for 48 h of N_2OR (14.8 µM) in the presence of 0, 7, 35, 70, 359 and 700 µM of cyanide (filled circles) and incubation of N_2OR (14 µM as final concentration in the assay) in the presence of 0, 491 and 655 µM of azide during 24 h (open circles).

6.4 Effect of nitric oxide on different forms of N_2OR

Nitric oxide interacts with various types of copper-containing proteins producing different effects [278], and there are studies reporting its interaction with N_2OR [130, 172].

The NO effect was investigated by titrating oxidized N_2OR, with 10 % and 50 % of "CuZ center" as CuZ*(4Cu1S), and monitoring changes in the visible spectra. Titration of N_2OR, with 50 % of "CuZ center" as CuZ*(4Cu1S), with NO concentration between 0 and 60 µM, exhibited an increase in the absorbance, especially at 640 nm (Figure 6.17A). At higher NO concentrations, perturbations at the CuA center were also observed in particular at 800 nm, but these differences might be due to its reduction. In fact, this is acceptable since no effect of NO has been previously reported on the CuA center of C*c*O [278].

An apparent dissociation constant of 8.0 ± 0.5 µM was determined at 640 nm demonstrating a high affinity of NO to N_2OR, when compared with the halides previously studied (Figure 6.17B).

In the case of a sample of N_2OR mainly with CuZ(4Cu2S), a sharp decrease in the absorbance at 550 nm was observed upon NO addition (in the range of 0 to 60 µM), suggesting that NO strongly perturbs the CuZ(4Cu2S) center (Figure 6.17C). Moreover, at the end of the titration, an emergence of an absorption band at 634 nm is observed suggesting the conversion of CuZ(4Cu2S) into CuZ*(4Cu1S). A decrease on the absorbance was also detected by spectroscopic (EPR and UV-visible) studies performed with *P. stutzeri* N_2OR, in which the presence of NO causes the loss of the hyperfine structure in both $g_{\parallel}$ and $g_{\perp}$ regions, and when NO is in large excess the formation of a new signal was reported [130]. Furthermore, in this species, an alteration of the initial spectrum of

oxidized N_2OR mainly with CuZ(4Cu2S) was also reported, with the formation of an absorption band at approximately 630 nm [279]. This alteration appears to be reversible to the initial form, CuZ(4Cu2S) upon air oxidation [279]. Interestingly, Frunzke *et al*. also state that the presence of NO in the CuZ(4Cu2S) form leads to a decrease in the specific activity of the enzyme, which is not re-established with the oxidation process, despite the similarity with the initial spectra [279].

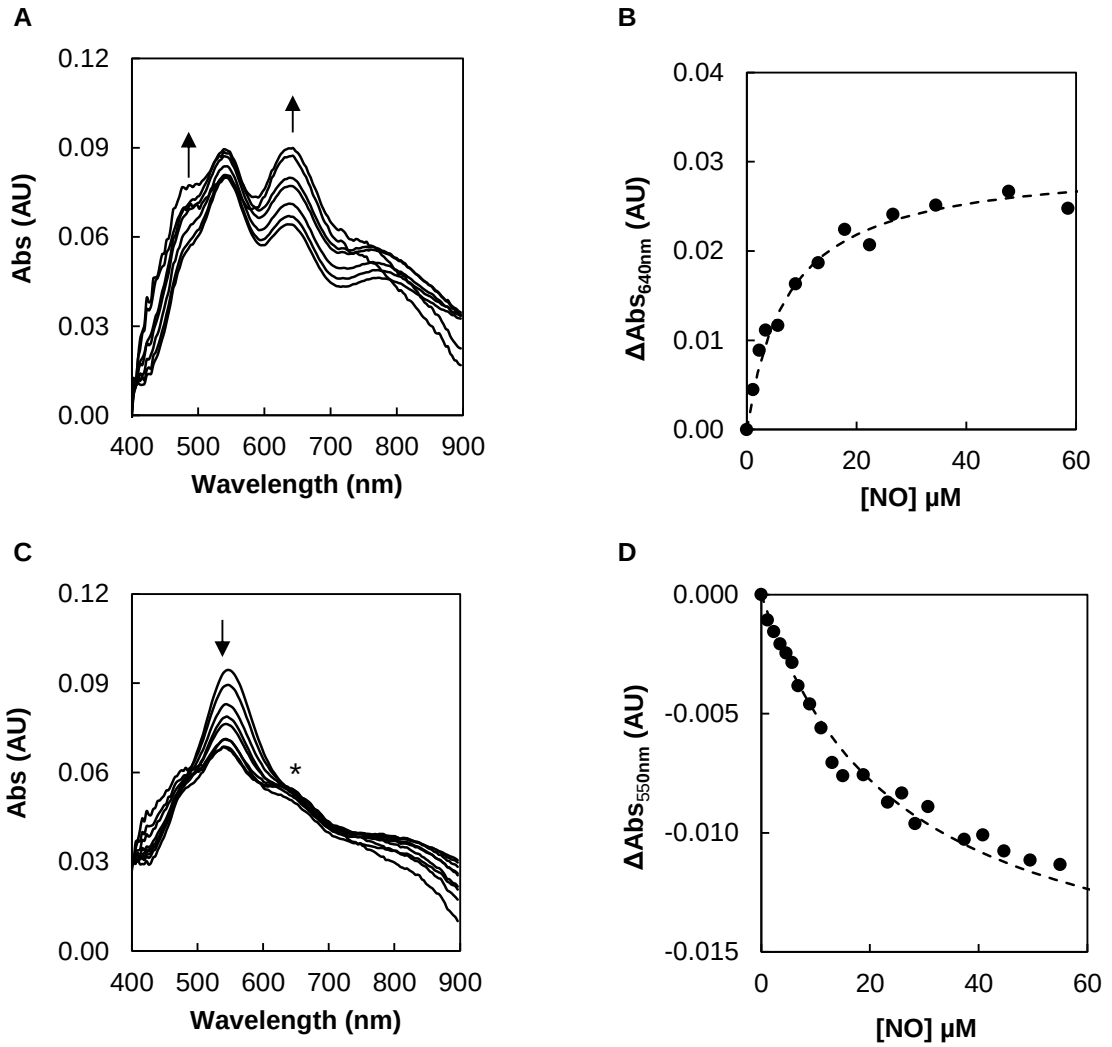

Figure 6.17 – Effect of NO titrated in the range 0 – 60 µM on the visible spectra of N_2OR. (A) N_2OR (40 µM), with 50 % of "CuZ center" as CuZ*(4Cu1S) was titrated with nitric oxide. (B) Dependence of spectral differences at 640 nm as a funtion of NO concentration. Data were fitted to a one binding site equation, and K_d^{app} of 8.0 ± 0.5 µM was determined. (C) Titration of N_2OR (18 µM), with 10 % of "CuZ center" as CuZ*(4Cu1S) with NO. (D) Dependence of spectra differences at 550 nm. Data were fitted to a one binding site equation and a K_d^{app} of 25 ± 1µM was determined. The arrows indicate spectral changes with the incubation time and the asterisk marks the appearance of a new band at 620 nm.

As no major perturbation was detected in the CuA center features, the absorbance difference at 550 nm was plotted as a function of NO concentration (Figure 6.17D). One binding site equation was used for the fitting, and an apparent binding constant of 25 ± 1 µM was estimated.

Our results indicate that NO is able to interact with both forms of "CuZ center" of N_2OR, which is in accordance with previously reported findings in *P. stutzeri* N_2OR [172]. However, the affinity of

this molecule for the CuZ*(4Cu1S) center is 3-times higher relative to the other form of "CuZ center", which is probably due to the availability of a labile coordinating position between Cu_I and Cu_{IV} on CuZ*(4Cu1S) center.

A sample of reduced N_2OR, with 10 % of "CuZ center" as CuZ*(4Cu1S) was also titrated with NO at similar concentrations as the other NO titrations. A small decrease in the absorbance intensity at 660 nm was observed (Figure 6.18A). Although such small variations are difficult to fit, a K_d^{app} of 25 ± 2 µM was estimated, which is identical to the one determined with oxidized CuZ(4Cu2S). These results indicating that NO affinity for the CuZ(4Cu2S) do not depend on the oxidation state of the center (Figure 6.18B).

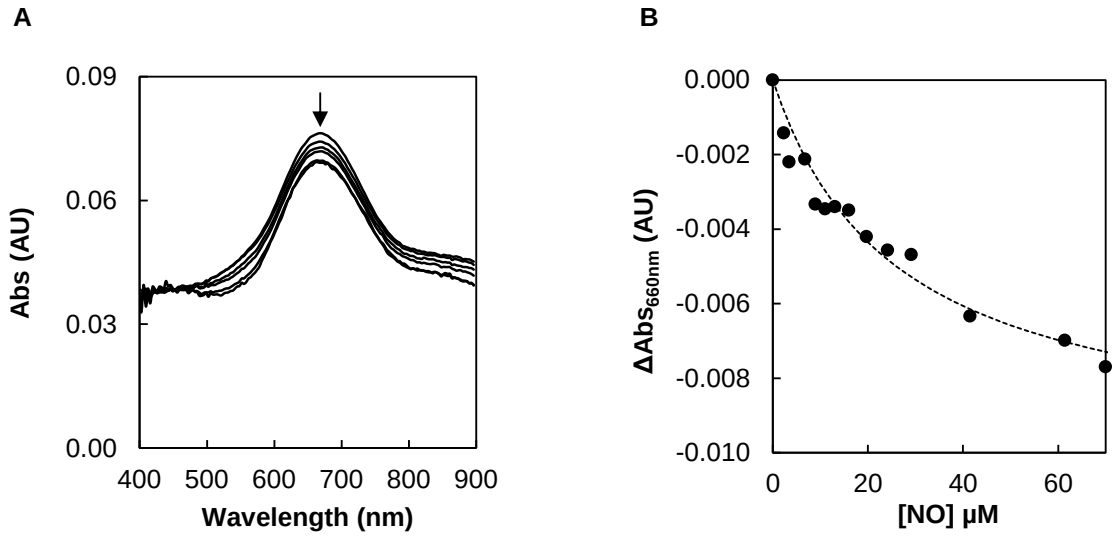

Figure 6.18 – Titration of N_2OR with NO, in the range 0 – 70 µM, followed by visible spectroscopy. (A) Titration of reduced N_2OR (18 µM), with 10 % of "CuZ center" as CuZ*(4Cu1S) with NO. (B) Dependence of spectra differences at 660 nm. Data were fitted to a one binding site equation and a K_d^{app} of 25 ± 2 µM was estimated. The arrows indicate spectral changes with the incubation time.

The effect of NO binding was also investigated as a function of time. The visible spectra of N_2OR, with 80 % of "CuZ center" as CuZ*(4Cu1S) in the presence of a 2.5-fold excess of NO was monitored for 48 h (Figure 6.19A). The main effects were detected at the CuA center features and no changes in the absorbance at 640 nm were observed. However, note that in this experiment only a small excess of NO over the protein was used.

Copper per protein (monomer) ratio was determined before (4.4 ± 0.2) and after 48 h of NO incubation (4.4 ± 0.1), showing that there were no copper losses after the reactivity of NO with this form of N_2OR, under the conditions used.

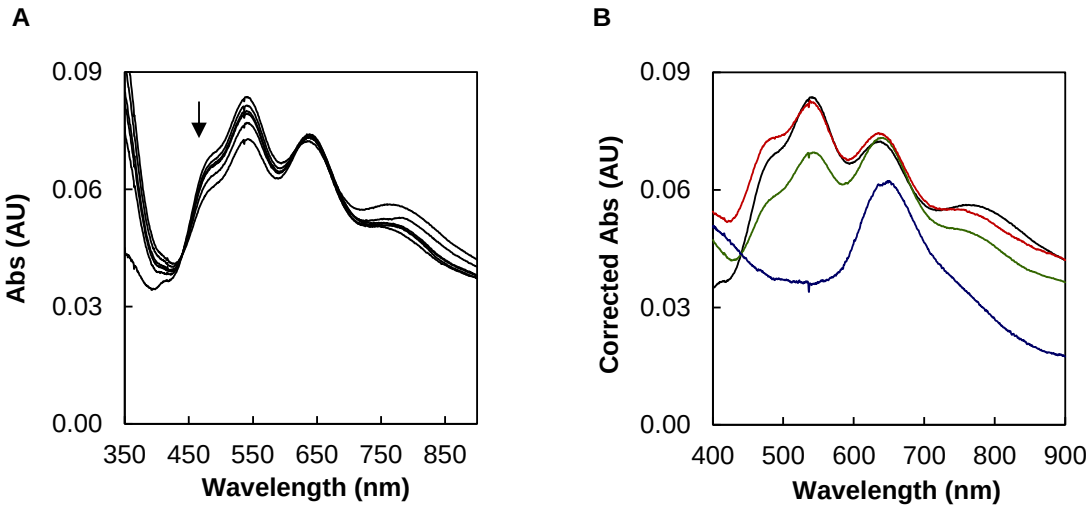

Figure 6.19 – Effect of nitric oxide (2.5-fold excess) on the visible spectra of 16 µM N_2OR, with 80 % of "CuZ center" as CuZ*(4Cu1S). (A) Changes in the visible spectra after 0, 3, 5, 8, 23 and 48 h. The arrow indicates the changes in the spectra with increasing incubation time. (B) The visible spectra of purified N_2OR (black), NO-incubated during 48 h (green), reduction of inhibited N_2OR by sodium dithionite (blue) and oxidation of inhibited N_2OR (red) are represented, being the absorbance corrected for the concentration of protein by modified Lowry method.

Oxidation and reduction of the NO-N_2OR complex were performed and the excess of reducing agents were removed by washing the sample 3 times with buffer. The results show that the perturbations observed during the incubation time, in the presence of 40 µM of NO, are reversible as the re-oxidation of the complex formed has a very similar spectrum as the initial oxidized N_2OR (Figure 6.19B). In addition, upon sodium dithionite reduction of NO-complex a band with a maximum at 640 nm was observed, indicating that CuZ*(4Cu1S) is intact under these conditions and no other species were formed (Figure 6.19B).

These results are in line with the EPR studies reported, as a new species was only observed in the presence of a high concentrations of NO [130].

Preliminary studies on the effect of this molecule on the specific activity of the enzyme suggested an inhibition, as the specific activity decreases, however further studies to determine the inhibition mechanism and also a K_i are needed.

6.5 Effect of EGTA, calcium and sulfide addition on the specific activity of N_2OR

The influence of EGTA, calcium and sulfide were tested on the enzymatic activity of N_2OR. N_2OR, with 50 % of "CuZ center" as CuZ*(4Cu1S), was incubated anaerobically for 5 h with 2 mM of calcium chloride or 6 h with 2 mM EGTA, followed by reduction in the presence of reduced methyl viologen. While the sample incubated with calcium retained 61 % of its initial activity, EGTA treated N_2OR retained only 15 %. In fact, previous assays in the presence of EGTA also reported copper loss [89]. Calcium, on the other hand, appears to have an effect on the enzyme

activity, however at the concentrations used only small differences in the spectrum were observed (data not shown).

Effect of sulfide on the enzymatic activity was also investigated through activation of N_2OR with reduced methyl viologen followed by incubation of the enzyme with equimolar amount of Na_2S, as well as 10 and 100 fold-excess of Na_2S, during 250 min (Figure 6.20). Our results showed that neither the amount of sulfide used nor the incubation time caused changes in the specific activity of the enzyme. Moreover, incubation of N_2OR with 100-fold excess of Na_2S before activation of the enzyme also does not seem to affect its specific activity. These results are in accordance with similar effects reported for *P. denitrificans* N_2OR treated with other sulfur-directed compounds (such as DTT and 2-Mercaptoethanol), in which it was reported a lack of effect on N_2OR [89]. Indeed, we can postulate that sulfur compounds are not very reactive with CuZ*(4Cu1S) center and the use of sulfide to convert CuZ*(4Cu1S) in CuZ(4Cu2S) can be a very challenging reaction.

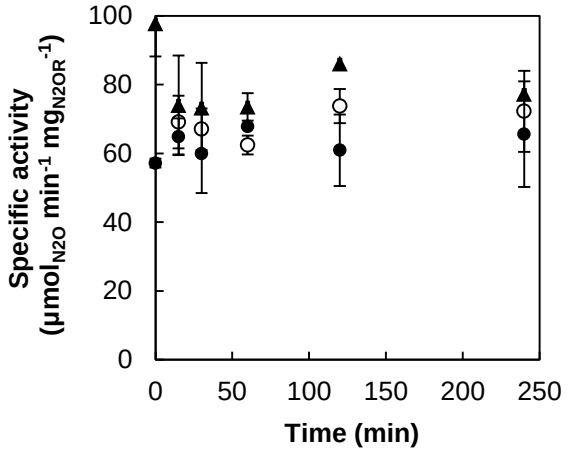

Figure 6.20 – Effect of sulfide on the enzymatic activity of N_2OR, with 50 % of "CuZ center" as CuZ*(4Cu1S). Different N_2OR:Na_2S ratios were investigated: 1:1 (filled circles), 1:10 (open circles) and 1:100 (filled triangles).

6.6 Conclusions

In this Chapter we have studied the binding of small molecules and their effects on N_2OR. The reactivity of some of them towards N_2OR was identified in previous studies, and our results and those previously reported are summarized in Table 6.4.

Table 6.4 – Summary of the effects of exogenous ligands on N_2OR. The different oxidation states of the four copper atoms in the "CuZ center" are presented together with their spectroscopic features.

Oxidation state	Ligand	Visible spectra	EPR	Ref.
$*[1Cu^{2+}: 3Cu^{1+}:S]^{3+}$	N_3^-	Decrease at 540 and 630 nm, new band at 375 nm		130, 172
$[2Cu^{2+}: 2Cu^{1+}:2S]^{2+}$ $*[1Cu^{2+}: 3Cu^{1+}:S]^{3+}$	N_3^-	Decrease at 400-800 nm	New lines at low-field	This work, 130, 172, 173, 280
$[2Cu^{2+}: 2Cu^{1+}:2S]^{2+}$	CN^-	Vanishing at 480 and 540 nm, new weak band at 640 nm	$g_{\parallel} = 2.25$, $g_{\perp} = 2.05$	130, 173
$*[1Cu^{2+}: 3Cu^{1+}:S]^{3+}$	CN^-	Bleaching absorbance in the visible region		This work
$[1Cu^{2+}: 3Cu^{1+}:2S]^{1+}$	CN^-	Loss of 640 nm band	Little hyperfine structure	157
$[2Cu^{2+}: 2Cu^{1+}:2S]^{2+}$	NO	Decrease at 550 nm, increase at 640 nm, new band at 345 nm	Loss of hyperfine lines, $g_{\parallel} = 2.25$; $g_{\perp} = 2.05$, $A_{\parallel} = 15.0$ mT	130, 172, 173
$[1Cu^{2+}: 3Cu^{1+}:2S]^{1+}$	NO	Decrease at 550 nm, increase at 640 nm	Two lines at lower field	130, 173 This work
$[2Cu^{2+}: 2Cu^{1+}:2S]^{2+}$	H_2O_2	Transient species, decrease of 640 nm	$g_{\parallel} = 2.26$, $g_{\perp} = 2.05$	130, 157
$[1Cu^{2+}: 3Cu^{1+}:2S]^{1+}$	H_2O_2	Vanishing of 640 nm band	Low-field hyperfine lines	*9*
$[2Cu^{2+}: 2Cu^{1+}:2S]^{2+}$	Cl^-	Decrease at 540 nm		172 This work
$*[1Cu^{2+}: 3Cu^{1+}:S]^{3+}$	Cl^-	Increase at 640 nm		This work
$[2Cu^{2+}: 2Cu^{1+}:2S]^{2+}$	Br^-	Decrease at 550 nm		This work
$[2Cu^{2+}: 2Cu^{1+}:2S]^{2+}$	F^-	No changes	Loss of hyperfine lines	89, 130 This work
$*[1Cu^{2+}: 3Cu^{1+}:S]^{3+}$	F^-	Decrease at 640 nm	—	This work
$[2Cu^{2+}: 2Cu^{1+}:2S]^{2+}$	CO	Decrease at 540 nm, new band at 660 nm	$A_{\parallel} = 2.4$ mT	173
$*[1Cu^{2+}: 3Cu^{1+}:S]^{3+}$ $[2Cu^{2+}: 2Cu^{1+}:2S]^{2+}$	I^-	Adduct formation at 650 nm	Two lines at lower field $g_{\parallel} = 2.24$, $g_{\perp} = 2.04$,	151 This work

Note: Oxidation states marked with (*) correspond to "CuZ center" as CuZ*(4Cu1S).

Some of these ligands exhibited interesting properties and the formation of new species with the active site was probably due to a ligand-metal complex formation.

Comparison between binding of halides to N_2OR was reported here for the first time. The reactivity of these small ions of the 17 group of the periodic table (fluoride, chloride, bromide and iodide) to different forms of N_2OR was investigated and our results indicate that their binding cannot be simply explained by the size of the anion. Furthermore, all the apparent binding constants determined for halides interaction with N_2OR were in the mM range, evidencing a low affinity, independent of the form of the "CuZ center" of N_2OR. From the four halides tested, iodide presented the most interesting effect since it was the only one that clearly showed the formation of a new species. This blue adduct was observed with CuZ(4Cu2S) and CuZ*(4Cu1S) forms of the active site, having very similar spectroscopic properties. Furthermore, the thermostability studies

exhibited similar denaturation temperatures not only between different forms of the enzyme but also in the iodide incubated samples. Such observations lead us to hypothesize a possible displacement of sulfur in CuZ(4Cu2S) by iodide binding, though activity of the enzyme does not seem to be affected.

Incubation of N_2OR with cyanide and azide exhibits an identical effect on the copper centers, as they caused the complete destruction of the center, and thus the mode of action of these molecules is not relevant for the substrate binding mechanism.

Nitric oxide, on the other hand, is more analogous to the substrate of the enzyme, which is in accordance with the apparent binding constants determined, that evidenced a high affinity of this molecule to the tetranuclear copper site. Indeed, the K_d^{app} determined (8.0 ± 0.5 µM), for a N_2OR with 50 % of "CuZ center" as CuZ*(4Cu1S), is about 5000-times lower than iodide binding (K_d^{app} = 40 ± 2 mM). Prospective studies of the influence of this molecule on the specific activity of N_2OR are still needed.

Chapter 7

Conclusions and Future Perspectives

7 Conclusions and Future Perspectives

For decades, N_2OR has been studied not only because of its essential and almost exclusive biological role in N_2O detoxification, but also due to its unique and complex catalytic center, making this project extremely challenging in the field of bioinorganic.

The work described in this thesis focused on the effect of pH on denitrification pathway and on isolated N_2OR, as well as on insights into the reactivity of the catalytic site of N_2OR. The main aims were to understand the environmental acidification linked to N_2O emissions and to clarify the catalytic mechanism of N_2OR during the reduction of its substrate, nitrous oxide.

Precious information relative to the denitrification pathway on the model organism *M. hydrocarbonoclasticus* was addressed through genome analysis, which showed that genes encoding to catalytic subunits of the denitrification enzymes, as well as accessory genes encoding proteins involved in the maturation of the enzymes are clustered together, which is uncommonly observed in denitrifiers.

The effect of pH on the denitrification pathway of *M. hydrocarbonoclasticus* was elucidated through controlled growth performed in a bioreactor (pH 6.5, 7.5 and 8.5). Under these different growth conditions transcriptomic analysis of denitrification genes was performed, showing that at low pH *nirS* gene expression, encoding cd_1NiR, was affected. Low cd_1NiR production, caused by acidic pH, explains the high nitrite levels that remained in the medium throughout the growth.

In addition, the ability of the whole-cells to reduce external NO and N_2O was analyzed at different pH values. The reduction rates profile observed at low pH was quite interesting as even though nitrite was not totally consumed at this acidic pH values, possibly as a consequence of low *nirS* expression and also nitrite reductase inactivation, NO was probably chemically produced as there was induction of *nor* genes. However, the whole-cells grown at more acidic pH were not able to reduced external N_2O.

Although several aspects are still not completely understood, it was clear that complete denitrification is affected at low pH and this can explain the high levels of N_2O observed in soils and aquatic systems when a drop in pH occurs [281, 282].

In parallel, N_2OR was isolated from growths at each pH condition, and despite the lower yield of purified protein from the acidic growth, relative to the other growths under microaerobic conditions, it is remarkable that the isolated N_2OR presents “CuZ center” mainly as CuZ*(4Cu1S), which has a high specific activity after activation. By opposition, from more neutral growth conditions, N_2OR was isolated with “CuZ center” mainly as CuZ(4Cu2S), which is a form of the enzyme with a very low specific activity *in vitro*, and up-to-now no activation mechanism has been identified. Growth conditions and purification strategies were established and constitute important advances in obtaining more homogeneous N_2OR preparations.

Interestingly, N_2OR isolated from these different growth conditions evidenced differences in the kinetic reactivity with the redox physiological electron donor, cytochrome c_{552} as we demonstrated that N_2O catalysis mediated through this electron donor is faster for the N_2OR with "CuZ center" mainly as CuZ*(4Cu1S) in its fully reduced state than using the reduced form of the CuZ(4Cu2S). These results also show that cytochrome c_{552} mediated reduction of N_2O *in vitro* does not justify the reduction rate of external N_2O by the whole-cells. This provided clues for the existence *in vivo* of an additional still unknown mechanism involving other proteins in the activation of N_2OR or even the formation of a supramolecular complex, as observed in *P. aeruginosa* [180], in the catalysis of N_2O.

In Chapter 4, the structural characterization and the redox behavior of both forms of the "CuZ center", CuZ*(4Cu1S) and CuZ(4Cu2S) were reported.

One of the challenges of this thesis was to obtain structural information of the different forms of the enzyme. In fact, progress from the only deposited structure of N_2OR from *M. hydrocarbonoclasticus* [126] was made and two additional structures were successfully obtained. These structures differ in their "CuZ center", with one having mainly CuZ*(4Cu1S) and solved at 2.4 Å, while the other presents CuZ(4Cu2S) in the reduced form and was solved at 1.9 Å. Comparison between these structures clearly evidenced a well-fitted second sulfur on the "CuZ center" of the higher resolution structure, similar to the previously reported *P. stutzeri* N_2OR structure, with "CuZ center" mainly as CuZ(4Cu2S) [152].

Another aspect of the dissimilarities between both forms of "CuZ center" lies on their completely different redox behavior, which was studied here through potentiometric and electrochemical methods. Reduction potentials of + 272 ± 10 mV and + 65 ± 10 mV *vs* SHE were determined by potentiometry for CuA and CuZ(4Cu2S) centers, respectively, at pH 7.6. The pH dependence on CuA center reduction potential indicates coupling of protonation to reduction behavior. A different behavior is observed for the CuZ(4Cu2S) reduction potential with pH, as a hysteresis was observed (except for the potentiometric titration performed at pH 7.6). The reduction potentials of the reductive titration can be analyzed considering a $1e^-/H^+$ coupled transfer mechanism, while in the oxidative direction no changes were observed on the reduction potential between pH 6.5 and pH 9.0 (~ 60 mV), which can be due to the presence of ionizable groups on the vicinity of "CuZ center", K447 that stabilizes the thiolate edge ligand in the reduced form and at low pH it is proposed that protonation of a histidine side chain that coordinates one of the copper atoms of "CuZ center" influences its redox properties.

Direct electrochemistry was used for the first time to characterize N_2OR. Two signals were detected at E°' = 385 ± 5 mV and E = + 70 ± 6 mV (*vs* SHE, at pH 7.0), and assigned to CuA and CuZ(4Cu2S) centers, respectively, although a slightly deviation relative to the potentiometric results was observed for the reduction potential of the CuA center. The pH dependence of reduction

potentials of CuA and CuZ(4Cu2S) centers analyzed by direct electrochemistry, showed a $1e^-/1H^+$ coupled mechanism for both centers.

The reactivity of N_2OR with exogenous ligands that usually can form complexes with other copper proteins was described in Chapter 6.

The titration of N_2OR with different halides proved that not all the ligands are able to interact with "CuZ center" and the most interesting effects on the visible spectrum were observed by iodide binding, which showed higher affinity for the reduced state of CuZ(4Cu2S) (K_d^{app} = 20 ± 2 mM). Interestingly, the spectra of iodide interacting with N_2OR, independently of the oxidation state of the centers, exhibited the formation of a blue adduct.

The first thermal stability of the holo-N_2OR was reported here, with two transitions being observed with a T_m of 51 ºC and 58 ºC, which did not show variation in the presence of 500-fold excess of potassium iodide.

The action of cyanide and azide ions towards the enzyme proved that copper centers were destroyed in their presence.

Another interesting effect was observed in the presence of nitric oxide. This ligand has a high affinity for the resting CuZ*(4Cu1S), with a K_d^{app} of 8.0 ± 0.5 µM being estimated. As proved, this ligand did not induce destruction of the copper centers and a promising NO-inhibited complex might be formed.

In Chapter 5, the catalytic mechanism of N_2OR was reviewed based on the current knowledge of the intervening species. The catalytically competent intermediate species, CuZº, observed from the direct reaction of the enzyme with a stoichiometric amount of N_2O was recently spectroscopically characterized and here its behavior with pH was established. At pH > 9.5 CuZ° is not formed, which we assigned to be due to K447 deprotonation, essential to stabilize CuZ° species. On the contrary, CuZ° decay is not pH dependent indicating that the species formed is most probably not stabilized by the nearby lysine.

In this study, it is reported for the first time the formation of CuZ', an intermediate species obtained upon oxidation of fully reduced CuZ*(4Cu1S) when low amounts of N_2O are present. This CuZ' species has a maximum absorption band at 617 nm and has its "CuZ center" in the [$1Cu^{2+}$-$3Cu^{1+}$] oxidation state, which cannot be easily oxidized or reduced. Although CuZ' species is not part of the catalytic cycle its formation opens new questions regarding its role.

Important new insights into the catalytic cycle were attained, as we proved that reduction of CuZº species to the fully reduced state [$4Cu^{1+}$] by sodium ascorbate occurs through IET from CuA center. This electron transfer occurs at a rate 10^4 faster than IET in the bimolecular reduction of CuA center in a N_2OR with "CuZ center" mainly as CuZ*(4Cu1S). The result obtained evidenced that an electron donor with a more positive reduction potential (in comparison to methyl viologen,

which reduction potential is most probably unattainable in the *M. hydrocarbonoclasticus* periplasm) is able to reduce CuZ° species, strengthening the relevance of the proposed mechanism.

Progresses in the understanding of denitrification pathway and the mechanism of the enzyme have been accomplished. Since there are some aspects that remain to be unravelled and are fundamental to be addressed, our future perspectives relative to this work are expressed below.

Future Perspectives

At the physiological level, many questions still remain to be answered such as:

i) Why is the reduction of N_2O by whole-cells affected by a slight drop of the pH?;

ii) Why the enzyme isolated from growths performed at low pH exhibits higher specific activity *in vitro*?;

iii) Which molecular mechanism in the cell is affected by pH to induce the formation of CuZ*(4Cu1S) as the main form of "CuZ center" in the isolated enzyme?

It is imperative to address these questions to better understand the role of the different forms of the enzyme and their catalytic mechanisms.

In the future, it would be interesting to test the activity of the enzyme containing "CuZ center" as CuZ(4Cu2S) in the presence of other proteins of the *nos* cluster. A more comprehensive proteomic study involving the periplasmic proteins and their identification by mass spectrometry, could provide a detailed analysis of the possible formation of a complex at more neutral pH values.

New electrochemical approaches, as the deposition of protein on self-assembled monolayers, might be fundamental for the determination of CuZ*(4Cu1S) potential, that until now has been difficult to be accomplished. The reduction potential of CuZ^o must also be determined, since we preview a positive potential for this form and in fact this species might have relevance *in vivo*.

Several aspects regarding the catalysis *in vivo* remain unanswered and several studies are still needed to understand the mechanism of reactivity of CuZ(4Cu2S) with N_2O, as the physiologic relevance of this form was pointed out. Up-to-now no activation mechanism for this form of the enzyme has been proposed, thus we hypothesized that this is a protective form of the enzyme and a displacement of the sulfur might be required for N_2O binding. In the future, it is imperative to explore the mechanism involved in CuZ(4Cu2S) activation, through spectroscopic and kinetic techniques.

Further studies on the kinetic interaction of N_2OR with nitric oxide are essential to understand if the inhibition occurs and identify the type of inhibition. Pressurization of different forms of crystals with NO and N_2O could be a key to understand the interaction of "CuZ center" and the substrate.

References

References

1. Rudolf, M.; Kroneck, P. M. H., The Nitrogen Cycle: Its Biology. In *Metal ions in Biological systems: Biogeochemical cycles of elements*, Sigel, A.; Sigel, H.; Sigel, R. K. O., Eds. Taylor & Francis Group: **2005,** pp 75-104.
2. Galloway, J. N.; Dentener, F. J.; Capone, D. G.; Boyer, E. W.; Howarth, R. W.; Seitzinger, S. P.; Asner, G. P.; Cleveland, C. C.; Green, P. A.; Holland, E. A.; Karl, D. M.; Michaels, A. F.; Porter, J. H.; Townsend, A. R.; Vorosmarty, C. J., Nitrogen Cycles: Past, Present, and Future. *Biogeochem.* **2004,** *70*, 153–226.
3. Thomson, A. J.; Giannopoulos, G.; Pretty, J.; Baggs, E. M.; Richardson, D. J., Biological sources and sinks of nitrous oxide and strategies to mitigate emissions. *Philos. Trans. R. Soc. Lond. B Biol. Sci.* **2012,** *367*, 1157-1168.
4. Cabello, P.; Roldán, M. D.; Moreno-Vivián, C., Nitrate reduction and the nitrogen cycle in archaea. *Microbiol.* **2004,** *150*, 3527-3546.
5. Bothe, H.; Ferguson, S. J.; Newton, W. E., *Biology of the Nitrogen Cycle*. Elsevier: Amsterdam, **2**007, pp 1-20.
6. Moura, I.; Maia, L. B.; Pauleta, S. R.; Moura, J. J. G., A bird's eye view of denitrification in relation to the nitrogen cycle. In *Metalloenzymes in Denitrification: Applications and Environmental Impacts 2017*, RSC: **2017**, pp 1-10.
7. Moreno-Vivián, C.; Cabello, P.; Martínez-Luque, M.; Blasco, R.; Castillo, F., Prokaryotic nitrate reduction: molecular properties and functional distinction among bacterial nitrate reductases. *J. Bacteriol.* **1999,** *181*, 6573-6584.
8. Lin, J. T.; Stewart, V., Nitrate assimilation by bacteria. *Adv. Microb. Physiol.* **1998,** *39*, 1-30.
9. Koops, H.-P.; Pommerening-Röser, A., Distribution and ecophysiology of the nitrifying bacteria emphasizing cultured species. *FEMS Microbiol. Ecol.* **2001,** *37*, 1-9.
10. Simon, J., Enzymology and bioenergetics of respiratory nitrite ammonification. *FEMS Microbiol. Rev.* **2002,** *26*, 285–309.
11. Jetten, M. S. M.; Strous, M.; van de Pas-Schoonen, K. T.; Schalk, J.; van Dongen, U. G. J. M.; van de Graaf, A. A.; Logemann, S.; Muyzer, G.; van Loosdrecht, M. C. M.; Kuenen, J. G., The anaerobic oxidation of ammonium. *FEMS Microbiol. Rev.* **1998,** *22*, 421–437.
12. Strous, M.; Fuerst, J. A.; Kramer, E. H.; Logemann, S.; Muyzer, G.; van de Pas-Schoonen, K. T.; Webb, R.; Kuenen, J. G.; Jetten, M. S., Missing lithotroph identified as new planctomycete. *Nature* **1999,** *400*, 446-449.
13. Kartal, B.; Maalcke, W. J.; de Almeida, N. M.; Cirpus, I.; Gloerich, J.; Geerts, W.; Op den Camp, H. J.; Harhangi, H. R.; Janssen-Megens, E. M.; Francoijs, K. J.; Stunnenberg, H. G.; Keltjens, J. T.; Jetten, M. S.; Strous, M., Molecular mechanism of anaerobic ammonium oxidation. *Nature* **2011,** *479*, 127-130.
14. *IPCC 2007 Working group I: the physical science basis*; Cambridge University Press: Cambridge, **2007**.
15. Ravishankara, A. R.; Daniel, J. S.; Portmann, R. W., Nitrous oxide (N_2O): The dominant ozone-depleting substance emitted in the 21st century. *Science* **2009,** *326*, 123-125.
16. Fowler, D.; Coyle, M.; Skiba, U.; Sutton, M. A.; Cape, J. N.; Reis, S.; Sheppard, L. J.; Jenkins, A.; Grizzetti, B.; Galloway, J. N.; Vitousek, P.; Leach, A.; Bouwman, A. F.; Butterbach-Bahl, K.; Dentener, F.; Stevenson, D.; Amann, M.; Voss, M., The global nitrogen cycle in the twenty-first century. *Philos. Trans. R. Soc. Lond. B Biol. Sci.* **2013,** *368*, 20130164.
17. Wuebbles, D. J., Atmosphere. Nitrous oxide: no laughing matter. *Science* **2009,** *326*, 56-57.
18. Richardson, D.; Felgate, H.; Watmough, N.; Thomson, A.; Baggs, E., Mitigating release of the potent greenhouse gas N_2O from the nitrogen cycle - could enzymic regulation hold the key? *Trends Biotechnol.* **2009,** *27*, 388-397.
19. Smith, P.; Martino, D.; Cai, Z.; Gwary, D.; Janzen, H.; Kumar, P.; McCarl, B.; Ogle, S.; O'Mara, F.; Rice, C.; Scholes, B.; Sirotenko, O.; Howden, M.; McAllister, T.; Pan, G.; Romanenkov, V.; Schneider, U.; Towprayoon, S.; Wattenbach, M.; Smith, J., Greenhouse gas mitigation in agriculture. *Philos. Trans. R. Soc. Lond. B Biol. Sci.* **2008,** *363*, 789-813.

20. Zumft, W. G.; Kroneck, P. M., Respiratory transformation of nitrous oxide (N_2O) to dinitrogen by Bacteria and Archaea. *Adv. Microb. Physiol.* **2007,** *52*, 107-227.
21. Zumft, W. G., Cell biology and molecular basis of denitrification. *Microb. Mol. Biol. Rev.* **1997,** *61*, 533-616.
22. Heylen, K.; Keltjens, J., Redundancy and modularity in membrane-associated dissimilatory nitrate reduction in Bacillus. *Front. Microbiol.* **2012,** *3*, 1-27.
23. Bell, L. C.; Richardson, D. J.; Ferguson, S. J., Periplasmic and membrane-bound respiratory nitrate reductases in *Thiosphaera pantotropha*. The periplasmic enzyme catalyzes the first step in aerobic denitrification. *FEBS Lett.* **1990,** *265*, 85-87.
24. Pauleta, S. R.; Dell'Acqua, S.; Moura, I., Nitrous oxide reductase. *Coord. Chem. Rev.* **2013,** *257*, 332-349.
25. Ghiglione, J. F.; Philippot, L.; Normand, P.; Lensi, R.; Potier, P., Disruption of *narG*, the gene encoding the catalytic subunit of respiratory nitrate reductase, also affects nitrite respiration in *Pseudomonas fluorescens* YT101. *J. Bacteriol.* **1999,** *181*, 5099-5102.
26. Gates, A. J.; Hughes, R. O.; Sharp, S. R.; Millington, P. D.; Nilavongse, A.; Cole, J. A.; Leach, E. R.; Jepson, B.; Richardson, D. J.; Butler, C. S., Properties of the periplasmic nitrate reductases from *Paracoccus pantotrophus* and *Escherichia coli* after growth in tungsten-supplemented media. *FEMS Microbiol Lett.* **2003,** *220*, 261-269.
27. Jüngst, A.; Braun, C.; Zumft, W. G., Close linkage in *Pseudomonas stutzeri* of the structural genes for respiratory nitrite reductase and nitrous oxide reductase, and other essential genes for denitrification. *Mol. Gen. Genet.* **1991,** *225*, 241-248.
28. Cantera, J. J.; Stein, L. Y., Molecular diversity of nitrite reductase genes (*nirK*) in nitrifying bacteria. *Environ. Microbiol.* **2007,** *9*, 765-776.
29. Nojiri, M.; Xie, Y.; Inoue, T.; Yamamoto, T.; Matsumura, H.; Kataoka, K.; Deligeer; Yamaguchi, K.; Kai, Y.; Suzuki, S., Structure and function of a hexameric copper-containing nitrite reductase. *Proc. Natl. Acad. Sci.***2007,** *104*, 4315-4320.
30. Ellis, M. J.; Grossmann, J. G.; Eady, R. R.; Hasnain, S. S., Genomic analysis reveals widespread occurrence of new classes of copper nitrite reductases. *J. Biol. Inorg. Chem.* **2007,** *12*, 1119-1127.
31. Arai, H.; Igarashi, Y.; Kodama, T., Expression of the nir and nor genes for denitrification of *Pseudomonas aeruginosa* requires a novel CRP/FNR-related transcriptional regulator, DNR, in addition to ANR. *FEBS Lett.* **1995,** *371*, 73-76.
32. Hendriks, J.; Oubrie, A.; Castresana, J.; Urbani, A.; Gemeinhardt, S.; Saraste, M., Nitric oxide reductases in bacteria. *Biochim. Biophys. Acta* **2000,** *1459*, 266–273.
33. Cramm, R.; Pohlmann, A.; Friedrich, B., Purification and characterization of the single-component nitric oxide reductase from *Ralstonia eutropha* H16. *FEBS Lett.* **1999,** *460*, 6-10.
34. Suharti; Heering, H. A.; de Vries, S., NO reductase from *Bacillus azotoformans* is a bifunctional enzyme accepting electrons from menaquinol and a specific endogenous membrane-bound cytochrome c_{551}. *Biochemistry* **2004,** *43*, 13487-13495.
35. Viebrock, A.; Zumft, W. G., Molecular cloning, heterologous expression, and primary structure of the structural gene for the copper enzyme nitrous oxide reductase from denitrifying *Pseudomonas stutzeri*. *J. Bacteriol.* **1988,** *170*, 4658-4668.
36. Simon, J.; Oliver, E.; Kroneck, P. M. H.; Zumft, W. G., The unprecedented nos gene cluster of *Wolinella succinogenes* encodes a novel respiratory electron transfer pathway to cytochrome *c* nitrous oxide reductase. *FEBS lett.* **2004,** *569*, 7-12.
37. González, P. J.; Correia, C.; Moura, I.; Brondino, C. D.; Moura, J. J., Bacterial nitrate reductases: Molecular and biological aspects of nitrate reduction. *J. Inorg. Biochem.* **2006,** *100*, 1015-1023.
38. Lanciano, P.; Vergnes, A.; Grimaldi, S.; Guigliarelli, B.; Magalon, A., Biogenesis of a respiratory complex is orchestrated by a single accessory protein. *J. Biol. Chem.* **2007,** *282*, 17468-17474.
39. Jormakka, M.; Richardson, D.; Byrne, B.; Iwata, S., Architecture of NarGH reveals a structural classification of Mo-bisMGD enzymes. *Structure* **2004,** *12*, 95-104.

40. Sparacino-Watkins, C.; Stolz, J. F.; Basu, P., Nitrate and periplasmic nitrate reductases. *Chem. Soc. Rev.* **2014,** *43*, 676-706.
41. Dias, J. M.; Than, M. E.; Humm, A.; Huber, R.; Bourenkov, G. P.; Bartunik, H. D.; Bursakov, S.; Calvete, J.; Caldeira, J.; Carneiro, C.; Moura, J. J.; Moura, I.; Romão, M. J., Crystal structure of the first dissimilatory nitrate reductase at 1.9 Å solved by MAD methods. *Structure* **1999,** *7*, 65-79.
42. Cutruzzolà, F., Bacterial nitric oxide synthesis. *Biochim. Biophys. Acta* **1999,** *1411*, 231-249.
43. Jain, R.; Shapleigh, J. P., Characterization of *nirV* and a gene encoding a novel pseudoazurin in *Rhodobacter sphaeroides* 2.4.3. *Microbiol.* **2001,** *147*, 2505-2515.
44. Han, C.; Wright, G. S.; Fisher, K.; Rigby, S. E.; Eady, R. R.; Hasnain, S. S., Characterization of a novel copper-haem *c* dissimilatory nitrite reductase from *Ralstonia pickettii*. *Biochem. J.* **2012,** *444*, 219-226.
45. Fülöp, V.; Moir, J. W.; Ferguson, S. J.; Hajdu, J., The anatomy of a bifunctional enzyme: structural basis for reduction of oxygen to water and synthesis of nitric oxide by cytochrome cd_1. *Cell* **1995,** *81*, 369-377.
46. Kawasaki, S.; Arai, H.; Kodama, T.; Igarashi, Y., Gene cluster for dissimilatory nitrite reductase (*nir*) from *Pseudomonas aeruginosa*: sequencing and identification of a locus for heme d_1 biosynthesis. *J. Bacteriol.* **1997,** *179*, 235-242.
47. Spiro, S., Nitrous oxide production and consumption: regulation of gene expression by gas-sensitive transcription factors. *Philos. Trans. R. Soc. Lond. B Biol. Sci.* **2012,** *367*, 1213-1225.
48. Shiro, Y., Structure and function of bacterial nitric oxide reductases: nitric oxide reductase, anaerobic enzymes. *Biochim. Biophys. Acta* **2012,** *1817*, 1907-13.
49. Suharti; Strampraad, M. J.; Schröder, I.; de Vries, S., A novel copper A containing menaquinol NO reductase from *Bacillus azotoformans*. *Biochemistry* **2001,** *40*, 2632-2639.
50. Al-Attar, S.; de Vries, S., An electrogenic nitric oxide reductase. *FEBS Lett.* **2015,** *589*, 2050-2057.
51. Prendergast-Miller, M. T.; Baggs, E. M.; Johnson, D., Nitrous oxide production by the ectomycorrhizal fungi *Paxillus involutus* and *Tylospora fibrillosa*. *FEMS Microbiol. Lett.* **2011,** *316*, 31-35.
52. Takaya, N., Dissimilatory nitrate reduction metabolisms and their control in fungi. *J. Biosci. Bioeng.* **2002,** *94*, 506-510.
53. Baumann, L.; Baumann, P.; Mandel, M.; Allen, R. D., Taxonomy of aerobic marine eubacteria. *J. Bacteriol.* **1972,** *110*, 402-429.
54. Sproer, C.; Lang, E.; Hobeck, P.; Burghardt, J.; Stackebrandt, E.; Tindall, B. J., Note: Transfer of *Pseudomonas nautica* to *Marinobacter hydrocarbonoclasticus*. *Int. J. Syst. Bacteriol.* **1998,** *48*, 1445-1448.
55. Gauthier, M. J.; Lafay, B.; Christen, R.; Fernandez, L.; Acquaviva, M.; Bonin, P.; Bertrand, J. C., *Marinobacter hydrocarbonoclasticus* gen. nov., sp. nov., a new, extremely halotolerant, hydrocarbon-degrading marine bacterium. *Int. J. Syst. Bacteriol.* **1992,** *42*, 568-576.
56. Granger, J.; Ward, B. B., Accumulation of nitrogen oxides in copper-limited cultures of denitrifying bacteria. *Limnol. Oceanogr.* **2003,** *48*, 313–318.
57. Felgate, H.; Giannopoulos, G.; Sullivan, M. J.; Gates, A. J.; Clarke, T. A.; Baggs, E.; Rowley, G.; Richardson, D. J., The impact of copper, nitrate and carbon status on the emission of nitrous oxide by two species of bacteria with biochemically distinct denitrification pathways. *Environ. Microbiol.* **2012,** *14*, 1788–1800.
58. Liu, B.; Mørkved, P. T.; Frostegård, A.; Bakken, L. R., Denitrification gene pools, transcription and kinetics of NO, N_2O and N_2 production as affected by soil pH. *FEMS Microbiol. Ecol.* **2010,** *72*, 407-417.
59. Van Den Heuvel, R. N.; Bakker, S. E.; Jetten, M. S. M.; Hefting, M. M., Decreased N_2O reduction by low soil pH causes high N_2O emissions in a riparian ecosystem. *Geobiology* **2011,** *9*, 294-300.
60. Torres, M. J.; Simon, J.; Rowley, G.; Bedmar, E. J.; Richardson, D. J.; Gates, A. J.; Delgado, M. J., Nitrous oxide metabolism in nitrate-reducing bacteria: physiology and regulatory mechanisms. *Adv. Microb. Physiol.* **2016,** *68*, 353-432.

61. Arai, H.; Mizutani, M.; Igarashi, Y., Transcriptional regulation of the nos genes for nitrous oxide reductase in *Pseudomonas aeruginosa*. *Microbiol.* **2003,** *149*, 29-36.
62. Bueno, E.; Mesa, S.; Bedmar, E. J.; Richardson, D. J.; Delgado, M. J., Bacterial adaptation of respiration from oxic to microoxic and anoxic conditions: redox control. *Antioxid. Redox Signal* **2012,** *16*, 819-852.
63. Spiro, S., The FNR family of transcriptional regulators. *Antonie Van Leeuwenhoek* **1994,** *66*, 23-36.
64. Körner, H.; Sofia, H. J.; Zumft, W. G., Phylogeny of the bacterial superfamily of Crp-Fnr transcription regulators: exploiting the metabolic spectrum by controlling alternative gene programs. *FEMS Microbiol. Rev.* **2003,** *27*, 559-592.
65. Crack, J. C.; Jervis, A. J.; Gaskell, A. A.; White, G. F.; Green, J.; Thomson, A. J.; Le Brun, N. E., Signal perception by FNR: the role of the iron-sulfur cluster. *Biochem. Soc. Trans.* **2008,** *36*, 1144-1148.
66. Green, J.; Crack, J. C.; Thomson, A. J.; LeBrun, N. E., Bacterial sensors of oxygen. *Curr. Opin. Microbiol.* **2009,** *12*, 145-151.
67. Crack, J. C.; Stapleton, M. R.; Green, J.; Thomson, A. J.; Le Brun, N. E., Mechanism of [4Fe-4S](Cys)4 cluster nitrosylation is conserved among NO-responsive regulators. *J. Biol.Chem.* **2013,** *288*, 11492-11502.
68. Hugo Cruz-Ramos ; Jason Crack ; Guanghui Wu ; Martin N. Hughes ; Colin Scott ; Andrew J. Thomson ; Jeffrey Green ; Poole, R. K., NO sensing by FNR: regulation of the *Escherichia coli* NO-detoxifying flavohaemoglobin, Hmp. *EMBO J.* **2002,** *21*, 3235–3244.
69. Schreiber, K.; Krieger, R.; Benkert, B.; Eschbach, M.; Arai, H.; Schobert, M.; Jahn, D., The anaerobic regulatory network required for *Pseudomonas aeruginosa* nitrate respiration. *J. Bacteriol.* **2007,** *189*, 4310-4314.
70. Stewart, V., Biochemical Society Special Lecture. Nitrate- and nitrite-responsive sensors NarX and NarQ of proteobacteria. *Biochem. Soc. Trans.* **2003,** *31*, 1-10.
71. Moir, J. W.; Wood, N. J., Nitrate and nitrite transport in bacteria. *Cell Mol. Life Sci.* **2001,** *58*, 215-224.
72. Wood, N. J.; Alizadeh, T.; Richardson, D. J.; Ferguson, S. J.; Moir, J. W., Two domains of a dual-function NarK protein are required for nitrate uptake, the first step of denitrification in *Paracoccus pantotrophus*. *Mol. Microbiol.* **2002,** *44*, 157-170.
73. Castiglione, N.; Rinaldo, S.; Giardina, G.; Cutruzzolà, F., The transcription factor DNR from *Pseudomonas aeruginosa* specifically requires nitric oxide and haem for the activation of a target promoter in *Escherichia coli*. *Microbiol.* **2009,** *155*, 2838-2844.
74. Lee, Y. Y.; Shearer, N.; Spiro, S., Transcription factor NNR from *Paracoccus denitrificans* is a sensor of both nitric oxide and oxygen: isolation of nnr* alleles encoding effector-independent proteins and evidence for a haem-based sensing mechanism. *Microbiol.* **2006,** *152*, 1461-1470.
75. Cutruzzolà, F.; Arcovito, A.; Giardina, G.; della Longa, S.; D'Angelo, P.; Rinaldo, S., Distal-proximal crosstalk in the heme binding pocket of the NO sensor DNR. *Biometals* **2014,** *27*, 763-773.
76. Pohlmann, A.; Cramm, R.; Schmelz, K.; Friedrich, B., A novel NO-responding regulator controls the reduction of nitric oxide in *Ralstonia eutropha*. *Mol. Microbiol.* **2000,** *38*, 626-638.
77. Tucker, N. P.; Le Brun, N. E.; Dixon, R.; Hutchings, M. I., There's NO stopping NsrR, a global regulator of the bacterial NO stress response. *Trends in Microbiol.* **2010,** *18*, 149-156.
78. Saunders, N. F. W.; Houben, E. N. G.; Koefoed, S.; De Weert, S.; Reijnders, W. N. M.; Westerhoff, H. V.; De Boer, A. P. N.; Van Spanning, R. J. M., Transcription regulation of the *nir* gene cluster encoding nitrite reductase of *Paracoccus denitrificans* involves NNR and NirI, a novel type of membrane protein. *Mol. Microbiol.* **1999,** *34*, 24–36.
79. Wunsch, P.; Zumft, W. G., Functional domains of NosR, a novel transmembrane iron-sulfur flavoprotein necessary for nitrous oxide respiration. *J. Bacteriol.* **2005,** *187*, 1992-2001.
80. Zumft, W. G., Biogenesis of the bacterial respiratory CuA, Cu-S enzyme nitrous oxide reductase. *J. Mol. Microbiol. Biotechnol.* **2005,** *10*, 154-166.

81. Wunsch, P.; Körner, H.; Neese, F.; Van Spanning, R. J.; Kroneck, P. M.; Zumft, W. G., NosX function connects to nitrous oxide (N_2O) reduction by affecting the Cu(Z) center of NosZ and its activity *in vivo*. *FEBS Lett.* **2005,** *579*, 4605-4609.
82. Wunsch, P.; Herb, M.; Wieland, H.; Schiek, U. M.; Zumft, W. G., Requirements for Cu(A) and Cu-S center assembly of nitrous oxide reductase deduced from complete periplasmic enzyme maturation in the nondenitrifier *Pseudomonas putida*. *J. Bacteriol.* **2003**, 887-896.
83. Honisch, U.; Zumft, W. G., Operon structure and regulation of the *nos* gene region of *Pseudomonas stutzeri*, encoding an ABC-Type ATPase for maturation of nitrous oxide reductase. *J. Bacteriol.* **2003,** *185*, 1895-1902.
84. Holloway, P.; McCormick, W.; Watson, R. J.; Chan, Y. K., Identification and analysis of the dissimilatory nitrous oxide reduction genes, *nosRZDFY*, of *Rhizobium meliloti*. *J. Bacteriol.* **1996,** *178*, 1505-1514.
85. Saunders, N. F.; Hornberg, J. J.; Reijnders, W. N.; Westerhoff, H. V.; de Vries, S.; van Spanning, R. J., The NosX and NirX proteins of *Paracoccus denitrificans* are functional homologues: their role in maturation of nitrous oxide reductase. *J. Bacteriol.* **2000,** *182*, 5211-5217.
86. Zhang, L.; Trncik, C.; Andrade, S. L.; Einsle, O., The flavinyl transferase ApbE of *Pseudomonas stutzeri* matures the NosR protein required for nitrous oxide reduction. *Biochim. Biophys. Acta* **2017,** *1858*, 95-102.
87. Matsubara, T.; Iwasaki, H., A New-type of Copper-Protein from *Alcaligenes faecalis*. *J. Biochem.* **1972,** *71*, 747-750.
88. Iwasaki, H.; Saigo, T.; Matsubara, T., Copper as a controlling factor of anaerobic growth under N_2O and biosynthesis of N_2O reductase in denitrifying bacteria. *Plant Cell Physiol.* **1980,** *21*, 1573-1584.
89. Snyder, S. W.; Hollocher, T. C., Purification and some characteristics of nitrous oxide reductase from *Paracoccus denitrificans*. *J. Biol. Chem.* **1987,** *262*, 6515-6525.
90. Coyle, C. L.; Zumft, W. G.; Kroneck, P. M.; Körner, H.; Jakob, W., Nitrous oxide reductase from denitrifying *Pseudomonas perfectomarina*. Purification and properties of a novel multicopper enzyme. *Eur. J. Biochem.* **1985,** *153*, 459-467.
91. Prudêncio, M.; Pereira, A. S.; Tavares, P.; Besson, S.; Cabrito, I.; Brown, K.; Samyn, B.; Devreese, B.; Van Beeumen, J.; Rusnak, F.; Fauque, G.; Moura, J. J.; Tegoni, M.; Cambillau, C.; Moura, I., Purification, characterization, and preliminary crystallographic study of copper-containing nitrous oxide reductase from *Pseudomonas nautica* 617. *Biochemistry* **2000,** *39*, 3899-3907.
92. Ferretti, S.; Grossmann, J. G.; Hasnain, S. S.; Eady, R. R.; Smith, B. E., Biochemical characterization and solution structure of nitrous oxide reductase from *Alcaligenes xylosoxidans* (NCIMB 11015). *Eur. J. Biochem.* **1999,** *259*, 651-659.
93. Sato, K.; Okubo, A.; Yamazaki, S., Characterization of a multi-copper enzyme, nitrous oxide reductase, from *Rhodobacter sphaeroides* f. sp. denitrificans. *J. Biochem.* **1998,** *124*, 51-54.
94. Berks, B. C.; Baratta, D.; Richardson, J.; Ferguson, S. J., Purification and characterization of a nitrous oxide reductase from *Thiosphaera pantotropha*. Implications for the mechanism of aerobic nitrous oxide reduction. *Eur. J. Biochem.* **1993,** *212*, 467-476.
95. Hulse, C. L.; Averill, B. A., Isolation of a high specific activity pink, monomeric nitrous oxide reductase from *Achromobacter cycloclastes*. *Biochem. Biophys. Res. Commun.* **1990,** *166*, 729-735.
96. Yamaguchi, K.; Kawamura, A.; Ogawa, H.; Suzuki, S., Characterization of nitrous oxide reductase from a methylotrophic denitrifying bacterium, *Hyphomicrobium denitrificans* A3151. *J. Biochem.* **2003,** *134*, 853-858.
97. McEwan, A. G.; Greenfield, A. J.; Wetzstein, H. G.; Jackson, J. B.; Ferguson, S. J., Nitrous oxide reduction by members of the family *Rhodospirillaceae* and the nitrous oxide reductase of *Rhodopseudomonas capsulata*. *J. Bacteriol.* **1985,** *164*, 823-830.
98. Teraguchi, S.; Hollocher, T. C., Purification and some characteristics of a cytochrome *c*-containing nitrous oxide reductase from *Wolinella succinogenes*. *J. Biol. Chem.* **1989,** *264*, 1972-1979.

99. Yoon, S.; Nissen, S.; Park, D.; Sanford, R. A.; Löffler, F. E., Nitrous oxide reduction kinetics distinguish Bacteria Harboring Clade I NosZ from Those Harboring Clade II NosZ. *Appl. Environ. Microbiol.* **2016,** *82*, 3793-3800.
100. Sanford, R.; Wagner, D. D.; Wu, Q.; Chee-Sanford, J. C.; Thomas, S. H.; Cruz-García, C.; Rodríguez, G.; Massol-Deyáe, A.; Krishnanif, K. K.; Ritalahtig, K. M.; Nisseng, S.; Konstantinidisb, K. T.; Löffler, E. E., Unexpected nondenitrifier nitrous oxide reductase gene diversity and abundance in soils. *Proc. Natl. Acad. Sci.* **2012,** *109*, 19709-19714.
101. Liu, X.; Gao, C.; Zhang, A.; Jin, P.; Wang, L.; Feng, L., The nos gene cluster from gram-positive bacterium *Geobacillus thermodenitrificans* NG80-2 and functional characterization of the recombinant NosZ. *FEMS Microbiol. Lett.* **2008,** *289*, 46-52.
102. Berks, B. C.; Palmer, T.; Sargent, F., The Tat protein translocation pathway and its role in microbial physiology. *Adv. Microb. Physiol.* **2003**, 187-254.
103. Palmer, T.; Sargent, F.; Berks, B. C., Export of complex cofactor-containing proteins by the bacterial Tat pathway. *Trends Microbiol.* **2005,** *13*, 175-180.
104. Heikkilä, M. P.; Honisch, U.; Wunsch, P.; Zumft, W. G., Role of the Tat ransport system in nitrous oxide reductase translocation and cytochrome cd_1 biosynthesis in *Pseudomonas stutzeri*. *J. Bacteriol.* **2001,** *183*, 1663-1671.
105. Lee, H. S.; Hancock, R. E.; Ingraham, J. L., Properties of a *Pseudomonas stutzeri* outer membrane channel-forming protein (NosA) required for production of copper-containing N_2O reductase. *J. Bacteriol.* **1989,** *171*, 2096-2100.
106. Dash, B. P.; Alles, M.; Bundschuh, F. A.; Richter, O. M.; Ludwig, B., Protein chaperones mediating copper insertion into the CuA site of the aa3-type cytochrome *c* oxidase of *Paracoccus denitrificans*. *Biochim. Biophys. Acta* **2015,** *1847*, 202-211.
107. Nittis, T.; George, G. N.; Winge, D. R., Yeast Sco1, a protein essential for cytochrome *c* oxidase function is a Cu(I)-binding protein. *J. Biol. Chem.* **2001,** *276*, 42520-42526.
108. Horng, Y. C.; Cobine, P. A.; Maxfield, A. B.; Carr, H. S.; Winge, D. R., Specific copper transfer from the Cox17 metallochaperone to both Sco1 and Cox11 in the assembly of yeast cytochrome *c* oxidase. *J. Biol. Chem.* **2004,** *279*, 35334-35340.
109. McGuirl, M. A.; Bollinger, J. A.; Cosper, N.; Scott, R. A.; Dooley, D. M., Expression, purification, and characterization of NosL, a novel Cu(I) protein of the nitrous oxide reductase (*nos*) gene cluster. *J. Biol. Inorg. Chem.* **2001,** *6*, 189-195.
110. Taubner, L. M.; McGuirl, M. A.; Dooley, D. M.; Copié, V., Structural studies of apo NosL, an accessory protein of the nitrous oxide reductase system: insights from structural homology with MerB, a mercury resistance protein. *Biochemistry* **2006,** *45*, 12240-12252.
111. Sullivan, M. J.; Gates, A. J.; Appia-Ayme, C.; Rowley, G.; Richardson, D. J., Copper control of bacterial nitrous oxide emission and its impact on vitamin B12-dependent metabolism. *Proc. Natl. Acad. Sci.* **2013,** *110*, 19926-19931.
112. Zumft, W. G.; Viebrock-Sambale, A.; Braun, C., Nitrous oxide reductase from denitrifying *Pseudomonas stutzeri*. Genes for copper-processing and properties of the deduced products, including a new member of the family of ATP/GTP-binding proteins. *Eur. J. Biochem.* **1990,** *192*, 591-599.
113. Cuypers, H.; Viebrock-Sambale, A.; Zumft, W. G., NosR, a membrane-bound regulatory component necessary for expression of nitrous oxide reductase in denitrifying *Pseudomonas stutzeri*. *J. Bacteriol.* **1992,** *174*, 5332-5339.
114. Jones, K., The chemistry of nitrogen. In *Comprehensive Inorganic Chemistry*, Pergamon Press: Oxford, 1975.
115. Itoh, M.; Matsuura, K.; Satoh, T., Involvement of cytochrome bc_1 complex in the electron transfer pathway for N_2O reduction in a photodenitrifier, *Rhodobacter sphaeroides* f. s. denitrificans. *FEBS Lett.* **1989,** *251*, 104-108.
116. Boogerd, F. C.; van Verseveld, H.W.; Stouthamer, A. H., Electron transport to nitrous oxide in *Paracoccus denitrificans*. *FEBS Lett.* **1980,** *113*, 279-284.
117. Richardson, D. J.; Bell, L. C.; McEwan, A. G.; Jackson, J. B.; Ferguson, S. J., Cytochrome c_2 is essential for electron transfer to nitrous oxide reductase from physiological substrates in *Rhodobacter capsulatus* and can act as an electron donor to the reductase *in vitro*. Correlation with photoinhibition studies. *Eur. J. Biochem.* **1991,** *199*, 677-683.

118. Moir, J. W. B.; Ferguson, S. J., Properties of a *Paracoccus denitrificans* mutant deleted in cytochrome c_{550} indicate that a copper protein can substitute for this cytochrome in electron transport to nitrite, nitric oxide and nitrous oxide. *Microbiol.* **1994,** *140*, 389-397.
119. Fujita, K.; Chan, J. M.; Bollinger, J.; Alvarez, M. L.; Dooley, D. M., Anaerobic purification, characterization and preliminary mechanistic study of recombinant nitrous oxide reductase from *Achromobacter cycloclastes*. *J. inorg. biochem.* **2007,** *101*, 1836-1844.
120. Rasmussen, T.; Brittain, T.; Berks, B. C.; Watmough, J.; Thomson, A. J., Formation of a cytochrome *c*-nitrous oxide reductase complex is obligatory for N_2O reduction by *Paracoccus pantotrophus*. *Dalton Trans.* **2005**, 3501-3506.
121. Zhang, C.-s.; Hollocher, T. C., The reaction of reduced cytochromes *c* with nitrous oxide reductase of *Wolinella succinogenes*. *Biochim. Biophys. Acta* **1993,** *1142*, 253-261.
122. Dell'acqua, S.; Pauleta, S. R.; Monzani, E.; Pereira, A. S.; Casella, L.; Moura, J. J. G.; Moura, I., Electron transfer complex between nitrous oxide reductase and cytochrome c_{552} from *Pseudomonas nautica*: kinetic, nuclear magnetic resonance, and docking studies. *Biochemistry* **2008,** *47*, 10852-10862.
123. Fujita, K.; Hirasawa-Fujita, M.; Brown, D. E.; Obara, Y.; Ijima, F.; Kohzuma, T.; Dooley, D. M., Direct electron transfer from pseudoazurin to nitrous oxide reductase in catalytic N_2O reduction. *J. inorg. biochem.* **2012,** *115*, 163-173.
124. Liu, M. Y.; Liu, M. C.; Payne, W. J.; Legall, J., Properties and electron transfer specificity of copper proteins from the denitrifier "*Achromobacter cycloclastes*". *J. Bacteriol.* **1986,** *166*, 604-608.
125. Brown, K.; Tegoni, M.; Prudêncio, M.; Pereira, A. S.; Besson, S.; Moura, J. J.; Moura, I.; Cambillau, C., A novel type of catalytic copper cluster in nitrous oxide reductase. *Nat. Struct. Biol.* **2000,** *7*, 191-195.
126. Brown, K.; Djinovic-Carugo, K.; Haltia, T.; Cabrito, I.; Saraste, M.; Moura, J. J.; Moura, I.; Tegoni, M.; Cambillau, C., Revisiting the catalytic CuZ cluster of nitrous oxide (N_2O) reductase. Evidence of a bridging inorganic sulfur. *J. Biol. Chem.* **2000,** *275*, 41133-41136.
127. Murphy, M. E.; Lindley, P. F.; Adman, E. T., Structural comparison of cupredoxin domains: domain recycling to construct proteins with novel functions. *Protein Sci.* **1997,** *6*, 761-770.
128. Page, C. C.; Moser, C. C.; Chen, X.; Dutton, P. L., Natural engineering principles of electron tunnelling in biological oxidation-reduction. *Nature* **1999,** *402*, 47-52.
129. Schneider, L. K.; Einsle, O., Role of calcium in secondary structure stabilization during maturation of nitrous oxide reductase. *Biochemistry* **2016,** *55*, 1433-1440.
130. Riester, J.; Zumft, W. G.; Kroneck, P. M., Nitrous oxide reductase from *Pseudomonas stutzeri*. Redox properties and spectroscopic characterization of different forms of the multicopper enzyme. *Eur. J. Biochem.* **1989,** *178*, 751-762.
131. Rasmussen, T.; Berks, B. C.; Butt, J. N.; Thomson, A. J., Multiple forms of the catalytic centre, CuZ, in the enzyme nitrous oxide reductase from *Paracoccus pantotrophus*. *Biochem. J.* **2002,** *364*, 807-815.
132. Dell'Acqua, S.; Pauleta, S. R.; Moura, J. J.; Moura, I., Biochemical characterization of the purple form of *Marinobacter hydrocarbonoclasticus* nitrous oxide reductase. *Philos. Trans R. Soc. Lond. B Biol. Sci.* **2012,** *367*, 1204-1212.
133. Pauleta, S. R.; Carreira, C.; Moura, I., Insights into Nitrous oxide reductase. In *Metalloenzymes in Denitrification: Applications and Environmental Impacts*, Moura, J. J. G.; Maia, L.; Pauleta, S. R., Eds. RSC: **2017**; pp 141-169.
134. Beinert, H., Copper A of cytochrome *c* oxidase, a novel, long-embattled, biological electron-transfer site. *Eur. J. Biochem.* **1997,** *245*, 521-532.
135. Beinert, H.; Griffiths, D. E.; Wharton, D. C.; Sands, R. H., Properties of the copper associated with cytochrome oxidase as studied by paramagnetic resonance spectroscopy. *J. Biol. Chem.* **1962,** *237*, 2337-2346.
136. Greenwood, C.; Hill, B. C.; Barber, D.; Eglinton, D. G.; Thomson, A. J., The optical properties of CuA in bovine cytochrome *c* oxidase determined by low-temperature magnetic-circular-dichroism spectroscopy. *Biochem. J.* **1983,** *215*, 303-316.

137. Thomson, A. J.; Greenwood, C.; Peterson, J.; Barrett, C. P., Determination of the optical properties of CuA(II) in bovine cytochrome *c* oxidase using magnetic circular dichroism as an optical detector of paramagnetic resonance. *J. Inorg. Biochem.* **1986,** *28*, 195-205.
138. Kroneck, P. M.; Antholine, W. A.; Riester, J.; Zumft, W. G., The cupric site in nitrous oxide reductase contains a mixed-valence [Cu(II),Cu(I)] binuclear center: a multifrequency electron paramagnetic resonance investigation. *FEBS Lett.* **1988,** *242*, 70-74.
139. Kroneck, P. M.; Antholine, W. E.; Kastrau, D. H.; Buse, G.; Steffens, G. C.; Zumft, W. G., Multifrequency EPR evidence for a bimetallic center at the CuA site in cytochrome *c* oxidase. *FEBS Lett.* **1990,** *268*, 274-276.
140. Antholine, W. E.; Kastrau, D. H.; Steffens, G. C.; Buse, G.; Zumft, W. G.; Kroneck, P. M., A comparative EPR investigation of the multicopper proteins nitrous-oxide reductase and cytochrome *c* oxidase. *Eur. J. Biochem.* **1992,** *209*, 875-881.
141. Kroneck, P. M.; Antholine, W. A.; Riester, J.; Zumft, W. G., The nature of the cupric site in nitrous oxide reductase and of CuA in cytochrome *c* oxidase. *FEBS Lett.* **1989,** *248*, 212-213.
142. Farrar, J. A.; Neese, F.; Lappalainen, P.; Kroneck, P. M. H.; Saraste, M.; Zumft, W. G.; Thomson, A. J., The electronic structure of CuA: a novel mixed-valence dinuclear copper electron-transfer center. *J. Am. Chem. Soc.* **1996,** *118*, 11501-11514.
143. Alvarez, M. L.; Ai, J.; Zumft, W.; Sanders-Loehr, J.; Dooley, D. M., Characterization of the copper-sulfur chromophores in nitrous oxide reductase by resonance raman spectroscopy: evidence for sulfur coordination in the catalytic cluster. *J. Am. Chem. Soc.* **2001,** *123*, 576-587.
144. Gamelin, D. R.; Randall, D. W.; Hay, M. T.; Houser, R. P.; Mulder, T. C.; Canters, G. W.; Vries, S. d.; Tolman, W. B.; Lu, Y.; Solomon, E. I., Spectroscopy of mixed-valence CuA-type centers: ligand-field control of ground-state properties related to electron transfer. *J. Am. Chem. Soc.* **1998,** *120*, 5246-5263.
145. Andrew, C. R.; Han, J.; Vries, S. d.; Oost, J. v. d.; Averill, B. A.; Loehr, T. M.; Sanders-Loehr, J., CuA of cytochrome *c* oxidase and the A Site of N_2O reductase are tetrahedrally distorted type 1 Cu cysteinates. *J. Am. Chem. Soc.* **1994,** *116*, 10805-10806.
146. Solomon, E. I.; Heppner, D. E.; Johnston, E. M.; Ginsbach, J. W.; Cirera, J.; Qayyum, M.; Kieber-Emmons, M. T.; Kjaergaard, C. H.; Hadt, R. G.; Tian, L., Copper active sites in biology. *Chem. Rev.* **2014,** *114*, 3659–3853.
147. Farrar, J. A.; Thomson, A. J.; Cheesman, M. R.; Dooley, D. M.; Zumft, W. G., A model of the copper centres of nitrous oxide reductase (*Pseudomonas stutzeri*). Evidence from optical, EPR and MCD spectroscopy. *FEBS Lett.* **1991,** *294*, 11-15.
148. Dell'Acqua, S.; Pauleta, S. R.; Paes de Sousa, P. M.; Monzani, E.; Casella, L.; Moura, J. J.; Moura, I., A new CuZ active form in the catalytic reduction of N_2O by nitrous oxide reductase from *Pseudomonas nautica*. *J. Biol. Inorg. Chem.* **2010,** *15*, 967-976.
149. Charnock, J. M.; Dreusch, A.; Körner, H.; Neese, F.; Nelson, J.; Kannt, A.; Michel, H.; Garner, C. D.; Kroneck, P. M.; Zumft, W. G., Structural investigations of the CuA centre of nitrous oxide reductase from *Pseudomonas stutzeri* by site-directed mutagenesis and X-ray absorption spectroscopy. *Eur. J. Biochem.* **2000,** *267*, 1368-1381.
150. Blackburn, N. J.; Barr, M. E.; Woodruff, W. H.; van der Oost, J.; de Vries, S., Metal-metal bonding in biology: EXAFS evidence for a 2.5 Å copper-copper bond in the CuA center of cytochrome oxidase. *Biochemistry* **1994,** *33*, 10401-10407.
151. Paraskevopoulos, K.; Antonyuk, S. V.; Sawers, R. G.; Eady, R. R.; Hasnain, S. S., Insight into catalysis of nitrous oxide reductase from high-resolution structures of resting and inhibitor-bound enzyme from *Achromobacter cycloclastes*. *J. Mol. Biol.* **2006,** *362*, 55-65.
152. Pomowski, A.; Zumft, W. G.; Kroneck, P. M. H.; Einsle, O., N_2O binding at a 4Cu:2S copper-sulphur cluster in nitrous oxide reductase. *Nature* **2011,** *477*, 234-237.
153. Schneider, L. K.; Wüst, A.; Pomowski, A.; Zhang, L.; Einsle, O., No laughing matter: the unmaking of the greenhouse gas dinitrogen monoxide by nitrous oxide reductase. *Met. Ions Life Sci.* **2014,** *14*, 177-210.
154. Dell'acqua, S.; Moura, I.; Moura, J. J.; Pauleta, S. R., The electron transfer complex between nitrous oxide reductase and its electron donors. *J. Biol. Inorg. Chem.* **2011,** *16*, 1241-1254.

155. Zumft, W. G.; Matsubara, T., A novel kind of multi-copper protein as terminal oxidoreductase of nitrous oxide respiration in *Pseudomonas perfectomarinus*. *FEBS Lett.* **1982,** *148*, 107-112.
156. Farrar, J. A.; Zumft, W. G.; Thomson, A. J., CuA and CuZ are variants of the electron transfer center in nitrous oxide reductase. *Proc. Natl. Acad. Sci.***1998,** *95*, 9891-9896.
157. Tuomas, H.; Kieron, B.; Mariella, T.; Christian, C.; Matti, S.; Kimmo, M.; Kristina, D.-C., Crystal structure of nitrous oxide reductase from *Paracoccus denitrificans* at 1.6 Å resolution. *Biochem. J.* **2003,** *369*, 77-88.
158. Rasmussen, T.; Berks, B. C.; Sanders-Loehr, J.; Dooley, D. M.; Zumft, W. G.; Thomson, A. J., The catalytic center in nitrous oxide reductase, CuZ, is a copper-sulfide cluster. *Biochemistry* **2000,** *39*, 12753-12756.
159. Wüst , A.; Schneider, L.; Pomowski, A.; Zumft, W. G.; Kroneck, P. M. H.; Einsle, O., Nature's way of handling a greenhouse gas: the copper-sulfur cluster of purple nitrous oxide reductase. *Biol. Chem.* **2012,** *393*, 1067-1077.
160. Johnston, E. M.; Dell'Acqua, S.; Ramos, S.; Pauleta, S. R.; Moura, I.; Solomon, E. I., Determination of the active form of the tetranuclear copper sulfur cluster in nitrous oxide reductase. *J. Am. Chem. Soc.* **2014,** *136*, 614-617.
161. Ghosh, S.; Gorelsky, S. I.; George, S. D.; Chan, J. M.; Cabrito, I.; Dooley, D. M.; Moura, J. J. G.; Moura, I.; Solomon, E. I., Spectroscopic, computational, and kinetic studies of the μ_4-sulfide-bridged tetranuclear CuZ cluster in N_2O reductase: pH effect on the edge ligand and its contribution to reactivity. *J. Am. Chem. Soc.* **2007,** *129*, 3955-3965.
162. Chen, P.; Cabrito, I.; Moura, J. J. G.; Moura, I.; Solomon, E. I., Spectroscopic and electronic structure studies of the μ_4-sulfide bridged tetranuclear Cu(Z) cluster in N_2O reductase: molecular insight into the catalytic mechanism. *J. Am. Chem. Soc.* **2002,** *134*, 10497-10507.
163. Chen, P.; DeBeer, G. S.; Cabrito, I.; Antholine, W. E.; Moura, J. J.; Moura, I.; Hedman, B.; Hodgson, K. O.; Solomon, E. I., Electronic structure description of the μ_4-sulfide bridged tetranuclear Cu(Z) center in N_2O reductase. *J. Am. Chem. Soc.* **2002,** *124*, 744-745.
164. Johnston, E. M.; Dell'Acqua, S.; Pauleta, S. R.; Moura, I.; Solomon, E. I., Protonation state of the Cu4S2 CuZ site in nitrous oxide reductase: redox dependence and insight into reactivity. *Chem. Sci.* **2015,** *6*, 5670-5679.
165. Oganesyan, V. S.; Rasmussen, T.; Fairhurst, S.; Thomson, A. J., Characterisation of Cu4S , the catalytic site in nitrous oxide reductase, by EPR spectroscopy. *Dalton Trans.* **2004**, 996-1002.
166. Chen, P.; Gorelsky, S. I.; Ghosh, S.; Solomon, E. I., N_2O reduction by the μ_4-sulfide-bridged tetranuclear CuZ cluster active site. *Angew. Chem. Int. Ed. Engl.* **2004,** *43*, 4132-4140.
167. Johnston, E. M.; Carreira, C.; Dell'Acqua, S.; Ghosh, S.; Pauleta, S. R.; Moura, I.; Solomon, E. I., Spectroscopic definition of the CuZ° intermediate in turnover of nitrous oxide reductase and molecular insight into the catalytic mechanism. *J. Am. Chem. Soc.* **2017,** *139*, 4462–4476.
168. Ghosh, S.; Gorelsky, S. I.; Chen, P.; Cabrito, I.; Moura, J. J. G.; Moura, I.; Solomon, E. I., Activation of N_2O reduction by the fully reduced μ_4-sulfide bridged tetranuclear CuZ cluster in nitrous oxide reductase. *J. Am. Chem. Soc.* **2003,** *125*, 15708-15709.
169. Tolman, W. B., Binding and activation of N_2O at transition-metal centers: recent mechanistic insights. *Angew. Chem. Int. Ed. Engl.* **2010,** *49*, 1018-1024.
170. Johnson, B. J.; Lindeman, S. V.; Mankad, N. P., Assembly, structure, and reactivity of Cu4S and Cu3S models for the nitrous oxide reductase active site, CuZ*. *Inorg. chem.* **2014,** *53*, 10611–10619.
171. Bar-Nahum, I.; Gupta, A. K.; Huber, S. M.; Ertem, M. Z.; Cramer, C. J.; Tolman, W. B., Reduction of nitrous oxide to dinitrogen by a mixed valent tricopper-disulfido cluster. *J. Am. Chem. Soc.* **2009,** *131*, 2812-2814.
172. Dooley, D. M.; Alvarez, M. L.; Rosenzweig, A. C.; Hollis, R. S.; Zumft, W. G., Exogenous ligand binding to *Pseudomonas stutzeri* nitrous oxide reductase. *Inorg. Chim. Acta* **1996,** *242*, 239-244.
173. Kroneck, P. M. H.; Riester, J.; Zumft, W. G.; Antholine, W. E., The copper site in nitrous oxide reductase. *Biol. Met.* **1990,** *3*, 103-109.

174. Almeida, R. M.; Dell' Acqua, S.; Moura, I.; Pauleta, S. R.; Moura, J. J. G., Electron Transfer and Molecular Recognition in Denitrification and Nitrate Dissimilatory Pathways. In *Metalloenzymes in Denitrification: Applications and Environmental Impacts 2017*, Moura, I.; Moura, J. J. G.; Maia, L.; Pauleta, S. R., Eds. RSC: **2017**; pp 252-286.
175. Kristjansson, J. K.; Hollocher, T. C., First practical assay for soluble nitrous oxide reductase of denitrifying bacteria and a partial kinetic characterization. *J. Biol. Chem.* **1980,** *255*, 704-707.
176. Frunzke, K.; Zumft, W. G., Rapid, single sample analysis of H_2, O_2, N_2, NO, CO, N_2O and CO_2 by isothermal gas chromatography: applications to the study of bacterial denitrification. *J. chromatogr. A* **1984,** *299*, 477-483.
177. Körner, H.; Frunzke, K.; Döhler, K.; Zumft, W. G., Immunochemical patterns of distribution of nitrous oxide reductase and nitrite reductase (cytochrome cd_1) among denitrifying *pseudomonads*. *Arch. Microbiol.* **1987,** *148*, 20-24.
178. SooHoo, C. K.; Hollocher, T. C., Purification and characterization of nitrous oxide reductase from *Pseudomonas aeruginosa* strain P2. *J. Biol. Chem.* **1991,** *266*, 2203-2209.
179. Wardman, P., The reduction potential of benzyl viologen: an important reference compound for oxidant/radical redox couples. *Free Radic. Res. Commun.* **1991,** *14*, 57-67.
180. Borrero-de Acuña, J. M.; Rohde, M.; Wissing, J.; Jänsch, L.; Schobert, M.; Molinari, G.; Timmis, K. N.; Jahn, M.; Jahn, D., Protein Network of the *Pseudomonas aeruginosa* Denitrification Apparatus. *J. Bacteriol.* **2016,** *198*, 1401-1413.
181. Chan, J. M.; Bollinger, J.; Grewell, C. L.; Dooley, D. M., Reductively activated nitrous oxide reductase reacts directly with substrate. *J. Am. Chem. Soc.* **2004,** *126*, 3030-3031.
182. Fujita, K.; Dooley, D. M., Insights into the mechanism of N_2O reduction by reductively activated N_2O reductase from kinetics and spectroscopic studies of pH effects. *Inorg. Chem.* **2007,** *46*, 613-615.
183. Mayhew, S. G., The redox potential of dithionite and SO-2 from equilibrium reactions with flavodoxins, methyl viologen and hydrogen plus hydrogenase. *Eur. J. Biochem.* **1978,** *85*, 535-547.
184. Dell'Acqua, S.; Pauleta, S. R.; Moura, I.; Moura, J. J. G., The tetranuclear copper active site of nitrous oxide reductase: the CuZ center. *J. Biol. Inorg. Chem.* **2011,** *16*, 183-194.
185. Michalski, W. P.; Hein, D. H.; Nicholas, D. J. D., Purification and characterization of nitrous oxide reductase from *Rhodopseudomonas sphaeroides* f.sp. *denitrificans*. *Biochim. Biophys. Acta* **1986,** *872*, 50-60.
186. Instruments, W. P., Isolate dissolved oxygen meter and oxygen electrode. UK, **2001**.
187. Grimaud, R.; Ghiglione, J. F.; Cagnon, C.; Lauga, B.; Vaysse, P. J.; Rodriguez-Blanco, A.; Mangenot, S.; Cruveiller, S.; Barbe, V.; Duran, R.; Wu, L. F.; Talla, E.; Bonin, P.; Michotey, V., Genome sequence of the marine bacterium *Marinobacter hydrocarbonoclasticus* SP17, which forms biofilms on hydrophobic organic compounds. *J. Bacteriol.* **2012,** *194*, 3539-3540.
188. Larkin, M. A.; Blackshields, G.; Brown, N. P.; Chenna, R.; McGettigan, P. A.; McWilliam, H.; Valentin, F.; Wallace, I. M.; Wilm, A.; Lopez, R.; Thompson, J. D.; Gibson, T. J.; Higgins, D. G., Clustal W and Clustal X version 2.0. *Bioinformatics* **2007,** *23*, 2947-2948.
189. Münch, R.; Hiller, K.; Grote, A.; Scheer, M.; Klein, J.; Schobert, M.; Jahn, D., Virtual Footprint and PRODORIC: an integrative framework for regulon prediction in prokaryotes. *Bioinformatics* **2005,** *21*, 4187-4189.
190. Bagos, P. G.; Nikolaou, E. P.; Liakopoulos, T. D.; Tsirigos, K. D., Combined prediction of Tat and Sec signal peptides with hidden Markov models. *Bioinformatics* **2010,** *26*, 2811-7.
191. Tan, K. P.; Nguyen, T. B.; Patel, S.; Varadarajan, R.; Madhusudhan, M. S., Depth: a web server to compute depth, cavity sizes, detect potential small-molecule ligand-binding cavities and predict the pK_a of ionizable residues in proteins. *Nucleic Acids Res.* **2013,** *41*, 314-321.
192. P. Baumann; L. Baumann, The marine Gram-negative eubacteria: genera *Photobacterium, Beneckea, Alteromonas, Pseudomonas, and Alcaligenes*. *The prokaryots*. Springer-Verlag: New York, **1981**.
193. Starkey, R. L., A study of spore formation and other morphological characteristics of *Vibrio desulfuricans*. *Arch. Mikrobiol.* **1938,** *9*, 268.

194. Granger, D. L.; Taintor, R. R.; Boockvar, K. S.; Hibbs, J. B., Measurement of nitrate and nitrite in biological samples using nitrate reductase and Griess reaction. *Methods Enzymol.* **1996,** *268*, 142-151.
195. Applied-Biosystems, Applied Biosystems Tutorial - Guide to Performing Relative Quantitation of Gene Expression Using Real-Time Quantitative PCR. **2004**.
196. Gomes, J. P.; Hsia, R. C.; Mead, S.; Borrego, M. J.; Dean, D., Immunoreactivity and differential developmental expression of known and putative *Chlamydia trachomatis* membrane proteins for biologically variant serovars representing distinct disease groups. *Microbes Infect.* **2005,** *7*, 410-20.
197. Galisa, P. S.; da Silva, H. A.; Macedo, A. V.; Reis, V. M.; Vidal, M. S.; Baldani, J. I.; Simoes-Araujo, J. L., Identification and validation of reference genes to study the gene expression in *Gluconacetobacter diazotrophicus* grown in different carbon sources using RT-qPCR. *J. Microbiol. Methods* **2012,** *91*, 1-7.
198. Takle, G. W.; Toth, I. K.; Brurberg, M. B., Evaluation of reference genes for real-time RT-PCR expression studies in the plant pathogen *Pectobacterium atrosepticum*. *BMC Plant Biol.* **2007,** *7*, 50.
199. Eleaume, H.; Jabbouri, S., Comparison of two standardisation methods in real-time quantitative RT-PCR to follow *Staphylococcus aureus* genes expression during *in vitro* growth. *J. Microbiol. Methods* **2004,** *59*, 363-70.
200. Metcalf, D.; Sharif, S.; Weese, J. S., Evaluation of candidate reference genes in *Clostridium difficile* for gene expression normalization. *Anaerobe* **2010,** *16*, 439-43.
201. Neretin, L. N.; Schippers, A.; Pernthaler, A.; Hamann, K.; Amann, R.; Jørgensen, B. B., Quantification of dissimilatory (bi)sulphite reductase gene expression in *Desulfobacterium autotrophicum* using real-time RT-PCR. *Environ. Microbiol.* **2003,** *5*, 660-671.
202. Edwards, K. J.; Saunders, N. A., Real-time PCR used to measure stress-induced changes in the expression of the genes of the alginate pathway of *Pseudomonas aeruginosa*. *J. Appl. Microbiol.* **2001,** *91*, 29-37.
203. Untergasser, A.; Cutcutache, I.; Koressaar, T.; Ye, J.; Faircloth, B. C.; Remm, M.; Rozen, S. G., Primer3—new capabilities and interfaces. *Nucleic Acids Research* **2012,** *40*, e115-e115.
204. Goodhew, C. F.; Brown, K. R.; Pettigrew, G. W., Haem staining in gels, a useful tool in the study of bacterial *c*-type cytochromes. *Biochim. Biophys. Acta* **1986,** *852*, 288-294.
205. Saraiva, L. M.; Fauque, G.; Besson, S.; Moura, I., Physico-chemical and spectroscopic properties of the monohemic cytochrome c_{552} from *Pseudomonas nautica* 617. *Eur. J. Biochem.* **1994,** *224*, 1011-1017.
206. Ohnishi, S. T.; Barr, J. K., A simplified method of quantitating protein using the biuret and phenol reagents. *Anal. Biochem.* **1978,** *86*, 193-200.
207. Outten, F. W.; Wood, M. J.; Munoz, F. M.; Storz, G., The SufE protein and the SufBCD complex enhance SufS cysteine desulfurase activity as part of a sulfur transfer pathway for Fe-S cluster assembly in *Escherichia coli*. *J. Biol. Chem.* **2003,** *278*, 45713-45719.
208. Hanna, P. M.; Tamilarasan, R.; McMillin, D. R., Cu(I) analysis of blue copper proteins. *Biochem. J.* **1988,** *256*, 1001-1004.
209. D'Arcy, A.; Mac Sweeney, A.; Haber, A., Using natural seeding material to generate nucleation in protein crystallization experiments. *Acta Crystallogr. D Biol. Crystallogr.* **2003,** *59*, 1343-1346.
210. Kabsch, W., Xds. *Acta Crystallogr. D Biol. Crystallogr.* **2010,** *66*, 125-132.
211. Evans, P. R.; Murshudov, G. N., How good are my data and what is the resolution? *Acta Crystallogr. D Biol. Crystallogr.* **2013,** *69*, 1204-1214.
212. Winn, M. D.; Ballard, C. C.; Cowtan, K. D.; Dodson, E. J.; Emsley, P.; Evans, P. R.; Keegan, R. M.; Krissinel, E. B.; Leslie, A. G.; McCoy, A.; McNicholas, S. J.; Murshudov, G. N.; Pannu, N. S.; Potterton, E. A.; Powell, H. R.; Read, R. J.; Vagin, A.; Wilson, K. S., Overview of the CCP4 suite and current developments. *Acta Crystallogr. D Biol. Crystallogr.***2011,** *67*, 235-242.
213. Vagin, A.; Teplyakov, A., Molecular replacement with MOLREP. *Acta Crystallogr. D Biol. Crystallogr.* **2010,** *66*, 22-25.

214. Emsley, P.; Cowtan, K., Coot: model-building tools for molecular graphics. *Acta Crystallogr. D Biol. Crystallogr.* **2004,** *60*, 2126-2132.
215. Murshudov, G. N.; Skubák, P.; Lebedev, A. A.; Pannu, N. S.; Steiner, R. A.; Nicholls, R. A.; Winn, M. D.; Long, F.; Vagin, A. A., REFMAC5 for the refinement of macromolecular crystal structures. *Acta Crystallogr. D Biol. Crystallogr.* **2011,** *67*, 355-367.
216. Chen, V. B.; Arendall, W. B.; Headd, J. J.; Keedy, D. A.; Immormino, R. M.; Kapral, G. J.; Murray, L. W.; Richardson, J. S.; Richardson, D. C., MolProbity: all-atom structure validation for macromolecular crystallography. *Acta Crystallogr. D Biol. Crystallogr.* **2010,** *66*, 12-21.
217. Dutton, P. L., Redox potentiometry: determination of midpoint potentials of oxidation-reduction components of biological electron-transfer systems. In *Methods Enzymol.*, **1978**; pp 411-435.
218. Carvalho, R. C.; Gouveia-Caridade, C.; Brett, C. M., Glassy carbon electrodes modified by multiwalled carbon nanotubes and poly(neutral red): a comparative study of different brands and application to electrocatalytic ascorbate determination. *Anal. Bioanal. Chem.* **2010,** *398*, 1675-1685.
219. Philippot, L., Denitrifying genes in bacterial and Archaeal genomes. *Biochim. Biophys. Acta* **2002,** *1577*, 355-376.
220. Andrade, S. L.; Einsle, O., The tricky task of nitrate/nitrite antiport. *Angew. Chem. Int. Ed. Engl.* **2013,** *52*, 10422-10424.
221. Yan, H.; Huang, W.; Yan, C.; Gong, X.; Jiang, S.; Zhao, Y.; Wang, J.; Shi, Y., Structure and mechanism of a nitrate transporter. *Cell Rep.* **2013,** *3*, 716-723.
222. Zheng, H.; Wisedchaisri, G.; Gonen, T., Crystal structure of a nitrate/nitrite exchanger. *Nature* **2013,** *497*, 647-651.
223. Jia, W.; Tovell, N.; Clegg, S.; Trimmer, M.; Cole, J., A single channel for nitrate uptake, nitrite export and nitrite uptake by *Escherichia coli* NarU and a role for NirC in nitrite export and uptake. *Biochem. J.* **2009,** *417*, 297-304.
224. Goddard, A. D.; Bali, S.; Mavridou, D. A.; Luque-Almagro, V. M.; Gates, A. J.; Dolores Roldán, M.; Newstead, S.; Richardson, D. J.; Ferguson, S. J., The *Paracoccus denitrificans* NarK-like nitrate and nitrite transporters-probing nitrate uptake and nitrate/nitrite exchange mechanisms. *Mol. Microbiol.* **2017,** *103*, 117-133.
225. Zumft, W. G., Nitric oxide reductases of prokaryotes with emphasis on the respiratory, heme-copper oxidase type. *J. Inorg. Biochem.* **2005,** *99*, 194-215.
226. de Boer, A. P.; van der Oost, J.; Reijnders, W. N.; Westerhoff, H. V.; Stouthamer, A. H.; van Spanning, R. J., Mutational analysis of the *nor* gene cluster which encodes nitric-oxide reductase from *Paracoccus denitrificans*. *Eur. J. Biochem.* **1996,** *242*, 592-600.
227. Bergaust, L. L.; Hartsock, A.; Liu, B.; Bakken, L. R.; Shapleigh, J. P., Role of *norEF* in denitrification, elucidated by physiological experiments with *Rhodobacter sphaeroides*. *J. Bacteriol.* **2014,** *196*, 2190-2200.
228. Heylen, K.; Vanparys, B.; Gevers, D.; Wittebolle, L.; Boon, N.; De Vos, P., Nitric oxide reductase (*norB*) gene sequence analysis reveals discrepancies with nitrite reductase (*nir*) gene phylogeny in cultivated denitrifiers. *Environ. Microbiol.* **2007,** *9*, 1072-1077.
229. Jones, C. M.; Stres, B.; Rosenquist, M.; Hallin, S., Phylogenetic analysis of nitrite, nitric oxide, and nitrous oxide respiratory enzymes reveal a complex evolutionary history for denitrification. *Mol. Biol. Evol.* **2008,** *25*, 1955-1966.
230. Lopes, H.; Besson, S.; Moura, I.; Moura, J. J., Kinetics of inter- and intramolecular electron transfer of *Pseudomonas nautica* cytochrome cd_1 nitrite reductase: regulation of the NO-bound end product. *J. Biol. Inorg. Chem.* **2001,** *6*, 55-62.
231. Besson, S.; Carneiro, C.; Moura, J. J.; Moura, I.; Fauque, G., A cytochrome cd_1-type nitrite reductase isolated from the marine denitrifier *Pseudomonas nautica* 617: purification and characterization. *Anaerobe* **1995,** *1*, 219-226.
232. Bali, S.; Lawrence, A. D.; Lobo, S. A.; Saraiva, L. M.; Golding, B. T.; Palmer, D. J.; Howard, M. J.; Ferguson, S. J.; Warren, M. J., Molecular hijacking of siroheme for the synthesis of heme and d_1 heme. *Proc. Natl. Acad. Sci.* **2011,** *108*, 18260-18265.
233. Zajicek, R. S.; Bali, S.; Arnold, S.; Brindley, A. A.; Warren, M. J.; Ferguson, S. J., d_1 haem biogenesis - assessing the roles of three *nir* gene products. *FEBS J.* **2009,** *276*, 6399-6411.

234. Storbeck, S.; Walther, J.; Müller, J.; Parmar, V.; Schiebel, H. M.; Kemken, D.; Dülcks, T.; Warren, M. J.; Layer, G., The *Pseudomonas aeruginosa nirE* gene encodes the S-adenosyl-L-methionine-dependent uroporphyrinogen III methyltransferase required for heme d_1 biosynthesis. *FEBS J.* **2009,** *276*, 5973–5982.
235. Adamczack, J.; Hoffmann, M.; Papke, U.; Haufschildt, K.; Nicke, T.; Bröring, M.; Sezer, M.; Weimar, R.; Kuhlmann, U.; Hildebrandt, P.; Layer, G., NirN protein from *Pseudomonas aeruginosa* is a novel electron-bifurcating dehydrogenase catalyzing the last step of heme d_1 biosynthesis. *J. Biol. Chem.* **2014,** *289*, 30753-30762.
236. de Boer, A. P.; Reijnders, W. N.; Kuenen, J. G.; Stouthamer, A. H.; van Spanning, R. J., Isolation, sequencing and mutational analysis of a gene cluster involved in nitrite reduction in *Paracoccus denitrificans*. *Antonie Van Leeuwenhoek* **1994,** *66*, 111-27.
237. Bali, S.; Palmer, D. J.; Schroeder, S.; Ferguson, S. J.; Warren, M. J., Recent advances in the biosynthesis of modified tetrapyrroles: the discovery of an alternative pathway for the formation of heme and heme d_1. *Cell Mol. Life Sci.* **2014,** *71*, 2837-2863.
238. Stern, A. M.; Liu, B.; Bakken, L. R.; Shapleigh, J. P.; Zhu, J., A novel protein protects bacterial iron-dependent metabolism from nitric oxide. *J. Bacteriol.* **2013,** *195*, 4702-4708.
239. Crack, J. C.; Green, J.; Thomson, A. J.; Le Brun, N. E., Iron-sulfur clusters as biological sensors: the chemistry of reactions with molecular oxygen and nitric oxide. *Acc. Chem. Res.* **2014,** *47*, 3196-3205.
240. Arai, H.; Kodama, T.; Igarashi, Y., Effect of nitrogen oxides on expression of the *nir* and *nor* genes for denitrification in *Pseudomonas aeruginosa*. *FEMS Microbiol. Lett.* **1999,** *170*, 19-24.
241. Trunk, K.; Benkert, B.; Quäck, N.; Münch, R.; Scheer, M.; Garbe, J.; Jänsch, L.; Trost, M.; Wehland, J.; Buer, J.; Jahn, M.; Schobert, M.; Jahn, D., Anaerobic adaptation in *Pseudomonas aeruginosa*: definition of the Anr and Dnr regulons. *Environ. Microbiol.* **2010,** *12*, 1719-1733.
242. Wing, H. J.; Williams, S. M.; Busby, S. J., Spacing requirements for transcription activation by *Escherichia coli* FNR protein. *J. Bacteriol.* **1995,** *177*, 6704-6710.
243. Härtig, E.; Schiek, U.; Vollack, K. U.; Zumft, W. G., Nitrate and nitrite control of respiratory nitrate reduction in denitrifying *Pseudomonas stutzeri* by a two-component regulatory system homologous to NarXL of Escherichia coli. *J. Bacteriol.* **1999,** *181*, 3658-3665.
244. Zhang, X.; DeMoss, J. A., Structure modification induced in the *narG* promoter by binding of integration host factor and NARL-P. *J. Bacteriol.* **1996,** *178*, 3971-3973.
245. Hahnke, S. M.; Moosmann, P.; Erb, T. J.; Strous, M., An improved medium for the anaerobic growth of *Paracoccus denitrificans* Pd1222. *Front. Microbiol.* **2014,** *5*, 18.
246. Baumann, B.; van der Meer, J. R.; Snozzi, M.; Zehnder, A. J., Inhibition of denitrification activity but not of mRNA induction in *Paracoccus denitrificans* by nitrite at a suboptimal pH. *Antonie Van Leeuwenhoek* **1997,** *72*, 183-9.
247. Bergaust, L.; Mao, Y.; Bakken, L. R.; Frostegård, A., Denitrification response patterns during the transition to anoxic respiration and posttranscriptional effects of suboptimal pH on nitrous oxide reductase in *Paracoccus denitrificans*. *Appl. Environ. Microbiol.* **2010,** *76*, 6387-96.
248. Spiro, S., Nitrous oxide production and consumption: regulation of gene expression by gas-sensitive transcription factors. *Philos. Trans. R. Soc. Lond. B Biol. Sci.* **2012,** *367*, 1213-25.
249. Vollack, K. U.; Zumft, W. G., Nitric oxide signaling and transcriptional control of denitrification genes in *Pseudomonas stutzeri*. *J. Bacteriol.* **2001,** *183*, 2516-2526.
250. Almeida, J. S.; Júlio, S. M.; Reis, M. A.; Carrondo, M. J., Nitrite inhibition of denitrification by *Pseudomonas fluorescens*. *Biotechnol. Bioeng.* **1995,** *46*, 194-201.
251. Hartop, K. R.; Sullivan, M. J.; Giannopoulos, G.; Gates, A. J.; Bond, P. L.; Yuan, Z.; Clarke, T. A.; Rowley, G.; Richardson, D. J., The metabolic impact of extracellular nitrite on aerobic metabolism of *Paracoccus denitrificans*. *Water Res.* **2017,** *113*, 207-214.
252. Bergaust, L.; Mao, Y.; Bakken, L. R.; Frostegård, A., Denitrification response patterns during the transition to anoxic respiration and posttranscriptional effects of suboptimal pH on nitrous oxide reductase in *Paracoccus denitrificans*. *Appl. Environ. Microbiol.* **2010,** *76*, 6387-6396.
253. Booth, I. R., Regulation of cytoplasmic pH in bacteria. *Microbiol. Rev.* **1985,** *49*, 359-378.

254. Slonczewski, J. L.; Fujisawa, M.; Dopson, M.; Krulwich, T. A., Cytoplasmic pH measurement and homeostasis in bacteria and archaea. *Adv. Microb. Physiol.* **2009,** *55*, 1-79.
255. Wilks, J. C.; Slonczewski, J. L., pH of the cytoplasm and periplasm of *Escherichia coli*: rapid measurement by green fluorescent protein fluorimetry. *J. Bacteriol.* **2007,** *189*, 5601-5607.
256. Demanèche, S.; Philippot, L.; David, M. M.; Navarro, E.; Vogel, T. M.; Simonet, P., Characterization of denitrification gene clusters of soil bacteria via a metagenomic approach. *Appl. Environ. Microbiol.* **2009,** *75*, 534-537.
257. Timóteo, C. G.; Pereira, A. S.; Martins, C. E.; Naik, S. G.; Duarte, A. G.; Moura, J. J. G.; Tavares, P.; Huynh, B. H.; Moura, I., Low-spin heme b_3 in the catalytic center of nitric oxide reductase from *Pseudomonas nautica*. *Biochemistry* **2011,** *50*, 4251–4262.
258. Ghosh; Kumar, M.; Jitumani, R.; Debajani, B.; Shyamalava, M., Role of the surface-exposed leucine 155 in the metal ion binding loop of the CuA domain of cytochrome *c* oxidase from *Thermus thermophilus* on the function and stability of the protein. *Biochemistry* **2012,** *51*, 2443-2452.
259. Gupta, S.; Warne, A.; Saraste, M.; Mazumdar, S., pH-induced conformational transition in the soluble CuA domain of *Paracoccus denitrificans* cytochrome oxidase. *Biochemistry* **2001,** *40*, 6180-6189.
260. Sanghamitra, N. J.; Mazumdar, S., Conformational dynamics coupled to protonation equilibrium at the CuA site of *Thermus thermophilus*: insights into the origin of thermostability. *Biochemistry* **2008,** *47*, 1309-1318.
261. Jung, H. H.; Yi, L., pH-dependent transition between delocalized and trapped valence states of a CuA center and its possible role in proton-coupled electron transfer. *Proc. Natl. Acad. Sci.* **2004,** *101*, 12842-12847.
262. Alvarez-Paggi, D.; Abriata, L. A.; Murgida, D. H.; Vila, A. J., Native Cu(A) redox sites are largely resilient to pH variations within a physiological range. *Chem. Commun.* **2013,** *49*, 5381-5383.
263. Dutton, P. L., Redox potentiometry: determination of midpoint potentials of oxidation-reduction components of biological electron-transfer systems. *Methods Enzymol.* **1978,** *54*, 411-35.
264. Hosseinzadeh, P.; Lu, Y., Design and fine-tuning redox potentials of metalloproteins involved in electron transfer in bioenergetics. *Biochim. Biophys. Acta* **2016,** *1857*, 557-81.
265. Gooding, J. J., Nanostructuring electrodes with carbon nanotubes: A review on electrochemistry and applications for sensing. *Electrochem. Acta* **2005,** *50*, 3049-3060.
266. Hu, C.; Hu, S., Carbon nanotube-based electrochemical sensors: principles and applications in biomedical systems. *J. Sensors* **2009,** *2009*, 40.
267. Brownson, D. A.; Banks, C. E., Graphene electrochemistry: an overview of potential applications. *Analyst.* **2010,** *135*, 2768-2778.
268. Balasubramanian, K.; Burghard, M., Chemically functionalized carbon nanotubes. *Small.* **2005,** *1*, 180-192.
269. Bard, A. J.; Faulkner, L. R., *Electrochemical Methods, Fundamentals andApplications*. Wiley: **2001**.
270. de Sousa, P. M.; Pauleta, S. R.; Gonçalves, M. L.; Pettigrew, G. W.; Moura, I.; Dos Santos, M. M.; Moura, J. J., Mediated catalysis of *Paracoccus pantotrophus* cytochrome *c* peroxidase by *P. pantotrophus* pseudoazurin: kinetics of intermolecular electron transfer. *J. Biol. Inorg. Chem.* **2007,** *12*, 691-698.
271. Nicholls D., Ferguson S. J., Quantitative Bioenergetics. In *Bioenergetics* Elsevier: **2013**, pp 27-53.
272. Ertem, M. Z.; Cramer, C. J.; Himo, F.; Siegbahn, P. E., N-O bond cleavage mechanism(s) in nitrous oxide reductase. *J. Biol. Inorg. Chem.* **2012,** *17*, 687-698.
273. Tepper, A. W.; Bubacco, L.; Canters, G. W., Structural basis and mechanism of the inhibition of the type-3 copper protein tyrosinase from *Streptomyces antibioticus* by halide ions. *J. Biol. Chem.* **2002,** *277*, 30436-30444.
274. Solomon, E. I.; Penfield, K. W.; Wilcox, D. E., Active sites in copper proteins an electronic structure overview *Struct. Bonding* **1983**, 1- 57.

275. Neese, F. Electronic Structure and spectroscopy of novel copper chromophores in biology. Universität Konstanz, Konstanz, **1997**.
276. Küpper, F. C.; Kroneck, P. M. H., Iodine bioinorganic chemistry: physiology, structures, and mechanisms. In *Iodine chemistry and applications*, Kaiho, T., Ed. wiley: **2015**; pp 557-589.
277. Privalov, P. L., Microcalorimetry of Proteins and Their Complexes. In *Protein Structure, Stability, and Interactions*, - Shriver, John W. ed.; Shriver, J. W., Ed. **2008**; pp 1-39.
278. Torres, J.; Wilson, M. T., The reactions of copper proteins with nitric oxide. *Biochim. Biophys. Acta* **1999,** *1411*, 310-322.
279. Frunzke, K.; Zumft, W. G., Inhibition of nitrous-oxide respiration by nitric oxide in the denitrifying bacterium *Pseudomonas perfectomarina*. *Biochim. Biophys. Acta* **1986,** *852*, 119-125.
280. Jin, H.; Thomann, H.; Coyle, C. L.; Zumft, W. G., Copper coordination in nitrous oxide reductase from *Pseudomonas stutzeri*. *J. Am. Chem. Soc.* **1989,** *111*, 4262-4269.
281. Bakken, L. R.; Bergaust , L.; Liu , B.; Frostegård, A., Regulation of denitrification at the cellular level: a clue to the understanding of N_2O emissions from soils. *Philos. Trans. R. Soc. Lond. B Biol. Sci.* **2012,** *367*, 1226-1234.
282. Liu, B.; Frostegård, Å.; Bakken, L. R., Impaired reduction of N_2O to N_2 in acid soils is due to a posttranscriptional interference with the expression of *nosZ*. *MBio.* **2014,** *5*, e011383-14.

Supplementary Information

Supplementary Information

S1. Score of the alignments of NarL, FNR and IHF motifs.

Table S1.1 – NarL, FNR and IHF putative nucleotide motifs in the promoter regions of denitrification gene clusters of *M. hydrocarbonoclasticus*. PRODORIC database was used to identify the sequences.

PWM (species)	Promotor region	Sequence	Score
NarL | *Pseudomonas aeruginosa* (strain ATCC 15692 / PAO1) / Maximum score:5.63	*narK*	**TACCTC**C	5.12
	narGHJV	**T**G**CTT**C**T**	5.29
	narGHJV	**T**G**CT**G**CT**	4.92
Fnr | *Escherichia coli* (strain K12) / Maximum score: 8.93	*narK*	**TTGA**GGATAG**TCAA**	7.14
	narGHJV	**TTGAT**CCCACA**CAA**	7.04
	narXL	**TTGA**CTATCC**TCAA**	7.92
	nirCF	**TT**A**AT**CAAT**ATCAA**	7.08
	nirSDLGHJEN	**TTGAT**ATTG**AT**T**AA**	7.30
	norCB3055DEF	**TTGAT**AATC**ATCAA**	8.47
	nosR	**TTGA**TTTTCC**TCAA**	8.16
	dnr	**TTGA**GCTAAG**TCAA**	7.27
IHF | *Escherichia* coli (strain K12) Maximum score: 7.67	*narK*	CCC**CAA**TGGT**TTA**TAA	6.39

Note: The nucleotides highlight in bold match their consensus sequence. PWM- position weight matrix.

S2. Analysis of pI and molecular mass of proteins encoded by the *nos* gene cluster or proposed to be the accessory proteins of N_2OR

Table S2.1 – Parameters (molecular mass and pI) of proteins encoding by the *nos* cluster.

Protein	Location	MM (kDa)	pI
NosL	periplasm (attached to the outer membrane)	19.3	4.5
NosY	membrane	24.3	5.0
NosF	cytoplasm	33.6	6.5
NosD	periplasm	44.4	4.9
N_2OR	periplasm	65.0	5.4
NosR	membrane	70.4	5.7
ApbE (MARHY1380)	attached to the membrane	34.8	4.5

S3. EPR spectrum of as-isolated *M. hydrocarbonoclasticus* N_2OR

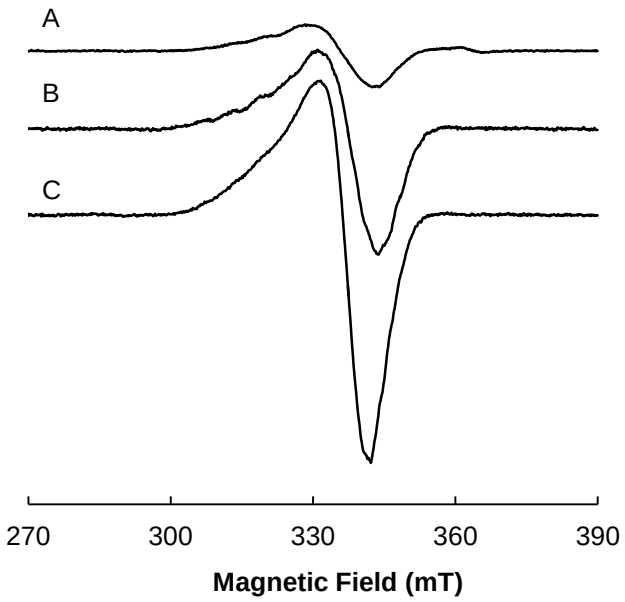

Figure S3.1 – X-band EPR spectra of as-isolated *M. hydrocarbonoclasticus* N_2OR from growths performed at different pH values: (A) $N_2OR_{pH8.5}$, (B) $N_2OR_{pH7.5}$ and (C) $N_2OR_{pH6.5}$. The instrument settings for the data acquisition were: microwave frequency, 9.65 GHz; microwave power, 2 mW; gain, $1x10^5$; temperature, 30 K.

S4. Behavior of the redox potential of CuZ(4Cu2S)

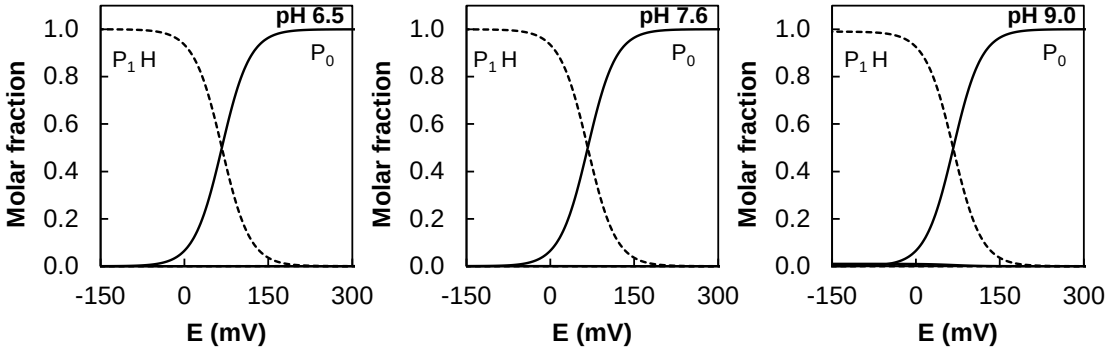

Figure S4.1 – Molar fraction of the four microstates of CuZ(4Cu2S) at pH 6.5, 7.6 and 9.0 (indicated in each panel). The curves were simulated considering one reduction potential (E = 67 mV), pK_{ox} = 3 and pK_{red} = 11. Solid and dashed lines indicate the deprotonated and protonated microstates, respectively. P_0 and P_0H represent the oxidized and oxidized protonated microstates and P_1 and P_1H represent the reduced and reduced protonated microstates.

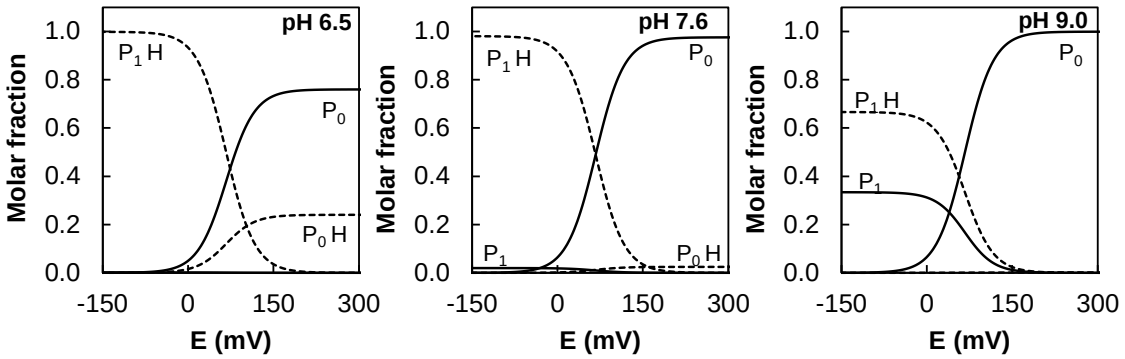

Figure S4.2 – Molar fraction of the four microstates of CuZ(4Cu2S) at pH 6.5, 7.6 and 9.0 (indicated in each panel). The curves were simulated considering one reduction potential (E = 67 mV), pK_{ox} = 6 and pK_{red} = 9.2. Solid and dashed lines indicate the deprotonated and protonated microstates, respectively. P_0 and P_0H represent the oxidized and oxidized protonated microstates and P_1 and P_1H represent the reduced and reduced protonated microstates.

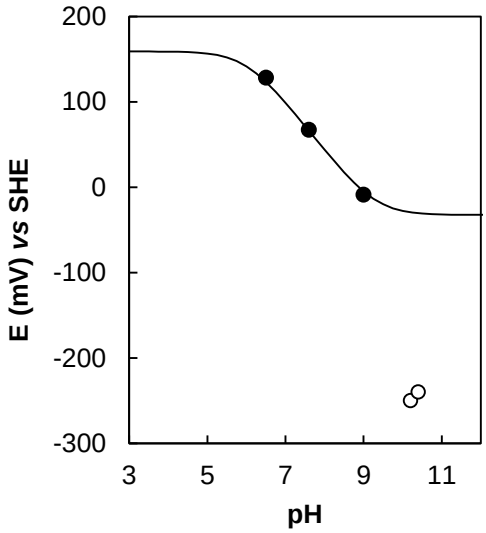

Figure S4.3 – pH dependence of the reduction potential of CuZ(4Cu2S). Data obtained for the reductive titration performed at pH 6.5, 7.6 and 9.0 (filled circles) were fitted to Equation S4.1, using pK_{ox} = 6 and pK_{red} = 9.3 and E_{lp} = 160 mV. The reductive titrations performed at pH 10.2 and 10.4 (open circles) are also represented.

The pH dependence with the reduction potential of CuZ(4Cu2S) was defined by two p*K* values, being the data fitted to the Equation S4.1.

$$E = E_{lp} + \frac{2.3RT}{nF} log_{10}\left(\frac{1+(\frac{K_{red}}{[H^+]})}{1+(\frac{K_{ox}}{[H^+]})}\right) \quad \text{(Eq S4.1)}$$

Where, E is the measured reduction potential, E_{lp} is the reduction potential at low pH (fully protonated form), and K_{ox} and K_{red} are the proton dissociation constants of the oxidized and reduced forms, respectively.

The pH dependence on the redox potential is given by the Nernst equation (Equation S4.2):

$$\mathrm{E} = E_1 + 58 \log_{10} \frac{\mathrm{P_0H} + \mathrm{P_0}}{\mathrm{P_1H} + \mathrm{P_1}} \quad \text{(Eq S4.2)}$$

The macroscopic stages are connected by one electron redox process, which can be described by a Nernst equation for each microstate (Equations S4.3 – S4.7):

$$\mathrm{P_0H} + \mathrm{P_0} + \mathrm{P_1H} + \mathrm{P_1} = 1 \quad \text{(Eq S4.3)}$$

P_0 and P_0H represent the oxidized and oxidized protonated microstates and P_1 and P_1H represent the reduced and reduced protonated microstates.

$$P_0H = \frac{1}{1+\frac{1}{10^{\left(\frac{E-E_1}{58}\right)}}\times\left(1+\frac{K_{ox}}{[H^+]}\right)} \quad \text{(Eq S4.4)}$$

$$P_0 = \frac{1}{1+\frac{1}{10^{\left(\frac{E-E_1}{58}\right)}}} - P_0H \quad \text{(Eq S4.5)}$$

$$P_1H = \frac{1}{\left(1+\frac{1}{10^{\left(\frac{E-E_1}{58}\right)}}\right)\times 10^{\left(\frac{E-E_1}{58}\right)}\times\left(1+\frac{K_{red}}{[H^+]}\right)} \quad \text{(Eq S4.6)}$$

$$P_1 = \frac{1}{\left(1+\frac{1}{10^{\left(\frac{E-E_1}{58}\right)}}\right)\times 10^{\left(\frac{E-E_{lp}}{58}\right)}} - \frac{1}{10^{\left(\frac{E-E_1}{58}\right)}\times\left(1+\frac{K_{red}}{[H^+]}\right)} \quad \text{(Eq S4.7)}$$

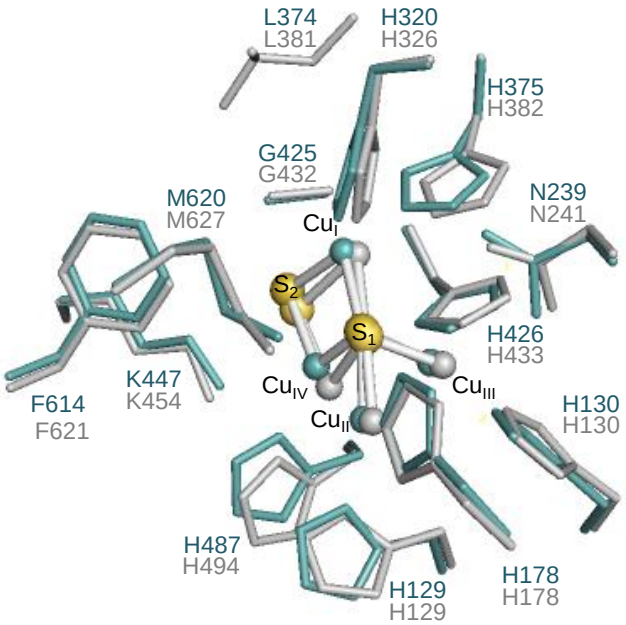

Figure S4.4 – Superposition of the amino acids residues at 5 Å from CuZ(4Cu2S) center. The *M. hydrocarbonoclasticus* N_2OR crystallized at pH 9.5 in a reduced state is colored in blue and the *P. stutzeri* N_2OR crystallized at pH 7.0 in the oxidized state is colored in grey. Copper atoms are represented as spheres, being colored according to the structure and the sulfur atoms are represented as yellow spheres. Residues are numbered according to primary sequence. Figure prepared with Pymol, using the structure obtained for purple crystal, in the case of *M. hydrocarbonoclasticus* N_2OR and the deposited structure of *P. stutzeri* N_2OR (PDB: 3SBQ).

S5. Formation and decay of CuZº at different pH values

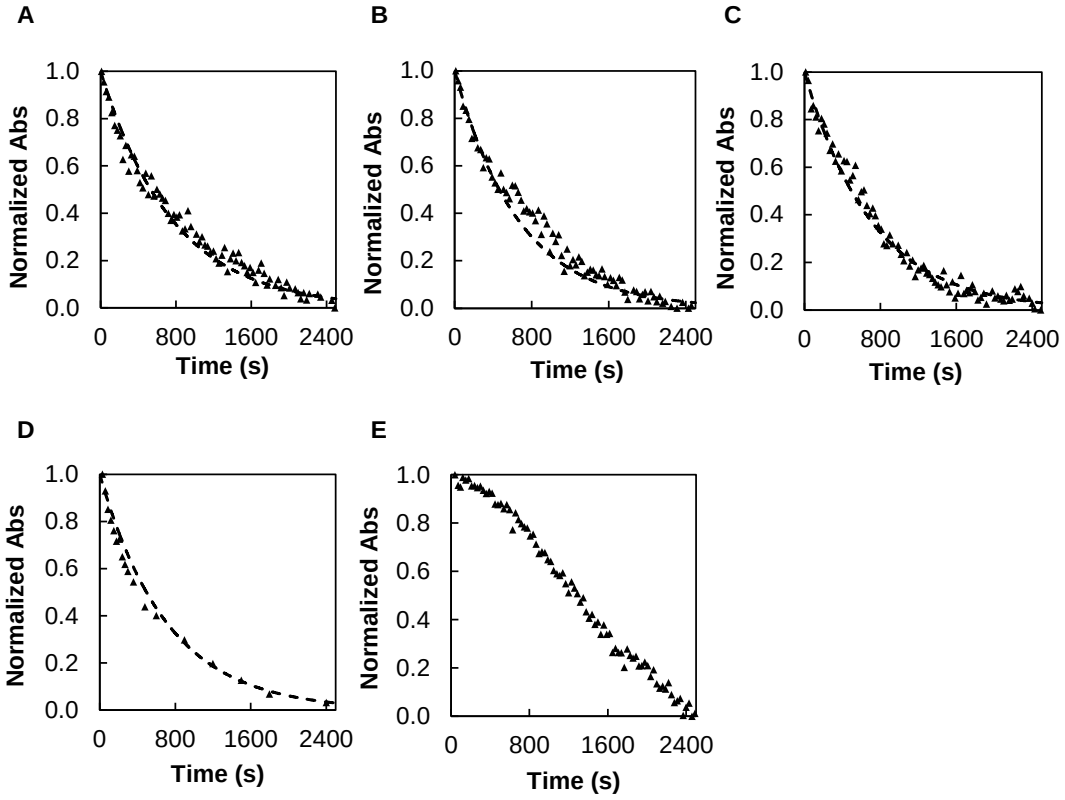

Figure S5.1 – Fittings of normalized time dependence of the decay of CuZº monitored at 683 nm at (A) pH 6.0, (B) 7.6, (C) 8.5, (D) 9.5 and (E) 9.7. Data (A-D) were fitted to single exponential, using the following parameters: (A) [N_2OR] = 19 µM; [N_2O] = 19 µM; $k_{formation}$ = 200 s^{-1}; k_{decay} = 1.3 ×10^{-3} s^{-1}, R^2 = 0.986; (B) [N_2OR] = 22 µM; [N_2O] = 19 µM; $k_{formation}$ = 200 s^{-1}; k_{decay} = 1.5 ×10^{-3} s^{-1}, R^2 = 0.873; (C) [N_2OR] = 19 µM; [N_2O] = 19 µM; $k_{formation}$ = 200 s^{-1}; k_{decay} = 1.5 ×10^{-3} s^{-1}, R^2 = 0.871; (D) [N_2OR] = 15 µM; [N_2O] = 20 µM; $k_{formation}$ = 200 s^{-1}; k_{decay} = 1.4 ×10^{-3} s^{-1}, R^2 = 0.699; (E) [N_2OR] = 19 µM; [N_2O] = 19 µM. The enzyme concentrations were determined for 60 % of "CuZ center" as CuZ*(4Cu1S).

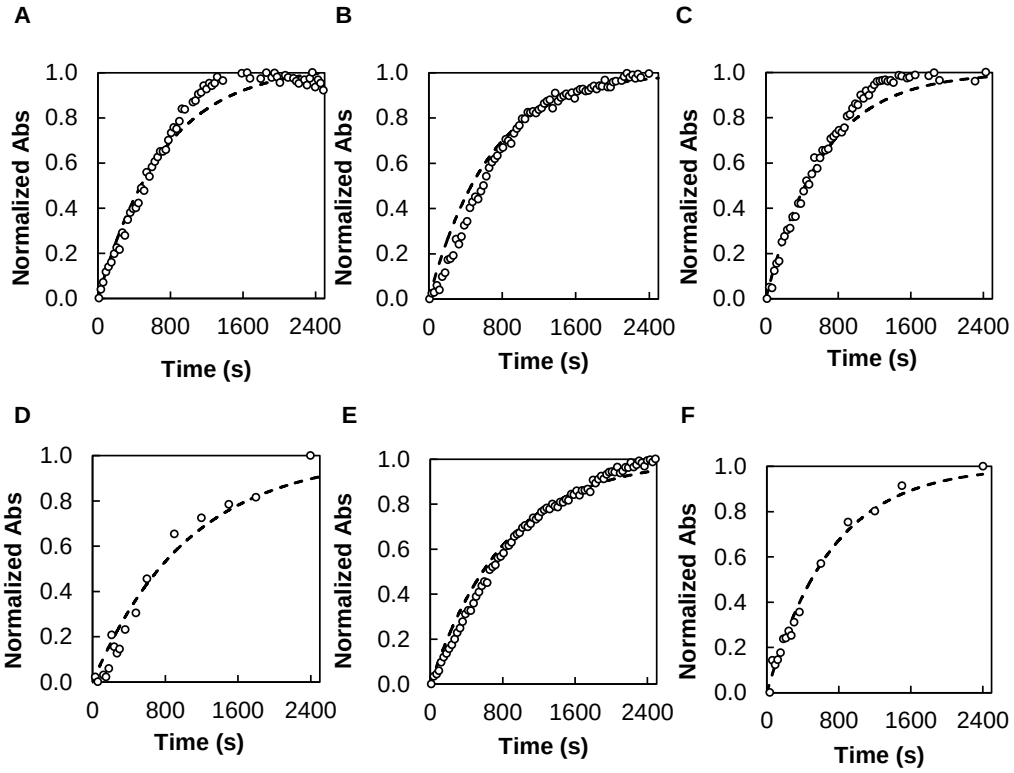

Figure S5.2 – Fittings of normalized time dependence of the formation of CuZ' intermediate species monitored at 614 nm at (A) pH 6.0, (B) 7.6, (C) 8.5, (D) 9.5, (E) 9.7 and (F) 10.0. Data were fitted using the equation A = 1- e^{-kt}. The best fit were obtained using the following parameters: (A) [N_2OR] = 19 µM; [N_2O] = 19 µM; $k_{formation}$ = 1.4 ×10^{-3} s^{-1}, R^2 = 0.645; (B) [N_2OR] = 22 µM; [N_2O] = 19 µM; $k_{formation}$ = 1.5 ×10^{-3} s^{-1}, R^2 = 0.696; (C) [N_2OR] = 19 µM; $k_{formation}$ = 1.6 ×10^{-3} s^{-1}, R^2 = 0.751; (D) [N_2OR] = 15 µM; [N_2O] = 20 µM; $k_{formation}$ = 1.0 ×10^{-3} s^{-1}, R^2 = 0.636; (E) [N_2OR] = 19 µM; [N_2O] = 19 µM; $k_{formation}$ = 1.1 ×10^{-3} s^{-1}, R^2 = 0.777; (F) [N_2OR] = 15 µM; [N_2O] = 20 µM; $k_{formation}$ = 1.4 ×10^{-3} s^{-1}, R^2 = 0.624;. The enzyme concentrations were determined for 60 % of "CuZ center" as CuZ*(4Cu1S).